SYNTHESIS, CHARACTERIZATION, AND APPLICATIONS OF ELECTROACTIVE POLYMERIC NANOSTRUCTURES FOR ORGANIC COATINGS

A Dissertation
Submitted to the Graduate Faculty
of the
North Dakota State University
of Agriculture and Applied Science

By

Abhijit Jagnnath Suryawanshi

In Partial Fulfillment of the Requirements
for the Degree of
DOCTOR OF PHILOSOPHY

Major Department:
Coatings and Polymeric Materials

June 2014

Fargo, North Dakota

North Dakota State University
Graduate School

Title

Synthesis, Characterization, and Applications of Electroactive Polymeric Nanostructures for Organic Coatings

By

Abhijit Jagnnath Suryawanshi

The Supervisory Committee certifies that this ***disquisition*** complies with North Dakota State University's regulations and meets the accepted standards for the degree of

DOCTOR OF PHILOSOPHY

SUPERVISORY COMMITTEE:

Dr. Victoria Johnston Gelling
Chair

Dr. Dean Webster

Dr. Andriy Voronov

Dr. Seth Rasmussen

Approved:

6/18/2014	Dean Webster
Date	Department Chair

ABSTRACT

Electroactive polymers (EAP) such as polypyrrole (PPy) and polyaniline (PANI) are being explored intensively in the scientific community. Nanostructures of EAPs have low dimensions and high surface area enabling them to be considered for various useful applications. These applications are in several fields including corrosion inhibition, capacitors, artificial muscles, solar cells, polymer light emitting diodes, and energy storage devices. Nanostructures of EAPs have been synthesized in different morphologies such as nanowires, nanorods, nanotubes, nanospheres, and nanocapsules. This variety in morphology is traditionally achieved using soft templates, such as surfactant micelles, or hard templates, such as anodized aluminum oxide (AAO). Templates provide stability and groundwork from which the polymer can grow, but the templates add undesirable expense to the process and can change the properties of the nanoparticles by integrating its own properties.

In this study a template free method is introduced to synthesize EAP nanostructures of PPy and PANI utilizing ozone oxidation. The simple techniques involve ozone exposure to the monomer solution to produce aqueous dispersions of EAP nanostructures. The synthesized nanostructures exhibit uniform morphology, low particle size distribution, and stability against agglomeration. Ozone oxidation is further explored for the synthesis of silver-PPy (Ag-PPy) core-shell nanospheres (CSNs). Coatings containing PPy nanospheres were formulated to study the corrosion inhibition efficiency of PPy nanospheres. Investigation of the coatings using electrochemical techniques revealed that the PPy nanospheres may provide corrosion inhibition against filiform corrosion by oxygen scavenging mechanism. Finally, organic corrosion inhibitors were incorporated in PPy to develop efficient corrosion inhibiting systems, by using the synergistic effects from PPy and organic corrosion inhibitors.

ACKNOWLEDGMENTS

I greatly appreciate Dr. Victoria Johnston Gelling for her valuable guidance, support, and time towards this disquisition. I am very lucky for being a member of Dr. Gelling's research group. My professional and personal life has positively progressed through the mentoring and supervision of Dr. Gelling.

I would like to thank my advisory committee members, Dr. Webster, Dr. Voronov, and Dr. Rasmussen for their unrestrained advice and support over the past four years. I would like to thank each one of you for your valuable time towards completion of my dissertation.

I was very fortunate to work alongside academically brilliant and supportive colleagues including Joe, Ken, Niteen, Kiran, Takeshi, Chris, Drew and Kashi. I would like to thank all of you for assisting me through the graduate school years and for extending your friendship outside of work. I would like to take this opportunity and thank all my friends who have shared with me their time, humor, success and happiness. I am grateful to the students, staff, and faculty at the Department of Coatings and Polymeric Materials for providing me the environment where I have always felt like a home away from home.

I am grateful towards Scott and Jayma at the Electron Microscopy Centre for their assistance during my research with the SEM and TEM. I would also like to thank Dr. Khan and Pumis at the Depatment of Civil Engineering for their help and guidance in the anti-bacterial research.

Finally, I would like to thank Army Research Laboratory (Grant number: W911NF-11-2-0027) for funding my graduate research.

DEDICATION

I dedicate this disquisition to my family. My parents, Jagnnath and Gayatri Suryawanshi have been a constant source of motivation and inspiration in my career. My brother Ajinkya's support has been very special and cannot be described in words. The three of you have been the pillars for my success. All of you constantly support me through all the endeavors I wish to embark on.

TABLE OF CONTENTS

LIST OF TABLES

LIST OF FIGURES

LIST OF SCHEMES

LIST OF ABBREVIATIONS

EAP .....Electroactive polymers

PANI ..... Polyaniline

PPy .....Polypyrrole

SDS .....Sodium dodecyl sulfate

SDBS..... Sodium dodecyl benzoyl sulfonate

CTAB..... Cetyltrimethylammonium bromid

PEG .....Poly(ethylene glycol)

AAO .....Anodic aluminum oxide

NSA..... β-napthalene sulfonic acid

CSA.....Camphorsulfonic acid

SELA..... Selenious acid

APS ..... Ammonium persulfate

CSNs .....Core shell nanostructures

PMMA .....Poly(methyl methacrylate)

PS .....Polystyrene

PVA.....Poly(vinyl alcohol)

POE .....Poly(oxyethylene)

PVPD ..... Poly (N-vinylpyrrolidone)

PTP..... Polythiophene

PA .....Polyacetylene

SVET.....Scanning vibrating electrode technique

TEM ..... Transmission electron microscopy

FTIR.....Fourier transform infrared spectroscopy

AFM.....Atomic force microscope

C-AFM ..... Conductive AFM

SEM ..... Scanning electron microscopy

DLS ..... Dynamic Light Scattering

CV ..... Cyclic voltammetry

XPS ..... X-ray photo-electron spectroscopy

HAS ..... Hemispherical sector analyzer

IEP ..... Iso-electric point

CPN ..... Conductive polymeric nanostructures

PVP ..... Polyvinyl pyrrolidone

PVA ..... Polyvinyl acetate

TGA ..... Thermogravimmetric analysis

PBS ..... Phosphate buffer saline

CFU ..... Colony forming units

LB ..... Luria Bertani

EIS ..... Electrochemical impedance spectroscopy

PDS ..... Potentiodynamic scans

OCP ..... Open circuit potential

CPE ..... Constant phase element

OCI ..... Organic Corrosion inhibitors

BTA ..... Benzotriazole

SCDM ..... Salicyaladoxime

QA ..... Quinaldic acid

MBT 2-mercaptobenzothiazole

LDHs ..... Layered double hydroxides

HAP ..... Hydroxyapetite

OCI-PPy.....OCI modified PPy

BTA-PPy.....BTA modified PPy

SCDM-PPy ..... SCDM modified PPy

QA-PPy.....QA modified PPy

LIST OF APPENDIX TABLES

LIST OF APPENDIX FIGURES

CHAPTER 1. INTRODUCTION TO ELECTROACTIVE POLYMERIC NANOSTRUCTURES

1.1. Introduction

Electroactive polymers (EAP), which may reduce or oxidize upon application of electric field, including polyaniline (PANI) and polypyrrolle (PPy) have garnered a lot of interest in the scientific community due to their application in various fields including electrochromic devices, supercapacitors, actuators, antistatic coatings, and anti-corrosion coatings.[1] The interest in EAPs (Figure 1.1), particularly PPy and PANI, is arrived from the fact that they are stable to the environmental degradation elements, are compatible to a variety of materials, and can be synthesized at a lower cost with minimum resources.[2-4]

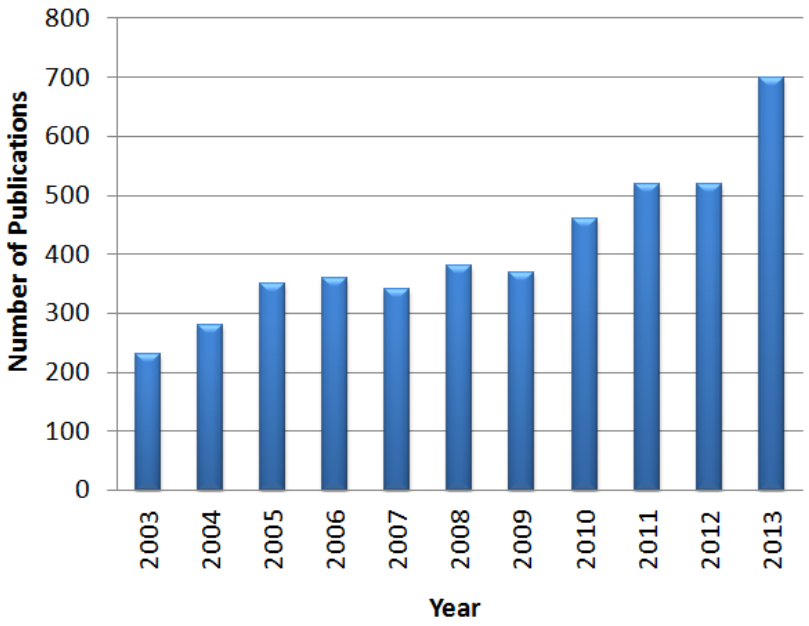

Figure 1.1. An estimate of increase in the research activity in the area of polypyrrole research
(*Note: Google scholar is used to estimate the number of publications. Excluded citations and patents*.)

Development of EAPs has been a multidisciplinary affair that enjoyed parallel attention from chemists, physicists and engineers. Another multidisciplinary field that is growing at a very

rapid pace is nanotechnology which over the years has provided practical market applications. Nanostructures of EAPs thus provide a unique opportunity to unite the fields of nanotechnology and that of EAPs to build advanced products that can cater to the future needs. Nanostructures of EAPs may be expected to yield better properties to their counterparts mainly due to increased surface area and high electrochemical activity. Additionally, due to increase in surface area, required loading levels of nanostructures are low as compared to microstructures.[5, 6]

EAPs are typically synthesized using either chemical oxidants or using electrochemical methods. The mechanism for oxidative polymerization of pyrrole as an example is provided in Scheme 1.1.[7, 8] Common chemical oxidants are iron(III) chloride, ammonium persulfate, and copper(II) perchlorate.[9] Chemical synthesis methods preside over electrochemical methods because of ease in synthesis.[10] The electrochemical route, however, is favorable where uniform films are to be obtained on desired metal substrates.[10, 11] Chemical synthesis method is often used in order to synthesize nanostructures of EAPs in bulk. A template can be used to synthesize nanostructures of EAPs; the template provides the support for the synthesis of nanostructures, the support can be a soft template such as surfactant micelle or hard template such as silica nanoparticles.[12-14] While templates are often advisable to achieve the desired morphology, the disadvantages associated with the templates are increased number of steps in the synthesis, modification of final properties of the product, and use of aromatic solvents for removal of templates.[12]

After synthesis, positively charged EAPs are associated with the anionic counterions for charge neutralization; for example if iron(III) chloride is used to synthesize PPy, chloride ions will be the anionic counterions for positively charged PPy. In a few applications such as corrosion inhibition, the counterion plays a crucial role in contributing to the corrosion

mitigation of metal and metal alloys. The corrosion inhibition anion is doped to the oxidized form of PPy, the anion is expected to release in a corrosion reaction consequently providing corrosion inhibition to metal and metal alloys.[15] A disadvantage associated with using conventional oxidants such as iron(III) chloride is that the chloride ion will stay with the positively charged PPy after oxidation. The chloride anions associated with PPy may aggravate the metallic corrosion by anodic dissolution.[16] Thus, it is desirable to use an oxidant which provides the freedom of choosing a counter-ion suitable to an application, for example ozone and hydrogen peroxide. However, it should also be noted that in the synthesis of PPy by ozone or hydrogen peroxide, PPy may be oxidatively doped.[17]

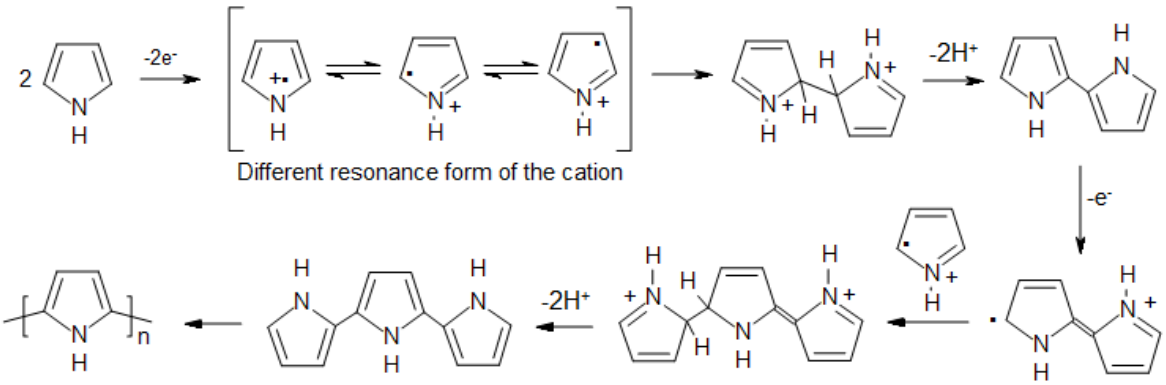

Scheme 1.1. Schematics of oxidative polymerization of pyrrole to PPy.

1.2. Nanostructures of EAPs using chemical oxidants

1.2.1 Polypyrrole

In a typical synthesis using conventional oxidants, cauliflower like microstructures of PPy are obtained (Figure 1.2). In order to synthesize nanostructures of PPy, an external medium such as a surfactant micelle or anodized aluminum oxide are used in the synthesis. Surfactants that are typically used for this purpose are sodium dodecyl sulfate (SDS), sodium dodecyl

benzene sulfonate (SDBS), cetyltrimethylammonium bromide (CTAB) or poly(ethylene glycol) (PEG). Surfactants assist in synthesizing nanostructures by acting as an anionic counterion to positively charged PPy, or by forming a micelle that provides a medium for nanostructure growth inside the micelle, or by hydrophobic interactions between the hydrophobic moieties of surfactant and PPy.[18] Reverse micelles where nanometer sized water containers are formed in the oil phase by surfactant aggregation have also been utilized to synthesize PPy nanotubes.[19]

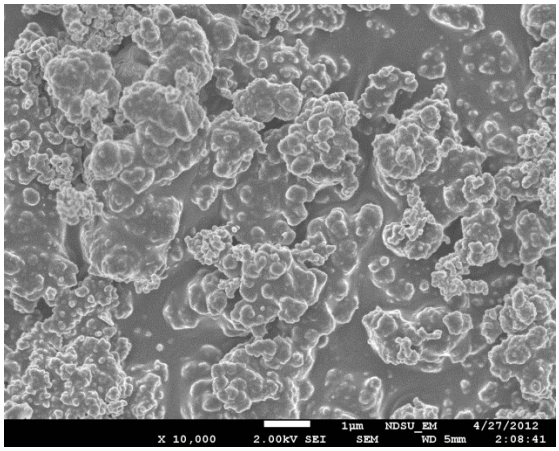

Figure 1.2. Cauliflower like PPy nanostructures synthesized using $FeCl_3$ as an oxidant.

Extensive research work by Zhang and team reveals the important role of surfactant type (anionic, cationic or non-ionic) and type of oxidizing agent to obtain nanostructures with varied nanostructures in the shape of wire, sphere and ribbon.[20] Spherical nanostructures (Figure 1.3a, 1.3d) were obtained when a non-ionic surfactant or a short-chain cationic surfactant was used for the PPy synthesis, due to the template provided by micelles. The layered mesostructures (Figure 1.3b) formed by long chain cationic surfactants and anions associated with the oxidizing agents, were thought to be providing the template for formation of wire and ribbon like PPy nanostructures. The use of anionic surfactants did not result in a specific nanostructure (Figure 1.3c) due to the doping effect of surfactant anions to positively charged PPy. Other factors that

affect the size and morphology of PPy nanostructures are monomer concentration, surfactant concentration and oxidant concentration.

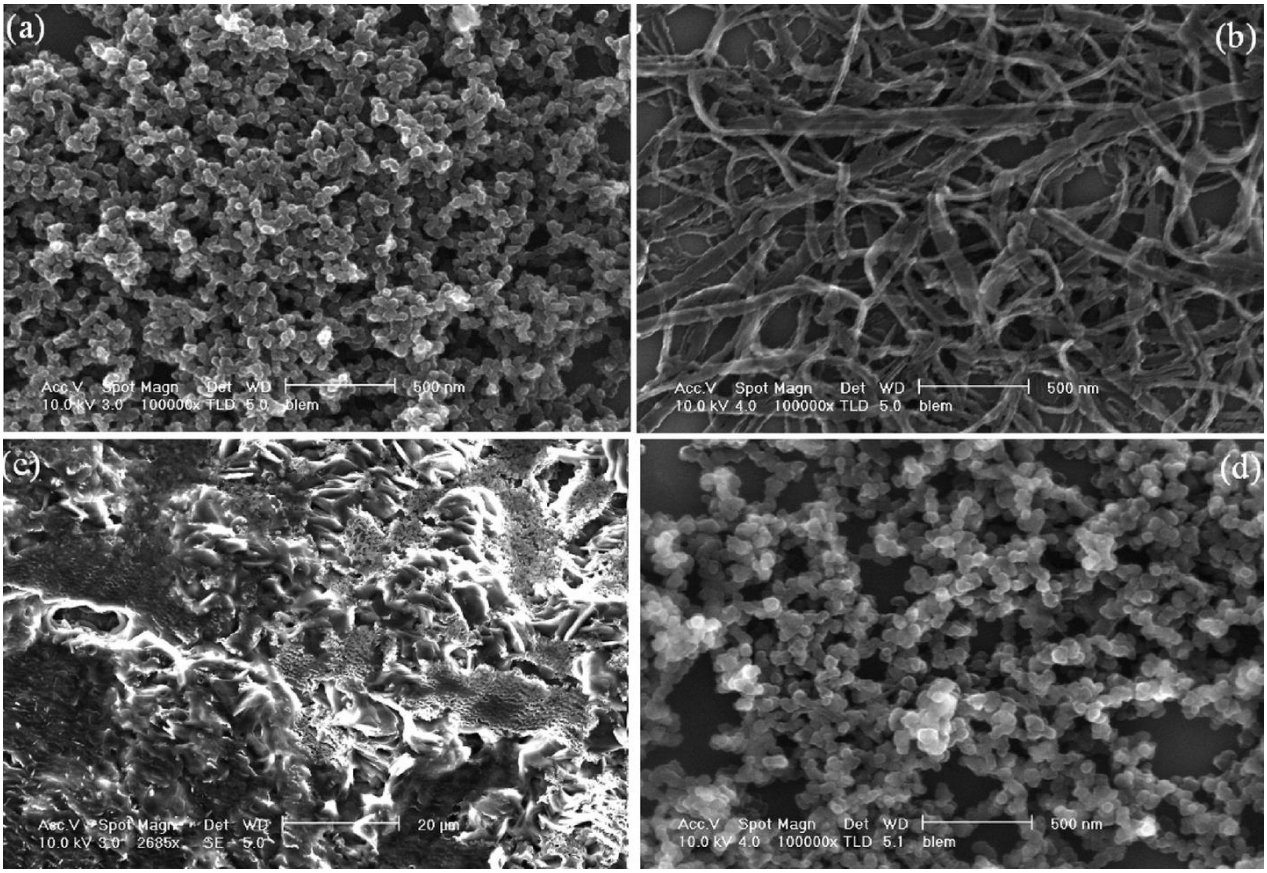

Figure 1.3. Effect of surfactant and oxidizing agent on PPy nanostructure morphology (a) spherical morphology using CTAB and $FeCl_3$, (b) ribbon morphology using CTAB and $(NH_4)_2S_2O_8$, (c) no specific morphology using SDS, (d) spherical morphology using poly(ethylene glycol) mono-p-nonylphenyl ether surfactant.
(*Note: Reprinted with permission from Zhang X, Zhang J, Song W, Liu Z (2006) Controllable synthesis of conducting polypyrrole nanostructures. The Journal of Physical Chemistry B 110 (3):1158-1165 Copyright (2006) American Chemical Society [20]*)

A hard template approach may be considered as a true template method where a physical support is provided to achieve desirable morphological features for EAP nanostructures.[6] Widely used supports are porous anodic aluminum oxide (AAO) membranes or solvent etched polymeric membranes. The support is immersed in the monomer solution; this is followed by addition of the oxidizing solution. The monomer fills the pores and polymerizes inside the pores

resulting in un-agglomerated particles of desired shapes and size. According to the application, after the completion of the synthesis, the template can be removed to get free nanostructures or the nanostructures can be kept inside the template for further use.[21] The positives of using a hard template are; the pores can be configured for various sizes and various morphologies ranging from spherical to cylindrical.[14]

In another scenario, inorganic nanostructures such as silica, halloysite or metal nanoparticles are used which act as a site for the growth of PPy nanostructures.[22] The nanoparticles are added to the solution containing pyrrole monomer and the oxidizing solution is added afterwards. The nanostructures act as a support where pyrrole polymerization takes place resulting into heterogeneous nanostructures consisting of polypyrrole and inorganic material. The heterogeneous nanostructures are valuable to the scientific community since they have the ability to possess properties of both the materials combined into a composite nanostructure. If desired the nanostructures may be removed utilizing aromatic solvents. Recently Zuo *et al.* synthesized PANI-PPy binary composite nanotubes using halloysite as a hard template; self assembled aniline on the tubular halloysite nanostructure was first polymerized.[23] The pyrrole monomer was subsequently assembled on the PANI-halloysite composite due to favoring interaction between the nitrogen groups and acidic N-H bonds. The PANI-PPy-halloysite binary composites were synthesized after polymerization of pyrrole. Further, hydrogen fluoride acid was used to etch out the halloysite nanostructure to obtain PANI-PPy binary nanocomposites.

Although templates have interesting applications towards synthesis of PPy nanostructures, it has a few limitations when compared to a template free approach. The template may modify the properties of PPy by incorporating its own properties, introducing a template may increase the number of steps in the synthesis, and hazardous solvents are used for removal

of the template. [12] Therefore, a template free approach is suggested where no external template is used for synthesis of PPy nanostructures. It should be noted that in literature the term 'template free' is also used as a substitute to 'soft template method' where surfactant aggregates are used for synthesis of nanostrucutres. In this work, the term 'template free' is used extensively to emphasize that no external soft or hard template is used in the synthesis.

In a template free approach, β-napthalene sulfonic acid (NSA) was found to be an effective dopant to achieve various nanostructures of PPy and PANI by Meixiang Wan and coworkers in early 2000s.[12] Concentration of NSA was shown to affect the resulting morphology of PPy resulting in varied morphologies with the shapes of grain, tubes and blocks. The varied morphologies with respect to NSA concentration were ascribed to the hydrophobic interaction of NSA with PPy.[24] In another study PPy nanofibres were synthesized upon addition of a small amount of bipyrrole to a conventional $FeCl_3$ oxidation of an aqueous solution of pyrrole. Bipyrrole, having lower oxidation potential than pyrrole, provides nucleation sites for the growth and morphology of PPy nanofibres.[25]

PPy nanostructures have also been synthesized in template free electrochemical methods.[26, 27] It is observed that the control over morphology and size of PPy nanostructures is limited with template free methods as compared to their counterparts mainly due to lack of the luxury of the physical template or surfactant aggregates for driving growth and morphology of nanostructures.

1.2.2. Polyaniline

In addition to PPy, PANI nanostructures have received considerable attention from the scientific community due to their thermal and environmental stability. Various nanostructures of PANI are possible including nanorods,[28, 29] nanotubes,[30, 31] nanowires[32, 33] and

nanospheres[34, 35] by soft template, hard template or template free methods. Methods described for PPy in the previous section can also be applied for synthesis of PANI nanostructures.

Acidic dopant anions have been found to be particularly useful for template free synthesis of PANI nanostructures. Over the years, various nanostructures have been prepared in several studies using anionic dopants such as camphorsulfonic acid (CSA), [36] selenious acid (SELA) [37] and NSA. Ratio of monomer to dopant was observed to play a major role in dictating the shape and size of the nanostructures. Amarnath *et al.* studied synthesis of PANI nanostructures in the presence of SELA as a dopant with ammonium persulfate (APS) as an oxidizing agent.[37] They observed that increasing dopant-monomer ratio from 0.03 to 2.0, the morphology of the PANI nanostructures changed from flakes to nanorods to nanospheres. The drastic variation in morphology with a small increase in the dopant amount was attributed to the SELA-Aniline interactions. In a complex between aniline and selinious anions, aniline acts as a hydrophobic medium while, selinious anion act as a hydrophilic medium. Thus, in an aqueous synthesis at higher SELA-aniline ratio spherical micelle would dominate (Figure 1.4a), while at lower SELA-aniline ratio rod like surfactant aggregates would dominate (Figure 1.4b, 1.4c).

Interfacial polymerization, in the interface of two immiscible solvents, was also utilized to synthesize various morphologies of PANI nanostructures including nanofibres and nanospheres.[38, 39] Recently, nano-emulsion systems utilizing non-ionic surfactants have been reported for the controlled synthesis of nano-grains or nano-fibres.[40] Oil-in-water emulsion provided with the PANI nano-fibres of 60 nm diameter and 0.5 μm length; while inverse water-in-oil nano emulsion provided with the nano-grains of 60-80 nm diameter. Nanocomposites of PANI with inorganic nanoparticles such as TiO_2, [41, 42] CeO_2, [43, 44] ZnO, [45, 46] SiO_2,

[47-49] V_2O_5 [50] and Fe_3O_4 [51-53] have also been synthesized for various applications. For example, Radhakrishnan and research group proposed TiO_2 – PANI nanocomposites as a potential additive for smart corrosion resistant coatings.

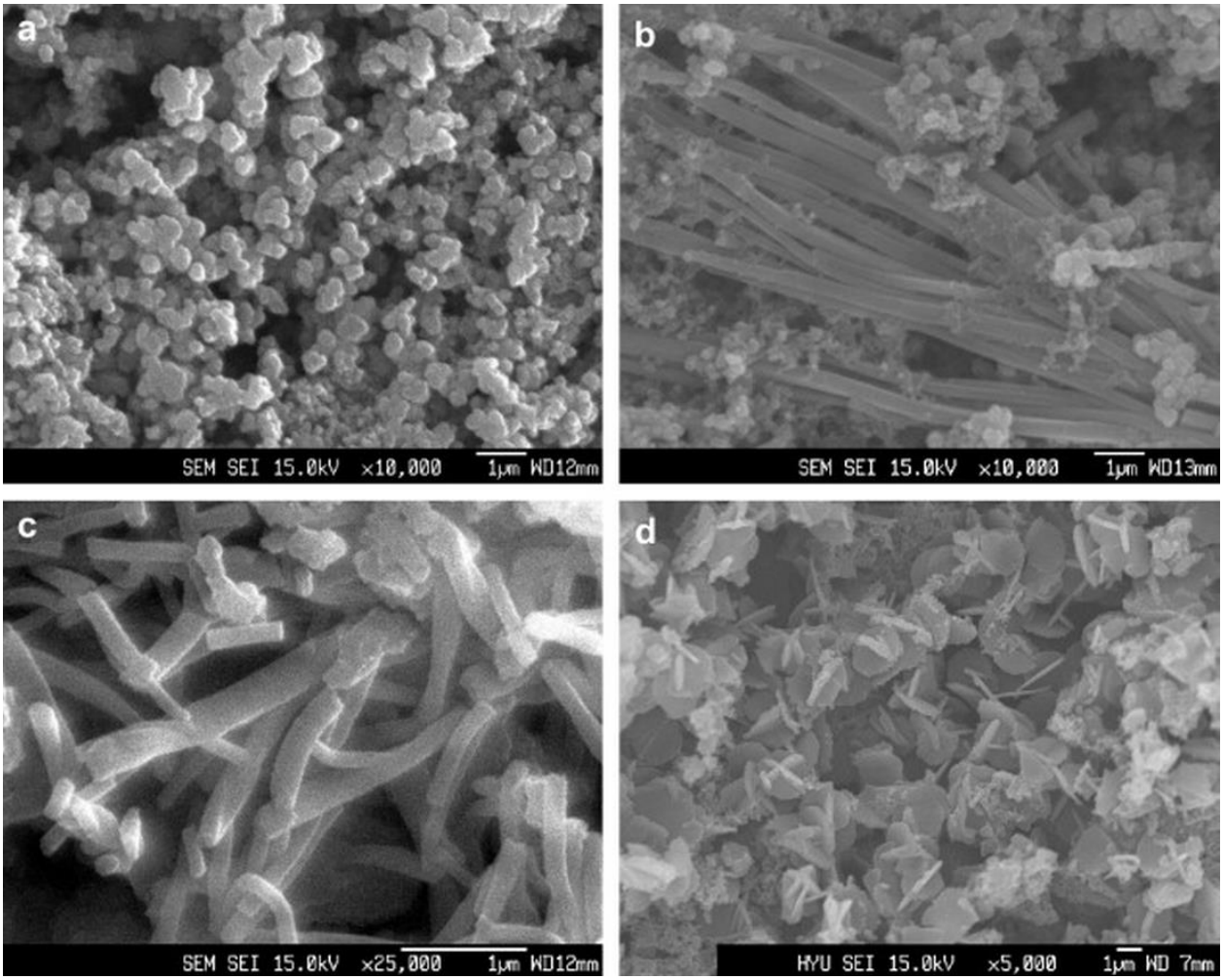

Figure 1.4. SEM images of PANI nanostructures synthesized using APS with SELA as a dopant. (a) dopant-monomer ratio = 2; (b) & (c) dopant-monomer ratio = 0.5 to 1.0 (d) dopant-monomer ratio 0.03.
(*Note: Reprinted with permission from Amarnath CA, Kim J, Kim K, Choi J, Sohn D (2008) Nanoflakes to nanorods and nanospheres transition of selenious acid doped polyaniline. Polymer 49 (2):432-437 Copyright (2008) Elsevier [37]*)

1.3. Core shell nanostructures of EAPs

Taking properties from two different materials for creating a new material with modified properties is the motivation for creating core shell nanostructures (CSNs). For instance magnetic and conductive properties have been achieved by incorporating Fe_3O_4 in the core of PANI [54] and PPy [55] shells. In semiconductor research, CSNs are formulated in order to fine tune band gap of final material.[56] CSNs with core materials including silica, metals, metal oxides, polymers, and carbon nanotubes; while shell materials consisting mainly of PPy and PANI have been reported regularly in the scientific literature.[57, 58]

In the synthesis of PPy and PANI when noble metal salts ($AgNO_3$, [60-66] $PdCl_2$, [67-72] $HAuCl_4$ [73, 74]) were used for oxidation, the noble metal salts oxidize pyrrole or aniline and reduce themselves to metal forms. This resulted in the synthesis of noble metal – EAP nanocomposites. Furthermore, to synthesize nanostructures out of noble metals and EAPs various methods were used which include use of surfactants and interfacial polymerization. The other reason for synthesizing CSNs of EAPs with traditional insulating polymers such as poly(methyl methacrylate) (PMMA) and polystyrene (PS) is to improve processability and mechanical properties of EAPs. Jang *et al.* have synthesized transparent thin films with PPy in the core and PMMA in the shell by a two-step microemulsion polymerization (Scheme 1.2, Figure 1.5). [59] CSNs with both PANI and PPy have also been reported with PS as the shell material. [75-77]

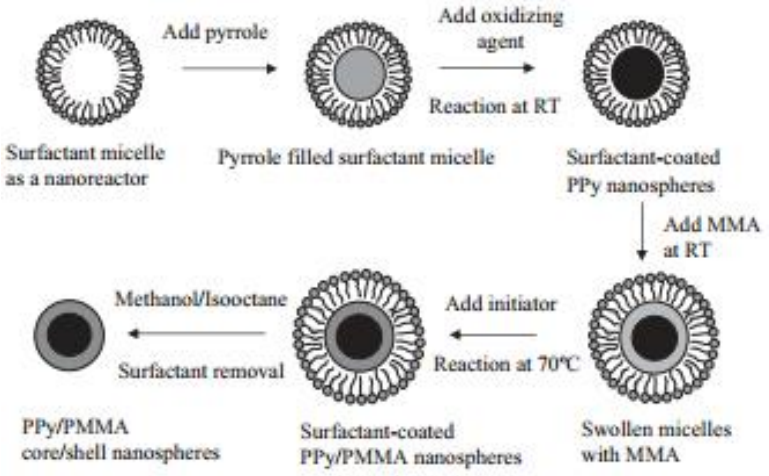

Scheme 1.2. Two step microemulsion to synthesize PPy/PMMA core shell nanospheres.

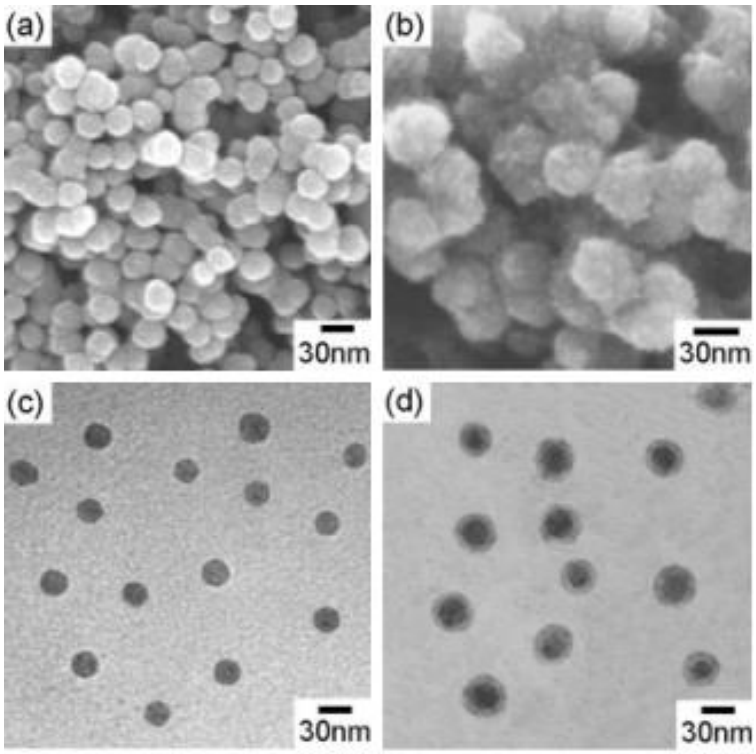

Figure 1.5. Left top: SEM image of PPy nanospheres; left bottom TEM image of PPy nanospheres; right top: SEM image of PPy/PMMA CSNs, right bottom: TEM image of PPy/PMMA CSNs.

(*Note: Scheme 1.2. and Figure 1.5. are reprinted with permission from Jang J, Oh JH (2005) Fabrication of a highly transparent conductive thin film from polypyrrole/poly (methyl methacrylate) core/shell nanospheres. Advanced Functional Materials 15 (3):494-502 Copyright © 2005 WILEY-VCH Verlag GmbH & Co. KGaA, Weinheim [59]*)

1.4. Aqueous dispersion stability of nanostructures of EAPs

It has long been acknowledged that, while it is important to synthesize nanostructure to achieve advanced properties arising out of higher surface activity, stability of the nanostructures to agglomeration is of paramount importance if the efficiency of the nanostructures is to be used to its full potential. The nanostructures are prone to agglomeration due to increased surface energy, increase surface area, and increased van der Waals forces of attraction. The three ways to provide dispersion stability are electrostatic repulsion, steric repulsion and electrosteric repulsion [1, 78] (Figure 1.6).

In electrostatic repulsion mechanism, like charges on the particle surface provide repulsive forces in order to offset the van der Waals forces of attraction.[79] Zeta potential is measured in order to describe the effectiveness of the repulsion forces between the particles against agglomeration. In steric stabilization mechanism, the polymer chains adsorbed on the nanostructures provide steric repulsion driven from the entropic restrictions of the adsorbed polymers. Poly(vinyl alcohol) (PVA), poly(oxyethylene) (POE), and poly (N-vinylpyrrolidone) (PVPD) are few of the common steric stabilizers for PANI and PPy stabilization.[80, 81] The hydrophobic-hydrophilic groups of the adsorbed polymer and thickness of the adsorbed layer play crucial part in determining the dispersion stability of nanostructures by steric stabilization method. Electrosteric repulsion method combines tools of both electrostatic repulsion and steric repulsion in order to provide extended stability and robustness to colloidal dispersions of nanostructures.[79, 80, 82]

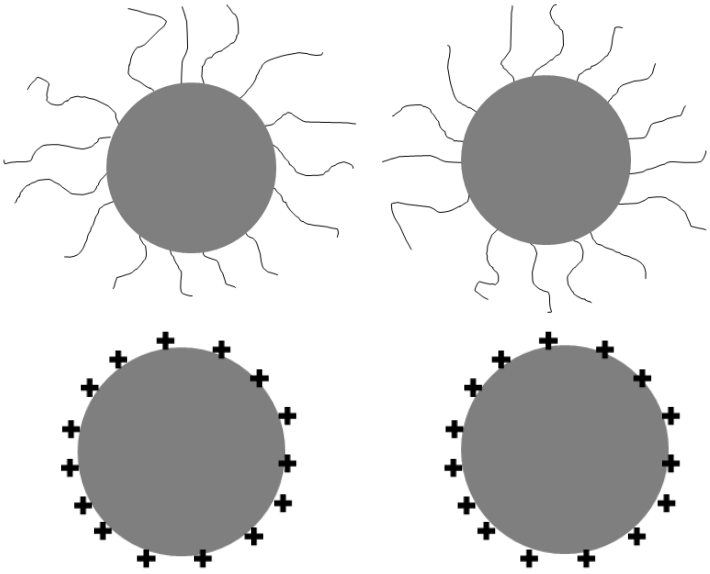

Figure 1.6. Top: steric repulsion; bottom: electrostatic repulsion.

Apart from achieving stability against agglomeration, in case of EAPs, a colloidal dispersion of EAP nanostructures circumvent the challenges with processing. The processing challenges arise from the fact that most EAPs are not soluble in common solvents, unless they are modified. Modification of EAP involves chemically modifying the monomer units in order to enhance the solubility in the solvent, however, modification may reduce the electrochemical properties of EAPs. Research group of S. P. Armes at the University of Sussex, UK, have performed extensive research work towards colloidal stability of PPy and PANI nanostructures. Colloidal dispersions of submicron PPy and PANI particles were prepared utilizing colloidal silica, which presented both steric and electrostatic effects for long term colloidal stability.[80, 82] PANI-copolymer latex composites were also prepared by chemical polymerization of aniline in the presence of copolymer latex.

Yang *et al.* utilized a bifuctional surfactant, polyoxyethylene nonylphenyl ether (PO-NPES) sulfate, in order to synthesize colloidal dispersions of PPy nanoparticles.[83] They observed that with increase in concentration of PO-NPES, the colloidal stability of the

nanoparticle improved, while the nanoparticle size decreased. PPy nanofibres produced utilizing a small amount of bipyrrole in chemical synthesis of PPy from pyrrole was observed to show colloidal stability over a period of one month.

1.5. Ozone as an oxidant for chemical synthesis of EAP nanostructures

In the past, particularly high oxidation potential of ozone as compared to most other oxidants had limited its use as an oxidizing agent for chemical synthesis of EAPs. Early reports indicated the formation of high molecular weight pyrrole black upon the reaction of ozone with pyrrole.[84, 85] Ozone was also investigated as a surface modifying agent and a surface grafting agent for EAPs with limited success.[86] Many research articles concluded that at high concentrations, ozone treatment disrupts conjugation in EAPs and over-oxidizes EAPs by introducing aldehydes and ketones in the EAPs structure. Ozone treatment consequently reduces the oxidation state of EPAs by substantially deprotonating them.[86] Ozone interaction with EAPs including PPy,[87] PANI, [88] polythiophene (PTP), [89] and polyacetylene (PA) [90] has been studied in the literature.

At low concentrations, ozone was able to dope PA films and was able to form charge-transfer complexes with PA.[90] Nowaczyk *et al.* showed that at low concentrations ozone was able to dope poly(3-alkylthiophenes)s, which resulted in increase in conductivity due to low levels of ozonization.[91] Since ozone, particularly at low concentrations, is able to dope EAPs rather than degrade them, Ando and coworkers investigated PANI films for optical ozone detection.[92]

The first studies of ozone as a secondary oxidant for the synthesis of PANI in the presence of iron(II) oxidants were reported in early 2000s.[93, 94] Traditional chemical synthesis methods for synthesizing EAPs use high oxidant to monomer ratios. The final product needs to

undergo excessive purification stages before it is used. In order to reduce the efforts put into purifying polymers off excess oxidizing agents and their byproducts, ozone was used as a catalyst to re-oxidize reduced oxidants back to their oxidized forms (Scheme 1.3). Ozone was able to significantly reduce the required amount of oxidant from the synthesis.

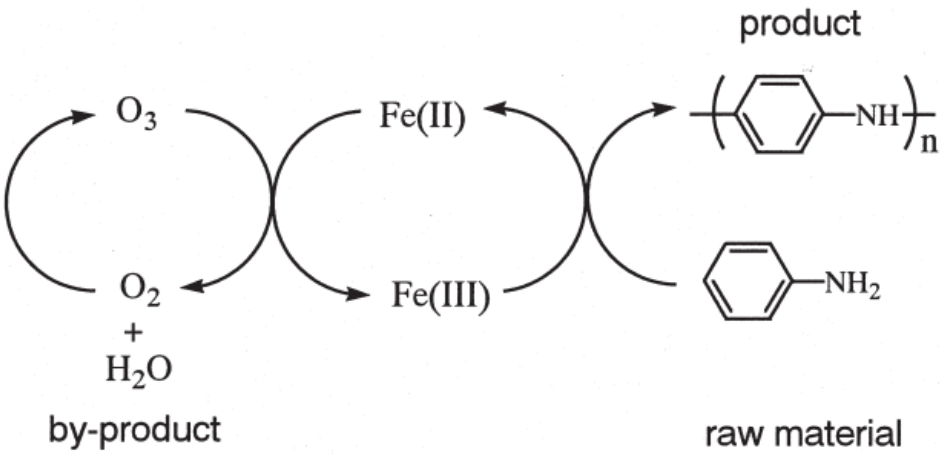

Scheme 1.3. Catalytic oxidation of aniline using ozone as a catalyst in presence of iron (III) oxidants.
(*Note: Reprinted with permission from Yan H, Kajita M, Toshima N (2002) Polymerization of aniline using iron (III) catalyst and ozone, and kinetics of oxidation reactions in the catalytic system. Macromolecular Materials and Engineering 287 (8):503-508 © 2002 WILEY-VCH Verlag GmbH & Co. KGaA, Weinheim from reference [94]*)

In this work, Initial thoughts of using ozone were to investigate the feasibility of ozone as an oxidant, to synthesize EAPs in the pure form, with a freedom of incorporating dopant of choice. Ozone presents numerous opportunities, particularly for aqueous chemical synthesis of EAPs, due to correlation between half-life of ozone in water with pH and temperature.[95, 96] With increase in pH the ozone decomposition rate in water is faster due to catalytic assistance from hydroxyl ions. Similarly, with increase in temperature of the reaction the ozone decomposition rate increases.[97, 98]

Initial studies from our laboratory with ozone had shown us that surprisingly uniform EAP nanostructures can be obtained with ozone oxidation.[99] The byproducts of the reaction

are oxygen and water, making the system environmentally friendly. The size of the nanostructures can be controlled by varying the temperature of the reaction.

1.6. Applications of EAP nanostructures: Focus on corrosion inhibition

EAP nanostructures have been successfully investigated for various applications, utilizing their electrochemical, optical and electrical properties. EAPs provide engineers and chemists the ability to tailor conductivity, redox states, morphology, size, and dopant choice to suit demanding applications. So far EAPs have been investigated for applications in electronic nanodevices, sensors, catalysis, energy storage, biomedical applications, microwave absorption, EMI shielding, electrorheological fluids, memory devices and corrosion prevention. Comprehensive list of applications of EAPs is reported in Table 1.1.[100]

Table 1.1. Applications of EAP nanostructures (*Note: Reorganized from reference [100]*)

<table>
<tr><td>Electronic Nanodevices</td><td>Sensors</td></tr>
<tr><td>• Field Effect Transistors and Diodes
• Polymer Light-Emitting Diodes
• Field-Emission and Electrochromic Displays</td><td>• Chemical and Gas Sensors
• Optical Sensors
• Biosensors</td></tr>
<tr><td>Catalysis</td><td>Energy storage</td></tr>
<tr><td>• Chemical and Photocatalysis
• Electrocatalysis</td><td>• Solar Cells
• Fuel Cells
• Lithium Ion Batteries
• Super Capacitors</td></tr>
<tr><td>Biomedical Applications</td><td>Microwave absorption & EMI Shielding</td></tr>
<tr><td rowspan="3">• Drug Delivery and Protein purification
• Tissue Engineering
• Actuators</td><td>Electrorheological Fluids</td></tr>
<tr><td>Memory devices</td></tr>
<tr><td>Corrosion Inhibition</td></tr>
</table>

1.6.1. Corrosion inhibition with EAP nanostructures

EAP nanostructures provide an environment friendly alternative to traditional carcinogenic corrosion inhibitor. The four general methods by which EAPs provide corrosion inhibition are: 1) Release of corrosion inhibiting dopant anions, 2) Passivation of metal alloys to more noble potentials, 3) Oxygen scavenging, and 4) Cathodic protection by reduced form of EAPs.

1.6.1.1. Release of corrosion inhibiting dopant anions

Also referred to as 'self healing additives', EAP nanostructures doped with organic corrosion inhibitors may release the organic corrosion inhibitors at the defect sites preventing metal and metal alloys from further corrosion.[101] At the defect site when the corrosion reaction is initiated EAPs become a cathode to the metal, thus gets reduced in the process with release of corrosion inhibiting anions on the defect site.[15, 102] A variety of corrosion inhibiting dopants can be incorporated in EAPs including vandate,[103] phosphate,[104-107] tungstate,[103, 108] and molybdate.[104, 109] Nanocomposites of PANI with camphorsulfonic acid (CSA) as a dopant were recently synthesized inside epoxy matrix and were shown to provide corrosion protection to mild steel substrates.[110] Recently the focus of using corrosion inhibiting dopant anions has been shifted to the use of larger anion molecules so as to prevent them from leaching out of the coatings.[104] In that regard benzene sulfonate, polysterensulfonate, and dodecyl sulfate have also been investigated.[15]

1.6.1.2. Passivation of metal alloys to more noble potentials

In their oxidized forms, EAPs have the ability to form a passive oxide layer by shifting the corrosion potential of metals to more noble potential thus providing corrosion protection.[111] The first corrosion inhibition application of EAPs was reported as an

electroactive coating that could passivate stainless steel for long periods of time in acid solutions.[112, 113] Since then, PANI and PPy were widely investigated for both steel and aluminum alloys; as a coating by itself and as a corrosion inhibiting additive in traditional organic coatings.

1.6.1.3. Oxygen scavenging

Oxygen is required in most cases for a corrosion reaction to occur. While oxygen scavengers are well known to the scientific community for their use as an additive in boilers, plumbing systems, water treatment plants, and petrochemical exploration; only recently EAPs were observed to be capable of scavenging oxygen. The reduced and neutral forms of EAPs were observed to dope oxygen and limit the corrosion reaction due to lack of oxygen on metal surface.[114] For instance, neutral and reduced forms of PPy were demonstrated to act as an oxygen scavenger initially for Al alloy AA 2024-T3 by Yan *et al.* thereby limiting availability of the oxygen for corrosion.[114]

1.6.1.4. Cathodic protection by reduced forms of EAPs

Metals and metal alloys can be protected using cathodic or sacrificial cathodic protection mechanisms wherein a more active metal preferentially corrodes over the metal being protected. Reduced forms of EAPs can get oxidized to neutral or oxidized forms at the expense of protecting the metal underneath the coating.[114, 115] Reduced form of poly(2,3-dihexylthieno[3,4-b]pyrazine) was shown to provide cathodic protection to Al alloy AA 2024-T3.[114] Scanning vibrating electrode technique (SVET) results on a coating with artificial defect demonstrated that the oxidation currents were observed on the coating whereas the reduction currents due to oxygen reduction were observed on the defect area. In the process reduced form of the polymer gets oxidized to a neutral form. Although this feature of EAPs has

not been investigated in detail, in the future, EAPs may be looked at as an organic alternative for sacrificial metal rich primers such as Zn-rich and Mg-rich primers.

1.7. Summary

In addition to their electrical, optical and electrochemical properties, EAP nanostructures provide improved efficiency over their counterparts owing to the high surface area and high electrochemical activity. Several synthetic methodologies have been introduced for the synthesis of EAP nanostructures either template based or template free. Better control over morphology and size is achieved with template based methods. Template free methods are advantageous since fewer steps are required in the synthesis, template does not modify properties of the final product, and the purification steps are not expensive. Colloidal dispersion of EAP nanostructures is essential in order to incorporate them in other polymers with better processing ability.

Ozone can be used as an effective oxidant for chemical synthesis of colloidal dispersion of EAP nanostructures in a template free and environment friendly method. Ozone synthesized EAP nanostructures can be fine tuned with the synthetic variants due to the dependence of ozone decomposition rate on pH and temperature of the water. Apart from the applications in biomedical, energy, corrosion, and electronic sectors, with the persistent development in EAP nanostructures more promising application may emerge in future.

1.8. Scope of the dissertation research

PPy and PANI nanostructures synthesized using ozone oxidation have been characterized for their chemical, morphological and electrochemical properties. The synthesis method is explored for the synthesis of CSNs consisting of Ag in the core and PPy in the shell. PPy nanostrucutres have been characterized for their corrosion inhibition utilizing traditional accelerated exposure techniques as well as utilizing modern electrochemical techniques. In order

to improve corrosion inhibition efficiency of PPy nanospheres a novel method is explored where organic corrosion inhibitors are incorporated inside the PPy nanospheres. It is believed that PPy nanospheres and organic corrosion inhibitors will work in cognizance to improve corrosion inhibition efficiency of the entire system.

1.9. References

1. Pecher, J. and S. Mecking, *Nanoparticles of conjugated polymers.* Chemical Reviews, 2010. **110**(10): p. 6260-6279.
2. Bhadra, S., et al., *Progress in preparation, processing and applications of polyaniline.* Progress in Polymer Science, 2009. **34**(8): p. 783-810.
3. Wang, L.-X., X.-G. Li, and Y.-L. Yang, *Preparation, properties and applications of polypyrroles.* Reactive and Functional Polymers, 2001. **47**(2): p. 125-139.
4. Ates, M., T. Karazehir, and A.S. Sarac, *Conducting Polymers and their Applications.* Current Physical Chemistry, 2012. **2**(3): p. 17.
5. Bhushan, B., *Introduction to nanotechnology*, in *Springer handbook of nanotechnology*. 2010, Springer. p. 1-13.
6. Pan, L., et al., *Conducting polymer nanostructures: template synthesis and applications in energy storage.* International journal of molecular sciences, 2010. **11**(7): p. 2636-2657.
7. Heth, C.L., D.E. Tallman, and S.C. Rasmussen, *Electrochemical study of 3-(N-alkylamino) thiophenes: experimental and theoretical insights into a unique mechanism of oxidative polymerization.* The Journal of Physical Chemistry B, 2010. **114**(16): p. 5275-5282.
8. Sadki, S., et al., *The mechanisms of pyrrole electropolymerization.* Chemical Society Reviews, 2000. **29**(5): p. 283-293.

9. Skotheim, T.A., Elsenbaumer, Ronald L, Reynolds, John R, *Handbook of conducting polymers*. 2 ed. 1997: MARCEL DEKKER, INC. 197-409.

10. Hatchett, D.W., M. Josowicz, and J. Janata, *Comparison of chemically and electrochemically synthesized polyaniline films.* Journal of The Electrochemical Society, 1999. **146**(12): p. 4535-4538.

11. Saldivar-Guerra, E. and E. Vivaldo-Lima, *Handbook of Polymer Synthesis, Characterization, and Processing*. 2013: John Wiley & Sons. 537-555.

12. Wan, M., *A Template-Free Method Towards Conducting Polymer Nanostructures.* Advanced materials, 2008. **20**(15): p. 2926-2932.

13. Martin, C.R., *Template synthesis of electronically conductive polymer nanostructures.* Accounts of Chemical Research, 1995. **28**(2): p. 61-68.

14. Yoon, H. and J. Jang, *Conducting-Polymer Nanomaterials for High-Performance Sensor Applications: Issues and Challenges.* Advanced Functional Materials, 2009. **19**(10): p. 1567-1576.

15. Hien, N., et al., *Role of doping ions in the corrosion protection of iron by polypyrrole films.* Electrochimica acta, 2005. **50**(7): p. 1747-1755.

16. Wang, J., C.C. Torardi, and M.W. Duch, *Polyaniline-related ion-barrier anticorrosion coatings: II. Protection behavior of polyaniline, cationic, and bipolar films.* Synthetic metals, 2007. **157**(21): p. 851-858.

17. Leonavicius, K., A. Ramanaviciene, and A. Ramanavicius, *Polymerization model for hydrogen peroxide initiated synthesis of polypyrrole nanoparticles.* Langmuir, 2011. **27**(17): p. 10970-10976.

18. Omastova, M., et al., *Synthesis and structural study of polypyrroles prepared in the presence of surfactants.* Synthetic metals, 2003. **138**(3): p. 447-455.

19. Jang, J. and H. Yoon, *Formation mechanism of conducting polypyrrole nanotubes in reverse micelle systems.* Langmuir, 2005. **21**(24): p. 11484-11489.

20. Zhang, X., et al., *Controllable synthesis of conducting polypyrrole nanostructures.* The Journal of Physical Chemistry B, 2006. **110**(3): p. 1158-1165.

21. Jackowska, K., A.T. Bieguński, and M. Tagowska, *Hard template synthesis of conducting polymers: a route to achieve nanostructures.* Journal of Solid State Electrochemistry, 2008. **12**(4): p. 437-443.

22. Yang, F., et al., *Preparation of uniform silica/polypyrrole core/shell microspheres and polypyrrole hollow microspheres by the template of modified silica particles using different modified agents.* Journal of colloid and interface science, 2006. **301**(2): p. 470-478.

23. Zuo, S., et al., *Preparation of polyaniline–polypyrrole binary composite nanotube using halloysite as hard-template and its characterization.* Chemical Engineering Journal, 2013. **228**: p. 1092-1097.

24. Liu, J. and M. Wan, *Synthesis, characterization and electrical properties of microtubules of polypyrrole synthesized by a template-free method.* Journal of Materials Chemistry, 2001. **11**(2): p. 404-407.

25. Tran, H.D., et al., *A Template-Free Route to Polypyrrole Nanofibers.* Macromolecular rapid communications, 2007. **28**(24): p. 2289-2293.

26. Zang, J., et al., *Template-free electrochemical synthesis of superhydrophilic polypyrrole nanofiber network.* Macromolecules, 2008. **41**(19): p. 7053-7057.

27. Debiemme-Chouvy, C., *Template-free one-step electrochemical formation of polypyrrole nanowire array.* Electrochemistry Communications, 2009. **11**(2): p. 298-301.

28. Bhadra, J. and D. Sarkar, *Self-assembled polyaniline nanorods synthesized by facile route of dispersion polymerization.* Materials Letters, 2009. **63**(1): p. 69-71.

29. Ding, S., H. Mao, and W. Zhang, *Fabrication of DBSA-doped polyaniline nanorods by interfacial polymerization.* Journal of Applied Polymer Science, 2008. **109**(5): p. 2842-2847.

30. Qiu, H., et al., *Conducting polyaniline nanotubes by template-free polymerization.* Macromolecules, 2001. **34**(4): p. 675-677.

31. Stejskal, J., et al., *The genesis of polyaniline nanotubes.* Polymer, 2006. **47**(25): p. 8253-8262.

32. Cao, Y. and T.E. Mallouk, *Morphology of template-grown polyaniline nanowires and its effect on the electrochemical capacitance of nanowire arrays.* Chemistry of materials, 2008. **20**(16): p. 5260-5265.

33. Liu, J., et al., *Templateless assembly of molecularly aligned conductive polymer nanowires: a new approach for oriented nanostructures.* Chemistry-A European Journal, 2003. **9**(3): p. 604-611.

34. Dhand, C., et al., *Preparation, characterization and application of polyaniline nanospheres to biosensing.* Nanoscale, 2010. **2**(5): p. 747-754.

35. Neelgund, G.M. and A. Oki, *A facile method for the synthesis of polyaniline nanospheres and the effect of doping on their electrical conductivity.* Polymer international, 2011. **60**(9): p. 1291-1295.

36. Zhang, L. and M. Wan, *Synthesis and characterization of self-assembled polyaniline nanotubes doped with D-10-camphorsulfonic acid.* Nanotechnology, 2002. **13**(6): p. 750.

37. Amarnath, C.A., et al., *Nanoflakes to nanorods and nanospheres transition of selenious acid doped polyaniline.* Polymer, 2008. **49**(2): p. 432-437.

38. Dallas, P., et al., *Characterization, magnetic and transport properties of polyaniline synthesized through interfacial polymerization.* Polymer, 2007. **48**(11): p. 3162-3169.

39. Chen, J., et al., *Novel interfacial polymerization for radially oriented polyaniline nanofibers.* Materials Letters, 2007. **61**(6): p. 1419-1423.

40. Rahy, A., et al., *Nano-emulsion use for the synthesis of polyaniline nano-grains or nano-fibers.* Polymers for Advanced Technologies, 2011. **22**(5): p. 664-668.

41. Sun, L., et al., *Preparation and characterization of polypyrrole/TiO_2 nanocomposites by reverse microemulsion polymerization and its photocatalytic activity for the degradation of methyl orange under natural light.* Polymer Composites, 2013. **34**(7): p. 1076-1080.

42. Pawar, S., et al., *Synthesis and characterization of polyaniline: TiO_2 nanocomposites.* International Journal of Polymeric Materials, 2010. **59**(10): p. 777-785.

43. Wang, S., et al., *Thermal stability of several polyaniline/rare earth oxide composites (I): polyaniline/CeO_2 composites.* Journal of thermal analysis and calorimetry, 2012. **107**(3): p. 1199-1203.

44. Huang, H. and Z.C. Guo. *Preparation and characterization of conductive polyaniline/cerium dioxide composites*. in *Materials Science Forum*. 2011. Trans Tech Publ.

45. Wang, G., et al., *Highly dispersed Co0. 5Zn0. 5Fe_2O_4/polypyrrole nanocomposites for cost-effective, high-performance defluoridation using a magnetically controllable microdevice.* Journal of hazardous materials, 2012. **237**: p. 1-9.

46. Eskizeybek, V., et al., *Preparation of the new polyaniline/ZnO nanocomposite and its photocatalytic activity for degradation of methylene blue and malachite green dyes under UV and natural sun lights irradiations.* Applied Catalysis B: Environmental, 2012. **119**: p. 197-206.

47. Lu, L., et al., *Synthesis and Characterization of SiO_2@ poly (4-vinylpyridine)@ Polypyrrole-Palladium Composites.* Journal of Polymer Materials, 2012. **29**(2).

48. Wang, W., et al., *Fabrication and characterization of multilayer SiO_2/polymethacrylic acid/polypyrrole composites and hollow polypyrrole microspheres.* Journal of Applied Polymer Science, 2012. **126**(3): p. 974-979.

49. Wu, J.-S., et al., *Chemical in situ polymerization of polypyrrole nanoparticles on the hydrophilic/hydrophobic surface of SiO_2 substrates.* Synthesis and Reactivity in Inorganic, Metal-Organic, and Nano-Metal Chemistry, 2012. **42**(8): p. 1064-1070.

50. Qu, Q., et al., *Core–shell structure of polypyrrole grown on V_2O_5 nanoribbon as high performance anode material for supercapacitors.* Advanced Energy Materials, 2012. **2**(8): p. 950-955.

51. Yao, T., et al., *Preparation of acid-resistant core/shell Fe_3O_4 @C materials and their use as catalyst supports.* Carbon, 2012. **50**(6): p. 2287-2295.

52. Fu, W. and Q. Zhou, *Fabrication of Fe_2O_3@ polypyrrole nanotubes and the catalytic properties under the ultrasound.* Journal of Wuhan University of Technology-Mater. Sci. Ed., 2013. **28**(5): p. 990-996.

53. Azadmanjiri, J., et al., *Synthesis and electromagnetic interference shielding properties of iron oxide/polypyrrole nanocomposites.* Polymer Engineering & Science, 2011. **51**(2): p. 247-253.

54. Deng, J., et al., *Magnetic and conducting Fe_3O_4–cross-linked polyaniline nanoparticles with core–shell structure.* Polymer, 2002. **43**(8): p. 2179-2184.

55. Chen, W., et al., *Magnetic and conducting particles: preparation of polypyrrole layer on Fe_3O_4 nanospheres.* Applied surface science, 2003. **218**(1): p. 216-222.

56. Ghosh Chaudhuri, R. and S. Paria, *Core/shell nanoparticles: classes, properties, synthesis mechanisms, characterization, and applications.* Chemical Reviews, 2011. **112**(4): p. 2373-2433.

57. Qian, T., et al., *Highly dispersed carbon nanotube/polypyrrole core/shell composites with improved electrochemical capacitive performance.* J. Mater. Chem. A, 2013. **1**(48): p. 15230-15234.

58. Jafarzadeh, M., I. Ab Rahman, and C.S. Sipaut, *Synthesis of silica–polypyrrole core–shell nanocomposite using in situ γ-aminopropyltriethoxysilane (APTES)-modified nanosilica.* Synthetic metals, 2012. **162**(5): p. 466-476.

59. Jang, J. and J.H. Oh, *Fabrication of a highly transparent conductive thin film from polypyrrole/poly (methyl methacrylate) core/shell nanospheres.* Advanced Functional Materials, 2005. **15**(3): p. 494-502.

60. Feng, X., et al., *Ag/polypyrrole core-shell nanostructures: Interface polymerization, characterization, and modification by gold nanoparticles.* The Journal of Physical Chemistry C, 2007. **111**(24): p. 8463-8468.

61. Wang, S. and G. Shi, *Uniform silver/polypyrrole core-shell nanoparticles synthesized by hydrothermal reaction.* Materials chemistry and physics, 2007. **102**(2): p. 255-259.

62. Muñoz-Rojas, D., et al., *Facile One-Pot Synthesis of Self-Assembled Silver@ Polypyrrole Core/Shell Nanosnakes.* Small, 2008. **4**(9): p. 1301-1306.

63. Yang, X. and Y. Lu, *Preparation of polypyrrole-coated silver nanoparticles by one-step UV-induced polymerization.* Materials Letters, 2005. **59**(19): p. 2484-2487.

64. Chen, A., et al., *Fabrication of Ag/polypyrrole coaxial nanocables through common ions adsorption effect.* Synthetic metals, 2006. **156**(2): p. 346-350.

65. Shi, Z., et al., *Room temperature synthesis of Ag/polypyrrole core–shell nanoparticles and hollow composite capsules.* Synthetic metals, 2010. **160**(19): p. 2121-2127.

66. Panigrahi, R. and S.K. Srivastava, *Ultrasound assisted synthesis of a polyaniline hollow microsphere/Ag core/shell structure for sensing and catalytic applications.* RSC Advances, 2013. **3**(21): p. 7808-7815.

67. Ohtaka, A., et al., *Polypyrrole–palladium nanocomposite-coated latex particles as a heterogeneous catalyst in water.* Catalysis letters, 2011. **141**(8): p. 1097-1103.

68. Hamasaki, H., et al., *Sterically stabilized polypyrrole–palladium nanocomposite particles synthesized by aqueous chemical oxidative dispersion polymerization.* Colloid and Polymer Science, 2013. **291**(1): p. 223-230.

69. Nie, G., L. Zhang, and Y. Cui, *Preparation of Pd nanoparticles deposited on a polyaniline/multiwall carbon nanotubes nanocomposite and their application in the Heck reaction.* Reaction Kinetics, Mechanisms and Catalysis, 2013. **108**(1): p. 193-204.

70. Ćirić-Marjanović, G., *Recent advances in polyaniline composites with metals, metalloids and nonmetals.* Synthetic metals, 2013. **170**: p. 31-56.

71. Fujii, S., et al., *Polypyrrole–Palladium Nanocomposite Coating of Micrometer-Sized Polymer Particles Toward a Recyclable Catalyst.* Langmuir, 2012. **28**(5): p. 2436-2447.

72. Zinovyeva, V.A., et al., *Highly Dispersed Palladium–Polypyrrole Nanocomposites: In-Water Synthesis and Application for Catalytic Arylation of Heteroaromatics by Direct C–H Bond Activation.* Advanced Functional Materials, 2011. **21**(6): p. 1064-1075.

73. Selvan, T., et al., *Gold–polypyrrole core–shell particles in diblock copolymer micelles.* Advanced materials, 1998. **10**(2): p. 132-134.

74. Xue, K., Y. Xu, and W. Song, *One-step synthesis of 3D dendritic gold@ polypyrrole nanocomposites via a simple self-assembly method and their electrocatalysis for H_2O_2.* Electrochimica acta, 2012. **60**: p. 71-77.

75. Okubo, M., S. Fujii, and H. Minami, *Production of electrically conductive, core/shell polystyrene/polyaniline composite particles by chemical oxidative seeded dispersion polymerization.* Colloid and Polymer Science, 2001. **279**(2): p. 139-145.

76. Vega-Rios, A., et al., *Electrical and electrochemical properties of polystyrene/polyaniline core–shell materials prepared with the use of a reactive surfactant as the polyaniline shell precursor.* Synthetic metals, 2013. **167**: p. 64-71.

77. Nair, S., E. Hsiao, and S.H. Kim, *Fabrication of electrically-conducting nonwoven porous mats of polystyrene–polypyrrole core–shell nanofibers via electrospinning and vapor phase polymerization.* Journal of Materials Chemistry, 2008. **18**(42): p. 5155-5161.

78. Gudarzi, M.M. and F. Sharif, *Characteristics of polymers that stabilize colloids for the production of graphene from graphene oxide.* Journal of colloid and interface science, 2010. **349**(1): p. 63-69.

79. Vincent, B. and J. Waterson, *Colloidal dispersions of electrically-conducting, spherical polyaniline particles.* J. Chem. Soc., Chem. Commun., 1990(9): p. 683-684.

80. Stejskal, J., et al., *Polyaniline dispersions. 6. Stabilization by colloidal silica particles.* Macromolecules, 1996. **29**(21): p. 6814-6819.

81. Armes, S., et al., *Aqueous colloidal dispersions of polyaniline formed by using poly (vinylpyridine)-based steric stabilizers.* Langmuir, 1990. **6**(12): p. 1745-1749.

82. Maeda, S. and S.P. Armes, *Preparation and characterisation of novel polypyrrole–silica colloidal nanocomposites.* J. Mater. Chem., 1994. **4**(6): p. 935-942.

83. Yang, C., et al., *Polypyrrole nanoparticles with high dispersion stability via chemical oxidative polymerization in presence of an anionic–non-ionic bifunctional polymeric surfactant.* Powder Technology, 2012. **217**: p. 134-139.

84. Angeli, A.P., A., *A new method of formation of pyrrole black.* Gazzetta Chimica Italiana, 1919. **49**(1): p. 154-8.

85. Freri, M., *Action of ozone on heterocyclic compounds. I. Pyrrole.* Gazzetta Chimica Italiana, 1932. **62**: p. 600-5.

86. Kang, E., et al., *Surface modification of electroactive polymer films by ozone treatment.* Surface and interface analysis, 1996. **24**(1): p. 51-58.

87. Cataldo, F. and M. Omastová, *On the ozone degradation of polypyrrole.* Polymer Degradation and Stability, 2003. **82**(3): p. 487-495.

88. Cataldo, F., *On the action of ozone on polyaniline.* Polymer Degradation and Stability, 2002. **75**(1): p. 93-98.

89. Czerwiński, W., J. Nowaczyk, and K. Kania, *Ozonization of electronic conducting polymersI. Copolymers based on poly [3-nonylthiophene]*. Polymer Degradation and Stability, 2003. **80**(1): p. 93-101.

90. Cataldo, F., *Ozone interaction with conjugated polymers—I. Polyacetylene.* Polymer Degradation and Stability, 1998. **60**(2): p. 223-231.

91. Nowaczyk, J., W. Czerwiński, and E. Olewnik, *Ozonization of electronic conducting polymers: II. Degradation or doping.* Polymer Degradation and Stability, 2006. **91**(9): p. 2022-2029.

92. Ando, M., et al., *Optical ozone detection by use of polyaniline film.* Solid state ionics, 2002. **152**: p. 819-822.

93. Toshima, N., et al., *Novel synthesis of polyaniline using iron (III) catalyst and ozone.* Chemistry Letters, 2000. **29**(12): p. 1428-1429.

94. Yan, H., M. Kajita, and N. Toshima, *Polymerization of aniline using iron (III) catalyst and ozone, and kinetics of oxidation reactions in the catalytic system.* Macromolecular Materials and Engineering, 2002. **287**(8): p. 503-508.

95. Gordon, G., *The chemistry and reactions of ozone in our environment.* Progress in Nuclear Energy, 1995. **29**: p. 89-96.

96. Sotelo, J.L., et al., *Ozone decomposition in water: kinetic study.* Industrial & engineering chemistry research, 1987. **26**(1): p. 39-43.

97. Ershov, B. and P. Morozov, *The kinetics of ozone decomposition in water, the influence of pH and temperature.* Russian Journal of Physical Chemistry A, 2009. **83**(8): p. 1295-1299.

98. Battino, R., T.R. Rettich, and T. Tominaga, *The solubility of oxygen and ozone in liquids.* Journal of physical and chemical reference data, 1983. **12**(2): p. 163-178.

99. Vetter, C.A., et al., *Novel Synthesis of Stable Polypyrrole Nanospheres Using Ozone.* Langmuir, 2011. **27**(22): p. 13719-13728.

100. Das, T.K. and S. Prusty, *Review on conducting polymers and their applications.* Polymer-Plastics Technology and Engineering, 2012. **51**(14): p. 1487-1500.

101. Stankiewicz, A., I. Szczygieł, and B. Szczygieł, *Self-healing coatings in anti-corrosion applications.* Journal of materials science, 2013. **48**(23): p. 8041-8051.

102. Kendig, M., M. Hon, and L. Warren, *'Smart'corrosion inhibiting coatings.* Progress in organic coatings, 2003. **47**(3): p. 183-189.

103. Yan, M., C.A. Vetter, and V.J. Gelling, *Corrosion inhibition performance of polypyrrole Al flake composite coatings for Al alloys.* Corrosion science, 2013. **70**: p. 37-45.

104. Kowalski, D., M. Ueda, and T. Ohtsuka, *Self-healing ion-permselective conducting polymer coating.* J. Mater. Chem., 2010. **20**(36): p. 7630-7633.

105. Hosseini, M., M. Sabouri, and T. Shahrabi, *Corrosion protection of mild steel by polypyrrole phosphate composite coating.* Progress in organic coatings, 2007. **60**(3): p. 178-185.

106. Sathiyanarayanan, S., S.S. Azim, and G. Venkatachari, *Corrosion protection of magnesium alloy ZM21 by polyaniline-blended coatings.* Journal of coatings technology and research, 2008. **5**(4): p. 471-477.

107. Pereira da Silva, J.E., S.I. Córdoba de Torresi, and R.M. Torresi, *Polyaniline acrylic coatings for corrosion inhibition: the role played by counter-ions.* Corrosion science, 2005. **47**(3): p. 811-822.

108. Kamaraj, K., et al., *Synthesis of tungstate doped polyaniline and its usefulness in corrosion protective coatings.* Electrochimica acta, 2011. **56**(25): p. 9262-9268.

109. Karpakam, V., et al., *Electrosynthesis of polyaniline–molybdate coating on steel and its corrosion protection performance.* Electrochimica acta, 2011. **56**(5): p. 2165-2173.

110. Pour-Ali, S., C. Dehghanian, and A. Kosari, *In situ synthesis of polyaniline-camphorsulfonate particles in epoxy matrix for corrosion protection of mild* Corrosion Science, Accepted April 2014.

111. Tallman, D., Y. Pae, and G. Bierwagen, *Conducting polymers and corrosion: polyaniline on steel.* Corrosion, 1999. **55**(8): p. 779-786.

112. DeBerry, D.W., *Modification of the electrochemical and corrosion behavior of stainless steels with an electroactive coating.* Journal of The Electrochemical Society, 1985. **132**(5): p. 1022-1026.

113. Mengoli, G., et al., *Anodic synthesis of polyaniline coatings onto Fe sheets.* Journal of Applied Polymer Science, 1981. **26**(12): p. 4247-4257.

114. Yan, M., et al., *Corrosion control coatings for aluminum alloys based on neutral and n-doped conjugated polymers.* Journal of The Electrochemical Society, 2009. **156**(10): p. C360-C366.

115. Jadhav, N., C.A. Vetter, and V.J. Gelling, *The effect of polymer morphology on the performance of a corrosion inhibiting polypyrrole/aluminum flake composite pigment.* Electrochimica acta, 2013. **102**: p. 28-43.

CHAPTER 2. NOVEL SYNTHESIS OF STABLE POLYPYRROLE NANOSPHERES UTILIZING OZONE[1]

(Published as "Novel Synthesis of Stable Polypyrrole Nanospheres Utilizing Ozone" Langmuir, 2011, **27** (22): p. 13719-13728)

2.1. Abstract

In this study, a novel and exceedingly simple method for the aqueous synthesis of stable, unagglomerated polypyrrole nanospheres was investigated. The method is template and surfactant free and uses only pyrrole monomer, water, and ozone. When the monomer concentration, exp[1]osure time to ozone, and temperature were varied, it was determined that the temperature was the critical factor controlling the particle size through particle size measurements via dynamic light scattering and transmission electron microscopy (TEM). From the particle size measurements, a particle size distribution with a number weighted mean diameter of 73 nm and a standard deviation of 18 nm was achieved. The particles were also investigated using zeta potential measurements, UV-Vis spectroscopy, Fourier transform infrared spectroscopy (FTIR), and thermal gravimetric analysis in an effort to determine the identity of the nanoparticles as well as the mechanism by which the nanoparticles are formed and stabilized.

Keywords: Polypyrrole, nanoparticles, agglomeration

[1] The material in this chapter was co-authored by Abhijit Suryawanshi and Victoria Gelling. Abhijit Suryawanshi had primary responsibility of executing reactions (R1-R43), analyzing samples, and summarizing results and conclusions. Abhijit Suryawanshi performed and/or coordinated FTIR, UV-vis, zeta potential, TEM and SEM techniques on the samples. Additionally, Abhijit Suryawanshi also contributed to the drafting of the two revised versions of this manuscript. Victoria Gelling provided guidance for design of experiments and to draw conclusions from the data. Victoria Gelling also served as a proof reader for the manuscript drafts.

2.2. Introduction

Because of their unique properties, there is currently great interest in polypyrrole nanoparticles and other carbon based nanoparticles for use in various applications such as chemical and biological sensors, optically transparent conducting materials, electrochromic devices, actuators, supercapacitors, photovoltaic cell, transistor, data storage, and surface protection.[1-5] Because of its environmental stability and high conductivity; polypyrrole has became interest of research in recent times.[6-14] When nanosized particles are synthesized, one challenge that is presented to researchers is to prevent agglomeration. This process is more pronounced with nanosized particles because of their increased surface area and therefore van der Waals interactions. Many attempts have been made to synthesize polypyrrole nanoparticles using a large number of different synthesis conditions.[15-20] From these studies, two main strategies have emerged to synthesize non-aggregated polypyrrole: hard and soft template processes.[18, 21-24]

Hard template processes use pores in "hard" materials, such as anodized aluminum oxide, to direct the growth of polypyrrole particles and wires and to prevent agglomeration.[25-27] After the synthesis, the templates must then be etched away usually with strong acids.[28] Another variation of the hard template approach is the coating of colloidal particles, such as silver or silica, with polypyrrole.[29-33] One issue with hard template processes is the high complexity and expense due to the very carefully controlled growth of oxide layers or colloidal particles to give precise and uniform pore or particle sizes. Soft template methods typically use surfactant micelles as a template for the formation of nanoparticles.[34-38] Microemulsion polymerization and reversed-microemulsion polymerization are examples of soft template based methods, wherein the structure and concentration of surfactant and monomers are critical factors

for controlling morphological parameters of products.[23] Soft template processes typically produce products in which the soft template can never be fully removed which will affect the properties of the product. Large amounts of surfactant are typically required, which adds to the expense of the process.

To circumvent the aforementioned issues, there have been some processes developed that either do not use traditional template systems or use a template that doubles as a dopant for the polypyrrole. One such process developed by Kim et al. uses a surfactant free emulsion system using water droplets in octanol as a soft template and $FeCl_3$ as the oxidant.[39] Li et al. employ a process that uses a dilute solution of rhodamine B as a molecular template that also acts as a dopant for the polypyrrole.[40] Henry et al. presents production of polypyrrole nanofibers using bipyrrole in oxidative polymerization of pyrrole.[41] Debiemme-Chouvy has obtained nanostructures with diameters in the range of 40–120 nm by electrodepositing polypyrrole in the presence of jointly non-acidic and weak-acidic anions.[42] In this study, a relatively simple method for the synthesis of unagglomerated polypyrrole nanospheres of a controlled size is outlined that utilizes water, pyrrole, and ozone in a one-pot, one-step, synthesis.

2.3. Experimental

Pyrrole was obtained from Sigma Aldrich and was freshly distilled before use. Millipore 18.2 MΩ water was the solvent used for the reaction. Ozone was obtained by flowing pure dried oxygen supplied by Air Gas through a model ATLAS 30 C ozone generator supplied by Absolute Ozone. Particle size measurements were carried out using a NICOMP 380 submicron particle sizer supplied by Particle Sizing Systems. A Gaussian analysis was applied to all data. For the transmission electron microscopy (TEM) images, 300 mesh Formvar/carbon coated grids were dipped into the solution containing the particles and immediately wicked off using filter

paper. After allowing the grid to dry, images were obtained using a JEOL JEM-100CX II Transmission Electron Microscope at 80 keV. UV - Vis spectra of the polypyrrole nanoparticles in water were recorded on Varian-5000 UV-Vis-NIR spectrophotometer. Thermal degradation analysis of the samples was performed using a thermogravimetric analysis instrument TGA Q 500 supplied by TA Instruments. The samples were heated from room temperature to 800˚ C at a heating rate of 20˚ C/min. The experiment was run in a stepwise isothermal fashion, meaning that, once weight loss was detected, the temperature was held steady until the weight loss stopped. The temperature was then ramped again until another weight loss was detected. In this way, it can be determined how much of the sample was lost at each temperature. The obtained results were analyzed using the software, Universal Analysis 2000. A Nicolet FT-IR spectrometer was used for the FT-IR characterization. A Veeco Dimension 3100 atomic force microscope (AFM) with contact mode and current sensing probe was used for conductive AFM (C-AFM) measurements to characterize pressed pellets of the nanoparticles for surface morphology and conductivity. C-AFM can be applied to materials with conductivity of 1 pA to 1 μA and an applied potential up to 12 V. Zeta potential was measured in water using a Zetasizer (Malvern Instruments, Worcestershire, U.K.).

All measurements were recorded at 25^{o}C. Samples were prepared for scanning electron microscopy (SEM) by sprinkling onto carbon tape attached to aluminum mounts. The sample was then coated with gold using a Balzers SCD 030 sputter coater. Images were obtained using a JEOL JSM-7600F Scanning Electron Microscope. Magnification, accelerating voltage values, and micron bars are listed in each figure.

The synthesis conditions for the first set of reactions as well as the particle size results for those reactions are shown in Table 2.1. The synthesis procedure for the first set of reactions was

as follows: 100 mL of Millipore water was placed in a 125 mL Erlenmeyer flask followed by 1.14 g of pyrrole. In the case of reaction D, 0.675 g of pyrrole was added. The mixture was then stirred until the pyrrole dissolved. Oxygen was provided to the ozone generator at a pressure of 20 psi and a flow rate of 0.2 liters/minute. According to the literature provided by Absolute Ozone, this flow rate should be producing an oxygen/ozone mixture that is 18% ozone by weight. For reactions A and D, the oxygen/ozone mixture was bubbled through the pyrrole solution for 60 seconds. For reaction C, the oxygen/ozone mixture was bubbled through the pyrrole solution for 30 seconds. After the ozone exposure was complete, any remaining ozone in the flask was removed by gently blowing a stream of air from a compressed air line. The flasks were then sealed with a rubber stopper and allowed to sit for 4 days.

Table 2.1. Summary of initial reactions

Reaction	Pyrrole (M)	Ozone Exposure (s)	Temperature (°C)	Mean Weighting	Mean Diameter (nm)	Standard Deviation (nm)
A	0.17	60	23	Number	324	16
				Volume	325	16
B	0.17	60	4	Number	73	18
				Volume	88	22
C	0.17	30	23	Number	266	78
				Volume	373	109
D	0.01	60	23	Number	288	32
				Volume	301	34

The procedure for reaction B was similar except that prior to the pyrrole being added to the Millipore water, the flask was placed in an ice bath until the water reached a temperature of 4° C. Pyrrole was then added and stirred. The oxygen/ozone mixture was then bubbled through the pyrrole solution while it remained in the ice bath. After ozone exposure, remaining ozone was removed with a stream of compressed air and the flask was sealed with a stopper and placed in a refrigerator at a temperature of 4° C for 4 days. The same reaction procedure was followed

for all the reactions in this work; the variants include temperature, molar concentration and ozone exposure time.

Table 2.2. Reactions for studying zeta potential measurement and particle size behavior as a function of monomer concentration and ozone exposure

Reaction	Conditions
	0.17 Molar
R – 1	30 Seconds Ozone Exposure
R – 2	60 Seconds Ozone Exposure
R – 3	120 Seconds Ozone Exposure
	0.34 Molar
R – 4	30 Seconds Ozone Exposure
R – 5	60 Seconds Ozone Exposure
R – 6	120 Seconds Ozone Exposure
	0.51 Molar
R – 7	30 Seconds Ozone Exposure
R – 8	60 Seconds Ozone Exposure
R – 9	120 Seconds Ozone Exposure
	0.68 Molar
R – 10	30 Seconds Ozone Exposure
R - 11	60 Seconds Ozone Exposure
R – 12	120 Seconds Ozone Exposure
	0.85 Molar
R – 13	30 Seconds Ozone Exposure
R – 14	60 Seconds Ozone Exposure
R - 15	120 Seconds Ozone Exposure

After the results from the first set of reactions were obtained, a larger set of reactions, shown in Table 2.2, was carried out in an effort to determine factors affecting the stability and formation of the nanoparticles. The reactions in Table 2.2 were performed at room temperature using the same pressure and flow rate as the previous reactions from Table 2.1. Additional reactions were performed to investigate the effect of pH in conjunction with ozone exposure on the synthesis reaction. The conditions used for these reactions are provided in Table 2.3.

Table 2.3. Reactions studying the effect of pH and ozone exposure on the synthesis of PPY nanoparticles

Reaction	Molar Concentration	pH	Ozone Exposure Time (s)	Temperature (˚C)
R-16	0.17	2	60	23
R-17	0.17	4	60	23
R-18	0.17	6	60	23
R-19	0.17	8	60	23
R-20	0.17	10	60	23
R-21	0.17	12	60	23
R-22	0.17	2	60	0
R-23	0.17	1.8	60	0
R-24	0.17	1.65	60	0
R-25	0.17	1.5	60	0
R-26	0.17	1.3	60	0
R-27	0.17	1.8	60	0
R-28	0.17	1.6	60	0
R-29	0.17	1.4	60	0
R-30	0.17	1.8	120	0
R-31	0.17	1.6	120	0
R-32	0.17	1.4	120	0
R-33	0.17	1.8	240	0
R-34	0.17	1.6	240	0
R-35	0.17	1.4	240	0
R-36	0.17	1	480	0
R-37	0.17	6.2	60	0
R-38	0.17	3.7	60	0
R-39	0.17	3.0	60	0
R-40	0.17	2.0	60	0
R-41	0.17	1.7	60	0
R-42	0.17	1.5	60	0
R-43	0.17	1.1	60	0

2.4. Results and discussion

The first reactions performed in this study (Table 2.1) were a survey to determine which factors may influence the particle size of the products of the reaction. The results from the Gaussian analysis of the particle size distributions from the various reactions are provided in Table 2.1. It is evident from these results that the duration of ozone exposure has a moderate effect on the mean particle size. When the ozone exposure time was reduced from 60 seconds to 30 seconds, the mean particle size was reduced by 58 nm. However, with this moderate decrease in the mean diameter of the particles there is a large increase in the standard deviation and, therefore, a decrease in the uniformity of the measured particle diameter. It is also evident that temperature has an influence on the resulting particle size. The number weighted mean particle diameter of reaction B, performed at 4℃ was 73 nm, while number weighted mean diameter of reaction A performed at 23℃ was 324 nm. This suggests that with decrease in temperature of reaction the particle size of nanospheres can be reduced. The effect of the temperature is by far the most drastic of the four variables. It may be possible that a mechanism similar to that of dispersion polymerization is taking place. It has been shown that, in dispersion polymerization, an increase in the rate of the reaction because of higher temperatures results in larger particle sizes.[43, 44] The curves of the data from which these numbers were calculated are provided in Figures 2.1. It is evident from these plots that particle distributions achieved from these reactions all approximate Gaussian behavior. The fact that these peaks are all Gaussian in nature indicates that there are likely not any large mechanistic differences induced by the variables that were changed in the reactions A-D. A bimodal distribution, for example, would indicate that some effect was causing a drastic difference in the products.

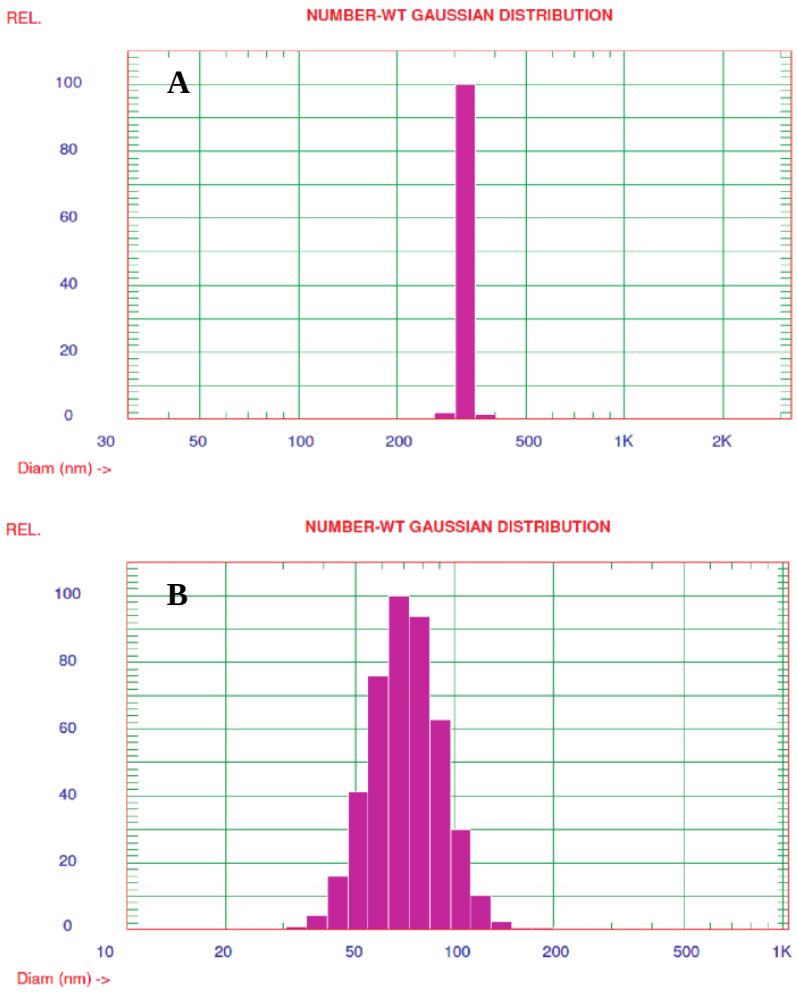

Figure 2.1. Plots of the particle size distribution for reactions A and B.

The analysis of reactions A and B via a transmission electron microscope is provided in Figure 2.3. It is clear in these images that both reactions yielded particles that were spherical in nature with very little agglomeration. The particle sizes presented in Figures 2.1 and 2.2 were verified with the TEM results presented in Figure 2.3. It is also interesting to note that the particles observed in Figure 2.3 display significant electron density, as indicated by the opacity of the particles, which may be an indication that there is a significant conjugation of the polypyrrole within the particles. Many nanosized polymer particles such as poly(methyl methacrylate) appear to be somewhat translucent under the TEM due to low electron density.[45]

In contrast to this, conducting polymers that have a high degree of unsaturation leading to much higher electron densities. The results obtained in this study are in good agreement with other TEM results for conducting polymer nanoparticles.[46, 47] When the hydrodynamic diameter measured by dynamic light scattering is compared to the diameters observed via TEM imaging, it is evident that the two techniques obtained similar results.

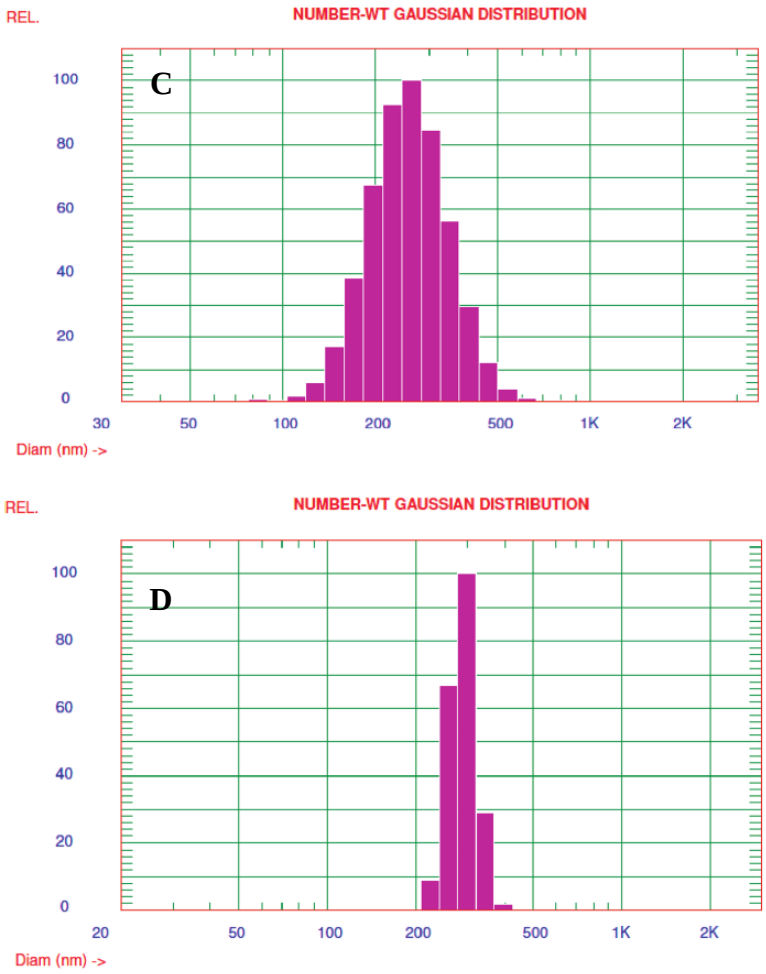

Figure 2.2. Plots of the particle size distribution for reactions C and D.

The diameter of the particles in panels b and c of Figure 2.3 were measured using Brava! software. The results were used to calculate an average and standard deviation for the data collected from the TEM images. As presented in Table 2.4, the average diameters of the particles

in the TEM images are remarkably similar to the results obtained using light scattering. The standard deviations, however, are very different. This is likely due to the fact that the sample sizes in the TEM images are much smaller than the sample sizes for the light scattering measurements; therefore, the standard deviations of the TEM data would be affected more by a few large agglomerations.

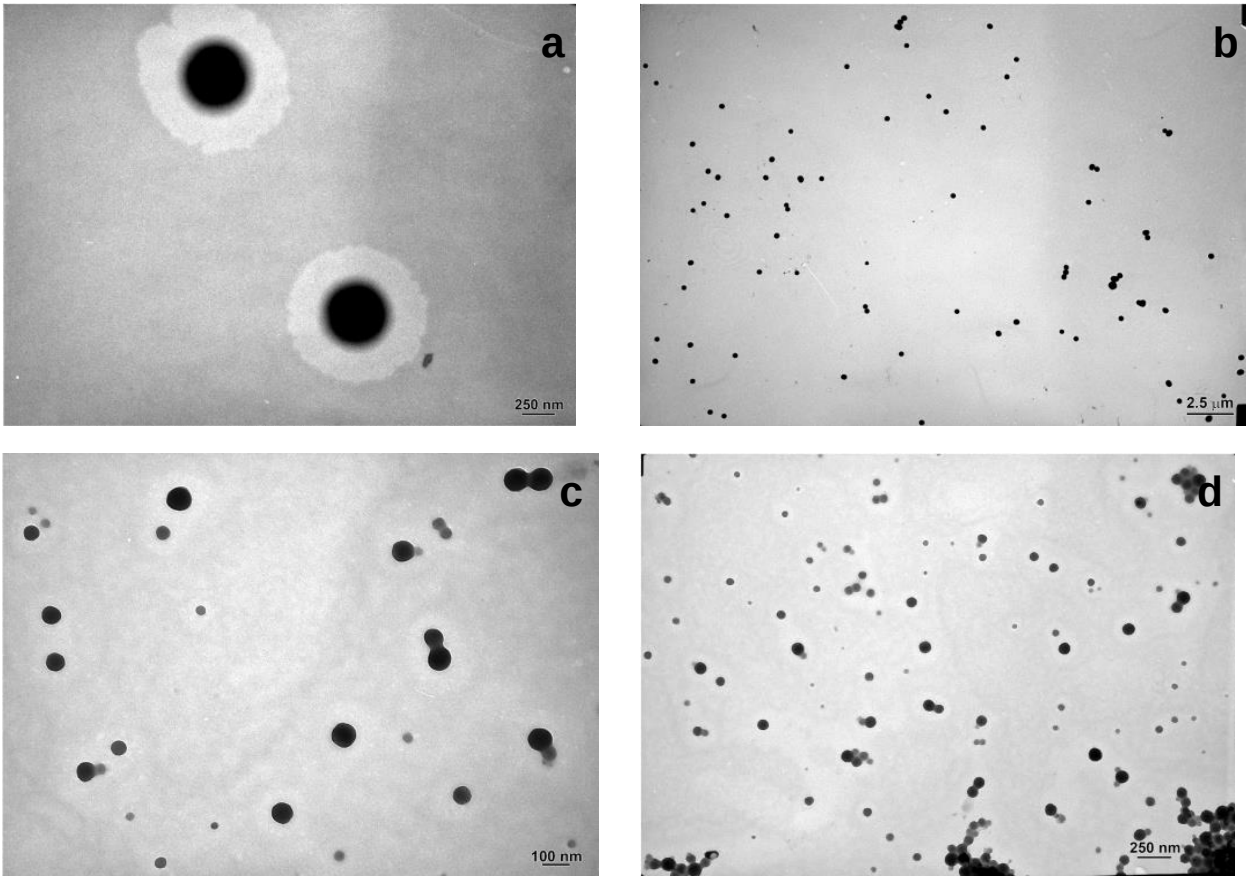

Figure 2.3. The TEM images of the particles produced from reaction A (a and b) and reaction B (c and d).

The results indicate that the hydrodynamic diameter of the particles does not differ greatly from the number-weighted diameter that was measured with TEM images. These results also indicate that the TEM images are likely to be a good representation of the amount of

agglomeration that is present during the light scattering measurements when the particles are still dispersed in water.

Table 2.4. Number-weighted mean particle diameter and the standard deviations for reactions A and B measured by TEM images

Reaction	Number of particles measured	Average (nm)	Standard deviation (nm)
A	66	317	142
B	95	82	104

After the aforementioned results were obtained for reactions A-D, further study (Table 2.2) was carried out to investigate any correlation between the monomer concentration, ozone exposure length, and particle size at room temperature. The TGA results for reactions R1-R3 are provided in Figure 2.4. It can be observed that with longer ozone exposure times, an increase in the thermal stability of the product resulted. This experiment was performed in an isothermal stepwise manner; therefore, it is possible to determine the percentage of the sample that was degraded at each temperature. The weight loss observed at lower temperatures starting at 150°C is associated with lower molecular-weight polypyrrole, such as dimers, trimers, and tetramers, while the weight loss seen at higher temperatures is associated with higher molecular-weight polypyrrole. It can be deteremined that, for reactions R-1 and R-2, the samples are approximately 60-70% high-molecular-weight polypyrrole, while the product from R-3 is 80-85% high-molecular-weight polypyrrole. This behavior could be indicative of a higher molecular weight product indicating that the ozone is initiating cationic radical polymerization of the polypyrrole similar to other initiators that act as oxidizing agents. This increase in molecular weight with more exposure to ozone indicates that the ozone is behaving in a similar fashion to other initiators for pyrrole polymerization. In the cationic radical polymerization mechanism, the higher the concentration of oxidant, the higher the molecular weight of the resultant polypyrrole.

However, it should be noted that longer ozone exposure may lead to overoxidation of polypyrrole.

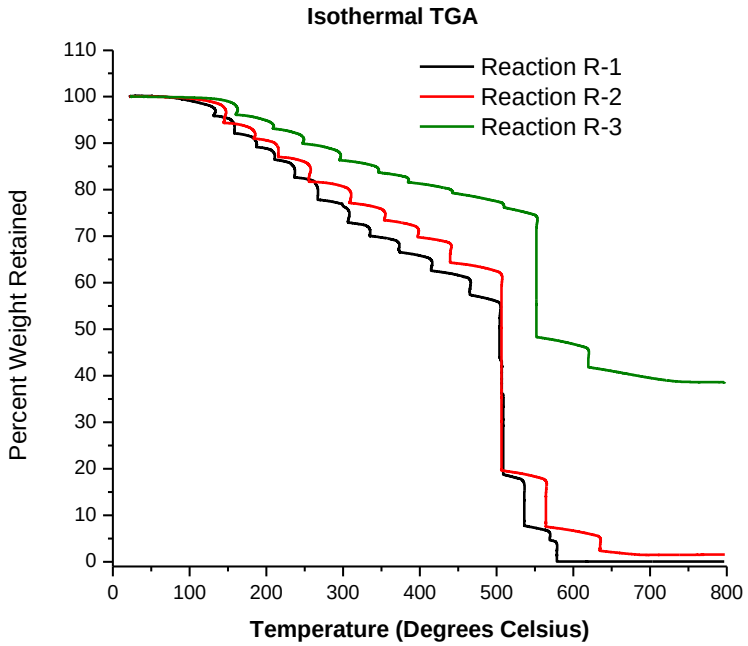

Figure 2.4. The plot of the isothermal TGA data collected from reactions R-1 through R-3.

TEM results for selected reactions from Table 2.2 are shown in Figure 2.5. It is evident from these results that there is a layer that has formed on the outside of the particles despite the absence of a surfactant in the synthesis reaction. It is thought that this layer may be responsible for the stabilization of the particle dispersion. It may be possible that this outer layer is composed of more polar overoxidized polypyrrole which could act as a steric stabilizer. The overoxidation of pyrrole may lead to oligomeric polypyrrole which may consist of carbonyl and carboxylic linkages. It is evident from Figure 2.5 that the outer layer varies in thickness due to varying synthesis conditions which could possibly be an explanation for observed agglomeration of the particles. For example, the layer observed on the particles produced from reaction R-10 appears to be thinner than the layers that can be observed in the other images, interestingly, this

same set displayed higher levels of agglomeration as well. Therefore, the particles would be composed of a polypyrrole core with a layer of overoxidized polypyrrole acting as a stabilizer on the outside of the particles. More evidence and a discussion on this hypothesis are provided below.

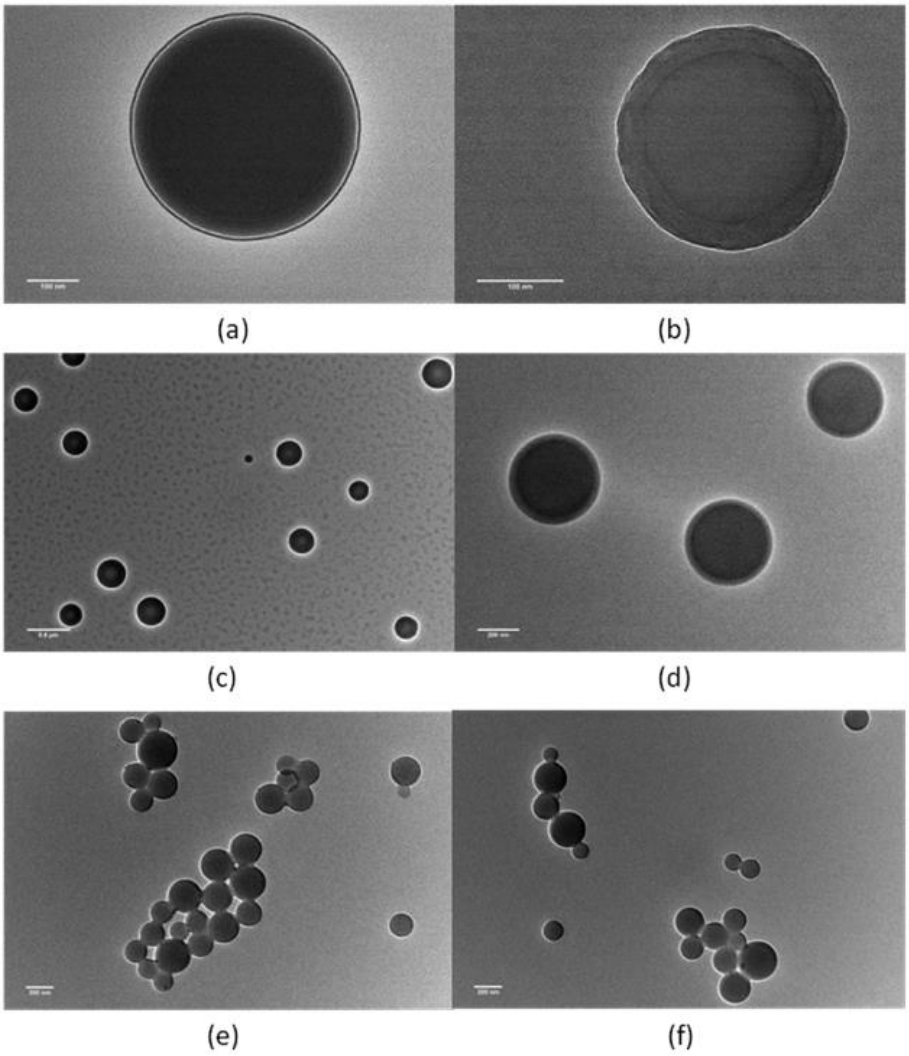

Figure 2.5. TEM images of the particles produced from R-13 (a), R-4 (b), R-9 (c), R-14 (d), and R-10 (e and f).

The influence of monomer concentration and ozone exposure is presented in Figure 2.6. It is evident that increased ozone exposure times and higher monomer concentration results in larger particle sizes at room temperature. It is also apparent that at higher monomer

concentrations the length of time that the reaction is exposed to ozone has a larger effect on particle size. These results may indicate that as the concentration of nanoparticles in the dispersions increases, the stability mechanism of the dispersion begins to become less effective, which leads to large agglomerations of particles. This may simply be due to a larger number of collisions between the particles leading to a higher agglomeration rate. Another possibility for the large diameters observed with higher concentrations of pyrrole, is the polymerization of large droplets of un-solubilized pyrrole.

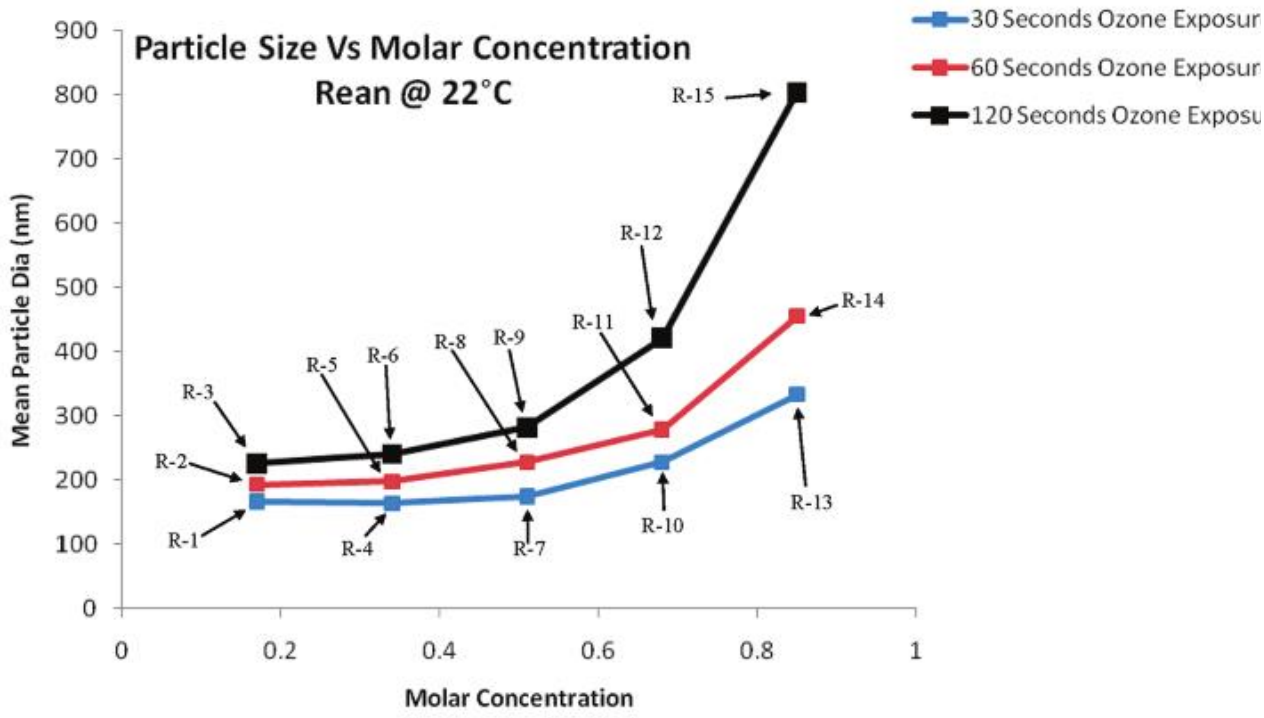

Figure 2.6. Molar concentration vs. mean particle diameter for reactions R-1 through R-15.

To determine the mechanism by which the nanoparticles are stabilized and whether the layer on the outside of the particles may be involved, zeta potential measurements were performed on the dispersions at a pH of 4.5 and at pH ranging from 4.2 to 1.2. The zeta potential results of all the reactions from Table 2.2 (R-1 to R-15 and R-37 to R-43) are presented in Table

2.5 and Table 2.6. For all of the reactions, the zeta potential was very near 0 mV this indicates that electrostatic repulsion is not likely the method of stabilization. Furthermore, no effect was observed on zeta potential with change in pH. Admittedly, ozone may cause the over-oxidation of polypyrrole. According to Cataldo et al., ozone slowly forms amide ketones on the α carbons and hydroxide groups on the ß carbons of a polypyrrole chain with some ring scission.[48]

Table 2.5. Zeta potential and yield data for reactions R-1 through R-15

Reaction		**Zeta potential (mV)**	**Yield (gm)**
	0.17 Molar		
R – 1	30 Seconds Ozone Exposure	0.069	0.01
R – 2	60 Seconds Ozone Exposure	-0.075	0.03
R – 3	120 Seconds Ozone Exposure	0.504	0.02
	0.34 Molar		
R – 4	30 Seconds Ozone Exposure	-0.077	0.02
R – 5	60 Seconds Ozone Exposure	-0.128	0.03
R – 6	120 Seconds Ozone Exposure	0.273	0.02
	0.51 Molar		
R – 7	30 Seconds Ozone Exposure	-0.077	0.03
R – 8	60 Seconds Ozone Exposure	-0.004	0.04
R – 9	120 Seconds Ozone Exposure	-0.239	0.04
	0.68 Molar		
R – 10	30 Seconds Ozone Exposure	0.060	0.03
R - 11	60 Seconds Ozone Exposure	0.045	0.03
R – 12	120 Seconds Ozone Exposure	-0.299	0.04
	0.85 Molar		
R – 13	30 Seconds Ozone Exposure	0.105	0.03
R – 14	60 Seconds Ozone Exposure	0.127	0.02
R - 15	120 Seconds Ozone Exposure	-0.142	0.03

If the layer surrounding the nanoparticles was comprised of overoxidized polypyrrole, it could possibly act as a sterically stabilizing layer. The ketone and hydroxyl functional groups that would form on the polypyrrole chains as a result of overoxidation would cause the outer

layers of the particles to be more polar and, therefore, more hydrophilic. This hydrophilicity would allow the chains to relax in the surrounding water. Aggregation would then require these surrounding chains to take on less relaxed conformations which would result in a decrease in entropy. Aggregation would therefore be entropically unfavorable.

Table 2.6. Zeta potential for reactions from R-37 to R-43

Reaction	pH Before Reaction	pH After Reaction	Zeta Potential (mV)
R - 37	6.2	4.2	0.036
R – 38	3.7	4	-0.062
R – 39	3	3.5	-0.090
R – 40	2	2.2	0.126
R – 41	1.7	1.8	-0.040
R – 42	1.5	1.5	-0.013
R – 43	1.1	1.2	-0.094

This hypothesis is further supported by the presence of a carbonyl peak and a hydroxyl peak in the FTIR results in Figure 2.7. The bands around 1489 (2,5-substituted pyrrole) and 1380 cm^{-1} may be assigned to polypyrrole ring vibrations.[49-51] The bands at 1220, and 1090 cm^{-1} may be corresponding to =C-H in plane vibrations while the band at 774 cm^{-1} and 881 cm^{-1} may correspond to out of plane vibrations indicating polymerization of pyrrole.[51, 52] The absorption peak at 1635 cm^{-1} likely correspond to a –C=O linkage. [52] The C=O structure at the β-C of pyrrole ring is typically due to the overoxidation of polypyrrole.[53] When the pH was reduced in R-24, the hydroxyl peak at approximately 3310 nm disappeared and the carbonyl peak at 1635 nm was reduced in intensity, indicating that there was less overoxidation of polypyrrole.

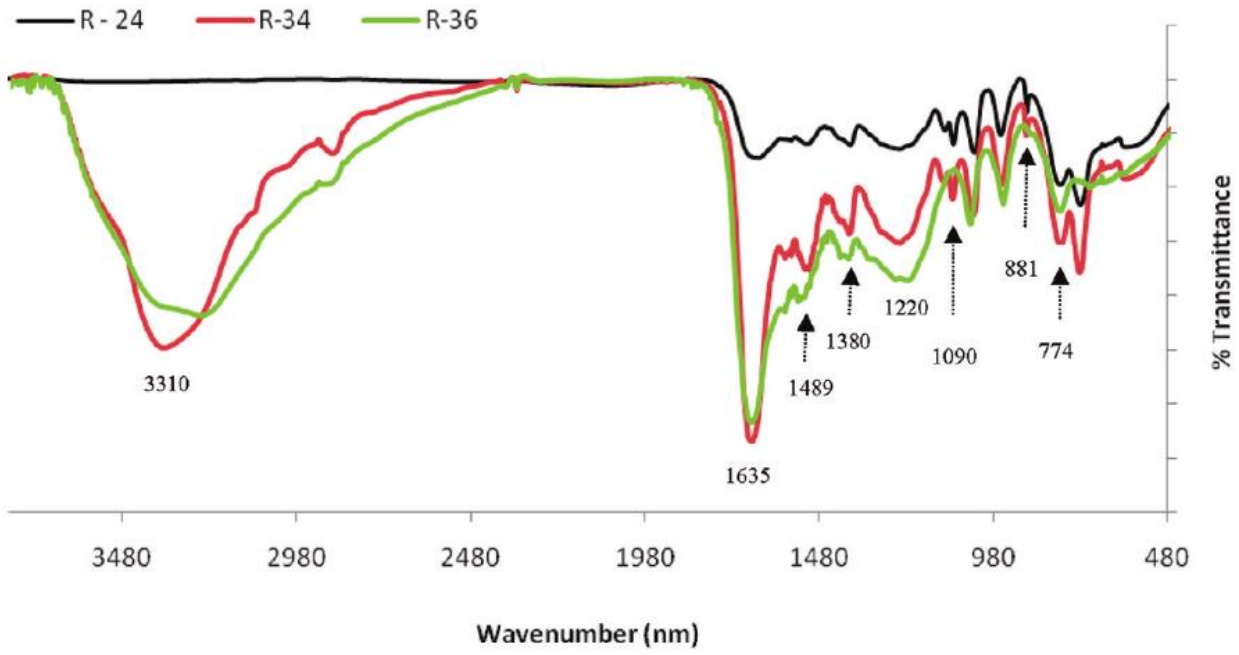

Figure 2.7. FTIR Spectra showing the effect of increased reaction time and reduced pH for reactions R-24, R-34, and R-36.

To further explore the layer surrounding the polypyrrole nanoparticles, high resolution SEM images of the nanoparticles were obtained to better determine the surface morphology of the outside layer surrounding them. These images can be seen in Figure 2.8. From these images, it is evident that the nanoparticles are fairly uniform in size and shape and that the outside layer surrounding the nanoparticles is quite smooth. This is not necessarily supportive of a steric stabilization mechanism. One would expect to see a rough surface due to the relaxed surface of the particles. One explanation of this may be that, in a near vacuum, devoid of electrolyte, any polymeric chains responsible for stabilization are in a different conformation.

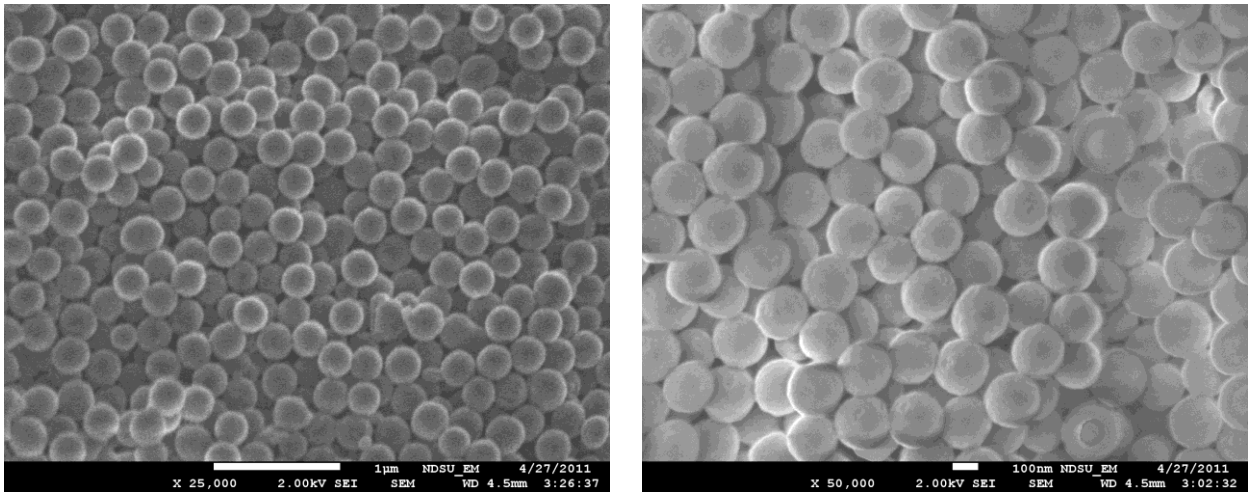

Figure 2.8. High resolution SEM images of the nanoparticles produced from reaction R-3 (Left) and reaction R-4 (Right).

The presence of overoxidized polypyrrole was also verified using the conductive AFM technique. In the 15 reactions in Table 2.2, the synthesized product does not exhibit conductivity that is measurable with this instrument. A typical set of images collected is shown in Figure 2.9. It is the far right image that would show measurable current as white areas in the image. The current detection threshold for this instrument is 1pA to 1µA with a maximum applied voltage of 12 V.

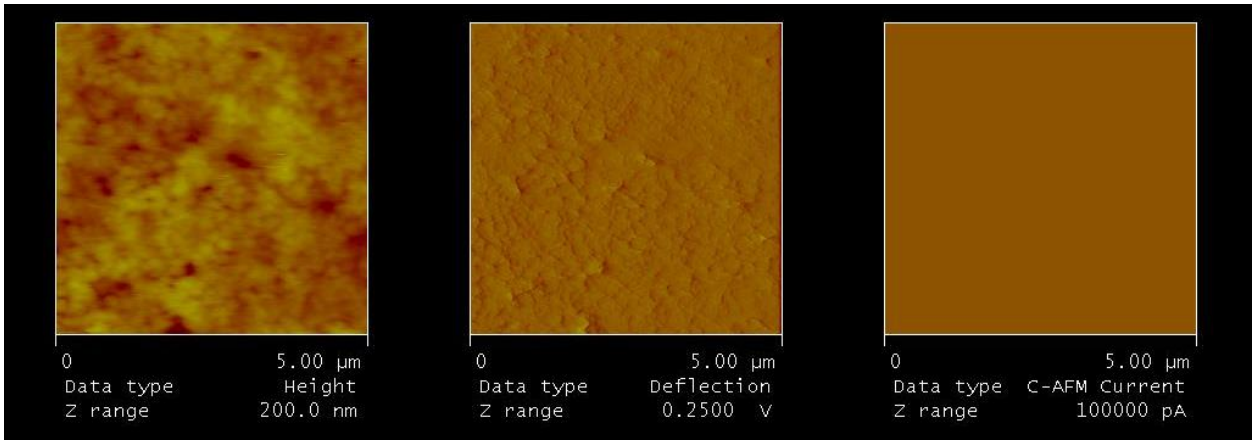

Figure 2.9. C-AFM images collected from a pressed pellet of the PPY nanoparticles.

If overoxidized oligomers are forming an insulating layer around the particles with more conductive polypyrrole at the center, it could disrupt conduction through a pressed pellet of the product and therefore prevent conductivity in the sample. This insulating behavior is due to the presence of the carbonyl functional groups which disrupt the conjugation of polypyrrole chains and therefore reduce the conductivity of polypyrrole.

Indeed, the overoxidation is most likely due to the use of water as the solvent. Novak has suggested in his work that carbonyl linkages form due to the reaction of pyrrole with water and hydroxy radicals, which are in abundance when ozone is dissolved in water.[54] This phenomenon is pH dependent; over-oxidation is thermodynamically more favorable at a basic pH, therefore, by adjusting the pH with hydrochloric acid, it was thought that a conductive product may be obtained.[54] An additional benefit of lower pH would be to decrease the rate of decomposition for ozone. Ozone dissociation in water is initiated by negatively charged OH^- ions, by decreasing the pH of the reaction solution, this reaction can be slowed, which may result in less overoxidation of the polypyrrole as well.[55] Therefore, it was necessary to investigate the effect that pH had on this synthesis reaction (Table 2.3). The effect of pH was studied using HCl and NaOH to adjust the pH of the synthesis solutions prior to ozone exposure. The dispersions produced from these reactions were observed visually for colloidal stability and with UV-Vis spectroscopy to detect the presence of bipolarons that would indicate conductivity. For this study, solutions of pyrrole in water were prepared at a pH of 2, 4, 6, 8, 10, and 12. It was observed visually that increasing the pH of the reaction above a pH of 4 caused agglomeration of the nanoparticles and that the least amount of agglomeration was observed at a pH 2. This effect was quite apparent because the destabilized particles fell out of dispersion quite rapidly and formed large particles on the bottom of the reaction vessel, while the stabilized particles stay in

dispersion for over 1 year. When the UV - vis spectra of the reactions R-17 and R-24 were analyzed (Figure 2.10), it could be concluded from the peaks at approximately 294 nm that the dispersions of nanoparticles contain large amounts of terpyrrole oligomers. [56] By reducing the pH of the reaction, it could be observed that the peak for terpyrrole oligomers became less intense and was shifted slightly towards higher wavelengths. This drop in intensity could indicate slightly less pyrrole monomer is being polymerized into terpyrrole.[56]

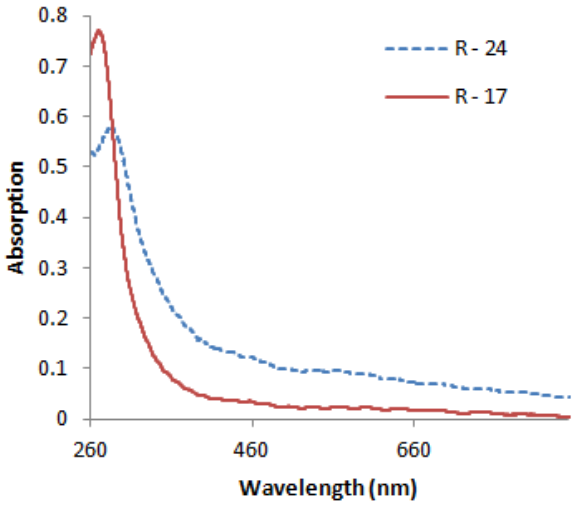

Figure 2.10. UV-Vis spectroscopy of reactions R-24 and R-17 (pH of 4 and 1.6).

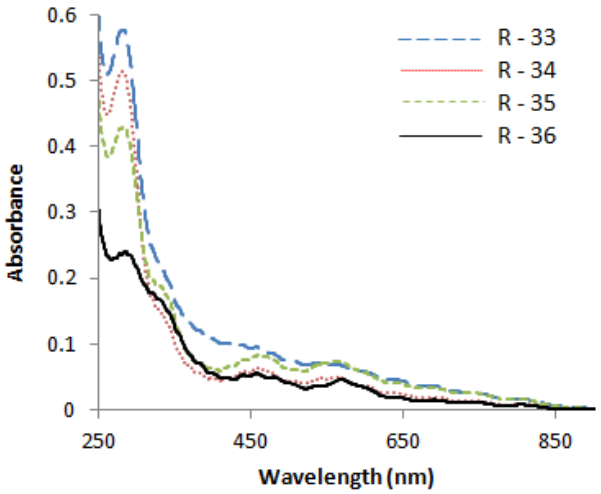

Figure 2.11. UV-Vis spectra results at increased reaction time, and reduced pH. (R-33 to R-36).

Reactions R-22 through R-26 were then carried out from a pH of 2 to a pH of 1.3 to determine if the stability or conductivity of the nanoparticles could be improved. The ozone exposure time was also increased for these reactions in an effort to increase the molecular weight of the polypyrrole. It was evident from visual assessment that the dispersions were not stable below a pH of 1.65. Therefore, while it may be beneficial to perform the synthesis reaction at a low pH, as this would provide significant chloride ions from the hydrochloric acid to act as dopant ions if the polypyrrole chains were oxidized to a conductive state, too low of a pH can cause agglomeration.

Figure 2.11 provides the results for the increased ozone exposure time and reduced pH on the UV-Vis spectra of the products. It can be observed that with reduction in pH, the terpyrrole peaks at approximately 300 nm were reduced, which suggests a decrease in the amount of terpyrrole in the final product.[56] The broad band at 475 nm, which has been assigned to the pi-pi* transition of polypyrrole, indicates that higher molecular weight polypyrrole is produced.[56-58] The peaks at 475 nm also show bipolaron absorption due to Cl^- ion doping.[59, 60] However, as earlier reported, the increase in reaction time is prone to producing agglomeration of nanoparticles and overoxidation of polypyrrole.

2.5. Conclusions

This study investigated the template-free synthesis of polypyrrole nanoparticles via chemical oxidative polymerization using ozone as the oxidizing agent. It was found that reaction temperature had the largest effect on particle size; with colder temperatures producing smaller particles. It was observed that there is a layer surrounding the particles that may be contributing to the stability of the nanoparticles. FTIR and UV-Vis results indicated that this layer is likely to be over-oxidized pyrrole monomers. Zeta potential measurements indicated that the mode by

which the particles were stabilized was steric stabilization. Future work will investigate the further decreasing of the reaction temperature by introducing co-solvents such as methanol. The removal of the overoxidized terpyrrole shell will be attempted through the use of solvents to investigate the nature of the core polypyrrole for stability and conductivity.

2.6. Acknowledgments

The authors would like to acknowledgment Army Research Laboratory for funding this project, grant #s W911NF-09-2-014, W911NF-10-2-0082, and W911NF-11-2-0027.

2.7. References

1. Aleshin, A.N., *Polymer nanofibers and nanotubes: Charge transport and device applications.* Advanced materials, 2006. **18**(1): p. 17-27.
2. Ambrosi, A., et al., *The application of conducting polymer nanoparticle electrodes to the sensing of ascorbic acid.* Analytica chimica acta, 2008. **609**(1): p. 37-43.
3. Fuhrmann-Lieker, T., et al., *Emissive materials, nanomaterials*. Advances in Polymer Science, ed. A.D. Abe, K.; Kobayashi, S.,. Vol. 199. 2006, Berlin, Germany: Springer.
4. Luo, X., et al., *Application of nanoparticles in electrochemical sensors and biosensors.* Electroanalysis, 2006. **18**(4): p. 319-326.
5. Ramanavičius, A., A. Ramanavičienė, and A. Malinauskas, *Electrochemical sensors based on conducting polymer—polypyrrole.* Electrochimica acta, 2006. **51**(27): p. 6025-6037.
6. MacDiarmid, A.G., *Polyaniline and polypyrrole: where are we headed?* Synthetic metals, 1997. **84**(1): p. 27-34.
7. Ruckenstein, E. and L. Hong, *Inverted emulsion pathway to polypyrrole and polypyrrole elastomer composites.* Synthetic metals, 1994. **66**(3): p. 249-256.

8. Selvaraj, M., et al., *Polypyrrole as a protective pigment in organic coatings.* Synthetic metals, 2008. **158**(21): p. 888-899.

9. Spinks, G.M., et al., *Electroactive conducting polymers for corrosion control.* Journal of Solid State Electrochemistry, 2002. **6**(2): p. 85-100.

10. Su, P.-G. and L.-N. Huang, *Humidity sensors based on TiO_2 nanoparticles/polypyrrole composite thin films.* Sensors and Actuators B: Chemical, 2007. **123**(1): p. 501-507.

11. Tallman, D.E., et al., *Electroactive conducting polymers for corrosion control.* Journal of Solid State Electrochemistry, 2002. **6**(2): p. 73-84.

12. Tamm, J., et al., *Electrochemical properties of polypyrrole/sulphate films.* Electrochimica acta, 1997. **42**(19): p. 2929-2934.

13. Wang, L.-X., X.-G. Li, and Y.-L. Yang, *Preparation, properties and applications of polypyrroles.* Reactive and Functional Polymers, 2001. **47**(2): p. 125-139.

14. Rohwerder, M. and A. Michalik, *Conducting polymers for corrosion protection: What makes the difference between failure and success?* Electrochimica acta, 2007. **53**(3): p. 1300-1313.

15. Hong, J.Y., H. Yoon, and J. Jang, *Kinetic Study of the Formation of Polypyrrole Nanoparticles in Water-Soluble Polymer/Metal Cation Systems: A Light-Scattering Analysis.* Small, 2010. **6**(5): p. 679-686.

16. Li, X.-G., et al., *Efficient synthesis of intrinsically conducting polypyrrole nanoparticles containing hydroxy sulfoaniline as key self-stabilized units.* The Journal of Physical Chemistry C, 2009. **113**(52): p. 21586-21595.

17. Liao, Y., X.-G. Li, and R.B. Kaner, *Facile synthesis of water-dispersible conducting polymer nanospheres.* ACS nano, 2010. **4**(9): p. 5193-5202.

18. Marinakos, S.M., et al., *Template synthesis of one-dimensional Au, Au-poly (pyrrole), and poly (pyrrole) nanoparticle arrays.* Chemistry of materials, 1998. **10**(5): p. 1214-1219.

19. Woo, H.-Y., et al., *Synthesis and dispersion of polypyrrole nanoparticles in polyvinylpyrrolidone emulsion.* Synthetic metals, 2010. **160**(7): p. 588-591.

20. Yang, C. and P. Liu, *Water-dispersed polypyrrole nanoparticles via chemical oxidative polymerization in the presence of a functional polyanion.* Reactive and Functional Polymers, 2010. **70**(10): p. 726-731.

21. Hulteen, J., *A general template-based method for the preparation of nanomaterials.* Journal of Materials Chemistry, 1997. **7**(7): p. 1075-1087.

22. Johnson, B.J., et al., *Template syntheses of polypyrrole nanowires and CdS nanoparticles in porous polymer monoliths.* Chemistry of materials, 2004. **16**(15): p. 2909-2917.

23. Pan, L., et al., *Conducting polymer nanostructures: template synthesis and applications in energy storage.* International journal of molecular sciences, 2010. **11**(7): p. 2636-2657.

24. Huczko, A., *Template-based synthesis of nanomaterials.* Applied Physics A, 2000. **70**(4): p. 365-376.

25. Jackowska, K., A.T. Bieguński, and M. Tagowska, *Hard template synthesis of conducting polymers: a route to achieve nanostructures.* Journal of Solid State Electrochemistry, 2008. **12**(4): p. 437-443.

26. Xu, Q., et al., *Controlled fabrication of gold and polypyrrole nanowires with straight and branched morphologies via porous alumina template-assisted approach.* Materials Letters, 2009. **63**(16): p. 1431-1434.

27. Yoo, S.-H., L. Liu, and S. Park, *Nanoparticle films as a conducting layer for anodic aluminum oxide template-assisted nanorod synthesis.* Journal of colloid and interface science, 2009. **339**(1): p. 183-186.

28. Wei, M. and Y. Lu, *Templating fabrication of polypyrrole nanorods/nanofibers.* Synthetic metals, 2009. **159**(11): p. 1061-1066.

29. Azioune, A., et al., *Synthesis and characterization of active ester-functionalized polypyrrole-silica nanoparticles: application to the covalent attachment of proteins.* Langmuir, 2004. **20**(8): p. 3350-3356.

30. Stejskal, J., et al., *Polyaniline dispersions. 6. Stabilization by colloidal silica particles.* Macromolecules, 1996. **29**(21): p. 6814-6819.

31. Yang, X., T. Dai, and Y. Lu, *Synthesis of novel sunflower-like silica/polypyrrole nanocomposites via self-assembly polymerization.* Polymer, 2006. **47**(1): p. 441-447.

32. Yang, X. and Y. Lu, *Preparation of polypyrrole-coated silver nanoparticles by one-step UV-induced polymerization.* Materials Letters, 2005. **59**(19): p. 2484-2487.

33. Percy, M., et al., *Synthesis of vinyl polymer-silica colloidal nanocomposites via aqueous dispersion polymerization.* Langmuir, 2003. **19**(6): p. 2072-2079.

34. Cheng, Q., et al., *Surfactant-assisted polypyrrole/titanate composite nanofibers: morphology, structure and electrical properties.* Synthetic metals, 2008. **158**(21): p. 953-957.

35. Li, G. and Z. Zhang, *Synthesis of dendritic polyaniline nanofibers in a surfactant gel.* Macromolecules, 2004. **37**(8): p. 2683-2685.

36. Meng, S., Z. Zhang, and M. Rouabhia, *Surfactant-templated crystalline polygon nanoparticles of heterocyclic polypyrrole prepared with Fenton's reagent.* Synthetic metals, 2010. **160**(1): p. 116-122.

37. Zhang, X., et al., *Inorganic/organic mesostructure directed synthesis of wire/ribbon-like polypyrrole nanostructures.* Chem. Commun., 2004(16): p. 1852-1853.

38. Stejskal, J., P. Kratochvíl, and M. Helmstedt, *Polyaniline dispersions. 5. Poly (vinyl alcohol) and poly (N-vinylpyrrolidone) as steric stabilizers.* Langmuir, 1996. **12**(14): p. 3389-3392.

39. Kim, S.W., H.G. Cho, and C.R. Park, *Fabrication of unagglomerated polypyrrole nanospheres with controlled sizes from a surfactant-free emulsion system.* Langmuir, 2009. **25**(16): p. 9030-9036.

40. Li, J., et al., *A novel route to synthesis of photoluminescent dye/polypyrrole nanoparticles: Effects of intermolecular energy transfer on nucleation and growth of polypyrrole.* Synthetic metals, 2008. **158**(10): p. 396-399.

41. Tran, H.D., et al., *A Template-Free Route to Polypyrrole Nanofibers.* Macromolecular rapid communications, 2007. **28**(24): p. 2289-2293.

42. Debiemme-Chouvy, C., *Template-free one-step electrochemical formation of polypyrrole nanowire array.* Electrochemistry Communications, 2009. **11**(2): p. 298-301.

43. Paine, A.J., *Dispersion polymerization of styrene in polar solvents. 7. A simple mechanistic model to predict particle size.* Macromolecules, 1990. **23**(12): p. 3109-3117.

44. Ober, C.K. and M.L. Hair, *The effect of temperature and initiator levels on the dispersion polymerization of polystyrene.* Journal of Polymer Science Part A: Polymer Chemistry, 1987. **25**(5): p. 1395-1407.

45. Jang, J. and H. Ha, *Fabrication of carbon nanocapsules using PMMA/PDVB core/shell nanoparticles.* Chemistry of materials, 2003. **15**(11): p. 2109-2111.

46. Jang, J., J.H. Oh, and G.D. Stucky, *Fabrication of ultrafine conducting polymer and graphite nanoparticles.* Angewandte Chemie International Edition, 2002. **41**(21): p. 4016-4019.

47. Jang, J. and J.H. Oh, *Facile Fabrication of Photochromic Dye–Conducting Polymer Core–Shell Nanomaterials and Their Photoluminescence.* Advanced materials, 2003. **15**(12): p. 977-980.

48. Cataldo, F. and M. Omastová, *On the ozone degradation of polypyrrole.* Polymer Degradation and Stability, 2003. **82**(3): p. 487-495.

49. Nicho, M. and H. Hu, *Fourier transform infrared spectroscopy studies of polypyrrole composite coatings.* Solar energy materials and solar cells, 2000. **63**(4): p. 423-435.

50. Chen, W., et al., *Magnetic and conducting particles: preparation of polypyrrole layer on Fe_3O_4 nanospheres.* Applied surface science, 2003. **218**(1): p. 216-222.

51. Vishnuvardhan, T., et al., *Synthesis, characterization and ac conductivity of polypyrrole/Y_2O_3 composites.* Bulletin of Materials Science, 2006. **29**(1): p. 77-83.

52. Li, Y. and R. Qian, *Electrochemical overoxidation of conducting polypyrrole nitrate film in aqueous solutions.* Electrochimica acta, 2000. **45**(11): p. 1727-1731.

53. Mostany, J. and B.R. Scharifker, *Direct microcalorimetric measurement of doping and overoxidation processes in polypyrrole.* Electrochimica acta, 1997. **42**(2): p. 291-301.

54. Novák, P., *Limitations of polypyrrole synthesis in water and their causes.* Electrochimica acta, 1992. **37**(7): p. 1227-1230.

55. Uhm, H.S., et al., *Increase in the ozone decay time in acidic ozone water and its effects on sterilization of biological warfare agents.* Journal of hazardous materials, 2009. **168**(2): p. 1595-1601.

56. Weng, Z. and X. Ni, *Oxidative polymerization of pyrrole photocatalyzed by TiO_2 nanoparticles and interactions in the composites.* Journal of Applied Polymer Science, 2008. **110**(1): p. 109-116.

57. Reece, D.A., et al., *Autopolymerization of pyrrole in the presence of a host/guest calixarene.* Macromolecules, 2005. **38**(5): p. 1616-1622.

58. Langsdorf, B.L., et al., *Partitioning and polymerization of pyrrole into perfluorosulfonic acid (Nafion) membranes.* The Journal of Physical Chemistry B, 2003. **107**(11): p. 2480-2484.

59. Song, M.-K., et al., *Synthesis and characterization of soluble polypyrrole doped with alkylbenzenesulfonic acids.* Synthetic metals, 2004. **141**(3): p. 315-319.

60. Lee, J., D. Kim, and C. Kim, *Synthesis of soluble polypyrrole of the doped state in organic solvents.* Synthetic metals, 1995. **74**(2): p. 103-106.

CHAPTER 3. STUDIES ON THE SYNTHESIS OF POLYPYRROLE SUBMICRON SPHERES UTILIZING OZONE OXIDATION

3.1. Introduction

A template free method to synthesize polypyrrole (PPy) nanospheres using ozone oxidation was introduced in the previous chapter. It was surprising to achieve uniform morphology and narrow particle size distribution in a surfactant free method. A detailed analysis of the reaction parameters was needed to answer a few of the questions that were raised in the previous research. In this chapter effect of co-solvent and effect of ozone concentration on the PPy submicron spheres synthesis has been studied using electron microscopy, UV-Vis spectroscopy, dynamic light scattering (DLS), and cyclic voltammetry (CV). Additionally, electrochemical activity of PPy has been investigated using CV and a possible stability mechanism is presented using X-ray photo-electron spectroscopy (XPS), and zeta potential measurements. Please note that the term submicron spheres is used henceforth instead of nanospheres in this chapter due to the particle size of spheres studied was above 100 nm.

We believe that the radicals produced due to oxidation of water with ozone may significantly affect PPy synthesis. Thus, it was important to study effect of solvent, with relatively low reactivity with ozone, on the PPy synthesis. Methanol was used as a co-solvent due to its low reactivity with ozone, thus limiting the number of reactive radicals that are produced during the reaction of ozone with water.[1-3] In neutral water the decomposition rate of ozone producing reactive hydroxyl radicals is 70 $M^{-1}s^{-1}$, whereas the reaction rate between methanol and ozone is 0.024 $M^{-1}s^{-1}$.[3, 4] Methanol also shows scavenging behavior towards hydroxyl radicals.[3] These two factors may explain how important the reactive radicals are in the synthesis of PPy, and secondly if the reactive radicals are over-oxidizing PPy.

It is known that in order to synthesize uniform particle size high nucleation rate is necessary particularly at the start of the reaction.[5] In this study ozone was introduced at various concentrations to investigate if the nucleation theory is applicable to PPy submicron sphere synthesis and if the ozone concentration has any effect on morphology and size of PPy. The fact that, uniform PPy submicron spheres are formed with a relatively narrow particle size distribution in a highly oxidative solution consisting of ozone; encouraged us to investigate how morphology and size of PPy will be affected by changing nucleation rates.

Dobrowolska and co-workers recently studied nucleation in surfactant free emulsion polymerization of styrene, in order to visualize the widely acknowledged 'coagulative nucleation' theory that results in uniform particles with relatively narrow particle size distribution.[6] The coagulative nucleation theory particularly for surfactant free emulsions suggests formation of small particles immediately after the reaction by homogeneous nucleation of oligomers. These primary particles consisting of small water insoluble oligomers further grow by polymerization with monomers available in the solution. Very low solubility of pyrrole and particularly pyrrole oligomers suggest 'coagulative nucleation' may be a possible mechanism in the formation of uniform PPy submicron spheres.

3.2. Materials and methods

Methanol and pyrrole were purchased from Sigma Aldrich. Methanol was ACS grade with assay ≥ 99.8%. Pyrrole was distilled before use. A typical reaction size was 100 ml. Pyrrole (1.14 gm) was dissolved in 100 ml 18 MΩ Millipore water (0.17 M pyrrole solution). Ozone was generated in the lab using ATLAS 30 C ozone generator, provided by Absolute Ozone, using pure dried oxygen. A typical reaction mixture was exposed to ozone by bubbling ozone/oxygen mixture through the solution for 60 seconds. The ozone/oxygen mixture contained 18% ozone by

weight. In the case of methanol concentration experiments, methanol was used as a co-solvent and was replaced with water in a systematic way. For example a 10% methanol volume reaction had 10% methanol and 90% 18 MΩ Millipore water with pyrrole dissolved in the mixture; and in similar manner for other reactions.

The ATLAS 30 C ozone generator had the capability to adjust the ozone concentration in the ozone/oxygen mixture by adjusting flow rate, current pot position, and gas pressure. For ozone concentration experiments, settings provided in Table 3.1 were used to obtain various ozone concentrations. These settings were used when ozone was exposed to various reaction for reactions designed to study effect of ozone concentration on the reactions.

Table 3.1. Ozone generator settings to obtain various ozone concentrations (*Note: reproduced from Atlas 30 Performance Chart*)

Reaction	Oxygen flow (SLPM) 90-92%	Gas press. (psig)	Current pot position	Ozone conc. (%W-W)
1	0.15	20.00	35.00	17.37
2	0.50	20.00	40.00	15.75
3	0.75	20.00	50.00	14.38
4	1.00	20.00	50.00	13.47
5	1.25	20.00	50.00	13.00

Particle size and particle size distribution was measured using a NICOMP 380 submicron particle sizer supplied by Particle Sizing Systems. For UV-Vis spectra, as synthesized dispersions were diluted to 10% of the initial dispersion by 18 MΩ Millipore water. Varian-5000 UV-Vis-NIR spectrophotometer was used to perform UV-Vis spectroscopy. JEOL JSM-7600F Scanning Electron Microscope (SEM) was used to obtain the images. Samples were prepared by sprinkling centrifuged and dried particles onto carbon tape attached to aluminum mounts. Balzers SCD 030 sputter coater was used to coat the samples with gold. Accelerating voltage values, scale bars and magnifications are listed in each figure. The cyclic voltammetry (CV) was performed using a standard three electrode setup provided by Gamry. Reference electrode was

Ag/AgCl, while counter electrode was platinum wire electrode. Electrolyte used was a 1.5M HCl solution. The dispersions were drop-coated on the platinum electrode which was used as a working electrode.

The (X-ray photoelectron spectroscopy) XPS measurements were performed using SSX-100 system (Surface Science Laboratories, Inc.) equipped with a monochromated Al K_α X-ray source, a hemispherical sector analyzer (HSA) and a resistive anode detector. The base pressure of the XPS system was 4.0×10^{-10} Torr. During the data collection, the pressure was ca. 1.0×10^{-8} Torr. Each sample was mounted on a piece of Al sticking tape on a separate sample holder to avoid cross contamination during sample handling. Care was taken to ensure the surface was fully covered with a sufficiently thick layer of the samples. All samples were nonconductive, and a low-energy electron beam (5 eV) was applied for charge neutralization. The X-ray spot size was 1×1 mm^2, which corresponded to an X-ray power of 200 W. The survey spectra were collected using 8 scans for each at 150 eV pass energy and 1 eV/step. The high resolution spectra were collected using 50 eV pass energy and 0.1 eV/step. Chlorine was seen in the samples after CV and Cl 2p high resolution scans were also collected. It should be noted that the two peaks after curve fitting were Cl $2p_{1/2}$ and Cl $2p_{3/2}$, rather than two different Cl chemical states. The atomic percentages were calculated from the survey spectrum using the ESCA 2005 software provided with the XPS system. For high resolution data, the lowest binding-energy C 1s peak (presumably, C-C/C-H peak) was set at 285.0 eV and used as the reference for all of the other elements. The curve fitting used a combination of Gaussian/Lorenzian function with the Gaussian percentages being at 80% or higher. Zeta potential was measured using Zetasizer (Malvern Instruments, Worcestershire, U.K.). All measurements were recorded at 25°C with as synthesized dispersions.

3.3. Results and discussion

3.3.1. Cyclic voltammetry

In order to assess electrochemical activity of PPy, platinum electrodes were drop coated with PPy submicron spheres directly from as-synthesized dispersion. The synthesis conditions for this reaction were standard, meaning water as a solvent and about 18% of ozone concentration. The electrodes were allowed to dry before performing CV scans. The PPy modified platinum electrode was working electrode in combination with platinum mesh counter electrode and Ag/AgCl reference electrode.

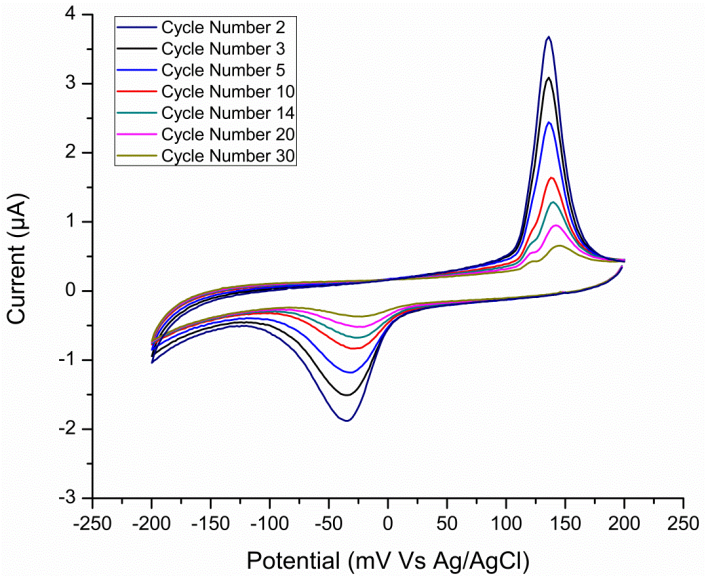

Figure 3.1. Cyclic voltammetry of PPy submicron spheres coated platinum electrode.

An oxidation peak was observed at approximately 150 mV while reduction peak was observed at approximately -45 mV (Figure 3.1). PPy submicron spheres show quasi-reversible redox behavior which is typical for chemically synthesized PPy.[7] The onset of oxidation was observed to be at approximately 115 mV while the onset of reduction was observed to be at approximately 5 mV. This large difference in the oxidation and reduction peaks may be due to

the smaller size of the PPy submicron spheres.[8] The oxidation and reduction current reduced with increase in scans and were significantly diminished after 30 scans.

3.3.2. Effect of ozone concentration

Effect of ozone concentration on particle size and morphology was studied at a series of ozone concentrations. At 17.31% concentration of ozone uniform spherical morphology was observed (Figure 3.3A). As the concentration of ozone was decreased a bimodal distribution was observed with particle size of approximately 250 nm and 1000 nm (Figure 3.3B). Further decrease in the concentration of ozone resulted into further increase in the particle size in the range of 1.5 µm to 2 µm (Figure 3.3C, 3.3D and 3.3E). The colloidal dispersion of PPy particles was not stable at lower concentrations of ozone as shown in Figure 3.2. This can be attributed to the increase in the gravitational forces due to increase in particle size (Figure 3.3). [9]

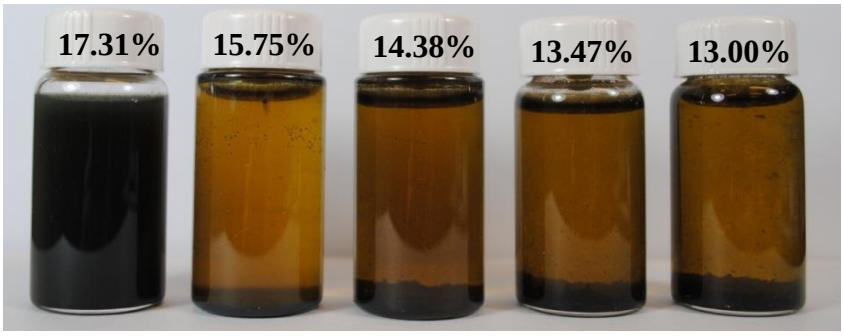

Figure 3.2. Colloidal stability after seven days of the reaction at various ozone concentrations.

The particle coagulation at lower ozone concentrations was also studied using dynamic light scattering. As a representative of low concentration reactions, dynamic light scattering was performed on the reaction with ozone concentration of 13.47% by weight over a period of 44 hours at regular intervals (Figure 3.3). Results immediately (Figure 3.4, 0 hour) after the reaction show nearly monodispere particle size distribution with average particle size of 160 nm. A developing bimodal distribution in the volume-wt nicomp distribution can be observed after four

hours of the synthesis (Figure 3.4). Further increase in the particle size and coagulation in the particles was observed as time progressed after the synthesis. These results are in agreement with the SEM results (Figure 3.3).

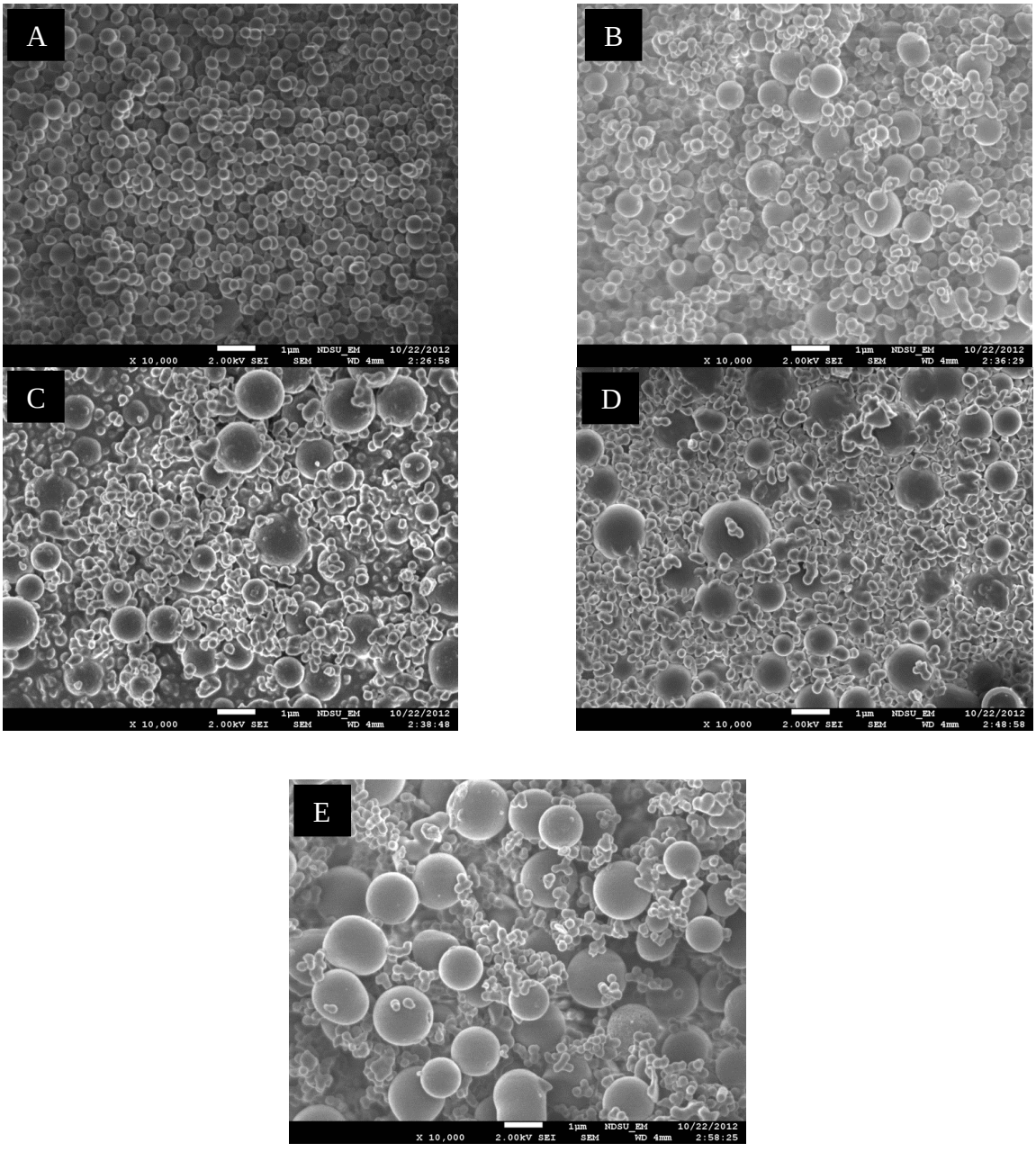

Figure 3.3. Effect of ozone concentration on morphology of PPy. SEM images of PPy at various ozone concentrations by weight A) 17.31% B) 15.75% C) 14.38% D) 13.47% E) 13%.

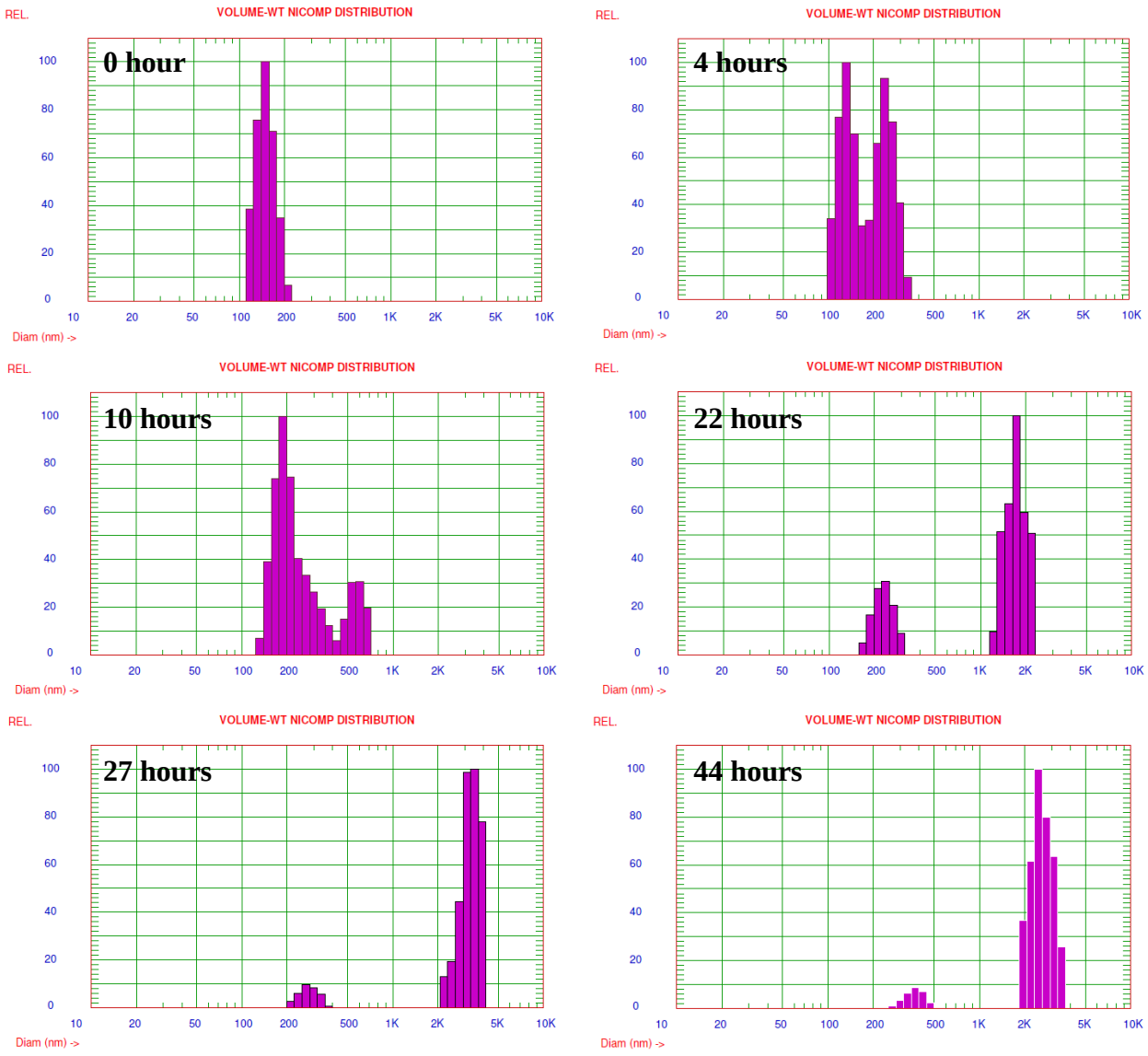

Figure 3.4. Analysis of particle size immediately after synthesis at regular time intervals, up to 44 hours, by dynamic light scattering.

The effect of ozone concentration on particle size may be explained by the nucleation, growth and particle size relationship in the PPy synthesis. It is possible that high concentrations of ozone may be providing higher amount of nucleating sites for subsequent PPy growth at higher nucleation rate. It is also known that to achieve uniform size distribution of particles all nuclei should form at the same time.[6, 10-12] Thus, the number of nuclei formed may be adequate for further growth of the PPy submicron spheres at 17.31% ozone concentration. While

at lower ozone concentrations the nucleation rate may be slower resulting in initially a bimodal size distribution and finally resulting in larger particles due to continuous incorporation of smaller particles in large particles (Figure 3.4). [13]

3.3.3. Effect of methanol concentration

It is suggested that water plays an important role in the synthesis of PPy submicron sphere dispersion, primarily due to reaction of ozone with water. Decomposition of ozone in neutral and basic water is facilitated by hydroxyl ions, which characteristically produce highly reactive free radical species including hydroxyl radicals. [14] The importance of reactive free radicals in the synthesis was studied using methanol as a co-solvent which has very low rate constant for the reaction with ozone in addition to its hydroxyl radicals scavenging ability.[1-3] Water was replaced with methanol at 10% by volume intervals from initial monomer solution. The effect of methanol concentration was characterized using UV-VIS spectroscopy, SEM, and CV. Seven days after the reaction the vial images were taken to demonstrate effect of methanol concentration on PPy synthesis and dispersion stability (Figure 3.6).

When methanol (100%) was used as the only solvent for the synthesis, PPY was not synthesized which is apparent from Figure 3.6. This may reveal the importance of reactive radicals produced during ozone oxidation of water for the synthesis of PPy. Furthermore, dispersion stability was adversely affected by introduction of methanol in the solvent particularly beyond 30% concentration.

Figure 3.5 shows UV VIS spectra of the dispersions at various concentrations of methanol; with increase in methanol concentration the intensity of peaks at approximately 450 nm and 590 nm increased up to 40% methanol concentration. The peaks at 450 nm and 590 nm

may be associated with $\pi - \pi^*$ transitions in PPy. [15-17] Further increase in the methanol concentration resulted in decrease in the intensity of the peaks.

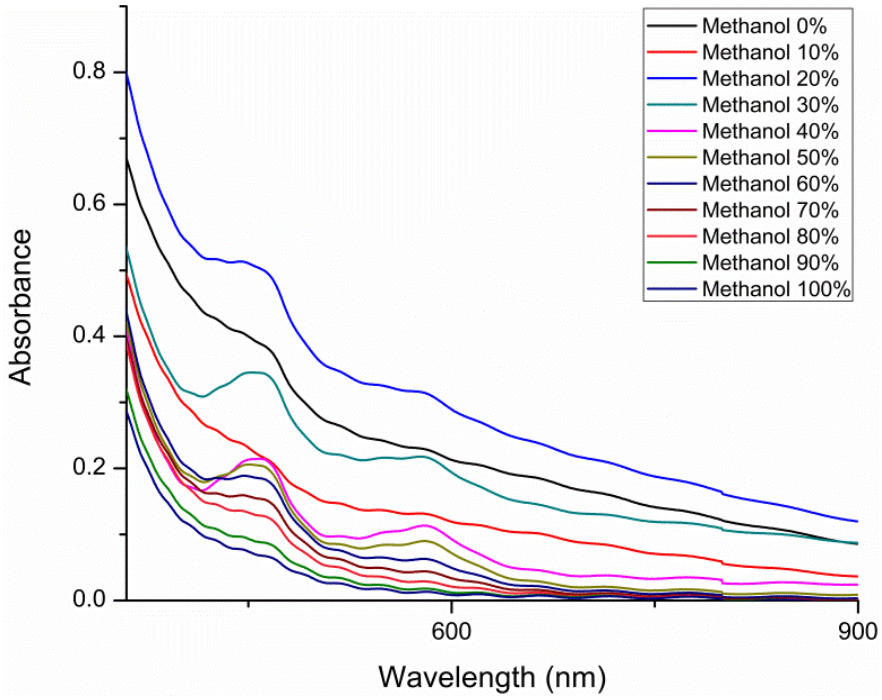

Figure 3.5. UV-Vis absorption spectra at various methanol concentrations in the solvent.

Figure 3.6. Image of vials after 7 days of the reaction at various methanol concentrations. (Methanol concentration on the vials in volume %)

In the synthesis of PPy submicron spheres utilizing ozone oxidation, it should be acknowledged that ozone and reactive radicals produced during water oxidation may over-oxidize PPy; adversely affecting the conjugation length, electrochemical activity, and

conductivity of PPy. [18, 19] Introducing methanol in the solvent may reduce the effect of ozone and reactive radicals due to slower oxidation of methanol by ozone. The over-oxidation may have been controlled with methanol as a co-solvent giving rise to increase in peak intensities in the UV-Vis spectroscopy (Figure 3.5).

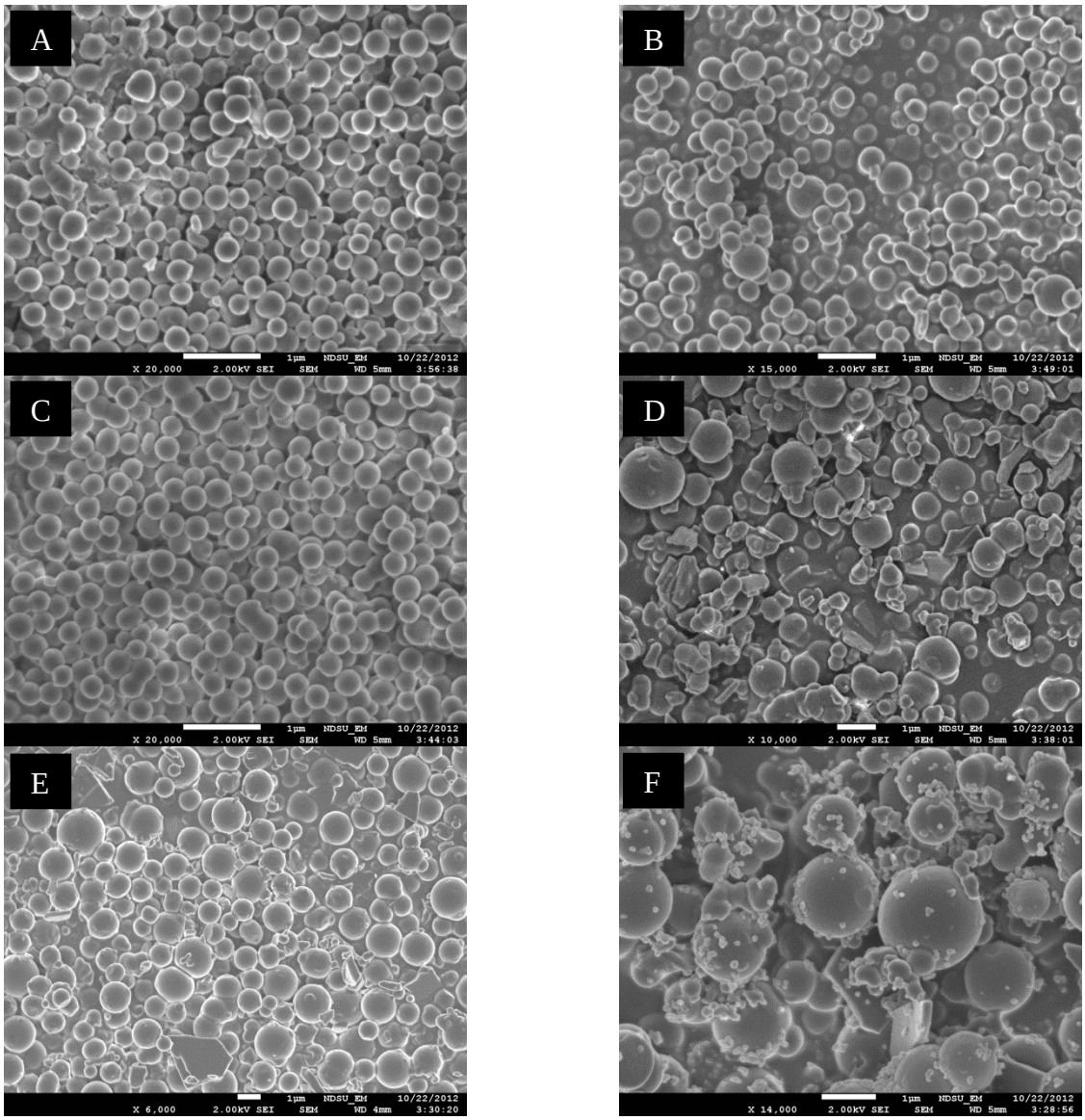

Figure 3.7. SEM images of PPy particles at various methanol concentrations in the solvent; methanol concentration by volume %; A) 0, B) 10, C) 20, D) 30, E) 40, F) 60.

Figure 3.7 shows SEM images of the synthesized particles at various concentrations of methanol in the solvent. Increase in particle size and particle size distribution can be observed

with increase in methanol concentration in the solvent mixture. This effect exacerbates beyond 20% concentration of methanol producing agglomerated non-uniform particles which in part explains the adverse impact on dispersion stability (Figure 3.6). Similar to ozone concentration experiments the increase in particle size with increase in methanol concentration can be attributed to the lower number of nucleating sites due to low reactivity of methanol to ozone

Thus, based on the ozone concentration and methanol concentration experiments it might be reasoned that the nucleation rate is indeed affecting the morphology and particle size of PPy. At lower nucleation rates, provided by lower ozone concentration and methanol introduction in the solvent, larger particles were observed; while at higher concentration of ozone, and when water was the only solvent for the reaction uniform PPy submicron spheres were observed (Figure 3.8).

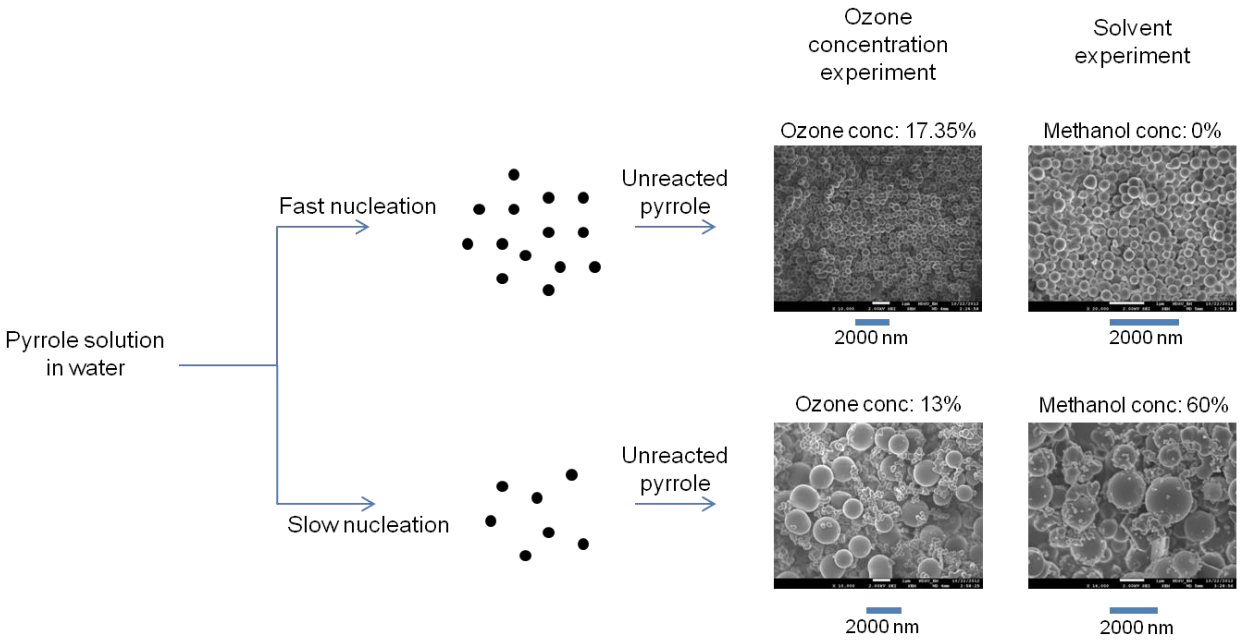

Figure 3.8. Schematic of nucleation effects on particle size.

Initial studies where particle size and particle size distribution were measured immediately after the reaction, it was observed that the particles form instantly after the reaction

(Figure 3.9), which is an indicative of burst nucleation.[11] The particles further coagulate to form uniform submicron spheres in the range of 200 nm to 300 nm (Figure 3.9). Although this experiment points towards nucleation coagulation as a possible mechanism for uniform submicron sphere formation, more experiments need to be performed in order to attest this to be the mechanism.[6] For instance, the samples can be freeze dried after a set period of intervals starting from immediately after the reaction and studied for their size and morphology using transmission electron microscopy (TEM).

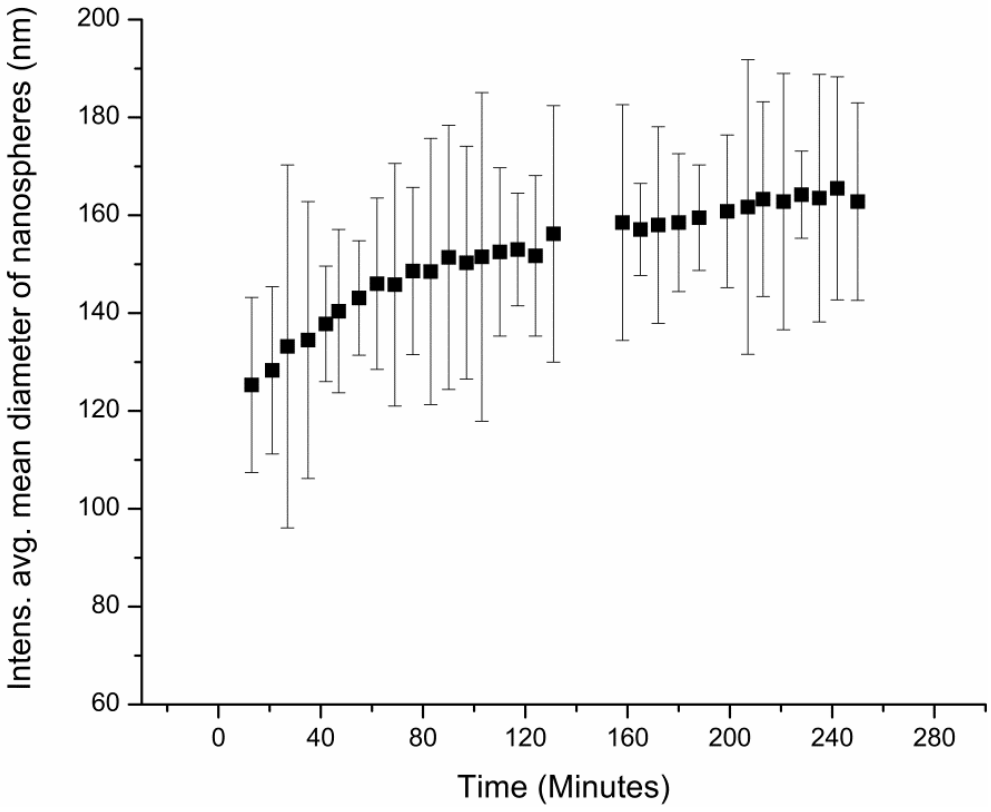

Figure 3.9. Particle size analysis with time.

CV was performed in order to investigate how the particle size may have affected the oxidation and reduction potential of the PPy. The PPy particles were drop coated on platinum electrodes directly from as-synthesized dispersions. Figure 3.10 shows CVs of PPy synthesized at 0%, 10%, 20%, 30% and 40% methanol concentration in the solvent. The CV curve indicated

shift from the quasi-reversible to irreversible behavior with incorporation of methanol. Onsets of oxidation potentials were estimated from CVs shown in Figure 3.10, and are reported in Table 3.2. The onset of oxidation potential was shifted towards more cathodic values (Table 3.2) with increase in the concentration of methanol in the solvent. It is possible that this shift is due to the increase in the particle size with the incorporation of methanol in the solvent (Figure 3.7). [20]

Table 3.2. Oxidation onsets from cyclic voltammetry (Figure 3.10)

Methanol concentration (Vol %)	E_{ox}^{onset} (mV)
0	82
10	80
20	90
30	-310
40	-290

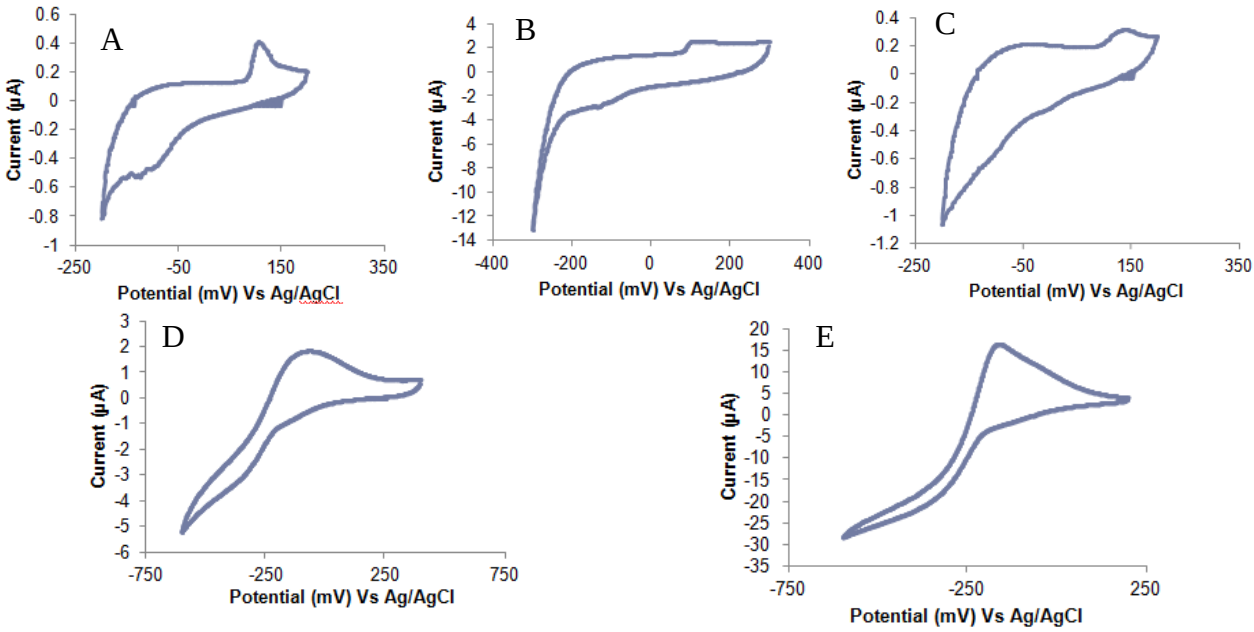

Figure 3.10. Cyclic voltammetry of PPy submicron spheres synthesized at various methanol concentrations. Methanol concentrations by volume %; A) 0%, B) 10%, C) 20%, D) 30%, E) 40%.

3.3.4. Stability analysis

In a broader perspective aqueous dispersion stability is provided by either of the three mechanisms namely electrostatic repulsion, steric stability or combination of electrostatic and steric stability.[21, 22] Zeta potential measurements and XPS were utilized to understand the possible stability mechanisms. Initial results had provided neutral zeta potentials for the aqueous dispersions at various pH values. However, after several trials it was observed that the batch of cuvettes may be malfunctioning leading to false results. A new batch of cuvettes was procured which provided more realistic zeta potential values for the aqueous dispersions at various pH values.

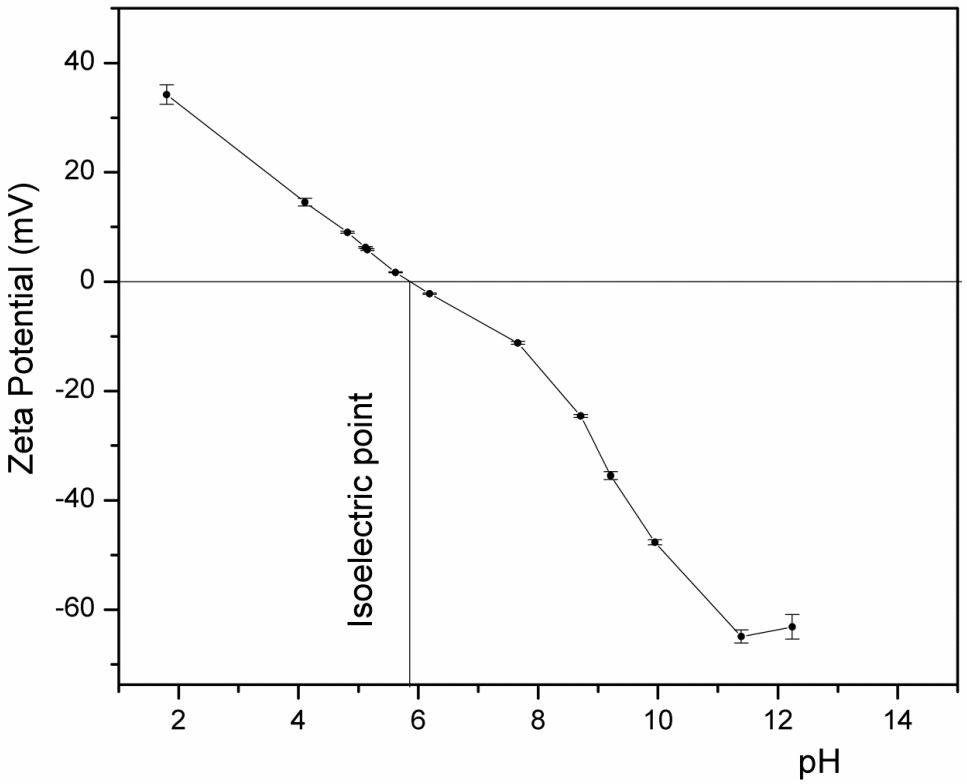

Figure 3.11. Zeta potential vs pH plot for as synthesized PPy dispersions.

The iso-electric point (IEP) of the dispersion was found to be 5.8 pH (Figure 3.11). At lower pH the dispersion is positively charged which may suggest that the PPy on the surface of

the submicron spheres may be protonated in acidic environments. While, the as synthesized PPy submicron sphere dispersions had zeta potential values of approximately 15 mV at a pH of 4. This may suggest that the surface charge on the PPy submicron spheres is positive and thus the nitrogens of the PPy on the surface of the submicron spheres may be protonated. Apart from that, the literature reveals that for good aqueous dispersion stability the magnitude of zeta potential should be higher than 30 mV.[23] Despite 15 mV of zeta potential the as-synthesized dispersions show prolonged dispersion stability indicating possibility of additional stability mechanism.

Table 3.3. Elemental surface composition of PPy submicron spheres

Elements	**Atom %**
Carbon	75.778
Nitrogen	15.108
Oxygen	9.114

XPS is a very relevant technique to understand surface characteristics especially because X-rays only penetrate about 10 nm inside the particles which allows characterizing the surface rather than bulk. XPS was performed on PPy, the results are shown in Figure 3.12. Elemental surface composition shows C/N ratio of approximately 5 (Table 3.3), while approximately 9% of oxygen was also detected in the periphery of PPy sub micron spheres. Both these results may suggest that the outer surface of PPy spheres may be overoxidized, leading into higher oxygen content and slightly higher C/N ratio.[24] Generally PPy has a C/N ratio of approximately 4. High resolution C 1s spectra of PPy submicron spheres (Figure 3.12B) shows distinct peak centered at 285 eV, two shoulder peaks were present at slightly higher energies of 288.2 eV and 292.0 eV. The peak at 285 eV are indicative of C-C and C-H bonds, while the peaks at 288.2 eV and 292.0 could be due to the presence of COO^- and C-N, $C\text{-}N^+$ species respectively.[25-32]

The central peak in the high resolution N 1s spectra (Figure 3.12C) was observed at 400.5 eV which may be attributed to $–N^+$ and –NH- species whereas the smaller shoulder peaks at

slightly lower energy (398.9 eV) can be attributed to the presence of –N= bonds.[25, 26, 28, 29, 31-35] The O 1s spectra (Figure 3.12D) of PPy show over-oxidation of PPy with the presence of distinct peak centered at 532.3 indicative of C=O and C-OH bonds, while the shoulder peak at 533.9 may be ascribed to COO^- species.[26, 30-32]

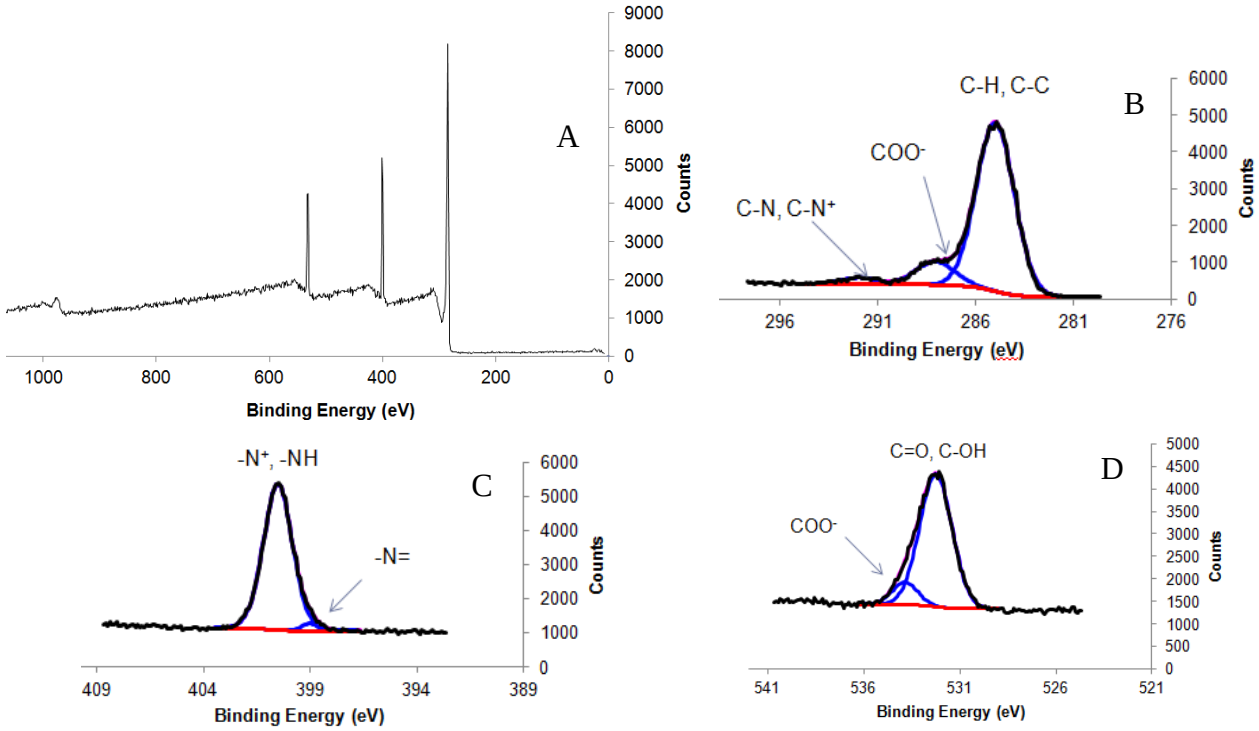

Figure 3.12. A) XPS spectrum survey of PPy submicron spheres B) High resolution C 1s spectra C) High resolution N 1s spectra D) High resolution O 1s spectra.

It may be concluded from XPS analysis that apart from the presence of the bonds associated with the presence of PPy, the outermost PPy could also be overoxidized resulting in the presence of hydrophilic carbonyl (C=O), hydroxyl (C=OH) and carboxylic (COO^-) linkages on the PPy backbone. The overoxidized PPy may thus provide steric stability to PPy submicron spheres against agglomeration in addition to the electrostatic repulsion described earlier. The steric stability may be resulting from hydrophilic character of carbonyl, hydroxyl and carboxylic

groups on hydrophobic PPy backbone particularly in the overoxidized PPy on the surface of spheres.

3.5. Conclusions

Drop coated PPy submicron spheres on platinum electrode show quasi-reversible electrochemical activity with oxidation peak at approximately 150 mV and reduction peak at approximately -45 mV. Ozone concentration affected PPy particle size as well as particle size distribution possibly due to decrease in nucleating sites with decrease in ozone concentration. Introduction of methanol had a similar effect on particle size and particle size distribution which could be due to low reactivity of methanol with ozone. Addition of methanol also positively affected electrochemical activity and $\pi - \pi^*$ transitions in PPy which was attributed to reduction in degree of over-oxidation of PPy. Zeta potential measurements and XPS suggest that the dispersion stability of PPy submicron spheres could be due to both electrostatic and steric effect.

3.6. References

1. Hoigné, J. and H. Bader, *Rate constants of reactions of ozone with organic and inorganic compounds in water—I: non-dissociating organic compounds.* Water Research, 1983. **17**(2): p. 173-183.
2. Von Sonntag, C. and U. Von Gunten, *Chemistry of ozone in water and wastewater treatment: From basic principles to applications*. 2012, London, UK: Iwa publishing. 320.
3. Mena, E., et al., *On ozone-photocatalysis synergism in black-light induced reactions: Oxidizing species production in photocatalytic ozonation versus heterogeneous photocatalysis.* Chemical Engineering Journal, 2012. **204-206**: p. 131-140.

4. Van Geluwe, S., L. Braeken, and B. Van der Bruggen, *Ozone oxidation for the alleviation of membrane fouling by natural organic matter: A review.* Water Research, 2011. **45**(12): p. 3551-3570.

5. Privman, V., *Diffusional nucleation of nanocrystals and their self-assembly into uniform colloids.* J. Optoelectronics Adv. Mater., 2008. **10**: p. 2827-2839.

6. Dobrowolska, M.E., J.H. van Esch, and G.J. Koper, *Direct visualization of "coagulative nucleation" in surfactant-free emulsion polymerization.* Langmuir, 2013. **29**(37): p. 11724-11729.

7. Ramachandran, K. and M.M. Lerner, *Electrochemical characterization of a polypyrrole/montmorillonite nanocomposite.* Journal of The Electrochemical Society, 1997. **144**(11): p. 3739-3743.

8. Fan, L.-Z. and J. Maier, *High-performance polypyrrole electrode materials for redox supercapacitors.* Electrochemistry Communications, 2006. **8**(6): p. 937-940.

9. Larsson, M., et al., *Suspension Stability; Why Particle Size, Zeta Potential and Rheology are Important.* Annual Transactions of the Nordic Rheology Society, 2012. **20**: p. 209-214.

10. Robb, D.T. and V. Privman, *Model of nanocrystal formation in solution by burst nucleation and diffusional growth.* Langmuir, 2008. **24**(1): p. 26-35.

11. Park, J., V. Privman, and E. Matijevic, *Model of formation of monodispersed colloids.* The Journal of Physical Chemistry B, 2001. **105**(47): p. 11630-11635.

12. Privman, V., *Mechanisms of Diffusional Nucleation of Nanocrystals and Their Self-Assembly into Uniform Colloids.* Annals of the New York Academy of Sciences, 2009. **1161**(1): p. 508-525.

13. Chern, C., *Emulsion polymerization mechanisms and kinetics.* Progress in Polymer Science, 2006. **31**(5): p. 443-486.

14. Ershov, B. and P. Morozov, *The kinetics of ozone decomposition in water, the influence of pH and temperature.* Russian Journal of Physical Chemistry A, 2009. **83**(8): p. 1295-1299.

15. Woo, H.-Y., et al., *Synthesis and dispersion of polypyrrole nanoparticles in polyvinylpyrrolidone emulsion.* Synthetic metals, 2010. **160**(7): p. 588-591.

16. Cheung, K., D. Bloor, and G. Stevens, *The influence of unusual counterions on the electrochemistry and physical properties of polypyrrole.* Journal of materials science, 1990. **25**(9): p. 3814-3837.

17. Bredas, J., et al., *Polarons and bipolarons in polypyrrole: Evolution of the band structure and optical spectrum upon doping.* Physical review. B, Condensed matter, 1984. **30**(2): p. 1023-1025.

18. Li, Y. and R. Qian, *Electrochemical overoxidation of conducting polypyrrole nitrate film in aqueous solutions.* Electrochimica acta, 2000. **45**(11): p. 1727-1731.

19. Krische, B. and M. Zagorska, *Overoxidation in conducting polymers.* Synthetic metals, 1989. **28**(1): p. 257-262.

20. Somani, P.R., *Synthesis and characterization of polyaniline dispersions.* Materials chemistry and physics, 2003. **77**(1): p. 81-85.

21. Pecher, J. and S. Mecking, *Nanoparticles of conjugated polymers.* Chemical Reviews, 2010. **110**(10): p. 6260-6279.

22. Gudarzi, M.M. and F. Sharif, *Characteristics of polymers that stabilize colloids for the production of graphene from graphene oxide.* Journal of colloid and interface science, 2010. **349**(1): p. 63-69.

23. Xu, R., C. Wu, and H. Xu, *Particle size and zeta potential of carbon black in liquid media.* Carbon, 2007. **45**(14): p. 2806-2809.

24. Atanasoska, L., K. Naoi, and W.H. Smyrl, *XPS studies on conducting polymers: polypyrrole films doped with perchlorate and polymeric anions.* Chemistry of materials, 1992. **4**(5): p. 988-994.

25. Kijewska, K., et al., *Photopolymerized polypyrrole microvessels.* Chemistry-A European Journal, 2012. **18**(1): p. 310-320.

26. Vasquez, M., et al., *Chlorine dopants in plasma synthesized heteroaromatic polymers.* Polymer, 2006. **47**(23): p. 7864-7870.

27. Silverstein, M. and I. Visoly-Fisher, *Plasma polymerized thiophene: molecular structure and electrical properties.* Polymer, 2002. **43**(1): p. 11-20.

28. Yuvaraj, H., J.J. Shim, and K.T. Lim, *Organic–inorganic polypyrrole-surface modified SiO2 hybrid nanocomposites: a facile and green synthetic approach.* Polymers for Advanced Technologies, 2010. **21**(6): p. 424-429.

29. Cho, Y. and R.B. Borgens, *The preparation of polypyrrole surfaces in the presence of mesoporous silica nanoparticles and their biomedical applications.* Nanotechnology, 2010. **21**(20): p. 205102.

30. Rajagopalan, R. and J.O. Iroh, *Characterization of polyaniline–polypyrrole composite coatings on low carbon steel: a XPS and infrared spectroscopy study.* Applied surface science, 2003. **218**(1): p. 58-69.

31. Malitesta, C., et al., *New findings on polypyrrole chemical structure by XPS coupled to chemical derivatization labelling.* Journal of Electron Spectroscopy and Related Phenomena, 1995. **76**: p. 629-634.

32. Ge, H., et al., *Study of overoxidized polypyrrole using X-ray photoelectron spectroscopy.* Polymer, 1994. **35**(3): p. 504-508.

33. Kang, E., et al., *X-ray photoelectron spectroscopic studies of polypyrrole synthesized with oxidative iron (III) salts.* Macromolecules, 1991. **24**(10): p. 2822-2828.

34. Tan, K., et al., *The chemical nature of the nitrogens in polypyrrole and polyaniline: A comparative study by x-ray photoelectron spectroscopy.* The Journal of chemical physics, 1991. **94**(8): p. 5382-5388.

35. Kang, E., K. Neoh, and K. Tan, *The intrinsic redox states in polypyrrole and polyaniline: a comparative study by XPS.* Surface and interface analysis, 1992. **19**(1-12): p. 33-37.

CHAPTER 4. STABLE POLYANILINE DISPERSIONS USING OZONE OXIDATION

4.1. Introduction

In recent years, polyaniline (PANI) has been rigorously investigated due to its high conductivity, easy doping/dedoping chemistry, excellent electrochemical properties, and good thermal and environmental stability.[1-5] PANI nano and submicron spheres, in addition to high conductivity and processing advantage, have low dimensions and high surface area, enabling them to be considered for various useful applications.[6] These applications are in a variety of fields, including corrosion inhibition, [4, 7-10] capacitors, [11-13] artificial muscles, [14] solar cells, [15-17] polymer light emitting diodes,[18-21] and energy storage devices.[22, 23]

PANI nanoparticles have been synthesized in many different morphologies such as nanowires, [24-27] nanorods/nanotubes, [28-30] nanospheres, [31, 32] and nanocapsules. [33, 34] This variety in morphology is traditionally attained using soft templates, such as surfactant micelles, [35-38] or hard templates, such as anodized aluminum oxide (AAO). [39-41] Templates provide stability and groundwork from which the polymer can grow, but the templates add undesirable expense to the process and can change the properties of the nanoparticles by integrating its own properties by acting as a dopant. [42] Positively charged PANI incorporates dopants, or negatively charged ions, throughout its structure to maintain charge neutrality. The dopants can change the electronic, magnetic, optical, and structural properties of PANI. Since the templates are often incorporated unintentionally, the templates must later be removed, which usually involves hazardous chemicals that can be detrimental to human health and the environment. [43] Consequently, there is growing interest in the research of template free synthesis of PANI nanoparticles leading to nanosphere and nanorod formation.

Multiple processes for template free syntheses, more commonly known as self assembly, of PANI nanospheres, nanotubes, and nanorods have been given in the scientific literature. [28, 44-56] Wei et al. reported the self assembly of PANI in the presence of β-napthalene sulfonic acid (NSA) as a dopant; they attributed formation of nanotubes to the self assembled micelle of the PANI-NSA salt. [55] Similarly, a one step synthesis of PANI/Au nanospheres is also reported by Zhang et al.; the self assembly mechanism is believed to be induced by p-toluene sulphonic scid-aniline micelle, which provides nucleation sites for further growth. [56] Park et al. have presented a synthesis of self assembled PANI microspheres by interfacial oxidative polymerization in the presence of tartaric acid as a dopant. [54] In addition, a self assembly of various desirable nanostructures of PANI using a step wise electrochemical deposition process is reported by Liu et al. [53] Chiou et al. have also synthesized PANI nanofibers and nanotubes by utilizing excess ammonium persulphate (APS) as the oxidizing agent. The dimer cation of aniline is oxidized by APS and acts as a surfactant, assisting in the process of self assembly. [52] Finally, the research group of Stejskal et al. has done extensive research in the field of polyaniline nanotubes and nanospheres by proposing mechanisms of formation of various morphologies. [38, 57-63]

The use of ozone as an oxidant for polymerization of conducting polymers has not yet been explored in the scientific community to its full potential. Even though Yan *et al*. reported catalytic oxidation of aniline using iron(III) and ozone in a 1 N HCl solution, the reaction of ozone and aniline without iron(III) and HCl was not considered in the report. [64] We believe that ozone is an effective oxidant by itself because of its reaction with water producing further oxidants that can be used to oxidize the aniline in solution. It should be noted that the chemistry of ozone in water is complex with a variety of mechanisms reported in the literature. The most

widely accepted reaction of ozone with water is initiated by hydroxide anions and produces highly reactive radicals that have an even higher oxidation potential than ozone itself. [65, 66] The half reaction culminating in hydroxyl radicals is shown in Scheme 4.1. Consequently, the ozone is reduced to molecular oxygen (Scheme 4.2). [67] If this reaction scheme is indeed accurate, it is important to note that the only byproducts of this reaction are oxygen and water, making ozone an environmentally friendly oxidant.

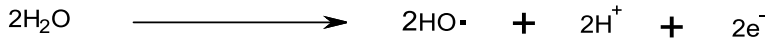

Scheme 4.1. Oxidation of water to hydroxyl radicals.

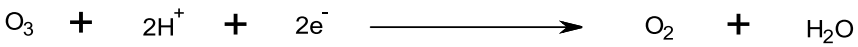

Scheme 4.2. Reduction of ozone to molecular oxygen and water.

In this chapter, we report the synthesis of self assembled PANI submicron spheres (SS) (100-500 nm) using ozone as the oxidant. This synthesis is unique because the reaction solution consists solely of aniline, ozone, and water and the byproducts are only water and oxygen. Effect of pH and effect of ozone exposure time on PANI synthesis is studied utilizing scanning electron microscopy (SEM), dynamic light scattering (DLS), Fourier transform infrared spectroscopy (FTIR), UV-Vis spectroscopy and zeta potential measurements.

4.2. Materials and methods

Aniline was obtained from Sigma Aldrich and was used as provided. Millipore 18.2 MΩ water was the solvent used for the reaction. Ozone was obtained by flowing pure dried oxygen supplied by Air Gas through a model ATLAS 30 C ozone generator supplied by Absolute Ozone.

In a typical experiment, a 0.02 molar solution of aniline was prepared in 18 MΩ Millipore water. Ten percent hydrogen chloride and 1 M sodium hydroxide solutions were used to adjust the pH of the experimental solution before the reaction. Oxygen was provided to the

ozone generator at a pressure of 20 psi and a flow rate of 0.2 liters/minute. According to the literature provided by Absolute Ozone®, this flow rate should be producing an oxygen/ozone mixture that is 18% ozone by weight. The oxygen/ozone mixture was bubbled through the 100 ml aniline solution for specified time (Table 4.1). After the ozone exposure was complete, any remaining ozone in the flask was removed by gently blowing a stream of air from a compressed air line over the reaction solution until fuming ceased. The reactions presented in this study (Table 4.1) were carried out at room temperature in 250 ml Erlenmeyer flasks. The dried particles were obtained after filtration and washing with copious amounts of 18 MΩ Millipore water. The residual water was removed by drying the powder samples at about 45°C-50°C.

Table 4.1. Reaction conditions with variation of pH

Reactions	Aniline (M)	pH before reaction	Ozone Exposure (Seconds)
R-1	0.02	2	60
R-2	0.02	4.03	60
R-3	0.02	6.05	60
R-4	0.02	8.15	60
R-5	0.02	10.18	60
R-6	0.02	12.04	60
R-7	0.02	7.6	10
R-8	0.02	7.6	30
R-9	0.02	7.6	60
R-10	0.02	7.6	120
R-11	0.02	7.6	180
R-12	0.02	7.6	240
R-13	0.02	7.6	300
R-14	0.02	7.6	360
R-15	0.02	7.6	600
R-16	0.02	7.6	900

Particle size measurements were performed using a NICOMP 380 submicron particle sizer supplied by Particle Sizing Systems®. UV-Vis spectra of the PANI SS in water were recorded on a Varian-5000 UV-Vis-NIR spectrophotometer. A Nicolet FTIR spectrometer was

used for the FTIR characterization. Samples were prepared for SEM by sprinkling centrifuged and dried particles onto carbon tape attached to aluminum mounts. The sample was then coated with gold using a Balzers SCD 030 sputter coater. Images were obtained using a JEOL JSM-7600F Scanning Electron Microscope. Magnification, accelerating voltage values, and micron bars are listed in each figure. Zeta potential measurements were obtained using Zetasizer (Malvern Instruments, Worcestershire, U.K.).

4.3. Results and discussions

In the previous chapters (Chapter 2 and Chapter 3), polypyrrole synthesis using ozone oxidation was investigated. The chemical oxidation of pyrrole and aniline to PPy and PANI respectively, follow the same principal mechanism.[68] This study was performed to examine if PANI SS can be synthesized in the similar conditions that were used for PPy synthesis. Experiments were designed to study the effect of pH of the reaction and ozone exposure time on the morphology and size of the PANI. A typical oxidation of aniline solution (0.02 M aniline) by ozone coexists with the decrease of pH of the solution due to continuous deprotonation of aniline in the process of polymerization. Figure 4.1 shows the decrease in pH of the solution after ozone exposure to a 0.02M solution of aniline at neutral pH confirming PANI synthesis.

It is known that pH of the reaction plays decisive role in the synthesis of various forms of PANI. Reactions were performed at various pH to examine the effect of pH on PANI synthesis. The color of the products obtained was brown which is associated with the reduced form of PANI, particularly in the basic and acidic conditions. However, the color of the synthesized PANI was greenish brown at acidic pH (Figure 4.2) while reddish brown at basic pH. This may indicate that the PANI SS synthesized in this study may be in the partially oxidized form especially at acidic pH.

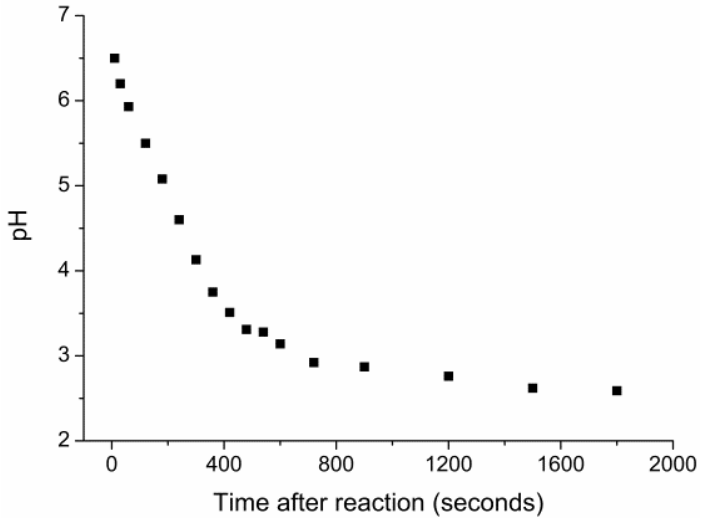

Figure 4.1. pH of the solution after 60 seconds of ozone exposure to a 0.02 M aniline solution.

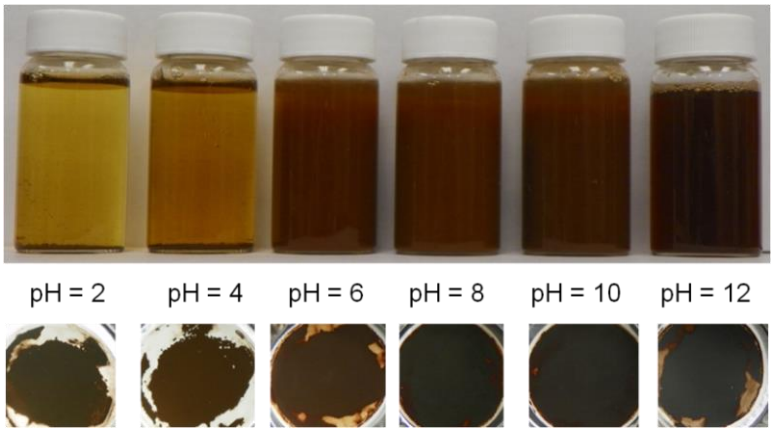

Figure 4.2. Top: vial images after seven days of the synthesis, Bottom: photographic image of the products obtained after washing and filtering.

The reactions performed at a pH of 6, 8 or 10 resulted in stable dispersion of PANI SS, while the reactions performed at acidic conditions (pH = 2 and pH = 4) resulted in unstable dispersions (Figure 4.2). At pH of 12, the reaction results in a transparent liquid with no visible particles. This could be explained by the early formation of carbonyl linkages due to the high radical concentration at neutral pH, which would restrict the growth of the polymer chain.

As already mentioned in previous chapters for PPy synthesis using ozone oxidation, the oxidation of aniline-water mixture with ozone is a complex reaction because of the formation of reactive radicals in ozone-water reaction. Ozone as well as the reactive radicals take part in the PANI synthesis. The ozone-water reaction is facilitated by hydroxide ions. Thus, the reaction rate of ozone with water is faster in basic solutions than in acidic solutions.

In a nutshell, the radical concentration may be higher in the basic solution, whereas the radical concentration may be lower in the acidic solutions. Due to this reason, it was expected that pH would have large impact on PANI particle size and morphology. Uniform sphereical morphology was obtained at a pH of 6 and 8. Insignificant decrease in the particle diameter was observed at a pH of 8 as compared to a pH of 6. A bimodal distribution was observed at a pH of 10, with a peak at 60 nm and another peak at 300 nm. The smaller spheres at a pH of 10 and pH of 8 could be due to the presence of more nucleating sites due to higher reactivity of ozone at neutral pH.

To determine the nature of the stability of the particles, zeta potential measurements were performed on PANI dispersions. The as synthesized dispersion has a pH of approximately 6 (pH before the reaction: 7.8); the pH of the dispersion was varied between pH of 1 and 13 using HCl and NaOH solutions. Figure 4.4 shows plots of zeta potential against pH for the dispersions. The isoelectric point of the dispersion was around a pH of 2.8.

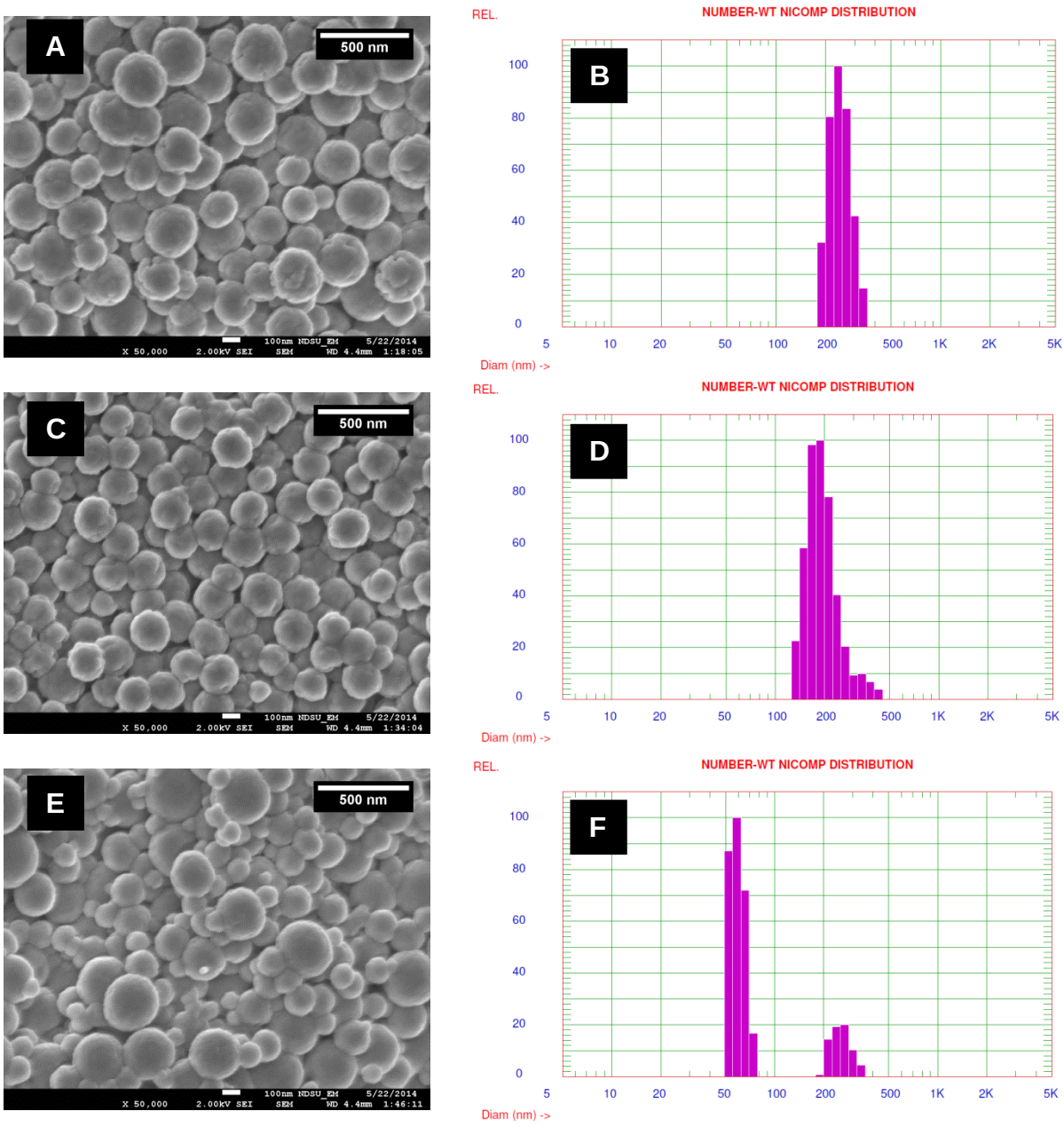

Figure 4.3. SEM images and dynamic light scattering results of PANI SS synthesized at various pH. A and B) pH = 6; C and D) pH = 8; E and F) pH = 10.

The negative zeta potential of -50 mV for as synthesized dispersions (pH = 6) indicate that the dispersions are stable due to electrostatic repulsion between individual particles. This result was encouraging mainly due to the fact that previous literature revealed multistep synthesis procedures to obtain colloidal dispersions of PANI using silica or surfactant.[69, 70]

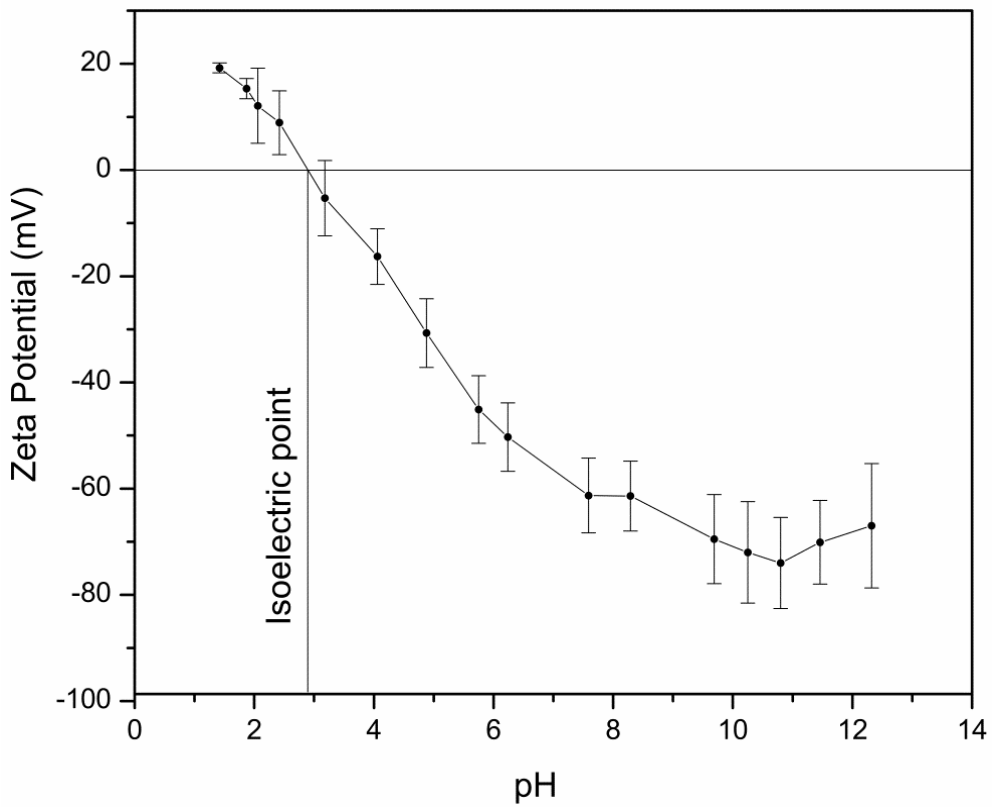

Figure 4.4. Effect of pH on the zeta potential of the PANI dispersion synthesized at a pH of 8.

The outer surface of the spheres may be consisting of overoxidized PANI oligomers providing electrostatic repulsion to spheres. The negative zeta potential also reveals that the PANI present on the outer surface of the spheres is deprotonated. X-ray photoelectron spectroscopy (XPS) will be performed in the future on the PANI spheres to confirm the surface overoxidation.

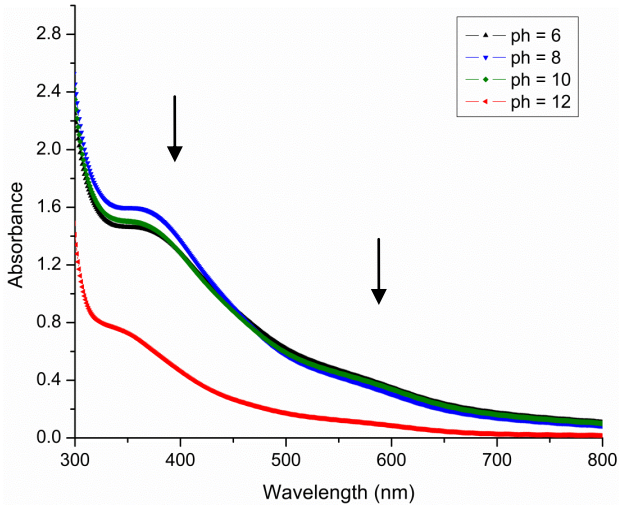

Figure 4.5. UV-Vis spectra of PANI dispersion synthesized at various pH.

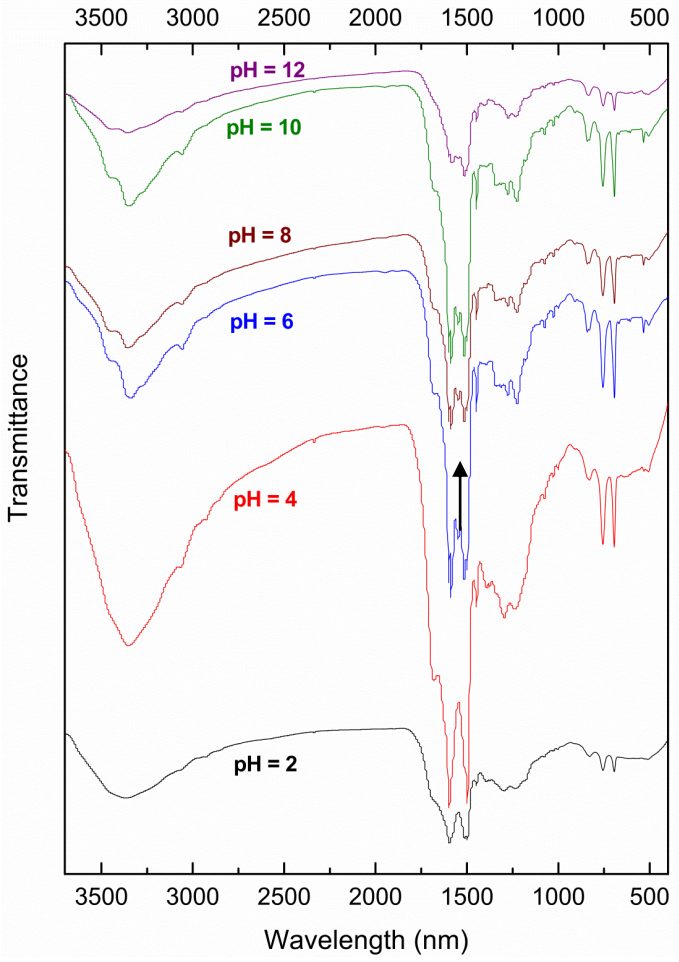

Figure 4.6. FTIR spectra of PANI synthesized at various pH.

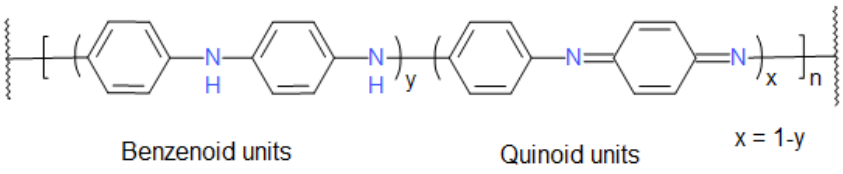

Scheme 4.3. Generic structure of PANI showing quinoid and benzenoid components.

The Fourier transform infrared spectra (Figure 4.6) of the synthesized PANI at various pH has characteristic quinoid and benzenoid C=C stretching at 1598 cm^{-1} and 1498 cm^{-1} respectively.[46, 51, 71] The absorption peaks at 1211 cm^{-1} and 1321 cm^{-1} that develops with increasing pH suggest a consequent increase in –C-N and –C=N stretching modes with aromatic conjugation.[51, 56] The peaks at 820 cm^{-1} may correspond to the C-H out of plane vibrations. [56, 72] The most significant change in the FTIR spectra of the PANI synthesized in acidic (pH = 2 and pH =4) conditions and in weak-acidic or basic conditions is the development of band at approximately 1540 cm^{-1} (for a pH of 6, 8 and 10). This band is reported to be corresponding to the substituted phenazine contaminations when PANI is synthesized in the neutral conditions. [73, 74] Furthermore, the ratio of quinoid peak (1598 cm^{-1}) intensity and benzenoid peak (1498 cm^{-1}) intensity provides an indication of the degree of oxidation in PANI (Scheme 4.3). The quinoid-benzenoid ratio for the PANI synthesized in this study was estimated to be between 1.02 and 1.05 for the pH of 2 to 10. While for a pH of 12 the quinoid-benzenoid ratio was 0.89 which may indicate reduced form of PANI containing more benzenoid units.

The effect of pH was further analyzed using UV-Vis spectroscopy, see Figure 4.5. The reaction done at pH 6, 8 and 10 show a distinct peak at 400 nm, with an emerging peak at 600 nm. These two peaks correspond to π-π^* transition of benzenoid and exciton absorption of the quinoid in the polymer chain.[46, 71, 75] The absence of the absorbance peaks at 400 nm and 600 nm for pH 12 may have been caused by the overoxidation of aniline due to reactive radicals

produced in a water ozone reaction at basic pH. This result is in agreement with the FTIR results mentioned above where quinoid-benzoid ratio was found to be lower for PANI synthesized at a pH of 12. Due to destabilization of the dispersion, UV-vis spectra for the reactions performed at pH = 2 and pH = 4 could not be obtained in similar conditions.

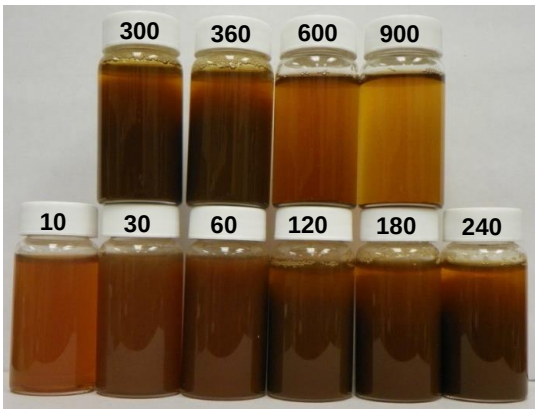

Figure 4.7. Vial images of the dispersions synthesized at various ozone exposure periods. (*Note: Ozone exposure in seconds on vials*)

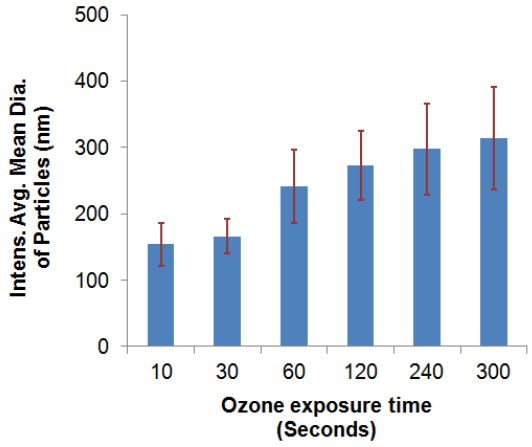

Figure 4.8. Effect of ozone exposure time on particle diameter of PANI SS.

The effect of ozone exposure time on the PANI synthesis was studied using SEM, UV-Vis and FTIR. Reactions were performed in ambient temperature with various ozone exposure durations from 10 seconds to 900 seconds. Stable dispersions of PANI SS were achieved until approximately 120 seconds of ozone exposure. Beyond 120 seconds the dispersions were

relatively unstable. Interestingly, particle size of the PANI SS increased with increasing ozone exposure time (Figure 4.8). This could be because with increase in the ozone exposure free aniline monomer and oligomers are getting oxidized even further, resulting in higher number of spheres which would increase the rate of agglomeration, resulting in larger spheres.

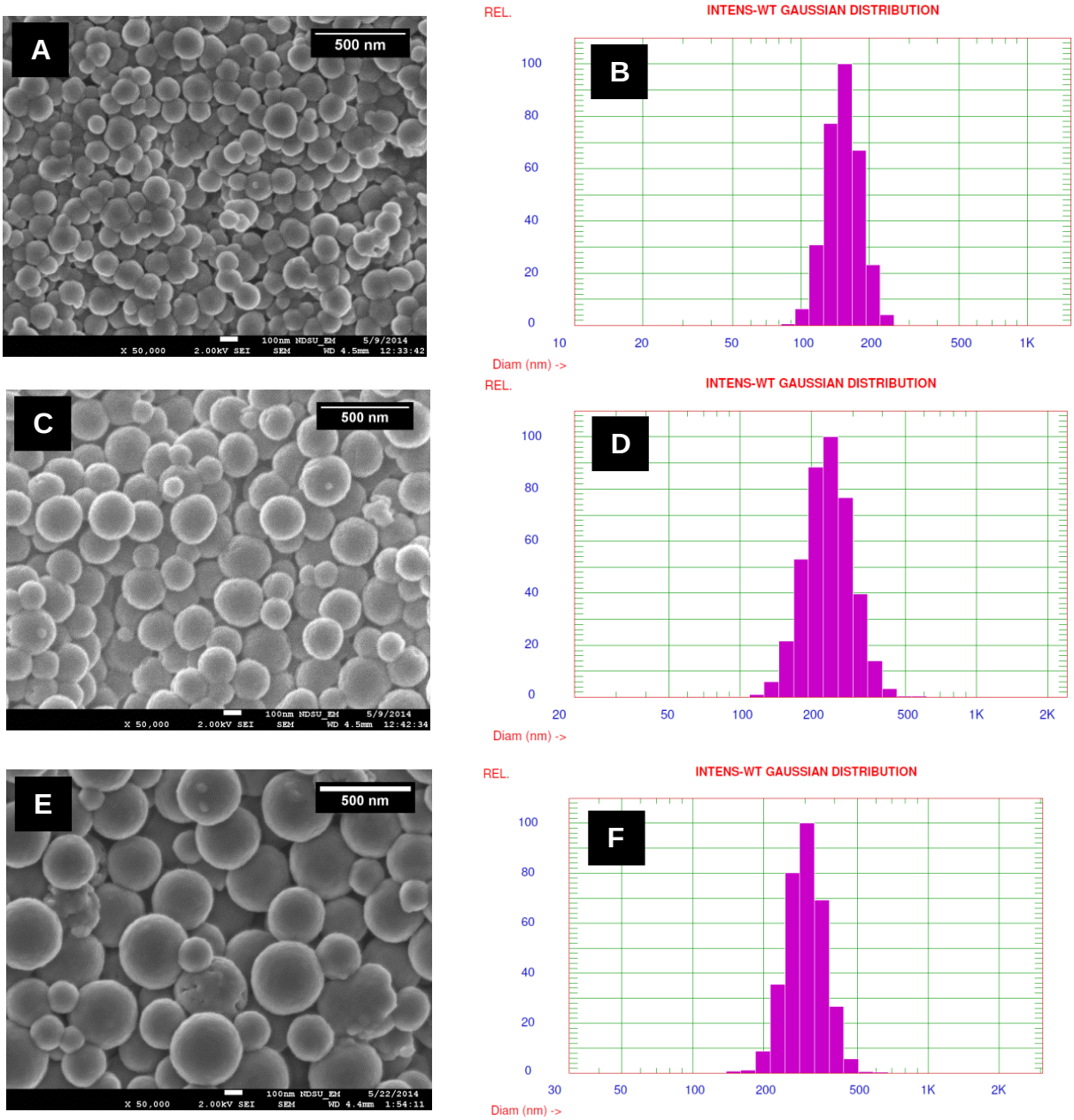

Figure 4.9. SEM images and dynamic light scattering results of PANI SS synthesized at various ozone exposure periods. A and B) 10 seconds; C and D) 30 seconds; E and F) 240 seconds.

Dynamic light scattering experiments (Figure 4.8 and Figure 4.9) show that the at 10 seconds of ozone exposure the particle diameter was about 150 nm, which increased up to 300 nm at 300 seconds of ozone exposure. These results compliment the analysis of the spheres via scanning and transmission electron microscopy (Figure 4.9). This increase size of the spheres may also be adversely affecting the stability of the dispersion (mentioned above) due to increased gravitational forces.

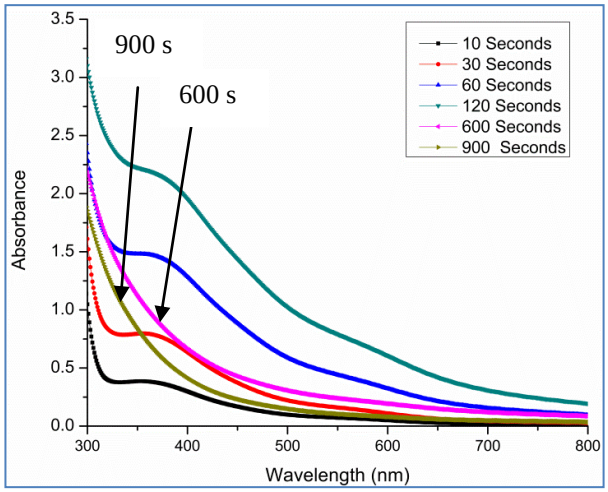

Figure 4.10. UV-Vis spectra of PANI dispersions synthesized at various ozone exposure periods.

High ozone exposure to aniline solution may overoxidize PANI and decrease the conjugation degree by incorporating more hydroxyl and carbonyl linkages on the PANI backbone. The FTIR spectra (Figure 4.11) for PANI did not change significantly with increase in the ozone exposure. However, the UV-Vis results (Figure 4.10) indicated that while the polaron/bipolaron absorbance peaks were present in the UV-vis spectra when ozone was exposed to the aniline solution up to 120 seconds; the polaron/bipolaron peaks were absent when ozone was exposed for 600 seconds and 900 seconds. This indicates the lack of conjugation in PANI when ozone is exposed to the aniline water solution for long periods.

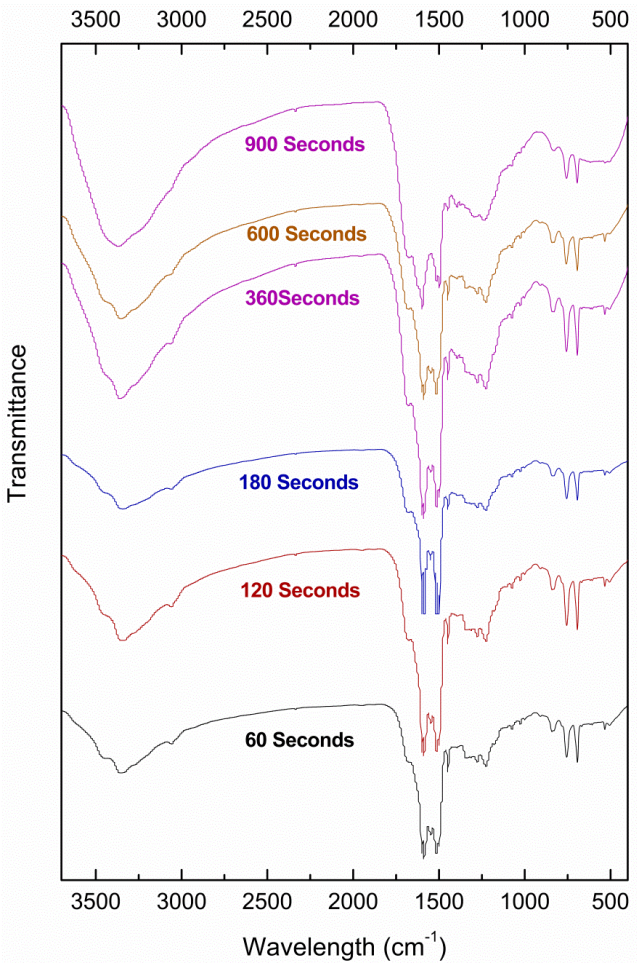

Figure 4.11. FTIR spectra of PANI dispersions synthesized at various ozone exposure periods.

4.4. Conclusion

Ozone was successfully used as an oxidant for the synthesis of stable polyaniline submicron sphere dispersions. Stable dispersions were achieved between pH of 6 and 10. The zeta potential of the as synthesized dispersion was -50 mV revealing the electrostatic repulsion mechanism for dispersion stability of PANI submicron spheres. FTIR and UV-Vis results indicated that the strong basic conditions are not suitable for the synthesis of PANI dispersions particularly because of higher ozone reactivity with water in basic conditions. Duration of ozone exposure was important in controlling the over-oxidation as well as particle size of PANI

submicron spheres. Higher ozone exposure resulted in the increase in the particle size as well as increase in the degree of overoxidation of PANI.

4.5. References

1. Kang, E., K. Neoh, and K. Tan, *Polyaniline: a polymer with many interesting intrinsic redox states.* Progress in Polymer Science, 1998. **23**(2): p. 277-324.
2. Pecher, J. and S. Mecking, *Nanoparticles of Conjugated Polymers.* Chemical reviews, 2010. **110**(10): p. 6260-6279.
3. Kulkarni, V.G., L.D. Campbell, and W.R. Mathew, *Thermal stability of polyaniline.* Synthetic Metals, 1989. **30**(3): p. 321-325.
4. Genies, E., et al., *Polyaniline: a historical survey.* Synthetic Metals, 1990. **36**(2): p. 139-182.
5. Bhadra, S., et al., *Progress in preparation, processing and applications of polyaniline.* Progress in Polymer Science, 2009. **34**(8): p. 783-810.
6. Huang, J., *Syntheses and applications of conducting polymer polyaniline nanofibers.* Pure and Applied Chemistry, 2006. **78**(1): p. 15-28.
7. Wei, Y., et al., *Polyaniline as corrosion protection coatings on cold rolled steel.* Polymer, 1995. **36**(23): p. 4535-4537.
8. McAndrew, T.P., et al. *Poly (aniline) in corrosion resistant coatings*. in *Polymer Material Science and Engineering Spring Meeting*. 1996. ACS Publications.
9. Wessling, B. and J. Posdorfer, *Corrosion prevention with an organic metal (polyaniline): corrosion test results.* Electrochimica Acta, 1999. **44**(12): p. 2139-2147.
10. Kraljic, M., Z. Mandic, and L. Duic, *Inhibition of steel corrosion by polyaniline coatings.* Corrosion Science, 2003. **45**(1): p. 181-198.

11. Huang, S.C., et al., *Polyaniline capacitors.* Synthetic Metals, 1993. **57**(1): p. 4047-4052.

12. Belanger, D., et al., *Characterization and long-term performance of polyaniline-based electrochemical capacitors.* Journal of the Electrochemical Society, 2000. **147**(8): p. 2923-2929.

13. Dong, B., et al., *Preparation and electrochemical characterization of polyaniline/multi-walled carbon nanotubes composites for supercapacitor.* Materials Science and Engineering: B, 2007. **143**(1-3): p. 7-13.

14. Shahinpoor, M., K.J. Kim, and M. Mojarrad, *Artificial muscles: applications of advanced polymeric nanocomposites*. 2007, Boca Raton, FL: Chapman & Hall/CRC. 480.

15. Tan, S., et al., *Polyaniline as a hole transport material to prepare solid solar cells.* Synthetic Metals, 2003. **137**(1-3): p. 1511-1512.

16. Chang, M.Y., et al., *Polymer solar cells incorporating one-dimensional polyaniline nanotubes.* Organic Electronics, 2008. **9**(6): p. 1136-1139.

17. Liu, Z., et al., *Polyaniline/TiO2 solar cells.* Synthetic Metals, 2006. **156**(9-10): p. 721-723.

18. Gaponik, N.P., D.V. Talapin, and A.L. Rogach, *A light-emitting device based on a CdTe nanocrystal/polyaniline composite.* Phys. Chem. Chem. Phys., 1999. **1**(8): p. 1787-1789.

19. Yang, Y. and Q. Pei, *Electron injection polymer for polymer light emitting diodes.* Journal of applied physics, 1995. **77**(9): p. 4807-4809.

20. Gustafsson, G., et al., *Flexible light-emitting diodes made from soluble conducting polymers.* Nature, 1992. **357**(6378): p. 477-479.

21. Yang, Y. and A. Heeger, *Polyaniline as a transparent electrode for polymer light emitting diodes: Lower operating voltage and higher efficiency.* Applied Physics Letters, 1994. **64**(10): p. 1245-1247.

22. Li, C. and R.H. Jung, *Polymer electrodes for energy storage devices and method of making same*. 1998, Motorola, Inc.

23. Gurunathan, K., et al., *Electrochemically synthesised conducting polymeric materials for applications towards technology in electronics, optoelectronics and energy storage devices.* Materials Chemistry and Physics, 1999. **61**(3): p. 173-191.

24. Wang, X., et al., *A facile route to ultra-long polyaniline nanowires and the fabrication of photoswitch.* Journal of colloid and interface science, 2009. **332**(1): p. 74-77.

25. Gupta, V. and N. Miura, *Large-area network of polyaniline nanowires prepared by potentiostatic deposition process.* Electrochemistry Communications, 2005. **7**(10): p. 995-999.

26. Huang, L., et al., *Polyaniline nanowires by electropolymerization from liquid crystalline phases.* J. Mater. Chem., 2002. **12**(2): p. 388-391.

27. Ma, Y., et al., *Polyaniline nanowires on Si surfaces fabricated with DNA templates.* Journal of the American Chemical Society, 2004. **126**(22): p. 7097-7101.

28. Bhadra, J. and D. Sarkar, *Self-assembled polyaniline nanorods synthesized by facile route of dispersion polymerization.* Materials Letters, 2009. **63**(1): p. 69-71.

29. Jiang, L. and Z. Cui, *One-step synthesis of oriented polyaniline nanorods through electrochemical deposition.* Polymer Bulletin, 2006. **56**(6): p. 529-537.

30. Zhang, Z. and M. Wan, *Nanostructures of polyaniline composites containing nano-magnet.* Synthetic Metals, 2003. **132**(2): p. 205-212.

31. Dhand, C., et al., *Preparation, characterization and application of polyaniline nanospheres to biosensing.* Nanoscale, 2010. **2**(5): p. 747-754.

32. Lei, Z., et al., *Structural evolution and electrocatalytic application of nitrogen-doped carbon shells synthesized by pyrolysis of near-monodisperse polyaniline nanospheres.* Journal of Materials Chemistry, 2009. **19**(33): p. 5985-5995.

33. Zhang, L. and P. Liu, *Polyaniline Micro/Nano Capsules via Facile Interfacial Polymerization Approach.* Soft Materials, 2010. **8**(1): p. 29-38.

34. Liu, P. and L. Zhang, *Hollow nanostructured polyaniline: Preparation, properties and applications.* Critical Reviews in Solid State and Material Sciences, 34, 2009. **1**(2): p. 75-87.

35. Cheng, Q., et al., *Surfactant-assisted polypyrrole/titanate composite nanofibers: Morphology, structure and electrical properties.* Synthetic Metals, 2008. **158**(21-24): p. 953-957.

36. Zhang, X., et al., *Inorganic/organic mesostructure directed synthesis of wire/ribbon-like polypyrrole nanostructures.* Chemical Communications, 2004(16): p. 1852-1853.

37. Meng, S., Z. Zhang, and M. Rouabhia, *Surfactant-templated crystalline polygon nanoparticles of heterocyclic polypyrrole prepared with Fenton's reagent.* Synthetic Metals, 2010. **160**(1-2): p. 116-122.

38. Stejskal, J., P. Kratochvíl, and M. Helmstedt, *Polyaniline dispersions. 5. Poly (vinyl alcohol) and poly (N-vinylpyrrolidone) as steric stabilizers.* Langmuir, 1996. **12**(14): p. 3389-3392.

39. Jackowska, K., A. Bieguński, and M. Tagowska, *Hard template synthesis of conducting polymers: a route to achieve nanostructures.* Journal of Solid State Electrochemistry, 2008. **12**(4): p. 437-443.

40. Xu, Q., et al., *Controlled fabrication of gold and polypyrrole nanowires with straight and branched morphologies via porous alumina template-assisted approach.* Materials Letters, 2009. **63**(16): p. 1431-1434.

41. Yoo, S.-H., L. Liu, and S. Park, *Nanoparticle films as a conducting layer for anodic aluminum oxide template-assisted nanorod synthesis.* Journal of Colloid and Interface Science, 2009. **339**(1): p. 183-186.

42. Pan, L., et al., *Conducting Polymer Nanostructures: Template Synthesis and Applications in Energy Storage.* International Journal of Molecular Sciences, 2010. **11**(7): p. 2636-2657.

43. Wei, M. and Y. Lu, *Templating fabrication of polypyrrole nanorods/nanofibers.* Synthetic Metals, 2009. **159**(11): p. 1061-1066.

44. Qiu, H., et al., *Conducting polyaniline nanotubes by template-free polymerization.* Macromolecules, 2001. **34**(4): p. 675-677.

45. Huang, K. and M. Wan, *Self-assembled polyaniline nanostructures with photoisomerization function.* Chemistry of Materials, 2002. **14**(8): p. 3486-3492.

46. Amarnath, C.A., et al., *Nanoflakes to nanorods and nanospheres transition of selenious acid doped polyaniline.* Polymer, 2008. **49**(2): p. 432-437.

47. Zhang, L. and M. Wan, *Self Assembly of Polyaniline—From Nanotubes to Hollow Microspheres.* Advanced Functional Materials, 2003. **13**(10): p. 815-820.

48. Liu, J. and M. Wan, *Synthesis, characterization and electrical properties of microtubules of polypyrrole synthesized by a template-free method.* Journal of Materials Chemistry, 2001. **11**(2): p. 404-407.

49. Wan, M. and J. Li, *Formation mechanism of polyaniline microtubules synthesized by a template free method.* Journal of Polymer Science Part A: Polymer Chemistry, 2000. **38**(13): p. 2359-2364.

50. Liang, L., et al., *Direct assembly of large arrays of oriented conducting polymer nanowires.* Angewandte Chemie, 2002. **114**(19): p. 3817-3820.

51. Zhang, Z., Z. Wei, and M. Wan, *Nanostructures of polyaniline doped with inorganic acids.* Macromolecules, 2002. **35**(15): p. 5937-5942.

52. Chiou, N.R., L.J. Lee, and A.J. Epstein, *Self-assembled polyaniline nanofibers/nanotubes.* Chemistry of Materials, 2007. **19**(15): p. 3589-3591.

53. Liu, J., et al., *Templateless assembly of molecularly aligned conductive polymer nanowires: a new approach for oriented nanostructures.* Chemistry–A European Journal, 2003. **9**(3): p. 604-611.

54. Park, M.C., Q. Sun, and Y. Deng, *Polyaniline microspheres consisting of highly crystallized nanorods.* Macromolecular Rapid Communications, 2007. **28**(11): p. 1237-1242.

55. Wei, Z., Z. Zhang, and M. Wan, *Formation mechanism of self-assembled polyaniline micro/nanotubes.* Langmuir, 2002. **18**(3): p. 917-921.

56. Zhang, L., et al., *Self Assembled Hollow Polyaniline/Au Nanospheres Obtained by a One Step Synthesis.* Macromolecular Rapid Communications, 2008. **29**(7): p. 598-603.

57. Gospodinova, N., et al., *Preparation and characterization of aqueous polyaniline dispersions.* European polymer journal, 1993. **29**(10): p. 1305-1309.

58. Stejskal, J., P. Kratochvíl, and A.D. Jenkins, *Polyaniline: forms and formation.* Collection of Czechoslovak chemical communications, 1995. **60**(10): p. 1747-1755.

59. Konyushenko, E.N., et al., *Polyaniline nanotubes: conditions of formation.* Polymer international, 2006. **55**(1): p. 31-39.

60. Stejskal, J., P. Kratochvil, and N. Radhakrishnan, *Polyaniline dispersions 2. UV--Vis absorption spectra.* Synthetic Metals, 1993. **61**(3): p. 225-231.

61. Stejskal, J., et al., *The genesis of polyaniline nanotubes.* Polymer, 2006. **47**(25): p. 8253-8262.

62. Stejskal, J., et al., *Oxidation of aniline: Polyaniline granules, nanotubes, and oligoaniline microspheres.* Macromolecules, 2008. **41**(10): p. 3530-3536.

63. Stejskal, J. and I. Sapurina, *On the origin of colloidal particles in the dispersion polymerization of aniline.* Journal of colloid and interface science, 2004. **274**(2): p. 489-495.

64. Yan, H., M. Kajita, and N. Toshima, *Polymerization of aniline using iron(III) catalyst and ozone, and kinetics of oxidation reactions in the catalytic system.* Macromolecular Materials and Engineering, 2002. **287**(8): p. 503-508.

65. Buehler, R.E., J. Staehelin, and J. Hoigne, *Ozone decomposition in water studied by pulse radiolysis. 1. Perhydroxyl (HO_2)/hyperoxide (O_2^-) and HO_3/O_3^- as intermediates.* The Journal of Physical Chemistry, 1984. **88**(12): p. 2560-2564.

66. Staehelin, J. and J. Hoigne, *Decomposition of ozone in water: rate of initiation by hydroxide ions and hydrogen peroxide.* Environmental Science & Technology, 1982. **16**(10): p. 676-681.

67. Johnson, D.C., D.T. Napp, and S. Bruckenstein, *Electrochemical reduction of ozone in acidic media.* Analytical Chemistry, 1968. **40**(3): p. 482-488.

68. Blinova, N.V., et al., *Polyaniline and polypyrrole: A comparative study of the preparation.* European polymer journal, 2007. **43**(6): p. 2331-2341.

69. Stejskal, J., et al., *Polyaniline dispersions. 6. Stabilization by colloidal silica particles.* Macromolecules, 1996. **29**(21): p. 6814-6819.

70. Yu, L., et al., *Preparation of aqueous polyaniline dispersions by micellar-aided polymerization.* Journal of Applied Polymer Science, 2003. **88**(6): p. 1550-1555.

71. Chen, S.A. and H.T. Lee, *Structure and properties of poly (acrylic acid)-doped polyaniline.* Macromolecules, 1995. **28**(8): p. 2858-2866.

72. Trchova, M., et al., *FTIR spectroscopic and conductivity study of the thermal degradation of polyaniline films.* Polymer Degradation and Stability, 2004. **86**(1): p. 179-185.

73. Sapurina, I.Y. and M. Shishov, *Oxidative Polymerization of Aniline: Molecular Synthesis of Polyaniline and the Formation of Supramolecular Structures, New Polymers for Special Applications*. 1 ed. 2012: InTech. 366.

74. Trchová, M. and J. Stejskal, *Polyaniline: The infrared spectroscopy of conducting polymer nanotubes (IUPAC Technical Report).* Pure & Applied Chemistry, 2011. **83**(10): p. 1803-1817.

75. Nguyen, M.T., et al., *Synthesis and properties of novel water-soluble conducting polyaniline copolymers.* Macromolecules, 1994. **27**(13): p. 3625-3631.

CHAPTER 5. TEMPLATE FREE METHOD FOR THE SYNTHESIS OF AG-PPY CORE-SHELL NANOSPHERES WITH INHERENT COLLOIDAL STABILITY

(Published as "Template free method for the synthesis of Ag–PPy core–shell nanospheres with inherent colloidal stability." *Synthetic Metals*197 (2014): 134-143)

5.1. Abstract

Stable aqueous dispersions of silver-polypyrrole core shell nanospheres have been synthesiszed using a template free method, utilizing the oxidative capabilities of ozone and silver nitrate. The core shell nanospheres possess antibacterial and electroactive properties. Silver nanoparticles which are produced due to reduction of silver nitrate by pyrrole provide sites for the nucleation and growth of the polypyrrole shell. The morphology of the nanospheres was studied using electron microscopy and dynamic light scattering, while X-ray photoelectron spectroscopy, Fourier transform infrared spectroscopy and UV VIS spectroscopy were used to study the chemical structure of the nanospheres. The electrochemical activity and thermal stability of the core-shell morphology has been studied using cyclic voltammetry and thermogravimetric analysis respectively. The core-shell nanospheres were studied for their antibacterial properties on *Pseudomonas putida* KT2440. The nanospheres reduced the viability of the strain as well as inhibited its growth.

Keywords: polypyrrole, core-shell, dispersion, nanospheres, antibacterial activity

5.2. Introduction

Advanced applications demand for optimized properties, consequently driving interest in the research areas dealing with heterogeneous materials. Core-shell nanostructures are one of such heterogeneous materials, with interesting properties derived from both the core and shell, and has prospective applications in several fields including drug delivery, catalysis, and

electronics[1]. Core-shell morphology also helps in mitigating difficulties associated with the processing of the nanostructures, encapsulating them inside a material which can be easily processed. Furthermore, the core-shell morphology with core of inorganic nanoparticles and shell of conducting polymers in particular can be used in sensors,[2, 3] semiconductor devices,[4] batteries[5, 6] and corrosion protection.[7, 8]

The core-shell morphologies of inorganic nanoparticles and conducting polymers have been synthesized for two reasons; one of which involves use of nanoparticles as a template for guiding synthesis of the conducting polymeric nanostructures (CPN),[9, 10] while the other is to fine tune the properties of the composite by utilizing properties of both conducting polymers and the inorganic nanoparticles.[11, 12] In the former strategy, either the CPN is recovered after removal of the template or the composite is used without the removal of the inorganic template.[9, 10, 13] In the latter case, the composite is characterized for advanced properties arising from the blend of the inorganic nanostructures and the organic conducting polymers. Several core-shell morphologies have been synthesized over the years. The conducting polymers often used are polypyrrole (PPy) and polyaniline (PANI), owing to their stability towards various environmental conditions, and the inorganic core of the composites have been various metals and metal oxides.[14, 15] This combination may help in fine tuning the thermal and electrical properties of the composites with respect to the application, by changing the dimensions of the core or the shell.[1]

The synthesis of such core-shell morphologies where conducting polymers are the shell becomes a challenge, mainly because of the insolubility of conducting polymers in many solvents.[16] The synthesis of stable aqueous dispersion of such morphologies is even more challenging due to the agglomeration of the particles due to van der Waals forces. More often, to

prevent agglomeration, colloidal stabilizers such as polyvinyl pyrrolidone (PVP) and polyvinyl acetate (PVA) are used. Wang and coworkers synthesized silver/PPy core shell nanostructures by one step hydrothermal reaction of pyrrole and silver nitrate using PVP as a colloidal stabilizer.[17] UV radiation was used in the presence of PVP and silver nitrate for synthesizing PPy coated silver nanoparticles in another report.[18] Interfacial polymerization in the presence of PVP was also utilized to synthesize core-shell nanostructures of silver and PPy.[19] Fujii *et al.* reported the synthesis of core shell morphologies of PPy and silver using PVA as a colloidal stabilizer.[20] This group further synthesized PANI-silver nanocomposites using PVA as a stabilizer.[21] However, it should be noted that the use of stabilizer for preparing stable suspensions might increase the cost of the synthesis and it may also change the properties of the synthesized nanostructures. Thus template free methods are highly desirable in which surfactant is not used for either the synthesis or the stabilization of the nanostructures.

Literature reveals only a few reports on the synthesis of core-shell morphologies of PPy and silver including those mentioned above, the template free method for synthesis of stable aqueous dispersions of core-shell morphologies of silver-PPy were not observed in the literature. Several other reports have been devoted to the study of nanocomposite formation with silver nanoparticles embedded in PPy or PANI matrix.[18, 22-27] A convenient template free route to synthesize core-shell silver-PPy nanoparticles was reported earlier, which unfortunately required hydrothermal conditions for the synthesis.[17, 25] Furthermore, previously described template free methods do not report aqueous dispersion stability and uniform morphology of silver-PPy nanostructures. It is important to note that the commercially viability of the nanostructures is derived from ease in processing, uniform morphology and convenient synthesis method. A

simple template free synthesis method is introduced in this study to synthesize aqueous dispersions of Ag-PPy core shell nanospheres.

Previously we have synthesized stable dispersions of PPy nanospheres, with uniform morphology and narrow size distribution, using ozone oxidation (Chapter 2).[28] Here, we present the template free synthesis of core-shell nanospheres (CSNs) of silver/PPy with the core as silver and the shell as PPy utilizing simple ozone oxidation. The silver nanoparticles are obtained *in-situ* by reduction of silver nitrate with pyrrole. The synthesized CSNs possess uniform spherical morphology with stability against agglomeration. The synthesized nanostructures are characterized using electron microscopy (EM), Fourier transform infrared spectroscopy (FTIR), X-Ray Photoelectron Spectroscopy (XPS) UV-visible spectroscopy (UV-VIS), cyclic voltammetry (CV) and thermogravimetric analysis (TGA). One of the most common applications of silver nanoparticles is for bacterial disinfection. It is well known that silver nanoparticles and free silver ions provide antibacterial properties by either adhering to the surface of the bacteria or by penetrating into the bacteria cell thereby damaging DNA.[29] Thus, antibacterial properties (growth inhibition and toxicity) of the CSNs containing silver nanoparticles in the core were studied on *Pseudomonas putida* KT2440. It is believed that this method can be extended to the synthesis of more such morphologies, varying the core from silver to other metal nanoparticles such as gold and palladium while varying the shell from PPy to other conducting polymers.

5.3. Materials and methods

Silver nitrate and pyrrole were obtained from Sigma Aldrich. Silver nitrate was used as received and pyrrole was distilled before use. A 1 M solution of silver nitrate and a 0.1 M solution of pyrrole were prepared, in Millipore water, in separate flasks. ATLAS 30 C ozone

generator, supplied by Absolute Ozone was used for obtaining ozone. Pure dried oxygen was supplied to the ozone generator at a pressure of 20 psi and flow rate of 0.2 L/min. According to the literature provided by Absolute Ozone this flow rate should produce oxygen/ozone mixture with 18% ozone by weight. Reactions were performed in a 125 ml Erlenmeyer flask at room temperature.

Ozone was bubbled through 100 ml of 0.1 M pyrrole solution (0.675 gm of pyrrole in 100 ml Millipore water) for 60 seconds under constant stirring. After the ozone exposure was complete excess ozone was removed by gently blowing a stream of air from compressed air line. Immediately after this, 1 M silver nitrate solution was added to the flask. The quantity of the silver nitrate solution was varied from 1 ml to 6.37 ml in various reactions (Table. 5.1). The reactions were kept stirring for 24 hours. The characterization of the sample was performed after 72 hours of the reactions. Table 5.1 lists the reactions performed with quantities of reactants used in each reaction. For example, for reaction R-1, ozone was bubbled for 60 seconds through 0.1 M, 100 ml solution of pyrrole in Millipore water at room temperature. Excess ozone was removed from the reaction after the completion of ozone exposure, using a gentle blow of air-stream from compressed air line. Immediately after this, 6.37 ml of 1 M silver nitrate solution was added to the flask. The reactions were performed while stirring at room temperature, and stirring was continued for 24 hours.

Particle size measurements were carried out using a NICOMP 380 submicron particle sizer supplied by Particle Sizing Systems. UV-Vis spectra of the CSNs in water were recorded on a Varian-5000 UV-Vis-NIR spectrophotometer. A Nicolet FTIR spectrometer was used for the FTIR characterization. Thermal analysis of the samples was performed using a thermogravimetric analysis instrument TGA Q 500 supplied by TA Instruments. The samples

were heated from room temperature to 800˚C at a heating rate of 20˚C/min. Samples were prepared for scanning electron microscopy (SEM) by sprinkling centrifuged and dried particles onto carbon tape attached to aluminum mounts. The sample was then coated with gold using a Balzers SCD 030 sputter coater. Images were obtained using a JEOL JSM-7600F Scanning Electron Microscope. Magnification, accelerating voltage values, and scale bars are listed in each figure. For the transmission electron microscopy (TEM) images, 300-mesh Formvar/carbon-coated grids were dipped into the solution containing the particles and immediately wicked off using filter paper. After the grid was allowed to dry, images were obtained using a JEOL JEM-100CX II transmission electron microscope at 80 keV. The cyclic voltammetry (CV) was performed using Gamry instrument framework, with Ag/AgCl reference electrode, and a platinum counter electrode. A 1.5 M HCl solution was used as an electrolyte. The dispersion was drop-coated on the platinum electrode. The XPS measurements were performed on an SSX-100 system (Surface Science Laboratories, Inc.) equipped with a monochromated Al K_α X-ray source, a hemispherical sector analyzer (HSA) and a resistive anode detector. The base pressure of the XPS system was 4.0×10^{-10} Torr. During the data collection, the pressure was ca. 1.0×10^{-8} Torr. Each sample was mounted on a piece of Al sticking tape on a separate sample holder to avoid cross contamination during sample handling. Care was taken to ensure the surface was fully covered with a sufficiently thick layer of the samples. All samples were nonconductive, and a low-energy electron beam (5 eV) was applied for charge neutralization. The X-ray spot size was 1×1 mm^2, which corresponded to an X-ray power of 200 W. The survey spectra were collected using 8 scans for each at 150 eV pass energy and 1 eV/step. The high resolution spectra were collected using 50 eV pass energy and 0.1 eV/step. Chlorine was seen in the samples after CV and Cl 2p high resolution scans were

also collected. It should be noted that the two peaks after curve fitting were Cl $2p_{1/2}$ and Cl $2p_{3/2}$, rather than two different Cl chemical states. The atomic percentages were calculated from the survey spectrum using the ESCA 2005 software provided with the XPS system. For high resolution data, the lowest binding-energy C 1s peak (presumably, C-C/C-H peak) was set at 285.0 eV and used as the reference for all of the other elements. The curve fitting used a combination of Gaussian/Lorenzian function with the Gaussian percentages being at 80% or higher.

The silver nanoparticles were tested for their antibacterial activity on *Pseudomonas putida* KT2440 (ATCC 47054). The culture was cultivated overnight at 37°C in 10 ml of Luria-Bertani (LB; 1% tryptone, 0.5% NaCl, 1% yeast extract) medium; after that, 1 ml of the culture was put into 200 ml of LB medium and it was shaken at 37°C for another 16 h. The bacteria were then pellitized and re-suspended in phosphate buffer saline (PBS) solution before the optical density at 600 nm (OD_{600}) of the cell suspension was adjusted to obtain the bacterial number equal to 10^6 colony forming units (CFU)/ml. Two types of tests were performed: the growth inhibition test and the toxicity test. For the growth inhibition test, 39 ml of the LB medium containing 10 mg of Ag/l of Ag/PPY nanoparticles was prepared in a bottle before adding 1 ml of the cell suspension. The bottle was shaken at room temperature (20°C) and 125 rpm for 24 h. At a sampling time, 100 µl of sample was taken to determine for the viability by the standard plate count method. The effects of Ag/PPY nanoparticles were compared with other two samples: the sample containing 10 mg/l of PPY nanoparticles and the sample containing 10 mg-Ag/l of bare silver nanoparticles synthesized from the method by Choi et al. [30]. In addition, a control sample having only cell suspension and LB medium was tested. For the toxicity test, 10 ml of the cell suspension was added to 30 ml of PBS solution containing 10 mg-Ag/ml of the

nanoparticles. The conditions of the experiment were as same as in the experiments for growth inhibition. The effects of Ag/PPy nanoparticles were also compared with the PPy nanoparticles, the bare Ag nanoparticles, and the control.

5.4. Results and discussion

Silver nitrate by itself is a poor oxidant for PPy synthesis with low oxidation potential which leads to longer reaction times[18] (Appendix Figure 1A). UV radiation and heat have been previously used to increase the rate of the reaction between pyrrole and silver nitrate to produce Ag-PPy nanocomposites.[17, 18] Initially, in order to increase the reaction rate, ozone was used as a co-oxidant in the synthesis, along with silver nitrate. Ozone oxidized pyrrole to PPy, while silver nitrate reduced itself to silver nanoparticles in the presence of pyrrole and pyrrole oligomers, leading to the formation of Ag-PPy nanocomposites (Appendix Figure 2A).

Table 5.1. Reaction Summary

Reaction	100 ml pyrrole Solution	Ozone exposure duration (Seconds)	1 M $AgNO_3$ Solution	Molarity of $AgNO_3$ in final reaction solution (M)
R-1	0.1 M	60	6.37 ml	0.060
R-2	0.1 M	60	4.25 ml	0.040
R-3	0.1 M	60	2.12 ml	0.020
R-4	0.1 M	60	1.50 ml	0.015
R-5	0.1 M	60	1.00 ml	0.010
R-6	0.1 M	60	--	--
R-7	0.1 M	--	4.25 ml	0.040
R-8	0.1 M	60	1.00 ml	0.010 (Addition after 5 minutes of ozone exposure)
R-9	0.1 M	60	1.00 ml	0.010 (Addition after 10 minutes of ozone exposure)
R-10	0.1 M	60	1.00 ml	0.010 (Addition after 30 minutes of ozone exposure)
R-11	0.1 M	60	1.00 ml	0.010 (Addition after 60 minutes of ozone exposure)

A basic procedure involved exposure of ozone to pyrrole solution in water, followed by addition of silver nitrate in the ozone exposed solution. Silver nitrate is added after ozone

exposure to make sure that the silver nanoparticles synthesized after reduction of silver nitrate by pyrrole is not in direct contact with ozone. If silver nitrate were added before the ozone exposure, silver nanoparticles formed by reduction of silver nitrate could have been oxidized to silver oxides. This thought process was explored to synthesize CSNs of silver and PPy. We have previously reported the use of ozone in the synthesis of uniform aqueous dispersion of PPy nanospheres.[28] The silver nitrate concentration was varied from 0.01 to 0.06 M, at 0.1M concentration of pyrrole and 60 seconds of ozone exposure (Table 5.1). The reaction without ozone oxidation produces agglomerated black powder after seven days of reaction time with low yield (Appendix Figure 1A).

In the synthesis of CSNs by template free methods, it is crucial to achieve uniform morphology by carefully controlling the concentration of each material. The concentration of core and shell materials should be such that the shell polymer covers the core inorganic nanostructures completely. In template based methods this issue is taken care by the amount of stabilizers that is used in the synthesis. The stabilizers such as PVP and PVA provide sites and templates, in the form of micelles for the nanostructure growth.[24]

However in template free synthesis methods, increasing quantity of shell material might result in formation of CSNs with more than one core nanoparticles embedded in a shell. Similarly, if core amount is more than the shell material, the shell material may not be sufficient to cover all the core nanoparticles, resulting in agglomeration of the nanoparticles to form nanocomposites (Appendix Figure 2A). This was evident from the TEM images (Figure 5.1) of the synthesized CSNs. Figure 5.1: A and B shows the TEM images of the reaction R -5, with 0.01 M concentration of silver nitrate, it can be observed that a single polyprrole shell contains

more than one silver nanoparticle. While in Figure 5.1: E and F the concentration of silver nitrate is 0.02, the agglomeration of PPy nanospheres was seen with silver nanoparticles embedded in it.

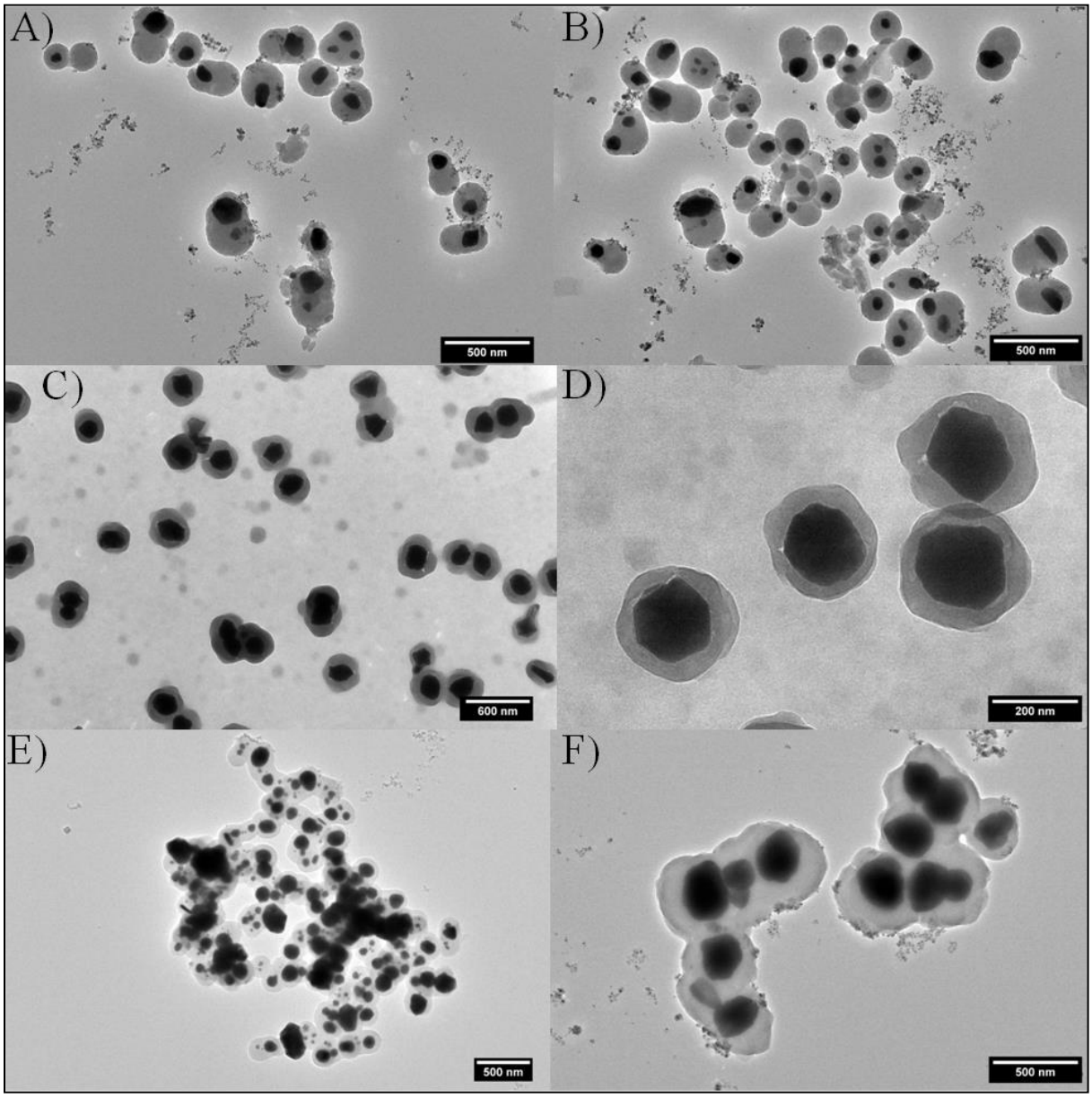

Figure 5.1. TEM Images of the PPy CSNs A & B) at 0.01 M silver nitrate concentration C & D) at 0.015 M silver nitrate concentration E & F) at 0.02 M silver nitrate concentration.

The optimum concentration of silver nitrate was 0.015 M (Figure 5.1: C and D), wherein every silver nanoparticle was observed to be coated with PPy. The shell thickness was 60 – 80

nm, while the core diameter was 150-200 nm. Higher concentration of silver nitrate resulted in the instability of dispersion and agglomeration of the nanocomposites (Appendix Figure 1A, Figure 2A, and Figure 3A C-E). The morphology of the nanospheres was also studied using dynamic light scattering and electron microscopy. Uniform spherical morphology and relatively narrow particle size distribution of CSNs was observed at 0.01M and 0.015 M silver nitrate concentrations (Appendix Figure 3A and Figure 5A).

XPS was performed on Ag-PPy CSNs ($AgNO_3$ 0.01M) (Figure 5.2A). Atom % detected for carbon, nitrogen, oxygen and silver were 76.85%, 14.511%, 8.426% and 0.206% respectively. Lower value of atom % of silver could be due to effectiveness of XPS for the depths of only about 10 nm from the surface of the sample. High resolution C1s, N1s, O1s and Ag3d scans are shown in Figure 5.2 (B-E) respectively.

In the C1s spectra (Figure 5.2B) the main peak at approximately 284.9 eV could correspond to C-H and C-C groups in PPy backbone, while the smaller peak at approximately 288.4 eV could correspond to C-OH, COO^- because of overoxidation of PPy.[31-34] The peaks at even higher binding energies of 291.7 eV could correspond to C-N or C-N^+. [33, 34] In the N1s spectra (Figure 5.2C) two major peaks were observed at approximately 400.4 eV and 398.9 eV which could be attributed to –NH and –N^+ groups respectively.[31, 33-35] The primary reason behind presence of oxygen in XPS survey scans could be due to overoxidation of PPy backbone; the peaks observed at around 532.28 in the O1s spectra (Figure 5.2D) could be due to C=O groups.[32, 33, 36] Two peaks were detected in the Ag3d spectra (Figure 5.2E) for silver at 374.8 eV and 368.7 eV which could correspond to Ag^0; [37-39] literature also reveals binding energies for Ag^0 of around 374 eV and 367.9 eV, [40-43] the positive shift of 0.8 eV in the two peaks may be because of the interactions between Ag and PPy.[44]

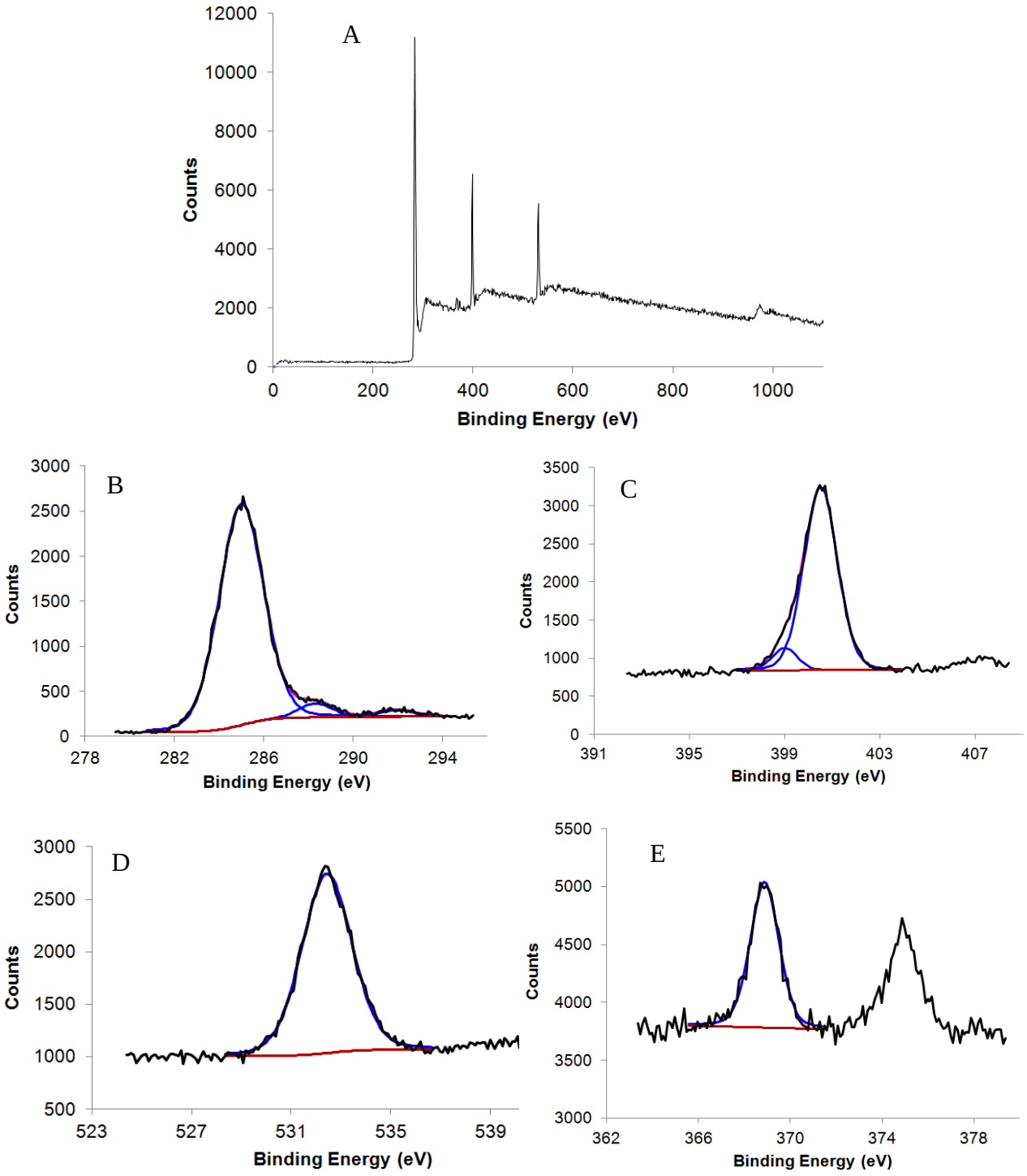

Figure 5.2. A) XPS survey scans for Ag-PPy CSNs (0.01M $AgNO_3$), B) C1s spectra Ag-PPy CSNs, C) High resolution N1s spectra Ag-PPy CSNs, and D) High resolution O1s spectra Ag-PPy CSNs E) High resolution Ag3d spectra Ag-PPy CSNs.

XPS experiment, in conclusion, confirms formation of PPy which could possibly be in the doped form due to presence of $–N^+$ groups. The presence of COO^-, C=O and C-OH groups due to overoxidation could be contributing to the stability of Ag-PPy CSNs against agglomeration. Although a detailed investigation of the stability mechanism is required, the presence of carboxylic anions on the periphery of Ag-PPy CSNs indicates possible electrostatic stability mechanism, in addition to the steric hindrance rendered by overoxidized PPy oligomers.

FTIR spectroscopy (Figure 5.3) was performed to study the effect of silver nitrate concentration on PPy synthesis, strong nitrate doping vibrations were observed at approximately 1385 cm^{-1} with the incorporation of silver nitrate in the reaction.[18, 45]

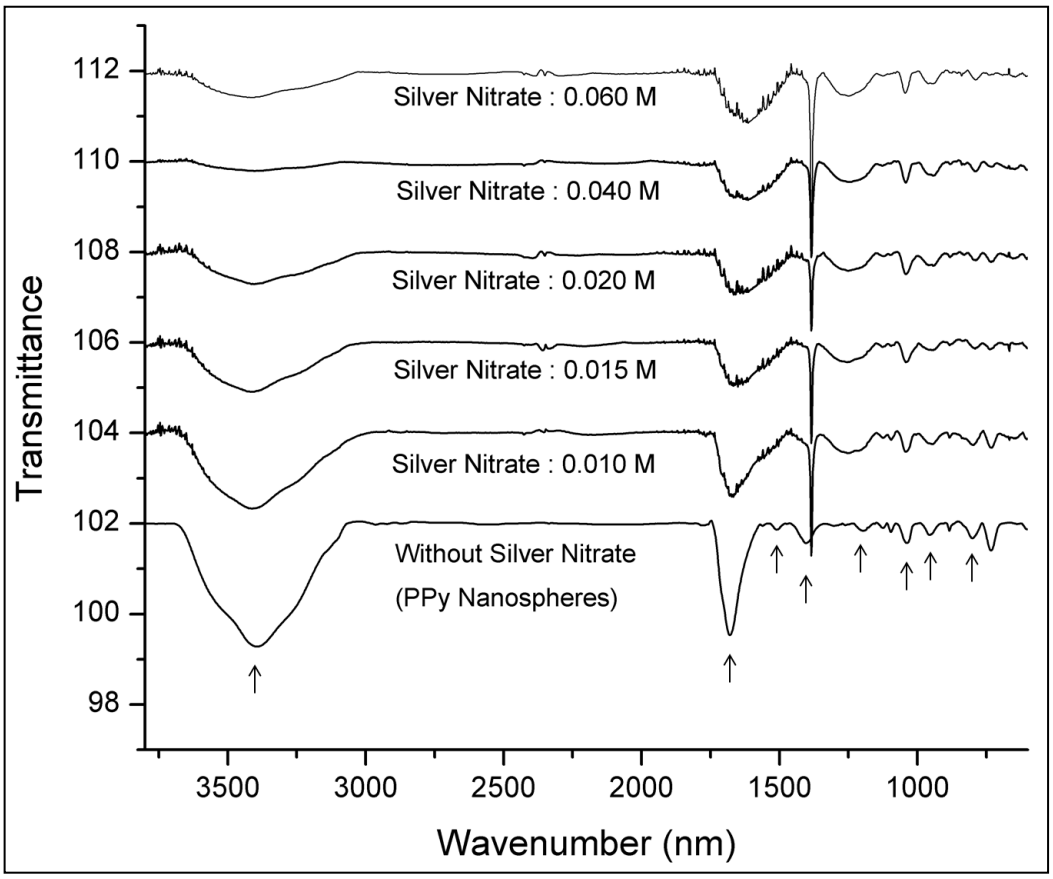

Figure 5.3. FTIR Spectrum of the reaction products with silver nitrate and without silver nitrate.

The characteristic bands present at approximately 770 cm^{-1} and 880 cm^{-1} might be ascribed to the C-H and C-C out of plane deformations, while the band present at approximately 1090 cm^{-1} may correspond to C-H in plane vibrations.[23, 46-49] The bands present at approximately 3400 cm^{-1} may be assigned to N-H stretching in PPy.[50] The characteristic bands that might correspond to C-N stretching vibrations and carbonyl linkages vibrations were observed to be shifted from 1374 cm^{-1} to 1273 cm^{-1} and from 1668 cm^{-1} to 1615 cm^{-1} respectively.[23, 51, 52] The blue shift of the characteristic bands to lower wavenumbers with increase in silver nitrate concentration is attributed to the interaction between PPy and silver.[52] The stabilizers or polymers interacting with metal nanoparticles often show such shifts owing to the conformation rearrangements.[53-55]

UV Vis spectroscopy (Figure 5.4) was performed on silver dispersions, CSNs and the PPy nanospheres to analyze the core shell morphology and the π-π^* transitions. At the lowest concentration of silver nitrate (0.01 M), most of the silver nanoparticles were coated by PPy (Figure 5.1 A & B), therefore, the peak for silver dispersion at approximately 400 nm was not observed in CSNs. On the other hand, similar peaks were observed for PPy nanospheres (without silver nitrate) and CSNs at approximately 460 nm, indicating that the silver/PPy core shell morphology was indeed synthesized. These peaks at 460 nm could correspond to π-π^* transition in PPy.[19, 24, 56] Increasing silver nitrate concentration did not seem to have adverse effect on electronic transition in PPy, however, the peak intensity at 600 nm increased with increase in silver nitrate concentration, this behavior is attributed to the increase in doping level of PPy.[57]

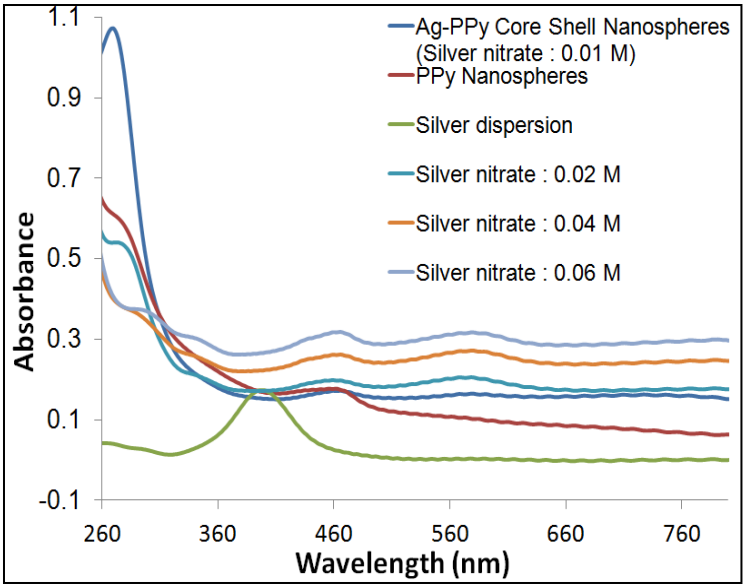

Figure 5.4. UV-Vis Spectroscopy of the CSNs, silver dispersion and PPY nanospheres without silver nitrate.

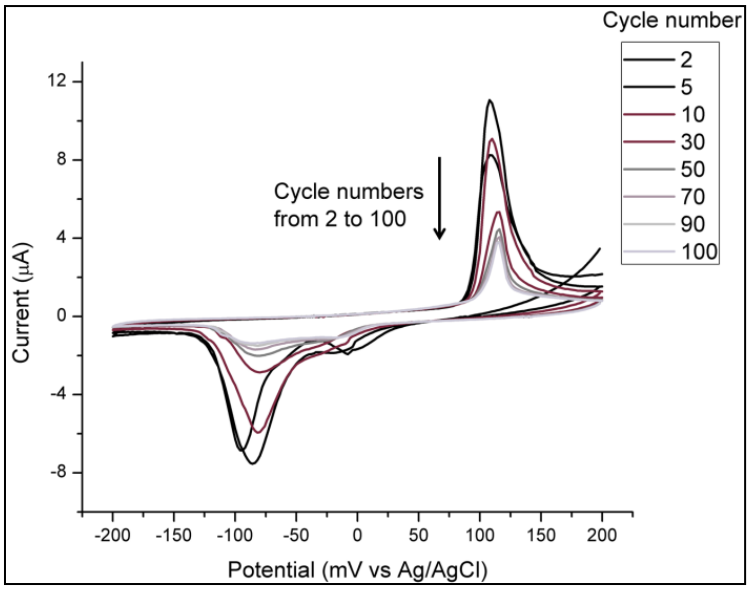

Figure 5.5. Cyclic voltammogram of CSNs showing the decrease in current peaks with increase in cycle numbers ($AgNO_3$ = 0.01 M).

Cyclic voltammetry was performed on the CSNs as well as on the PPy nanospheres (without silver nitrate) in HCl solution as an electrolyte against Ag/AgCl reference electrode. PPy nanospheres show oxidation and reduction peak approximately at 140 mV and -40 mV respectively, while the CSNs show oxidation and reduction peaks at approximately 120 mV and

-80 mV (Figure 5.6). The reversible redox peaks of Ag/Ag+ are situated around 57 mV (vs Ag/AgCl)[58], the shift in the peak of CSNs could be attributed to the electronic interaction between PPy and silver nanoparticles.[58]

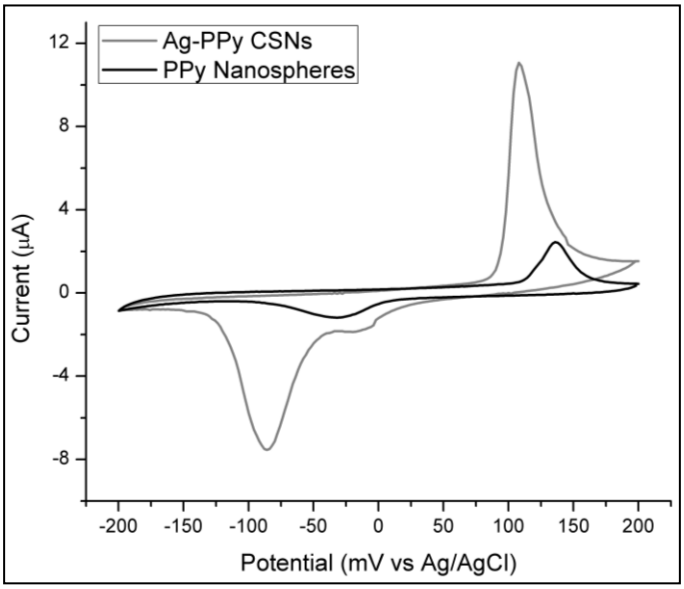

Figure 5.6. Cyclic voltammogram of CSNs ($AgNO_3$ = 0.01 M) and PPy nanospheres showing change in the peak location due to interaction between PPy and silver.

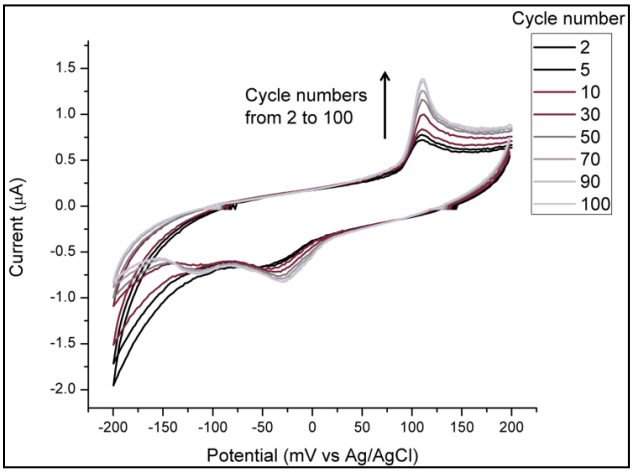

Figure 5.7. Cyclic voltammogram of silver/PPY nanocomposites showing the increase in the current peaks due to penetration of electrolyte through the composite ($AgNO_3$ = 0.06 M).

It was also observed that the peak intensity of the CSN decreased with the increase in cycle numbers due to the reduction in redox activity of PPy in the shell (Figure 5.5). However, in the nanocomposites (Figure 5.7) with silver nanoparticles embedded in the matrix (not core-shell morphology), the anodic and cathodic peak intensity was observed to be increasing. This could be due to increased exposure of the electrolyte to the silver nanoparticles embedded in the composite with increase in number of cycles. Near the 90^{th} cycle, it was observed that the peak intensities remained almost constant indicating complete penetration of the electrolyte through the PPy matrix. In order to confirm this observation XPS was performed on these samples before and after cyclic voltammetry (Appendix Figure 6A A-D and Table 1A). Atom % of silver was observed to increase from 0.206% to 2.027% after cyclic voltammetry for Ag-PPy CSNs, whereas much larger increase in atom % of silver was observed for Ag-PPy nanocomposites from 0.326% to 4.581%.

Scheme 5.1. Oxidation of pyrrole to PPy and reduction of silver cation to silver.

The mechanism of the formation of core-shell morphology could be attributed to the hydrophobicity of silver nanoparticles synthesized in-situ during the reaction (Figure 5.8). It is likely that the fast nucleation of the PPy chains by ozone oxidation and reduction of the silver nitrate to silver nanoparticles occur concurrently. Un-reacted pyrrole and pyrrole oligomers may reduce Ag^{+} (silver nitrate) to Ag^{0} (silver nanoparticles) (Scheme 5.1).

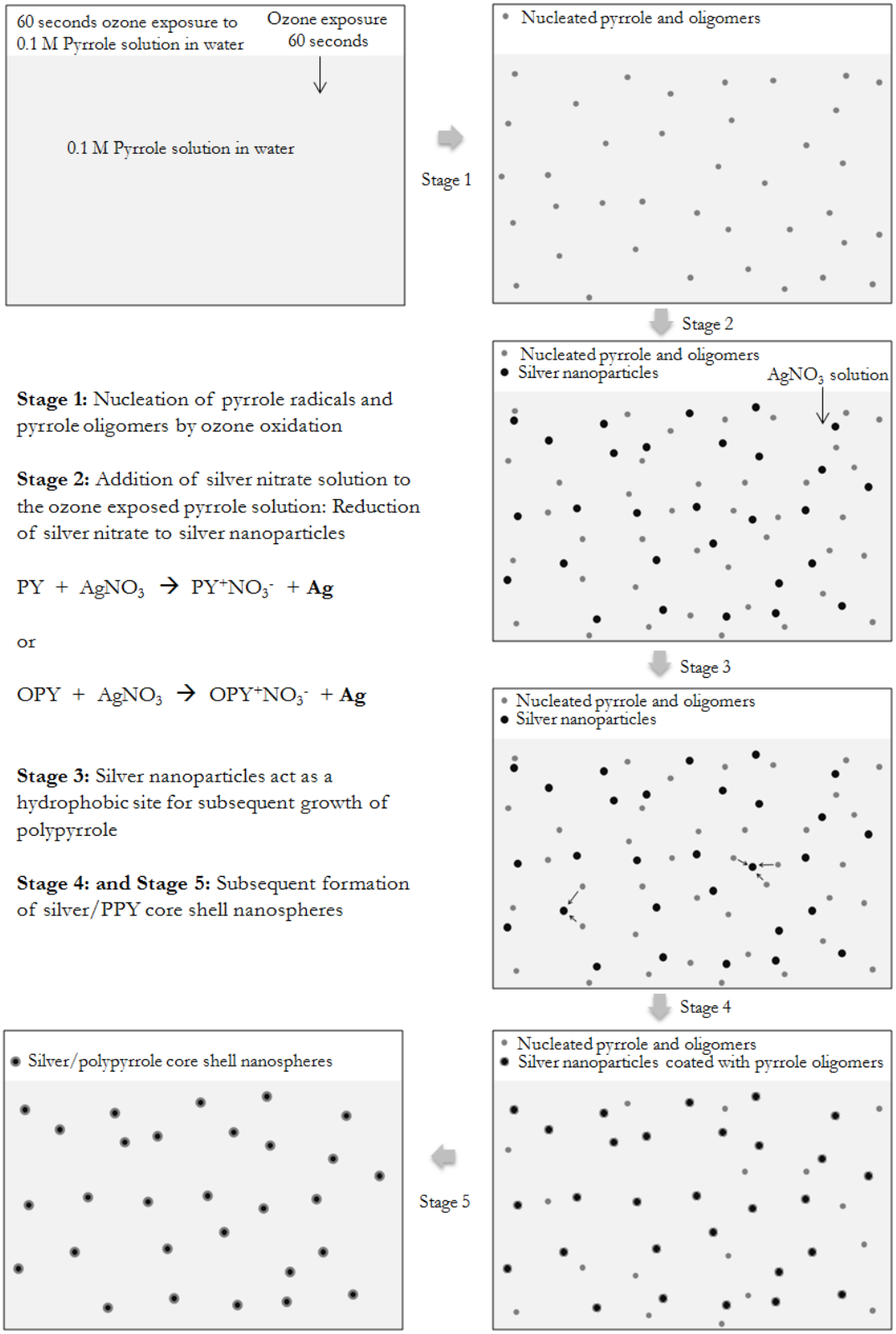

Stage 1: Nucleation of pyrrole radicals and pyrrole oligomers by ozone oxidation

Stage 2: Addition of silver nitrate solution to the ozone exposed pyrrole solution: Reduction of silver nitrate to silver nanoparticles

$PY + AgNO_3 \rightarrow PY^{+}NO_3^{-} + \mathbf{Ag}$

or

$OPY + AgNO_3 \rightarrow OPY^{+}NO_3^{-} + \mathbf{Ag}$

Stage 3: Silver nanoparticles act as a hydrophobic site for subsequent growth of polypyrrole

Stage 4: and Stage 5: Subsequent formation of silver/PPY core shell nanospheres

Figure 5.8. Representation of hypothesized mechanism for Silver/PPy core shell morphology.

The hydrophobic nature of the silver nanoparticles may be providing the sites for nucleation and further growth of the PPy shell.[50] The metal-π interactions between silver and PPy may also be prevalent in the initial deposition of PPy on silver nanoparticles. As explained earlier, the uniformity in the core shell morphology could be dependent on the silver nitrate concentration. The critical parameter could also be addition time of silver nitrate after ozone exposure to the pyrrole solution. The proposed mechanism was evaluated based on the experiments wherein silver nitrate solution was added after the ozone exposure (after 5, 10, 30 and 60 minutes) (Figure 5.9).

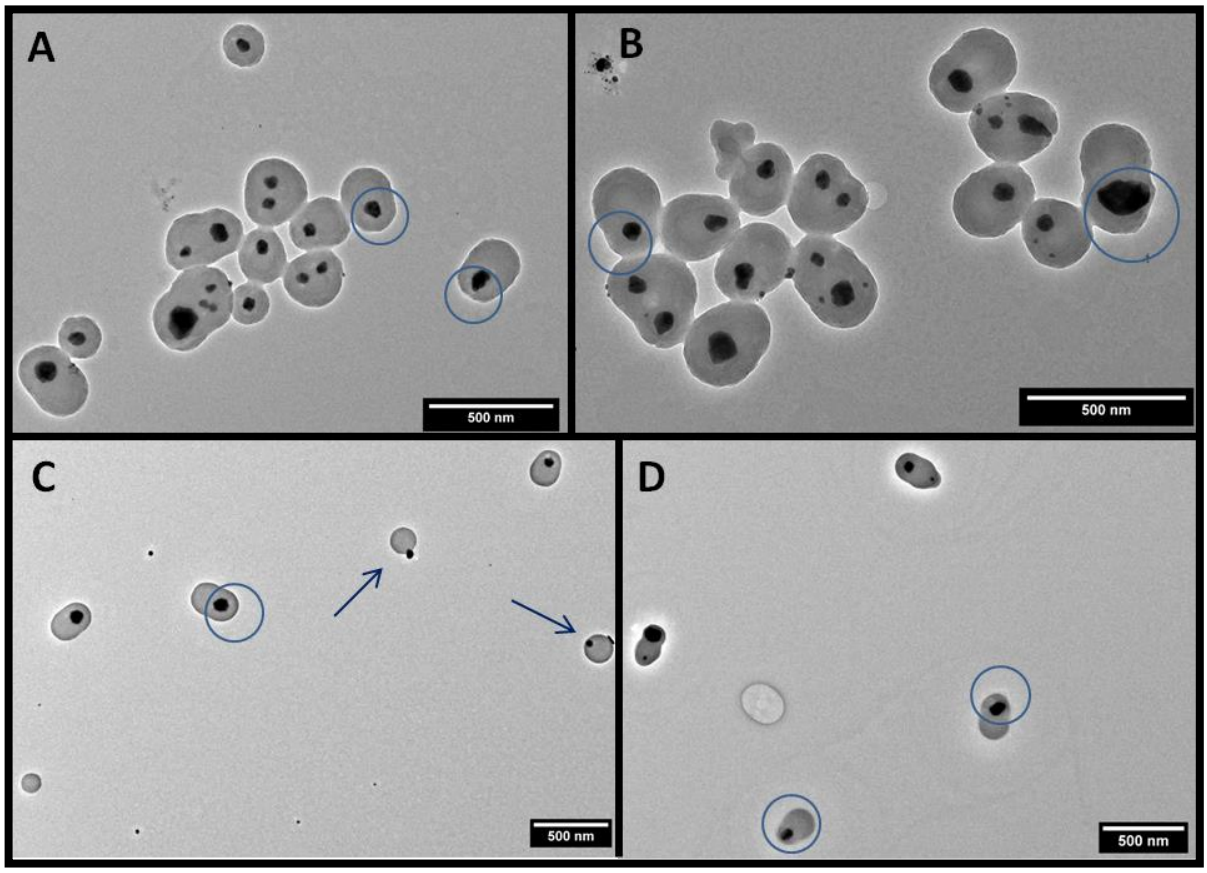

Figure 5.9. TEM images of nanospheres synthesized at various addition times of silver nitrate in ozone exposed pyrrole solution (A: after 5 minutes B: after 10 minutes C: after 30 minutes and D: after 60 minutes)
(*Note: Circles and arrows are shown to present examples of non-uniform core-shell morphology.)*

When silver nitrate solution was added immediately after ozone exposure, the probability of achieving uniform core shell morphology increases, because the processes of PPy nanosphere formation and silver nanoparticle formation occur concomitantly. However, if silver nitrate solution is added after several minutes of ozone exposure, the silver nanoparticles tend not to be in the center of the core, but were observed to be on one side of the nanosphere (Figure 5.9). A few nanoparticles were also observed to be adhering to the polypyrrole nanosphere instead of forming core shell morphology.

Analysis of particle size after ozone exposure in the absence silver nitrate reveals that the particle size of the nanospheres increases gradually, (Figure 5.10) which could result in non-uniform core-shell morphology, for example if silver nitrate solution is added in ozone exposed pyrrole solution after 60 minutes, the silver nanoparticles could be approximately 70 nm away from the core of PPy nanospheres.

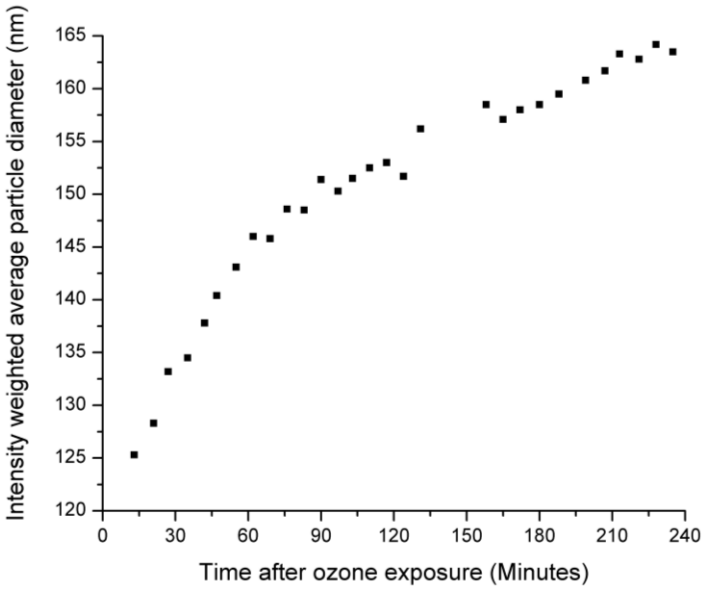

Figure 5.10. Particle size of PPy nanospheres in the absence of silver nitrate solution over time after 60 seconds of ozone exposure.

The nanospheres synthesized using only ozone show stability against agglomeration in water. The stability was attributed to the hydrophilic overoxidized pyrrole oligomers in the outermost part of the nanospheres[28]. The C=O, C-OH, COO^- groups were also observed in the XPS analysis to support this argument (Figure 5.2). However, the stability of the CSN dispersions is also dependent on the silver nitrate concentration. The reaction at 0.01 M concentration was stable in water, while the reactions at higher concentrations were not stable, indicating that the stability of the dispersion may not be achieved if all the silver nanoparticles are not successfully covered with PPy shell. Thermogravimetric analysis (Appendix Figure 4A) indicated that the weight percentage of silver nanoparticles in the final composites varied from approximately 45% to 65% by weight, for the reaction with 0.015 M concentration, for which uniform core shell morphology was obtained, silver nanoparticle concentration was observed to be 53% by weight. Apparently, higher concentration of silver nanoparticle would reduce dispersion stability of the aqueous dispersions, both due to insufficient shell amount available for silver nanoparticles and due to higher density of silver nanoparticles.

Silver nanoparticles are well known antibacterial agents.[29] The Ag-PPy CSNs may provide antibacterial properties despite a thick layer of PPy surrounding Ag nanoparticles. This is due to the inherent porous morphology of PPy.[59, 60] Antibacterial properties of Ag-PPy CSNs ($AgNO_3$ = 0.01M) were studied on a highly versatile bacteria *Pseudomonas putida* KT2440. The study was performed on four samples containing Ag-PPy CSNs, Bare Ag nanoparticles, PPy nanospheres and Control (Blank). The experiments were performed in such a manner that the concentration of silver is similar in Ag-PPy CSNs and bare Ag nanoparticles. The growth inhibition study was conducted by growing *P. putida* KT2440 in Luria Bertani (LB) Medium in the presence of the nanoparticles (Figure 5.11). The Ag/PPY CSNs reduced the

number of bacteria that are inoculated in the first 12 h. Even though the re-growth of bacteria was observed at 24 h, overall growth of the bacteria was controlled as compared to the samples containing PPy nanospheres and the control.

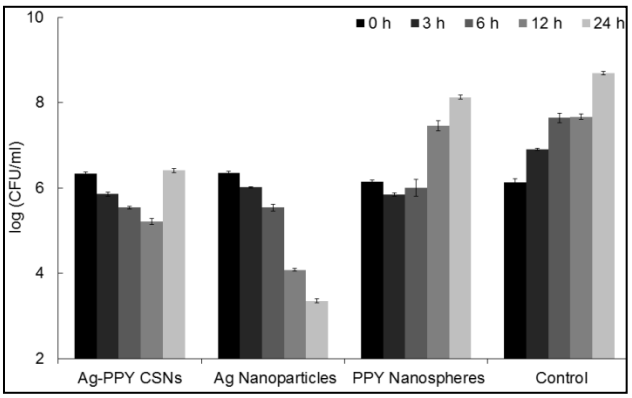

Figure 5.11. Inhibition of bacterial growth in the presence of LB medium due to Ag-PPy CSNs.

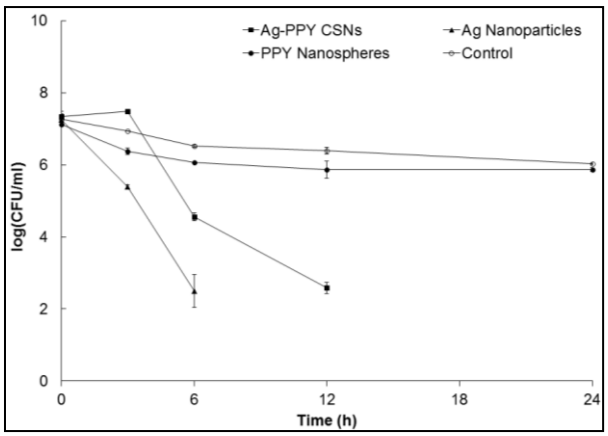

Figure 5.12. Toxicity of the Ag-PPy CSNs to the bacteria.

The bare Ag nanoparticles showed higher inhibition than the Ag-PPY CSNs as the number of bacteria kept decreasing in 24 h even though their silver concentrations are equal. This could be due to smaller size (40-60 nm) of bare silver nanoparticles as compared to silver nanoparticles (60-120 nm) in the Ag-PPy CSNs[61, 62]. The lesser efficiency of Ag-PPy CSNs than bare Ag nanoparticles could also be due to effect of PPy shells surrounding Ag nanoparticles. For the toxicity test, the LB medium was not added with the bacterial cells; therefore, no growth of bacteria was observed even in the control sample (Figure 5.12).

The results are in accordance with the previously described growth inhibition test. The Ag-PPy CSNs showed high toxicity to the bacteria, the number of bacteria decreased 10^5 times after 12 h of exposure, and no bacteria was observed in the sample at 24 h. On the other hand, PPy nanoparticles did not show any toxicity to the bacteria, and the cell number was almost equal to the control. Similar to the growth inhibition test, the bare Ag nanoparticles showed higher toxicity than the Ag/PPy nanoparticles. It should be noted that the antibacterial studies were performed on the as synthesized dispersions of Ag-PPy CSNs. Thus it may be possible that the silver nanoparticles and silver ions in the dispersion (in addition to the CSNs) also participated in the antibacterial activity of the Ag-PPy CSNs.

It is obvious that the method that we have developed can be extended to other conducting polymer and inorganic nanoparticles combinations, which are being explored in the author's laboratory. At this point it seems that the salts which oxidize pyrrole and reduce itself to metal nanoparticles can be used to synthesize those particular metals – PPy CSNs for example gold (III) chloride trihydrate and palladium chloride to synthesize gold-PPy and palladium-PPy CSNs respectively. Potential applications of Ag-PPy CSNs may be in antibacterial flexible inks on food packaging, and in the biomedical coatings[29].

5.5. Conclusions

Template free method for synthesis of stable dispersion of Ag-PPy core shell nanostructures was described. The shell thickness was approximately 60-80 nm while the core diameter was approximately 150-250 nm. Thermogravimetric analysis indicated that the CSNs contain approximately 53% silver nanoparticles by weight. The formation of the core-shell morphology was characterized using electron microscopy, XPS, UV Vis spectroscopy, FTIR and cyclic voltammetry. It is possible that the hydrophobic nature of silver nanoparticles synthesized

in-situ is providing sites for the growth of PPy shell, while the dispersion stability is observed to be dependent on the silver nitrate concentration; excess silver nanoparticles may hinder the stability of the dispersion. In cyclic voltammetry experiments CSNs show reduction and oxidation peaks at approximately -80 mV and 120 mV respectively. The CSNs were also observed to be effective antibacterial agent with respect to toxicity as well as growth of the bacteria. This method could be implemented further for the synthesis of gold-PPy and palladium-PPy core shell nanospheres.

5.6. Acknowledgments

This work was supported by the funds of Army Research Laboratory (Grant number: W911NF-11-2-0027). X-ray photoelectron spectroscopy was carried out in the Characterization Facility, University of Minnesota, which receives partial support from NSF through the MRSEC program The antibacterial studies were performed by the Department of Civil Engineering at North Dakota State University.

5.7. References

1. Ghosh Chaudhuri, R. and S. Paria, *Core/Shell Nanoparticles: Classes, Properties, Synthesis Mechanisms, Characterization, and Applications.* Chemical Reviews, 2011. **112**(4): p. 2373-2433.
2. Kabir, L. and S. Mandal, *Methanol sensing characteristics of conducting polypyrrole-silver nanocomposites.* The European Physical Journal Applied Physics, 2012. **58**(02).
3. Kate, K.H., et al., *Nano-Silver Mediated Polymerization of Pyrrole: Synthesis and Gas Sensing Properties of Polypyrrole (PPy)/Ag Nano-Composite.* Journal of Nanoscience and Nanotechnology, 2011. **11**(9): p. 7863-7869.

4. Li, F., et al., *Organic bistable devices based on core/shell CdSe/ZnS nanoparticles embedded in a conducting poly (N-vinylcarbazole) polymer layer.* Applied Physics Letters, 2007. **91**(12): p. 122111-122111-3.

5. Scrosati, B. and C.A. Vincent, *Polymer electrolytes: the key to lithium polymer batteries.* MRS Bulletin, 2000. **25**(03): p. 28-30.

6. Lee, J.W., Y. Anguchamy, and B.N. Popov. *Discharge Characteristics of Polypyrrole/Silver Vanadium Oxide Composite Used for Lithium Primary Batteries*. in *ECS Transactions*. 2007. ECS.

7. Malinauskas, A., J. Malinauskiene, and A. Ramanavičius, *Conducting polymer-based nanostructurized materials: electrochemical aspects.* Nanotechnology, 2005. **16**: p. R51.

8. Chen, W., et al., *Magnetic and conducting particles: preparation of polypyrrole layer on Fe_3O_4 nanospheres.* Applied surface science, 2003. **218**(1-4): p. 216-222.

9. Zhu, C.L., et al., *Synthesis of core/shell metal oxide/polyaniline nanocomposites and hollow polyaniline capsules.* Nanotechnology, 2007. **18**: p. 275604.

10. Liu, P. and L. Zhang, *Hollow nanostructured polyaniline: Preparation, properties and applications.* Critical Reviews in Solid State and Materials Sciences, 2009. **34**(1-2): p. 75-87.

11. Jang, J., *Conducting polymer nanomaterials and their applications.* Adv Polymer Sci: Emissive Materials Nanomaterials 2006. **199**: p. 189-260.

12. Lellouche, J.P., *Magnetic Core Conducting Polymer Shell Nanocomposites for DNA Attachment and Hybridization.* Nanotechnologies for the Life Sciences, 2005.

13. Hao, L., et al., *Fabrication of silica core-conductive polymer polypyrrole shell composite particles and polypyrrole capsule on monodispersed silica templates.* Synthetic metals, 2003. **139**(2): p. 391-396.

14. Zhang, L. and M. Wan, *Polyaniline/TiO2 composite nanotubes.* The Journal of Physical Chemistry B, 2003. **107**(28): p. 6748-6753.

15. Armes, S., et al., *Conducting polymer-colloidal silica composites.* Polymer, 1991. **32**(13): p. 2325-2330.

16. Gangopadhyay, R. and A. De, *Conducting polymer nanocomposites: a brief overview.* Chemistry of materials, 2000. **12**(3): p. 608-622.

17. Wang, S. and G. Shi, *Uniform silver/polypyrrole core-shell nanoparticles synthesized by hydrothermal reaction.* Materials chemistry and physics, 2007. **102**(2): p. 255-259.

18. Yang, X. and Y. Lu, *Preparation of polypyrrole-coated silver nanoparticles by one-step UV-induced polymerization.* Materials Letters, 2005. **59**(19): p. 2484-2487.

19. Feng, X., et al., *Ag/polypyrrole core-shell nanostructures: Interface polymerization, characterization, and modification by gold nanoparticles.* The Journal of Physical Chemistry C, 2007. **111**(24): p. 8463-8468.

20. Fujii, S., et al., *One-step synthesis of polypyrrole-coated silver nanocomposite particles and their application as a coloured particulate emulsifier.* J. Mater. Chem., 2007. **17**(36): p. 3777-3779.

21. Fujii, S., et al., *Facile one-step route to polyaniline–silver nanocomposite particles and their application as a colored particulate emulsifier.* Synthetic metals, 2010. **160**(13): p. 1433-1437.

22. Dallas, P., et al., *Interfacial polymerization of pyrrole and in situ synthesis of polypyrrole/silver nanocomposites.* Polymer, 2007. **48**(7).

23. Jing, S., et al., *Synthesis and characterization of Ag/polypyrrole nanocomposites based on silver nanoparticles colloid.* Materials Letters, 2007. **61**(23-24): p. 4528-4530.

24. Chen, A., et al., *Formation process of silver-polypyrrole coaxial nanocables synthesized by redox reaction between $AgNO_3$ and pyrrole in the presence of poly (vinylpyrrolidone).* The Journal of Physical Chemistry B, 2005. **109**(39): p. 18283-18288.

25. Muñoz-Rojas, D., et al., *Facile One-Pot Synthesis of Self-Assembled Silver@ Polypyrrole Core/Shell Nanosnakes.* Small, 2008. **4**(9): p. 1301-1306.

26. Nghia, N.D. and N.T. Tung. *Preparation and characterization of hybrid materials based on polypyrrole and silver nanoparticles*. 2009. IOP Publishing.

27. Pinter, E., et al., *Characterization of polypyrrole-silver nanocomposites prepared in the presence of different dopants.* The Journal of Physical Chemistry B, 2005. **109**(37): p. 17474-17478.

28. Vetter, C.A., et al., *Novel Synthesis of Stable Polypyrrole Nanospheres Utilizing Ozone.* Langmuir, 2011. **27**(22): p. 13719–13728.

29. Ataeefard, M. and S. Sharifi, *Antibacterial flexographic ink containing silver nanoparticles.* Progress in organic coatings, 2014. **77**(1): p. 118-123.

30. Choi, O.K., et al., *The inhibitory effects of silver nanoparticles, silver ions, and silver chloride colloids on microbial growth.* Water Research, 2008. **42**(12): p. 3066-3074.

31. Spurlock, L., *XPS characterization of nanosized overoxidized polypyrrole films on graphite electrodes.* Analyst, 1999. **124**(8): p. 1215-1221.

32. Idla, K., et al., *An XPS and AFM study of polypyrrole coating on mild steel.* Surface and interface analysis, 1997. **25**(11): p. 837-854.

33. Rajagopalan, R. and J.O. Iroh, *Characterization of polyaniline–polypyrrole composite coatings on low carbon steel: a XPS and infrared spectroscopy study.* Applied surface science, 2003. **218**(1): p. 58-69.

34. Pfluger, P. and G. Street, *Chemical, electronic, and structural properties of conducting heterocyclic polymers: A view by XPS.* The Journal of chemical physics, 1984. **80**: p. 544.

35. Saoudi, B., et al., *XPS study of the adsorption mechanisms of DNA onto polypyrrole particles.* Spectroscopy: An International Journal, 2004. **18**(4): p. 519-535.

36. Malitesta, C., et al., *New findings on polypyrrole chemical structure by XPS coupled to chemical derivatization labelling.* Journal of Electron Spectroscopy and Related Phenomena, 1995. **76**: p. 629-634.

37. Wang, W., et al., *The preparation and characterization of the cross-linked Ag–AgCl/polypyrrole nanocomposite.* Synthetic metals, 2010. **160**(19): p. 2203-2207.

38. Wang, P., et al., *Synthesis of highly efficient Ag@ AgCl plasmonic photocatalysts with various structures.* Chemistry-A European Journal, 2010. **16**(2): p. 538-544.

39. Zhang, H., et al., *Tuning Photoelectrochemical Performances of Ag−TiO_2 Nanocomposites via Reduction/Oxidation of Ag.* Chemistry of materials, 2008. **20**(20): p. 6543-6549.

40. Babu, K.F., et al., *One pot synthesis of polypyrrole silver nanocomposite on cotton fabrics for multifunctional property.* Carbohydrate polymers, 2012. **90**(4): p. 1557-1563.

41. Romand, M., M. Roubin, and J.-P. Deloume, *X-ray photoelectron emission studies of mixed selenides $AgGaSe_2$ and Ag_9GaSe_6.* Journal of Solid State Chemistry, 1978. **25**(1): p. 59-64.

42. Yang, X., et al., *Facial synthesis of polypyrrole/silver nanocomposites at the water/ionic liquid interface and their electrochemical properties.* Materials Letters, 2010. **64**(17): p. 1918-1920.

43. Wei, Y., et al., *One-step UV-induced synthesis of polypyrrole/Ag nanocomposites at the water/ionic liquid interface.* Nanoscale research letters, 2010. **5**(2): p. 433-437.

44. Deng, J., et al., *Magnetic and conducting Fe_3O_4–polypyrrole nanoparticles with core-shell structure.* Polymer international, 2003. **52**(7): p. 1182-1187.

45. Chen, A., H. Wang, and X. Li, *One-step process to fabricate Ag–polypyrrole coaxial nanocables.* Chemical communications, 2005(14): p. 1863-1864.

46. Bhat, N., A. Gadre, and V. Bambole, *Structural, mechanical, and electrical properties of electropolymerized polypyrrole composite films.* Journal of Applied Polymer Science, 2001. **80**(13): p. 2511-2517.

47. Rinaldi, A., et al., *Solid phase photopolymerization of pyrrole in poly (vinylchloride) matrix.* European polymer journal, 2005. **41**(11): p. 2711-2717.

48. Vishnuvardhan, T., et al., *Synthesis, characterization and ac conductivity of polypyrrole/Y_2O_3 composites.* Bulletin of Materials Science, 2006. **29**(1): p. 77-83.

49. Thombare, J., et al., *Synthesis of Hydrophilic Polypyrrole Thin Films by Silar Method.* Materials Physics and Mechanics, 2013. **16**: p. 118-125.

50. Chen, A., et al., *Fabrication of Ag/polypyrrole coaxial nanocables through common ions adsorption effect.* Synthetic metals, 2006. **156**(2): p. 346-350.

51. Li, Y. and R. Qian, *Electrochemical overoxidation of conducting polypyrrole nitrate film in aqueous solutions.* Electrochimica acta, 2000. **45**(11): p. 1727-1731.

52. Xing, S. and G. Zhao, *One-step synthesis of polypyrrole–Ag nanofiber composites in dilute mixed CTAB/SDS aqueous solution.* Materials Letters, 2007. **61**(10): p. 2040-2044.

53. Hershkovits, E., A. Tannenbaum, and R. Tannenbaum, *Polymer adsorption on curved surfaces: a geometric approach.* The Journal of Physical Chemistry C, 2007. **111**(33): p. 12369-12375.

54. Schneider, G. and G. Decher, *From functional core/shell nanoparticles prepared via layer-by-layer deposition to empty nanospheres.* Nano letters, 2004. **4**(10): p. 1833-1839.

55. Singho, N.D., et al., *FTIR Studies on Silver-Poly (Methylmethacrylate) Nanocomposites via In-Situ Polymerization Technique.* International Journal of Electrochemical Science, 2012. **7**(6).

56. Street, G., et al., *Preparation and characterization of neutral and oxidized polypyrrole films.* Molecular Crystals and Liquid Crystals, 1982. **83**(1): p. 253-264.

57. Barisci, J., et al., *Electrochemical preparation of polypyrrole colloids using a flow cell.* Colloids and Surfaces A: Physicochemical and Engineering Aspects, 1997. **126**(2-3): p. 129-135.

58. Hodko, D., M. Gamboa-Aldeco, and O.J. Murphy, *Photopolymerized silver-containing conducting polymer films. Part I. An electronic conductivity and cyclic voltammetric investigation.* Journal of Solid State Electrochemistry, 2009. **13**(7): p. 1063-1075.

59. Sun, M., et al., *Nano-wire networks of sulfur–polypyrrole composite cathode materials for rechargeable lithium batteries.* Electrochemistry Communications, 2008. **10**(12): p. 1819-1822.

60. Hallik, A., et al., *On the porosity of polypyrrole films.* Synthetic metals, 2007. **157**(24): p. 1085-1090.

61. Choi, O.K. and Z.Q. Hu, *Size dependent and reactive oxygen species related nanosilver toxicity to nitrifying bacteria.* Environmental Science and Technology, 2008. **42**(12): p. 4583-4588.

62. Morones, J.R., et al., *The bactericidal effect of silver nanoparticles.* Nanotechnology, 2005. **16**(10): p. 2346-2353.

CHAPTER 6. CORROSION INHIBITION ASSESSMENT OF MONODISPERSE POLYPYRROLE NANOSPHERES

6.1. Abstract

In this study polypyrrole (PPy) nanospheres were investigated for their corrosion inhibition properties. Aqueous dispersions of uniformly dispersed PPy nanospheres were synthesized using ozone oxidation. Inherent stability against agglomeration was displayed utilizing electron microscopy, dynamic light scattering and spin coating. Coating formulations were prepared in commercial water borne epoxy amine system. The coatings were applied on cold rolled steel as well as Al 2024 substrates. Corrosion inhibition assessment of PPy nanospheres was done utilizing accelerated salt spray exposure and electrochemical impedance spectroscopy. The results indicate that the coatings containing PPy nanospheres had increased corrosion inhibition than control coatings. The PPy nanospheres possibly provided corrosion inhibition through oxygen scavenging or cathodic protection which has been studied using potentiodynamic scans and galvanic corrosion experiements.

6.2. Introduction

Electro-active polymers (EAPs) such as polypyrrole (PPy) and polyaniline (PANI) have been shown to provide corrosion inhibition to metal and metal alloys and have been regarded as a possible alternative to carcinogenic hexavalent chrome based pigments and surface treatments. Pertinent to various synthesis methods and doping alternatives, EAPs provide corrosion protection via anodic protection,[1, 2] passivation,[1, 3] self healing, [4, 5] oxygen scavenging or cathodic protection.[6-8] Literature on corrosion inhibition studies of EAPs can be classified in two ways, firstly EAPs are electro-polymerized on substrates followed by investigation of corrosion protection properties, and secondly chemically synthesized EAPs are added in coating

formulations which are applied on the substrate followed by investigation of corrosion inhibition properties. Chemically synthesized EAPs have several advantages over the first method owing to the cost, efficiency, porosity and flexibility limitations of electro-polymerization of pyrrole and aniline on metal substrates.[9-11] Although chemical synthesis of EAPs affords scalable methodologies, the final product presents challenges in terms of processing, especially when compared to electro-polymerization where uniform films of EAPs can be obtained on metal substrates.[12] Furthermore, electro-polymerization of PPy onto metal substrates often requires a non-aqueous bath resulting into use of organic solvent.[13, 14]

PPy and PANI synthesized by chemical oxidation methods have poor mechanical and film forming properties. PPy in particular is insoluble in common solvents which add to the challenges in processing. More often these materials are processed like pigments and then formulated in coating systems; the processing involves grinding, sonication and use of surfactants for wetting and stabilization; which is neither cost effective nor facile. Although nano-sized EAPs have been shown to be more efficient than micron-sized EAPs,[15] the poor dispersion and agglomeration remain an issue with their commercial use in coating formulations. A possible solution for the problems associated with the use of nano-EAPs in coating formulations could be the use of aqueous dispersions of nano-EAPs which are inherently resistant to agglomeration. Aqueous dispersions of nano-EAPs will allow efficient distribution of nanoparticles throughout the coating at a lower concentration in the formulation.

Corrosion inhibition behavior of nano-EAPs has not been studied to its full potential, however nanocomposites consisting of EAPs with mica,[16, 17] alumina,[18, 19] carbon nanotube, [20] clay [21-23] or titanium dioxide [24, 25] have been studied for their corrosion inhibition properties for steel and aluminum alloys. Furthermore, chemically synthesized PPy

nanoparticles have received a very little attention as compared to PANI nanoparticles. Bagherzadeh *et al.* have studied nanoemeraldine salt PANI as an anticorrosive additive for water based epoxy formulations, [26] while Wessling *et al.* have used electrochemical techniques and traditional accelerated exposure techniques to determine anticorrosion mechanism of PANI nanoparticles.[27] More recently, Mahmoudian *et al.* have investigated anticorrosive performance of PANI nanotubes and PANI nanofibres.[28] Nano-EAPs have potential in various fields including electronics, solar energy, sensors and corrosion inhibition, in accordance various nanostructures have been synthesized for their possible use in these fields. However, if we divide the EAPs current literature in two parts viz. synthesis and application, particularly for chemically synthesized EAPs, it can be observed that there is a scarcity in EAPs literature dealing with its applications once they have been synthesized and characterized.

In this work, we have synthesized stable aqueous dispersions of PPy and PANI nanospheres previously, in a template free synthesis procedure using ozone oxidation.[29, 30] The nanospheres are inherently resistant to agglomeration and possess uniform and mono-disperse morphology. In this study, corrosion inhibition properties and a possible mechanism for corrosion inhibition is presented for PPy nanospheres. Coatings are formulated with water dispersible epoxy, water reducible amine crosslinking agent, and water dispersed PPy nanospheres making it an environmentally friendly coating formulation. The coatings are applied on both cold rolled steel (CRS) substrate and Aluminum 2024 – T3 alloy for corrosion inhibition assessment. Corrosion inhibition properties are assessed using electrochemical impedance spectroscopy (EIS), potentiodynamic scans (PDS), scanning vibrating electrode technique (SVET), galvanic corrosion, EIS modeling and ASTM B 117 salt spray exposure. It was observed that the coatings containing PPy nanospheres significantly delay the corrosion of

substrate underneath as well as protect the substrate longer than the control coatings without PPy nanospheres. A proposed mechanism for corrosion protection is also discussed.

6.3. Experimental details

Pyrrole was purchased from Sigma-Aldrich. Beckopox VEP 2381W/55WA and Beckopox EH 623W/80WA were graciously supplied by Cytec. BYK 348 and BYK 1710 were graciously supplied by BYK.

PPy nanospheres were synthesized as described earlier.[29] In a simple procedure 0.01 M pyrrole solution was prepared in 18 MΩ Millipore water. Ozone was exposed to the prepared pyrrole solution from an ozone generator supplied by Absolute Ozone, which generates approximately 18% of ozone in ozone/oxygen mixture, upon supply of oxygen at a pressure of 20 psi and flow rate of 0.2 L/min. Ozone was bubbled through 100 ml pyrrole solution for 60 seconds. Ozone exposure was followed by removal of fumes which were generated in the reaction by blowing a stream of air. The reactions were allowed to sit for 4-7 days after which the samples were filtered and washed with Millipore water at least three times to remove unreacted pyrrole and pyrrole oligomers. The PPy nanospheres were dried in a convection oven to remove residual water.

Dried PPy nanospheres were sonicated in Millipore water for 30 minutes to re-disperse the nanospheres in water. To this dispersion water reducible amine Beckopox EH 623W/80WA was added and the sample was further sonicated for 10 minutes. Water based epoxy Beckopox VEP 2381W/55WA was added to the formulation along with wetting agent BYK 348 and defoamer BYK 1710. This sample was stirred for 5 minutes using magnetic stirrer. The formulation was thinned down with Millipore water and was provided allowed to sit for 5 minutes. The formulations were applied on sand blasted CRS and sand blasted Al 2024 substrate

using a drawdown bar. The panel dimensions were 3 in x 6 in. Panels were air dried for at least seven days after application. Two different dry film thickness of 30-35 µm and 70-80 µm were applied. Table 6.1 provides details of the formulations prepared.

Table 6.1. Formulation Summary

Components	Commercial name	F-1 (Wt %)	F-2 (Wt %)	F-3 (Wt %)
PPy nanospheres		00.42	00.85	01.25
Millipore water		14.00	14.00	14.00
Water reducible amine	Beckopox EH 623W/80WA	12.00	12.00	12.00
Water based epoxy	Beckopox VEP 2381W/55WA	54.10	54.10	54.10
Wetting agent	BYK 348	00.52	00.52	00.52
Defoamer	BYK 1710	00.52	00.52	00.52
Millipore water		18.44	18.01	17.61
Total		**100**	**100**	**100**
% solids of PPy		1.03	2.06	3.00

Characterization: Dry film thickness of the prepared panels was measured using Positector 6000 coating thickness gauge. EIS, PDS and galvanic corrosion experiments were performed using Gamry Reference 600 Potentiostats with Gamry Framework Version 5.58 software. For EIS 5% NaCl solution was used as and electrolyte. A three electrode setup was used for EIS experiments consisting of a platinum mesh counter electrode, saturated calomel reference electrode and coated substrate as a working electrode. Electrochemical cells were prepared by adhering a PVC pipe with 7.6 cm length and 2.4 cm inner diameter to the coated substrate using marine adhesive goop at least 24 hours prior to the immersion in the electrolyte. The samples were scanned in the range of 100,000 – 0.1 Hz of frequency range at an AC voltage of 10 mV. EIS was performed in triplicates to ensure reproducibility and accuracy of the results. Modeling of EIS data was conducted using ZView 2 software by Scribner Associates Inc. PDS was performed on the coated substrates with the similar setup as described above. The experiment was performed starting from below 500 mV of open circuit potential (OCP) until above 500 mV of OCP at a scan rate of 10 mV/s. The open circuit was measured for 10 minutes

to achieve a stable potential before the start of the PDS experiement. The experiment was performed on triplicates.

The experimental set-up for galvanic corrosion is illustrated in previous publications.[31] The cell had two compartments. The materials required for the setup were two glass cylinders 7.6 cm long and 2.4 cm inner diameter, two O-shaped rubber rings, two metal clips, one saturated calomel reference electrode, bare Al 2024 panels, and the coated substrate of interest. The first compartment consisted of the glass cylinder attached to the coated substrate using a metal clip and rubber ring. The second compartment consisted of the glass cylinder attached to the bare Al 2024 using a metal clip and rubber ring. The coated substrate was working electrode while the bare Al 2024 was a counter electrode. Reference electrode was inserted in the first compartment. First compartment was purged with nitrogen while the second compartment was purged with Air. The two compartments were connected utilizing a salt bridge. Diluted Harrison's solution was used as an electrolyte in both the compartments. Galvanic corrosion experiments were performed using Gamry Reference 600 potentiostats in zero resistance ammeter mode to yield data of mixed potential and coupling current with time for 24 hours. Galvanic corrosion experiments were performed on triplicates to ensure reproducibility and accuracy of the results. SVET measurements were performed on coated panels on Al 2024 with a small defect made using a razor blade. The instrument was supplied by Applicable Electronics Inc. Electrolyte used was 0.5% NaCl solution. Pt-Ir microelectrode with a platinum black deposited tip was supplied by Microprobe Inc. The quasi-reference electrode was a platinum black coated platinum wire electrode. The vibrating probe was at a distance of approximately 120 μm above the substrate.

After at least seven days of air drying, the coatings were exposed to accelerated salt spray test according to ASTM B117 standard. Coated panels were masked on the edges and on the non-coated areas before exposure. The panels were scribed in X shape prior to the exposure. The panels were removed periodically for visual assessment of the corrosion in scribed and un-scribed areas. The exposure test was performed on triplicates. Spin coating was performed using Laurell spin coater model number WS-400B-8NPP-LITE/AS. 0.4 ml of as synthesized dispersion was spread on the glass slide of about 1 inch × 1 inch before spin coating. The spin coating was performed for 30 seconds at 3000 RPM. JEOL JEM-100CX II transmission electron microscope was used for TEM images. In PPy nanosphere solution a 300-mesh Formvar/carbon-coated grid was dipped and removed. The grid was immediately wicked off using a filter paper. Scanning electron microscopy (SEM): Centrifuged and dried PPy nanospheres were sprinkled on a carbon tape attached to aluminum mounts. The nanospheres were coated with gold using a Balzers SCD 030 sputter coater. JEOL JSM-7600F Scanning Electron Microscope was used for obtaining SEM images.

6.4. Results and discussion

The efficiency of aqueous dispersions of PPy nanospheres, with respect to uniform distribution of nanospheres throughout the coating, was quite evident when the coatings were formulated and were applied on the substrate. Figure 6.1A shows SEM image of PPy nanospheres which were spin-coated on glass substrates. Figure 6.1B and Figure 6.1C shows SEM and TEM images of bulk PPy nanospheres after the synthesis. Number-wt Gaussian distribution of PPy nanosphere dispersion is shown in Figure 6.1D. Figure 6.1A-D illustrates uniform morphology of PPy nanospheres as well as their resistance to agglomeration which is

advantageous for the coating formulations if the nanospheres were to be utilized to their full potential.

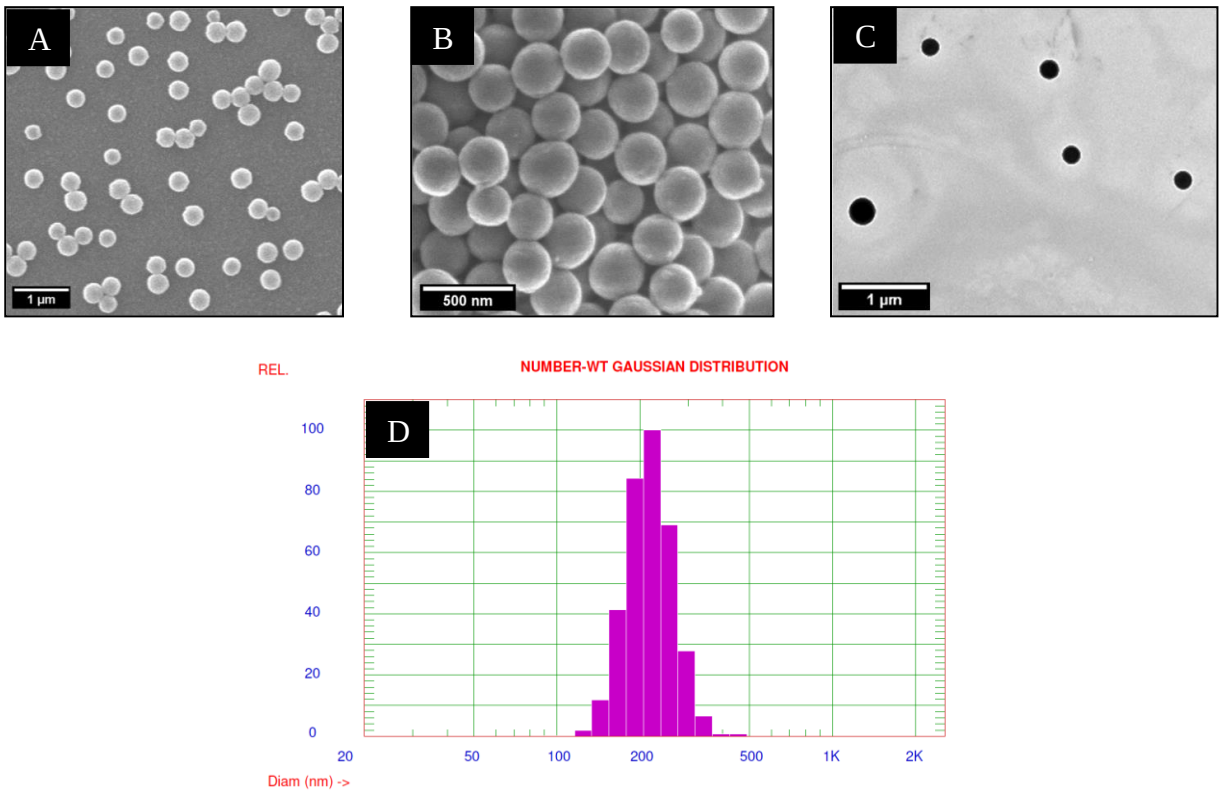

Figure 6.1. A) SEM image of PPy nanospheres spin-coated on glass substrate, B) SEM image of bulk PPy nanospheres after synthesis, C) TEM image of PPy nanosphere from aqueous dispersion, and D) Number-wt gaussian distribution of PPy nanosphere dispersion.

Passivating aluminum alloys such as Al 2024 undergo corrosion starting with pitting corrosion due to the cathodic sites formed by copper inclusions in the alloy, the dissolution and spreading of copper on the surface exacerbates corrosion reaction leading to failure.[32] This is particularly true in the case of Al2024 which constitutes of approximately 3% copper.[33] In the case of substrates covered with organic coatings, filiform corrosion occurs after ingress of the corrosive species through the coatings. Initial corrosion assessment was done on the coatings (DFT 30-35 µm) with 1% PPy nanospheres. The results were compared with coatings (DFT 30-35 µm) without PPy nanospheres. Figure 6.2 shows the photographs taken after 0, 168, 1900,

2572 and 3916 Hrs of ASTM B 117 salt spray exposure. It can be clearly observed that filform corrosion appears on the panels coated with epoxy amine coatings without PPy nanospheres as early as 168 hours of exposure to accelerated salt spray environment. For the coatings containing PPy nanospheres, only a slight discoloration of the coatings was observed over the exposure duration.

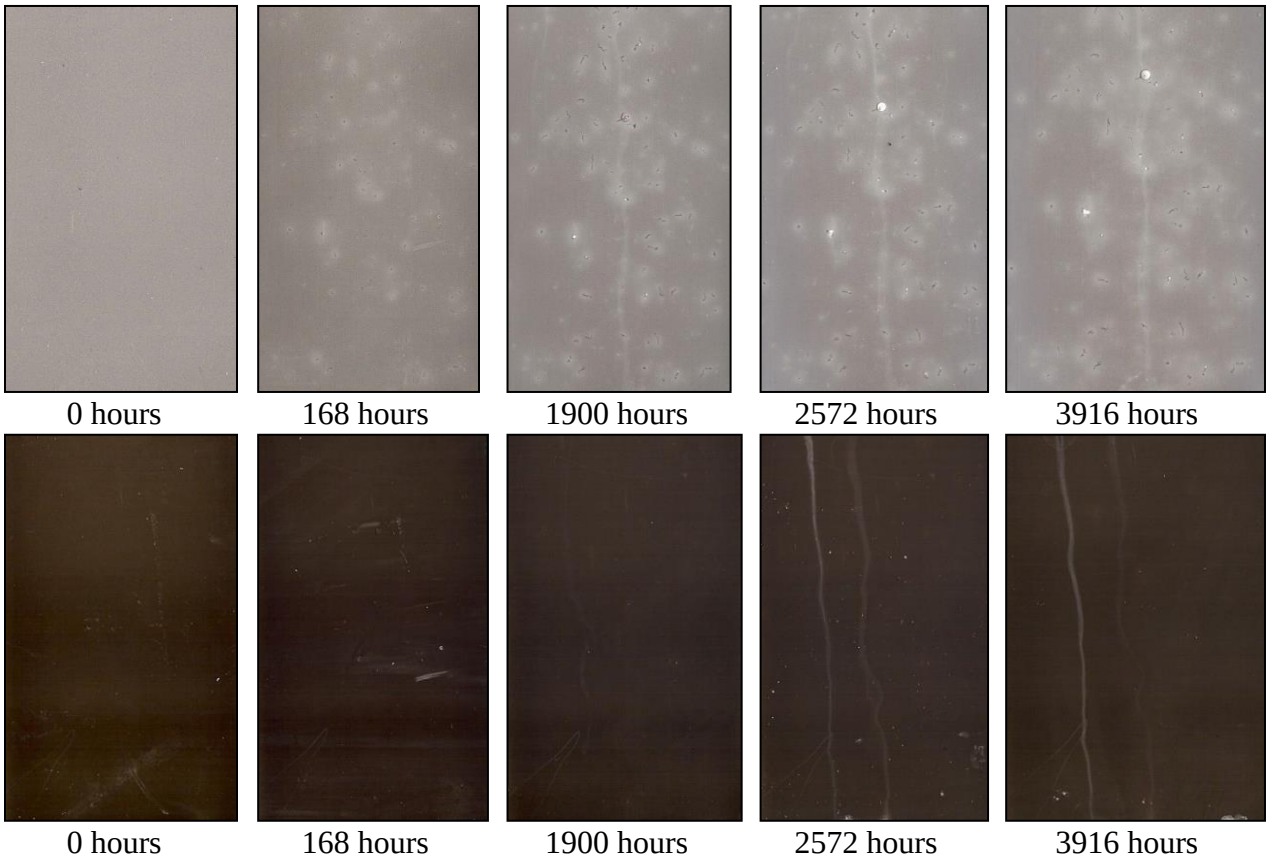

Figure 6.2. Photographs of Al 2024 panels coated with epoxy amine after exposure to ASTM B 117 salt spray. (Top row: Without PPy nanospheres, bottom row: with 1% PPy nanospheres)

Further effectiveness of PPy nanospheres as a corrosion inhibitor was investigated on coated panels with artificial defect (x-scribe) (DFT 70-80 µm). Figure 6.3 shows photographs taken at periodic intervals of scribed panels exposed to accelerated ASTM B 117 salt spray, for control coatings and for coatings containing 1%, 2% and 3% PPy nanospheres by weight on Al 2024 substrates. It can be observed that the coatings without PPy nanospheres show formation of

blistering and accumulation of corrosion product in the blisters much earlier than the coatings containing PPy nanospheres.

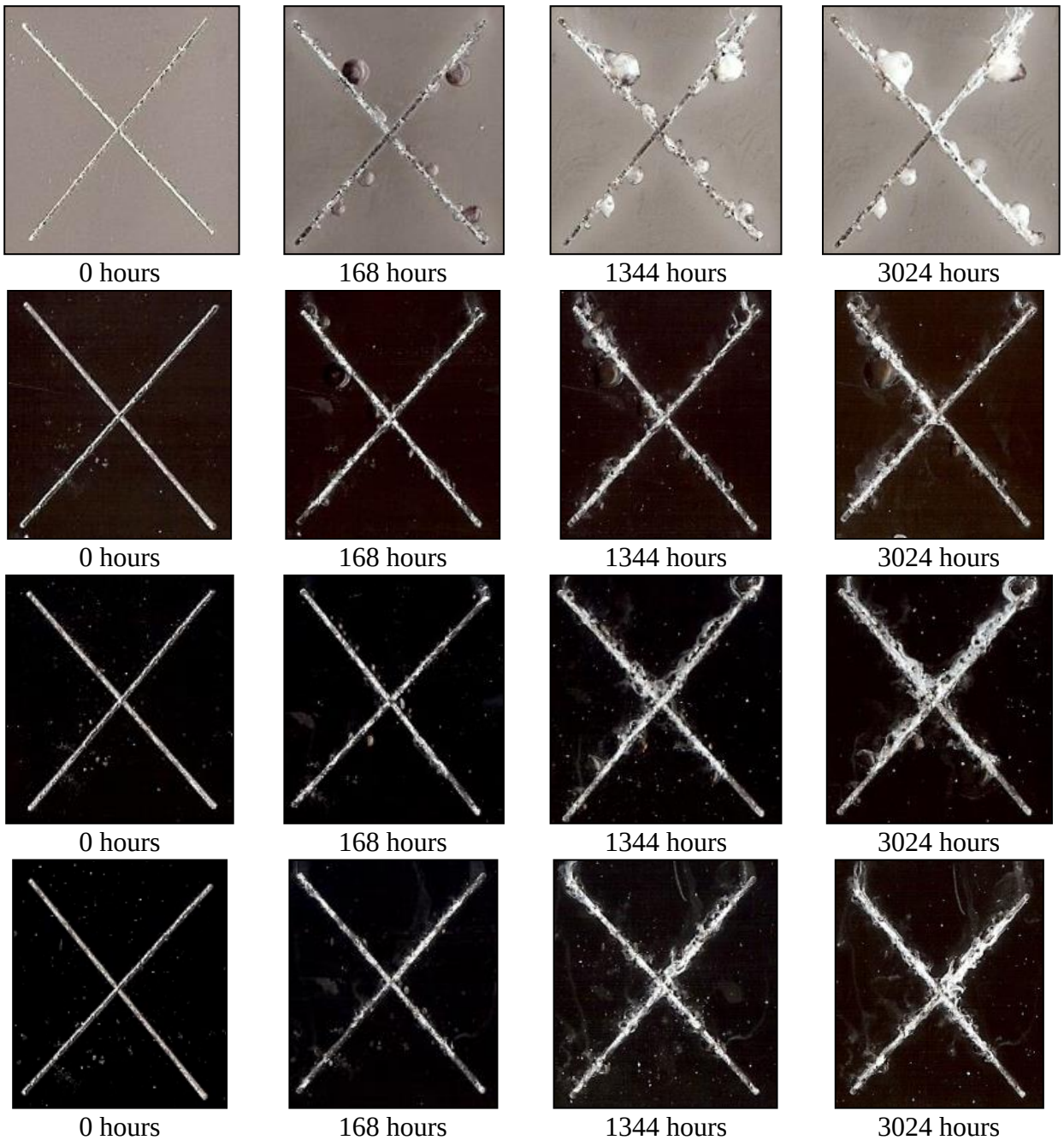

Figure 6.3. Photographs of Al 2024 panels coated with epoxy amine after exposure to ASTM B 117 salt spray. (Top row: without PPy nanospheres, second row: with 1% PPy nanospheres, third row: with 2% PPy nanospheres, and fourth row: with 3% PPy nanospheres).

Results of corrosion inhibition of coatings containing PPy nanospheres for CRS substrate are presented in Figure 6.4. It can be clearly seen in Figure 6.4 that all the coatings show growth of corrosion product in the scribed area after 48 hours of exposure.

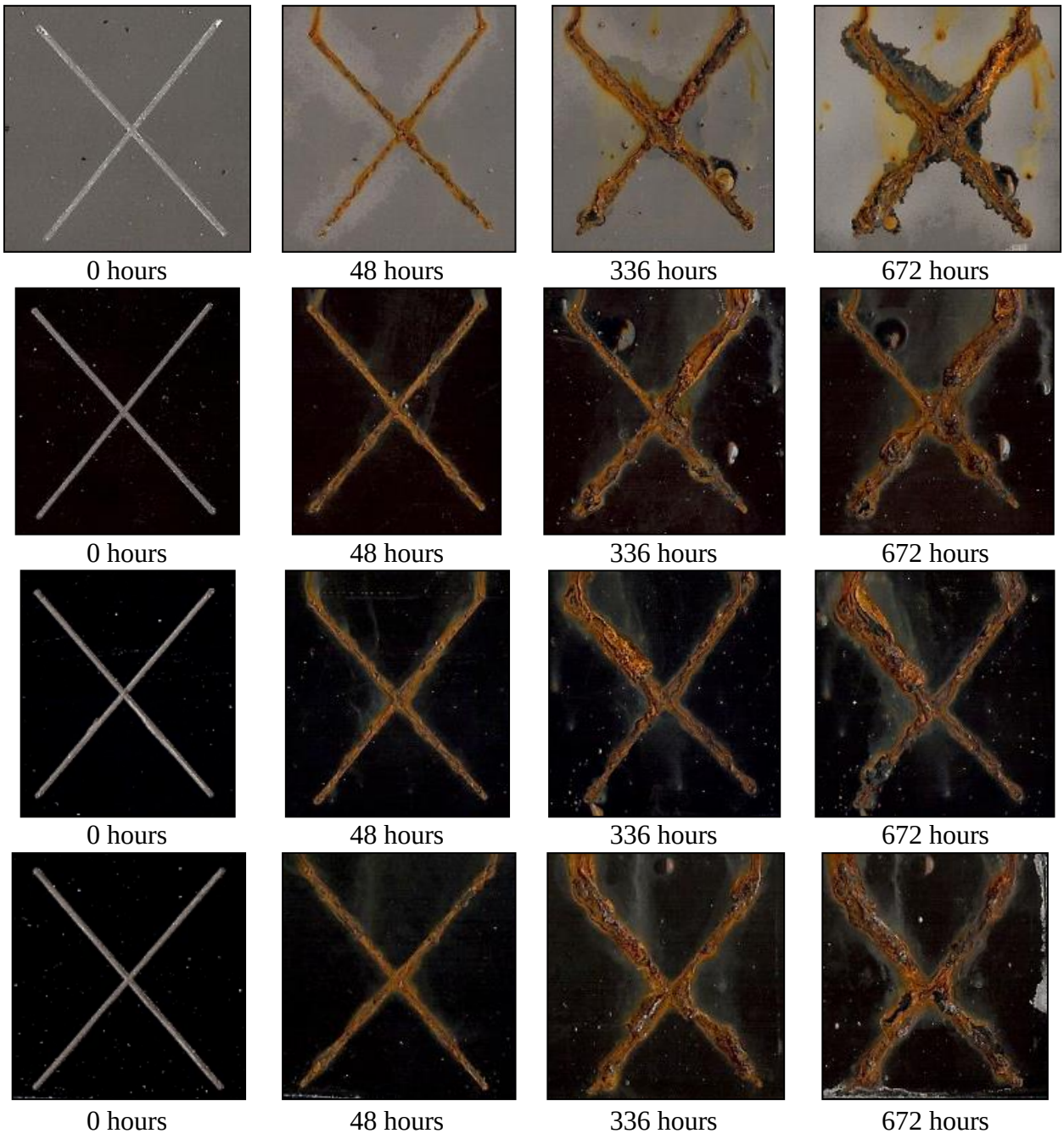

Figure 6.4. Photographs of CRS panels coated with epoxy amine after exposure to ASTM B 117 salt spray. (Top row: Without PPy nanospheres, second row: with 1% PPy nanospheres, third row: with 2% PPy nanospheres, and fourth row: 3% PPy nanospheres).

However, for the control coatings without PPy nanospheres the process of exfoliation starts at 336 hours of exposure to the salt spray. After 672 hours exfoliation of the coatings near scribed area can be observed in the control coatings, whereas, for the coatings containing PPy nanospheres no sign of exfoliation of the coating was observed at the end of 672 hours of exposure.

In order to quantitatively analyze corrosion inhibition properties of PPy nanospheres, EIS was employed for epoxy-amine panels with and without PPy nanospheres, on both CRS and Al 2024 substrates (DFT 70-80 µm). Figure 6.5 shows bode phase and bode modulus plots for control and for the coatings containing 1% PPy nanospheres on Al 2024. Impedance at low frequency of 0.01 Hz indicates barrier properties of the coatings. It was observed that the low frequency impedance was higher than 10^8 Ω for coatings containing 1% PPy nanospheres until 1848 hours of immersion in 5% NaCl solution (Figure 6.5A). While for control coatings after 336 hours of constant immersion, the low frequency impedance dropped below 10^8 Ω (Figure 6.5B). In contrast to the control coating, the phase angle for coating containing PPy nanospheres remained at -90° for all frequencies except at frequencies lower than 10^0 Hz, irrespective of the immersion time after 12 hours of constant immersion. For control coating the phase angle seem to increase starting at approximately 10^2 Hz from 12 to 1848 hours, with a clear second peak indicating saturation of the coating with electrolyte and initiation of corrosion reactions. It can be also observed that, for control coatings, after approximately 500 hours of constant immersion the low frequency impedance tends to show slight increase in its value possibly because of blockage of defects by corrosion product. Circuit modeling of EIS data will further clarify this argument in future discussion.

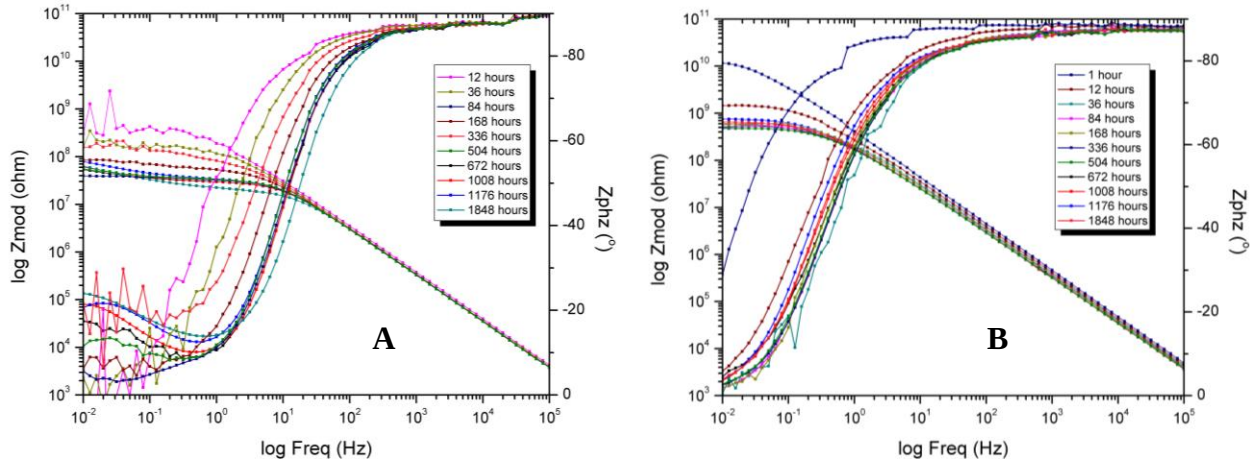

Figure 6.5. A) Bode phase and modulus plots for control coatings without PPy nanospheres on Al 2024 and B) Bode phase and modulus plots for coatings with 1% PPy nanospheres on Al 2024.

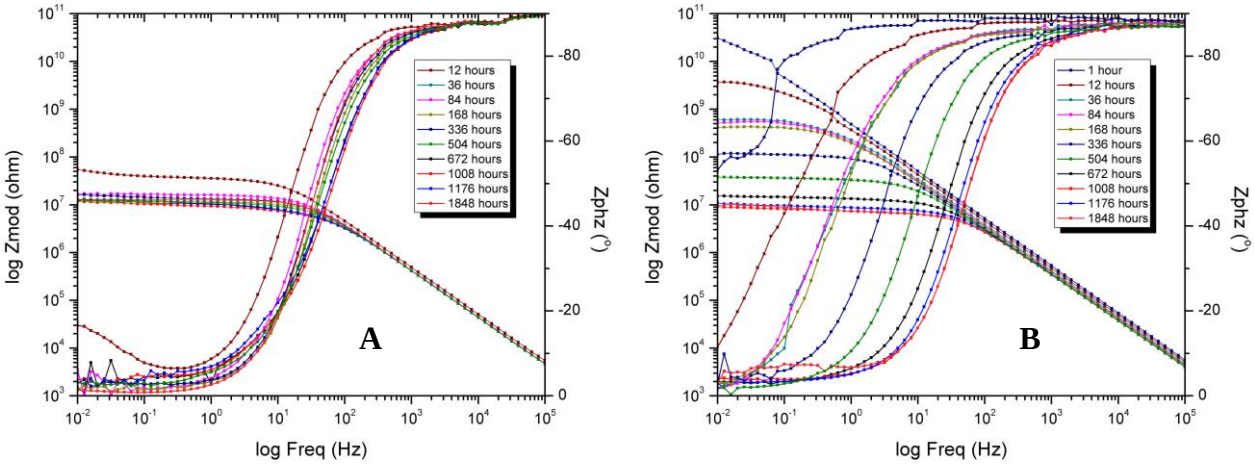

Figure 6.6. A) Bode phase and modulus plots for control coatings without PPy nanospheres on CRS and B) Bode phase and modulus plots for coatings with 1% PPy nanospheres on CRS.

Please note that data for the first hour is not included for control coatings due to noise present in all the replicates of the sample which interfered with clear analysis of data if included. Figure 6.6 shows bode phase and bode modulus plots for control coating without PPy nanospheres and for the coating containing 1% PPy nanospheres on CRS substrate. 12 hour low frequency impedance for control coating was lower than 10^8 Ω (Figure 6.6A); while for coatings containing 1% PPy nanospheres it was higher than 10^9 Ω (Figure 6.6B). The phase angle plot for control coating showed two time constants as early as 12 hours in electrolyte solution. For

coatings containing PPy nanospheres the phase angle remained at -90°, except at very low frequencies until 336 hours in electrolyte solution. In conclusion from bode phase and modulus plots it was observed that the coatings containing 1% PPy nanospheres showed improved corrosion inhibition and better barrier properties than control coatings without PPy nanospheres.

Data obtained from EIS was fitted to the equivalent circuits shown in Figure 6.7. ZView software from Scribner Associates Inc. was used for fitting the EIS data. In the equivalent circuits shown in Figure 6.7. R_s, CPE_c, and R_c corresponds to solution resistance, coating constant phase element and coating resistance respectively. W_s correspond to Warburg element in the later phase of constant immersion when aggressive corrosion reactions are occurring. Equivalent circuit shown in Figure 6.7A is used for fitting initial data when the coatings remain defect free through initial periods of penetration of electrolyte. Figure 6.7B shows equivalent circuit used for later parts of immersion period when the system shows more than one time constant possibly due to pores/defects after initial breakaway of coating barrier. Fitting was performed at the lowest possible chi-square value, the example plots showing the agreement between EIS data and fitting result is shown in Figure 6.7C.

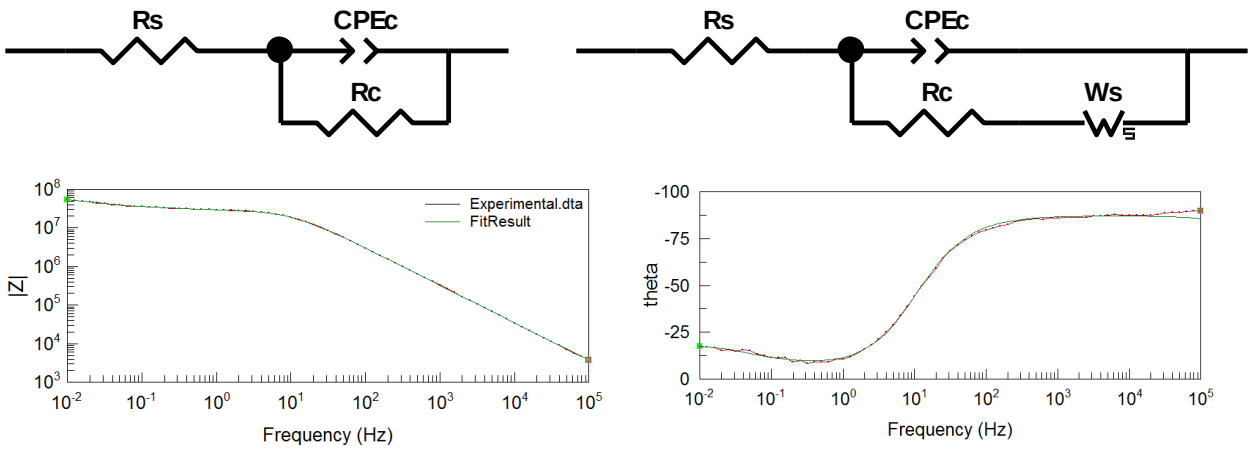

Figure 6.7. A) (Top left) Equivalent circuit corresponding to intact coating, B) (Top right) Equivalent circuit corresponding to coating with defect, and C) (Bottom row) Example plots showing agreement between experimental data and fitting results.

In the case of imperfect behavior of capacitance, constant phase element (CPE) that depicts the behavior of a double layer can be used instead of pure capacitor.[16, 34, 35] The CPE can be described by Equation 6.1 and Equation 6.2. In accordance with the experimental results obtained by electrochemical impedance spectroscopy and ASTM salt spray exposure, the results of circuit modeling provide trends showing corrosion inhibition properties of PPy nanospheres. The data obtained from circuit modeling was graphed with respect to immersion time (Figure 6.8 and 9). For the coatings containing PPy nanospheres R_c was higher as compared to the control coatings until 1800 hours for Al 2024 substrates and until 1100 hours for CRS substrate. As was observed with analysis of experimental bode modulus curves for control coatings on CRS substrate (Figure 6.6A), the R_c rapidly decreased until approximately 150 hours and then showed a slight increase (Figure 6.9A). The increase in the R_c after initial drop could be attributed to the corrosion product blocking the coating defects.

$$Z_{CPE} = \frac{(j\omega)^{-n}}{Y_0} \qquad \text{Equation 6.1}$$

$$n = \frac{\alpha}{\pi/2} \qquad \text{Equation 6.2}$$

Where,
- Z_{CPE}: Electrical impedance of CPE (Ω)
- ω: angular frequency (rad/s)
- n: Value between 0 and1 based on the coatings behavior; ideal capacitor or ideal resistor respectively
- Y_0: CPE constant (1/Ω)
- α: Phase angle for CPE (rad)

On the both CRS and Al 2024 substrates, after an initial increase in the capacitance of the coatings, it was observed that the capacitance remained fairly constant. This behavior is often observed with organic coatings where initially capacitance increases due to ingress of electrolyte in the coatings and once the coating is saturated with the electrolyte the capacitance remains

unchanged with immersion time. For the coatings containing PPy nanospheres the capacitance values were higher than the control coatings. Diffusion coefficients for the coatings were calculated using Equation 6.3. It is possible that 1% PPy nanospheres may have increased the compactness of the coating reflecting a lower diffusion coefficient values as compared to control coatings (Table 6.2).[36]

$$\frac{\log(C_t/C_0)}{\log(C_s/C_0)} = \sqrt{\frac{4Dt}{L^2\pi}} \qquad \text{Equation 6.3}$$

Where, C_t: Coating capacitance at time t

C_0: Coating capacitance at t = 0

C_S: Coating capacitance at saturation

D: Water diffusion coefficient

L: Coating thickness

Diffusion coefficient of the coatings was calculated using equation 6.3.[37] The initial coating capacitance at time t = 0 can be determined by extrapolating the time vs. capacitance curves to 0 hours (Figure 6.8B and Figure 6.9B). For Al 2024 substrates the diffusion coefficient for control coating was 7.11×10^{-14} m^2/s; while for the coatings containing PPy nanospheres the diffusion coefficient was 1.45×10^{-14} m^2/s. Similarly, for CRS substrates the diffusion coefficient was 2.65×10^{-14} m^2/s; while for the coatings containing PPy nanospheres the diffusion coefficient was 2×10^{-14} m^2/s. The decrease in diffusion coefficient could be due to good interaction between PPy nanosphere and the epoxy-amine binder and could be due to increased compactness of the coatings in the presence of nanospheres. The decreased diffusion coefficient can be correlated to the improved corrosion protection of the coatings due to slow transport of the corrosive electrolyte through the coating.

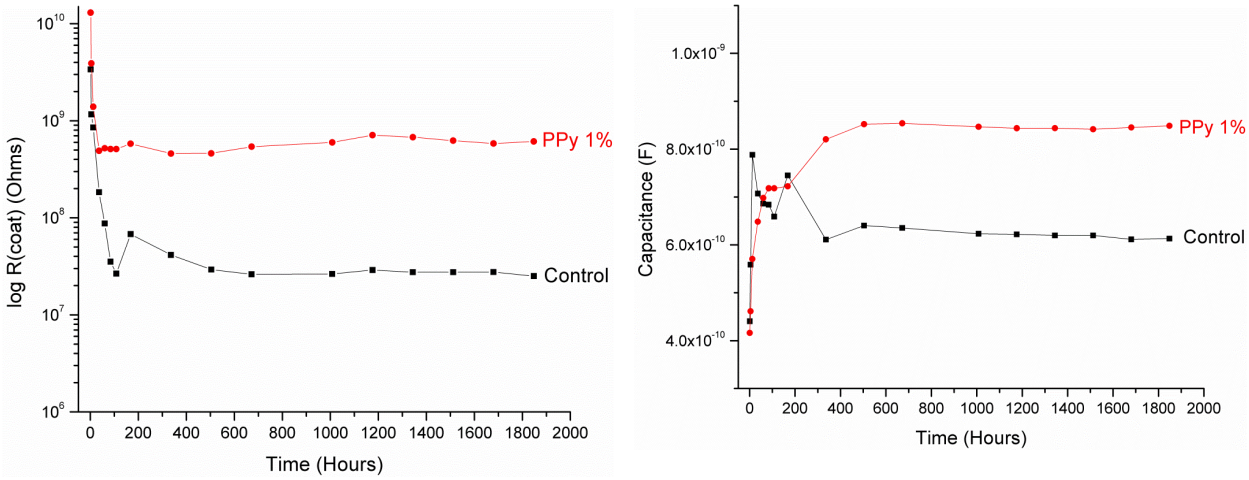

Figure 6.8. A) Left - $R_{(coat)}$ over time for control coatings without PPy nanospheres on Al 2024. B) Right - Capacitance over time for coatings with 1% PPy nanospheres on Al 2024.

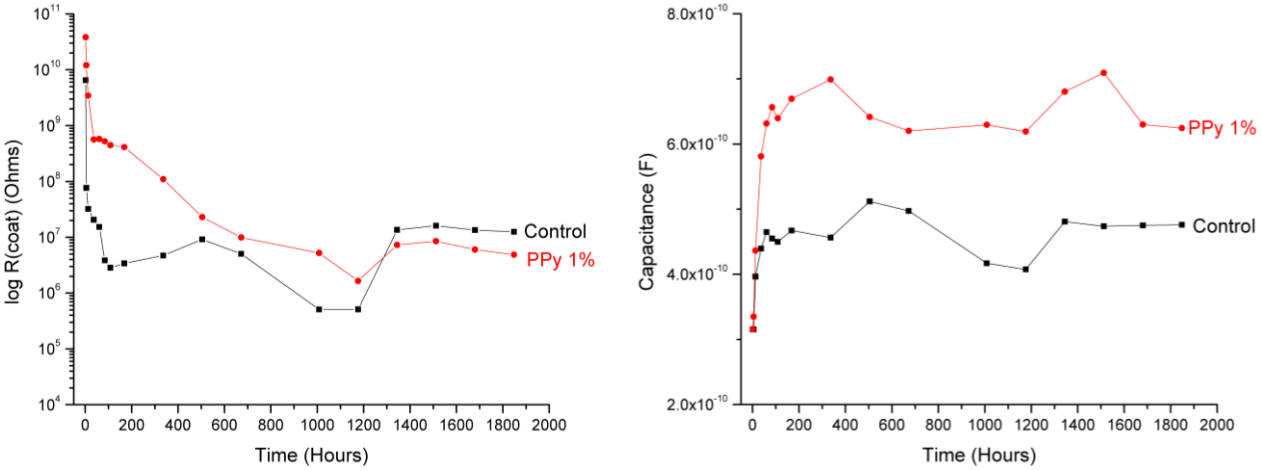

Figure 6.9. A) Left - $R_{(coat)}$ over time for control coatings without PPy nanospheres on CRS, and B) Right - Capacitance over time for coatings with 1% PPy nanospheres on CRS.

At this point, analysis of ASTM B 117 salt spray and EIS studies imply that the PPy nanospheres are indeed corrosion inhibitive. However, they are less effective as a corrosion inhibitor for CRS substrate as compared to aluminum substrate. As described briefly in the introduction section, multiple mechanisms have been proposed to explain corrosion inhibition attributes of EAPs. Few of the mechanisms such as anodic protection, passivation, self-healing or oxygen scavenging are explained in the literature in great details.

In this study, in order to understand the mechanism of the corrosion protection of the PPy nanospheres two tests were performed. Since PPy nanospheres performed better on Al 2024 with respect to corrosion inhibition, the mechanistic experiments were restricted to Al 2024 substrate. Potentiodynamic scans (PDS) were performed on the coatings containing PPy nanospheres as well as control coatings. While the coatings were under immersion in 5% NaCl solution, PDS experiments were performed after 24 hours of constant immersion. Secondly, galvanic corrosion experiments were performed on the coated samples coupled with uncoated Al 2024 substrates. The coatings were under constant immersion for 48 hours in DHS solution. The coupling current and the mixed potential generated during the galvanic interaction between the substrate and the coating were recorded for 48 hours.

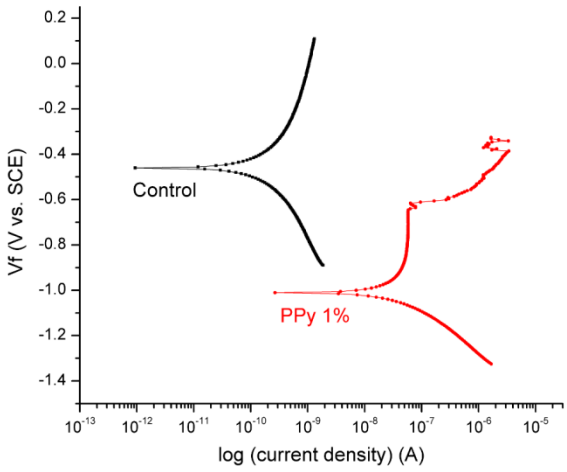

Figure 6.10. Potentiodynamic scans after 24 hours immersion in 5% NaCl (Al 2024).

Figure 6.10. presents potentiodynamic scans of the control coatings and the coating with 1% PPy nanospheres; the corrosion potential was approximately -1000 mV and was lower than the corrosion potential of control coatings. The corrosion protection afforded by the pigments which are more active than the Al 2024 substrates is described as cathodic corrosion protection, which may be associated with the corrosion protection mechanism of PPy nanospheres. This is

particularly true if the PPy is either in reduced or neutral form (n-doped PPy). More active corrosion potential (Figure 6.10 A and B) as compared to control coatings may suggest that the PPy is not in completely oxidized form. It is well known that oxidized PPy shifts the corrosion potential to more noble potential as opposed to reduced or neutral PPy.

If the coatings containing PPy nanospheres provide cathodic protection to Al 2024 substrates, the coupling current in the galvanic corrosion experiment should show higher coupling current as compared to the control coatings without PPy nanospheres. Figure 6.11A shows the coupling current curves against time under constant immersion for both control coatings as well as for coatings with 1% PPy nanospheres. It can be clearly observed that initially the coupling current is significantly higher in the experimental sample than the control. This indicates a possible cathodic protection by PPy nanospheres. However, as the immersion time progressed it was observed that the coupling current decreased without falling below the values of control coatings. Figure 6.12 provides the SVET current density maps for the coatings containing 1% PPy nanospheres on Al 2024 substrates. Both anodic as well as cathodic currents were observed on the scribed area in the centre indicating formation of a typical corrosion cell. If cathodic protection is provided the cathodic currents are observed in the defect site whereas anodic currents are observed on the coated area.[16] This suggests that there could be additional corrosion protection mechanisms at play.

The two mechanisms that explain the corrosion inhibition could be oxygen scavenging by neutral or reduced PPy before oxygen reaches the metal surface. This will hinder the corrosion process due to reduced supply of oxygen for the corrosion reaction.[31, 38] Secondly, the interaction between neutral PPy and active components of aluminum alloy may cause the PPy to be more cathodic than aluminum alloy thereby providing corrosion protection.[39]

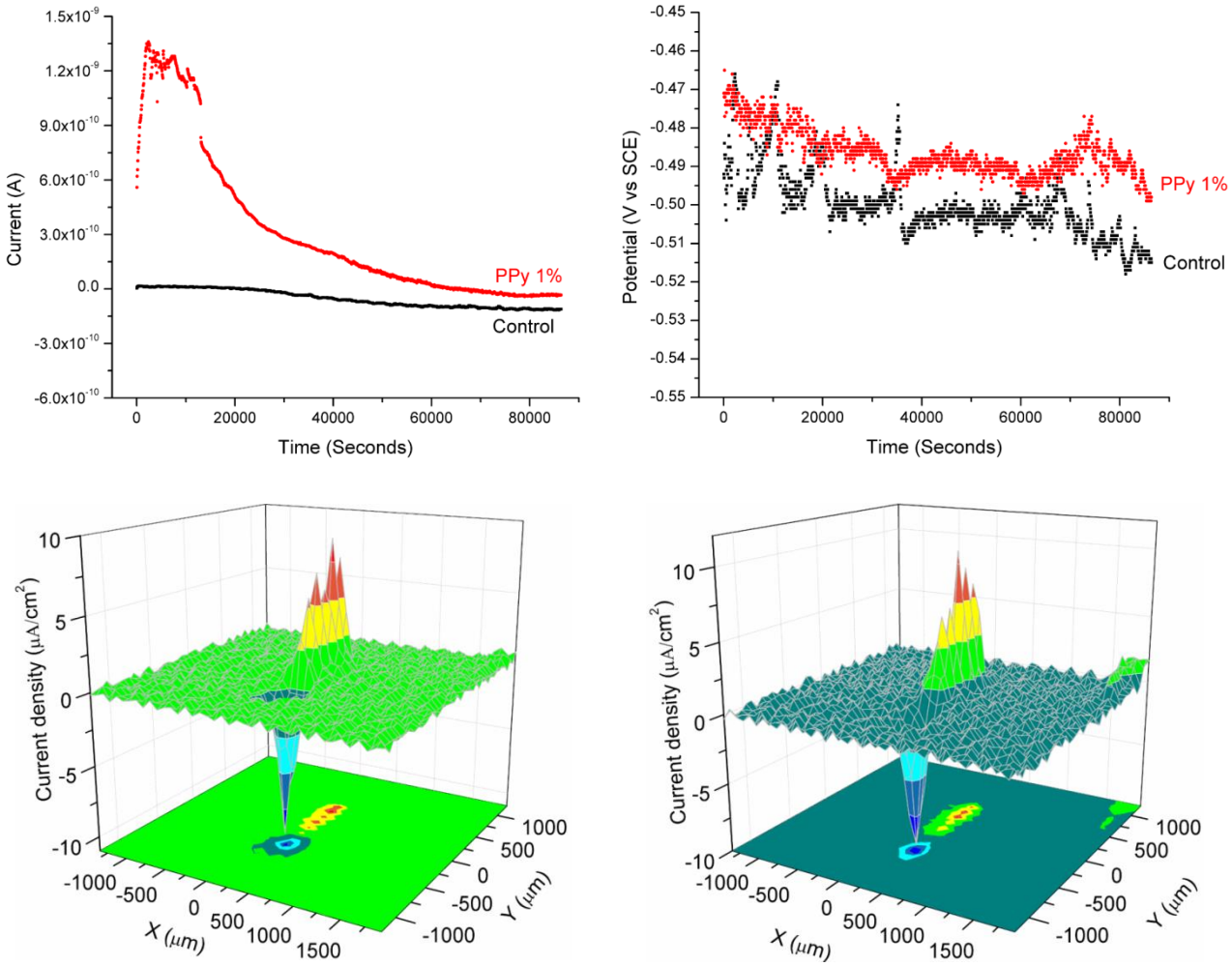

Figure 6.11. A) Top left - Coupling current Vs time, B) Top right - Mixed potential Vs. time, and C) Bottom row - SVET current density maps on coatings containing 1% PPy nanospheres. (Immersion in 0.5% NaCl solution left: 4 hours right: 44 hours)

6.5. Conclusion

Aqueous dispersion of monodisperse PPy nanospheres was synthesized using ozone oxidation. Formulations were prepared in water borne epoxy-amine coatings and were casted on cold rolled steel and Aluminum 2024 substrates. The results of accelerated salt spray exposure and electrochemical impedance spectroscopy suggest that the PPy nanospheres are corrosion inhibitive. Possible reasons for corrosion inhibition of PPy nanospheres were investigated using potentiodynamic scans and galvanic corrosion experiments. It was observed that the PPy

nanospheres may provide corrosion inhibition through oxygen scavenging or cathodic protection mechanism, which needs to be established further to reach to a concrete mechanism for corrosion protection. In future, the PPy nanospheres synthesized and characterized in this study may prove to be a promising alternative to carcinogenic corrosion inhibiting pigments.

6.6. References

1. Lu, W.-K., R.L. Elsenbaumer, and B. Wessling, *Corrosion protection of mild steel by coatings containing polyaniline.* Synthetic metals, 1995. **71**(1): p. 2163-2166.
2. Tansuğ, G., et al., *Mild steel protection with epoxy top coated polypyrrole and polyaniline in 3.5% NaCl.* Current Applied Physics, 2007. **7**(4): p. 440-445.
3. Sitaram, S., J. Stoffer, and T. O'Keefe, *Application of conducting polymers in corrosion protection.* Journal of Coatings Technology, 1997. **69**(866): p. 65-69.
4. Paliwoda-Porebska, G., et al., *On the development of polypyrrole coatings with self-healing properties for iron corrosion protection.* Corrosion science, 2005. **47**(12): p. 3216-3233.
5. Radhakrishnan, S., et al., *Conducting polyaniline–nano-TiO_2 composites for smart corrosion resistant coatings.* Electrochimica acta, 2009. **54**(4): p. 1249-1254.
6. Tallman, D.E., et al., *Electroactive conducting polymers for corrosion control.* Journal of Solid State Electrochemistry, 2002. **6**(2): p. 73-84.
7. Yan, M., et al., *Neutral and n-Doped Conjugated Polymers for Corrosion Control of Aluminum Alloys.* ECS Transactions, 2009. **16**(52): p. 183-194.
8. Breslin, C., A. Fenelon, and K. Conroy, *Surface engineering: corrosion protection using conducting polymers.* Materials & design, 2005. **26**(3): p. 233-237.

9. Straetmans, U., M. Soltau, and F. Straetmans, *Polymeric corrosion inhibiter for metal surfaces and the production thereof*. 2012, Straetmans Hightac Gmbh.

10. Tüken, T., G. Tansuğ, and M. Erbil, *Polypyrrole films modified with graphite layer on mild steel.* Progress in organic coatings, 2007. **59**(1): p. 88-94.

11. Agfa-Gevaert, N., *Conductive Polymers.* Flexible Flat Panel Displays, 2005. **3**: p. 135.

12. Yıldırım, M. and İ. Kaya, *A comparative study of aminothiazole-based polymers synthesized by chemical oxidative polymerization.* Synthetic metals, 2012. **162**(5): p. 436-443.

13. Shinde, V., et al., *Synthesis of corrosion inhibitive poly (2, 5-dimethylaniline) coatings on low carbon steel.* Journal of materials science, 2006. **41**(10): p. 2851-2858.

14. Tallman, D., et al., *Direct electrodeposition of polypyrrole on aluminum and aluminum alloy by electron transfer mediation.* Journal of The Electrochemical Society, 2002. **149**(3): p. C173-C179.

15. Alam, J., et al., *Corrosion-protective performance of nano polyaniline/ferrite dispersed alkyd coatings.* Journal of coatings technology and research, 2008. **5**(1): p. 123-128.

16. Jadhav, N., C.A. Vetter, and V.J. Gelling, *The Effect of Polymer Morphology on the Performance of a Corrosion Inhibiting Polypyrrole/Aluminum Flake Composite Pigment.* Electrochimica acta, 2013. **102**: p. 28-43.

17. Jadhav, N. and V.J. Gelling, *Synthesis and Characterization of Micaceous Iron Oxide/Polypyrrole Composite Pigments and Their Application for Corrosion Protection of Cold Rolled Steel.* Corrosion, 2014. **70**(5): p. 464-474.

18. He, J., D.E. Tallman, and G.P. Bierwagen, *Conjugated polymers for corrosion control: Scanning vibrating electrode studies of polypyrrole-aluminum alloy interactions.* Journal of The Electrochemical Society, 2004. **151**(12): p. B644-B651.

19. Gergely, A., et al., *Corrosion protection of cold-rolled steel by zinc-rich epoxy paint coatings loaded with nano-size alumina supported polypyrrole.* Corrosion science, 2011. **53**(11): p. 3486-3499.

20. Ioniţă, M. and A. Prună, *Polypyrrole/carbon nanotube composites: Molecular modeling and experimental investigation as anti-corrosive coating.* Progress in organic coatings, 2011. **72**(4): p. 647-652.

21. Yeh, J.M., C.P. Chin, and S. Chang, *Enhanced corrosion protection coatings prepared from soluble electronically conductive polypyrrole-clay nanocomposite materials.* Journal of Applied Polymer Science, 2003. **88**(14): p. 3264-3272.

22. Yeh, J.-M., et al., *Enhancement of corrosion protection effect in polyaniline via the formation of polyaniline-clay nanocomposite materials.* Chemistry of materials, 2001. **13**(3): p. 1131-1136.

23. Hosseini, M., et al., *Effect of polypyrrole–montmorillonite nanocomposites powder addition on corrosion performance of epoxy coatings on Al 5000.* Progress in organic coatings, 2009. **66**(3): p. 321-327.

24. Ferreira, C., S. Domenech, and P. Lacaze, *Synthesis and characterization of polypyrrole/TiO_2 composites on mild steel.* Journal of Applied Electrochemistry, 2001. **31**(1): p. 49-56.

25. Lenz, D.M., M. Delamar, and C.A. Ferreira, *Application of polypyrrole/TiO_2 composite films as corrosion protection of mild steel.* Journal of Electroanalytical Chemistry, 2003. **540**: p. 35-44.

26. Wessling, B. and J. Posdorfer, *Nanostructures of the dispersed organic metal polyaniline responsible for macroscopic effects in corrosion protection.* Synthetic metals, 1999. **102**(1): p. 1400-1401.

27. Bagherzadeh, M., et al., *Using nanoemeraldine salt-polyaniline for preparation of a new anticorrosive water-based epoxy coating.* Progress in organic coatings, 2010. **68**(4): p. 319-322.

28. Mahmoudian, M., Y. Alias, and W. Basirun, *Effect of narrow diameter polyaniline nanotubes and nanofibers in polyvinyl butyral coating on corrosion protective performance of mild steel.* Progress in organic coatings, 2012.

29. Vetter, C.A., et al., *Novel Synthesis of Stable Polypyrrole Nanospheres Using Ozone.* Langmuir, 2011. **27**(22): p. 13719-13728.

30. Suryawanshi, A.J., J. Lamb, and V.J. Gelling, *Synthesis of Stable Polypyrrole and Polyaniline Nanospheres.* Advances in Science and Technology, 2013. **79**: p. 7-15.

31. Yan, M., C.A. Vetter, and V.J. Gelling, *Electrochemical investigations of polypyrrole aluminum flake coupling.* Electrochimica acta, 2010. **55**(20): p. 5576-5583.

32. Lamaka, S., et al., *High effective organic corrosion inhibitors for 2024 aluminium alloy.* Electrochimica acta, 2007. **52**(25): p. 7231-7247.

33. Leblanc, P. and G. Frankel, *A study of corrosion and pitting initiation of AA2024-T3 using atomic force microscopy.* Journal of The Electrochemical Society, 2002. **149**(6): p. B239-B247.

34. Tahmassebi, N., S. Moradian, and S. Mirabedini, *Evaluation of the weathering performance of basecoat/clearcoat automotive paint systems by electrochemical properties measurements.* Progress in organic coatings, 2005. **54**(4): p. 384-389.

35. Zhou, Q. and Y. Wang, *Comparisons of clear coating degradation in NaCl solution and pure water.* Progress in organic coatings, 2013. **76**(11): p. 1674-1682.

36. Moreno, C., et al., *Characterization of Water Uptake by Organic Coatings Used for the Corrosion Protection of Steel as Determined from Capacitance Measurements.* International Journal of Electrochemical Science, 2012. **7**(8): p. 8444-8457.

37. Allahar, K.N., et al., *Water transport in multilayer organic coatings.* Journal of The Electrochemical Society, 2008. **155**(8): p. F201-F208.

38. Yan, M., C.A. Vetter, and V.J. Gelling, *Corrosion inhibition performance of polypyrrole Al flake composite coatings for Al alloys.* Corrosion science, 2013. **70**: p. 37-45.

39. Yan, M., et al., *Corrosion control coatings for aluminum alloys based on neutral and n-doped conjugated polymers.* Journal of The Electrochemical Society, 2009. **156**(10): p. C360-C366.

CHAPTER 7. ORGANIC CORROSION INHIBITOR INCORPORATED POLYPYRROLE FOR CORROSION INHIBITION OF ALUMINUM ALLOY 2024-T3

7.1. Introduction

Copper is an important alloying element for aluminum alloy Al 2024-T3, on the grounds that it provides significant strength to the pure aluminum.[1] This has driven to its widespread use in the aerospace industry. However, the increase of copper as an alloying element in the aluminum alloys adversely affects the corrosion resistance. [2-5] Pure aluminum is resistive to corrosive environments particularly in neutral solutions, afforded by the passivating and barrier effect of the well adhered oxide layer.[4, 5] Susceptibility of Al 2024-T3 towards corrosion is considered to be because of the inter-granular and pitting corrosion due to alloying elements present in Al 2024, especially due to the cathodic effect of copper. It is reasoned that the copper granules present a galvanic interaction with the anodic aluminum matrix resulting in pitting corrosion of aluminum. [2, 3, 5] This phenomenon worsens with time as copper spreads on the aluminum, as a result of dealloying, providing larger cathodes to the aluminum anode. [3] Considering the growing use of Al 2024 in the industry and the regulatory ban on carcinogenic corrosion inhibitors; the scientific research on the development of environment friendly corrosion inhibitors for Al 2024-T3 has grown over the years.

In the previous chapter, polypyrrole (PPy) nanospheres were investigated for their corrosion inhibition activity for aluminum alloy Al 2024-T3 substrates. It was believed that the reduced form of PPy may be scavenging oxygen in the interface of coating and substrate, consequently preventing filiform (under-film) corrosion. In this chapter, organic corrosion inhibitors (OCI) modified PPy are proposed; to circumvent the aforementioned issue of galvanic interaction between granular copper and aluminum matrix in Al 2024-T3. The OCIs which form

an insoluble complex with copper and reduce the galvanic interaction between copper and aluminum are incorporated (or entrapped) in PPy nanospheres during the synthesis. The intent was to use the synergistic effect, from oxygen scavenging by PPy nanospheres, and from the reduction of galvanic interaction between aluminum and copper by OCIs; to design efficient corrosion inhibiting additives. The OCIs employed in this study are benzotriazole (BTA), salicyaladoxime (SCDM) and quinaldic acid (QA). Interestingly, a literature survey indicated no studies in reference to the synergistic effects of electroactive polymers (EAPs) and OCIs. Incorporation of OCIs in EAP's for instance PPy and polyaniline (PANI) will be appealing to the corrosion scientists with regards to the additives with enhanced corrosion inhibition efficiency.

When present in an electrolyte solution, OCIs have previously been shown to provide improved anticorrosion activity towards Al 2024-T3 by forming a protective oxide layer on the substrate.[3, 6, 7] The challenge, however, is to use OCIs for long term protection of metal alloys especially by incorporating OCIs in organic coatings. Distribution, delivery and dissolution are three important factors for achieving corrosion inhibition from OCIs. Since they are small molecules they tend to wash away from the coatings. If the OCIs have low solubility the dispersion and delivery to the substrate is inefficient. [8] A solution to these challenges is to incorporate OCIs in containers of organic or inorganic particles, which can further be embedded in the coating matrix to be applied on the Al 2024-T3 substrates. Inert micro and nano particles, for instance halloysite nanocontainers and [9, 10] mesoporous silica,[11, 12] are used for delivering benzotriazole (BTA). Additionally, in a study reported by Poznyak and coworkers, organic corrosion inhibitors, QA and 2-mercaptobenzothiazole (MBT), were loaded in the layered double hydroxides (LDHs). [13] Hydroxyapetite (HAP) microparticles were also utilized as reservoirs for OCIs including SCDM, 8-hydroxyquinilne, lanthanum (III) and cerium (III).

[14] Nanocontainers composed of layer by layer assembly of polyeletrolyte on slilica nanoparticles were also reported to be self regulating the release of BTA on demand.[8]

Polymeric microcapsules or containers have greater advantages as compared to inorganic particles due to improved compatibility with the polymeric coatings. Recently, polystyrene nanocontainers for BTA were developed by Li *et al.* that showed self healing character as well as pH sensitive release for steel substrates.[15] Polymeric nanocapsules containing MBT were synthesized and investigated for their corrosion resistance performance in a water based epoxy system on aluminum 5083 by Plawecka and co-workers.[16]

The advantage of using OCI modified PPy (OCI-PPy) is the synergism achieved from utilization of both the container, PPy in this case, and the released OCI. In the previous scientific studies the containers are inert and do not particularly take part in the corrosion prevention except for the release of the OCIs. We have previously demonstrated synthesis of dispersions of PPy nanospheres utilizing ozone oxidation in water. The PPy nanospheres are produced spontaneously in water with a coagulative growth in the particle size up to a few hours. In this study, the objective was to incorporate OCIs during the particle growth phase of PPy nanospheres consequently producing PPy particles embedded with OCIs. BTA, SCDM and QA are incorporated in PPy at various concentrations from 0.005 M to 0.02 M. The OCI-PPy particles are characterized utilizing scanning electron microscopy (SEM), Fourier transform infrared spectroscopy (FTIR) and thermogravimmetric analysis (TGA). UV Vis spectroscopy is used to study the release behavior of the three OCIs. The OCI-PPy was further incorporated in water based epoxy-amine coating and was studied for their corrosion inhibition for Al 2024-T3 using traditional accelerated salt spray exposure techniques and electrochemical impedance spectroscopy (EIS).

7.2. Materials and methods

7.2.1. Materials

BTA, SCDM, QA, and pyrrole were purchased from Sigma-Aldrich. BTA, SCDM, and QA were used as received. Pyrrole was distilled before use. The epoxy dispersion (Beckopox VEP 2381W/55WA) and water reducible amine (Beckopox EH 623W/80WA) were kindly provided by Cyte. BYK 348 and BYK 1710 were kindly provided by BYK. Supor-100 0.1µm, 47 mm diameter filter were purchased from PALL Life Sciences. Mesoporus Silica 200 nm was purchased from Sigma Aldrich.

7.2.2. Synthesis of OCI-PPy

In a typical synthesis, 0.67 gm of pyrrole was dissolved in 18 MΩ Millipore water. Ozone was generated using the ozone generator purchased from Absolute Ozone. Pure oxygen was supplied to the ozone generator. 18% by weight ozone was produced in ozone/oxygen mixture at a pressure of 20 psi and flow rate of 0.2 L/min. The produced ozone was bubbled through the pyrrole solution for 60 seconds. After the ozone exposure, the residual ozone was removed by a gentle stream of air through the compressed air line. After about two minutes, OCIs were added to the solution and the solution was kept under magnetic stirring for 24 hours. The OCIs were added at the molar concentrations of 0.001M, 0.005M, 0.01M and 0.02M. Same procedure was followed for all three corrosion inhibitors including BTA, SCDM, and QA. In this manner 12 reactions were performed as shown in Table 7.1. A control reaction was also performed without the addition of any OCIs. After four days of the synthesis, the particles were filtered using Supor-100 0.1µm, 47 mm diameter filter and were washed at least three times with excess amount of 18 MΩ Millipore water or until clear filtrate was received. The particles were then dried for 24 hours at approximately 45°C before characterizing.

Table 7.1. Reaction summary

Benzotriazole (BTA)	Salicylaldoxime (SCDM)	Quinaldic acid (QA)
BTA: 0.001M	SCDM: 0.001 M	QA: 0.001 M
BTA: 0.005M	SCDM: 0.005 M	QA: 0.005 M
BTA: 0.01M	SCDM: 0.01 M	QA: 0.01 M
BTA: 0.02M	SCDM: 0.02 M	QA: 0.02 M

7.2.3. Characterization

FTIR was performed utilizing a Nicolet FTIR spectrometer, while UV-Vis spectroscopy was performed using Varian-500 UV-Vis-NIR spectrophotometer. Release studies were performed in 100 ml 18 MΩ Millipore water with 30 mg of the washed and dried particles. The dispersion was kept under magnetic stirring. At periodic intervals about 5 ml of the dispersion was filtered through a Whatman GD/X syringe membrane filter (pore size-0.2 μm, diameter 25 mm). UV-Vis spectroscopy was performed on the filtrate. The release of OCIs was monitored with respect to the peaks of individual OCIs. For example, a dilute solution of BTA provides absorbance peak at the wavelength of 260 nm and 278 nm. The release of BTA from BTA-PPy was thus monitored through increase in the absorbance of the peak at 260 nm.

TGA was performed using TGA Q 500 instrument supplied by TA instruments. At a heating rate of 20°C/min the samples were heated from room temperature to 800°C in air. SEM was performed using JEOL JSM-7600F electron microscopy. Particles were first centrifuged and dried before sprinkling on the carbon tape attached to aluminum mounts. Gold was coated onto the particles using a Balzers SCD 030 sputter coater. Magnification, accelerating voltage values and scales bars are provided on the figures.

7.2.4. Formulations for coating systems

For corrosion inhibition studies, BTA-PPy, SCDM-PPy and QA-PPy were synthesized at 0.02 M concentrations of BTA, SCDM and QA respectively. Six formulations were prepared utilizing the formulation provided in Table 7.2. The centrifuged and dried particles were redispersed in Millipore water by sonicating for about 10 minutes. Water reducible amine was added to this dispersion and was simply mixed using a small spatula. Epoxy dispersion was added to this mixture followed with the addition of wetting agent and defoamer. This formulation was stirred using magnetic stirrer for about 5 minutes. The remaining Millipore water in the formulation was used for thinning down the formulation. The formulations were further allowed to sit for 5 minutes before application. Aluminum alloy 2024-T3 panels were sand blasted and cleaned using hexanes prior to application. The formulations were applied using a drawdown bar to achieve a dry film thickness of 70-90 µm. The panels were allowed to air dry at ambient conditions for at least seven days before characterizing.

Table 7.2. Formulation summary

Components	**Commercial name**	**F-1 (Wt %)**
The synthesized particles 1. BTA-PPy 2. SCDM-PPy 3. QA-PPy 4. Silica (As received) 5. Control (Without additive) 6. Control-PPy		00.42
Millipore water		14.00
Water reducible amine	Beckopox EH 623W/80WA	12.00
Water based epoxy	Beckopox VEP 2381W/55WA	54.10
Wetting agent	BYK 348	00.52
Defoamer	BYK 1710	00.52
Millipore water		18.44
Total		**100**
% solids of the particles		1.03

7.2.5. Corrosion inhibition studies

Accelerated salt spray exposure according to the standard ASTM B117 was used for accelerated salt spray testing. Prohesion conditions were performed according to ASTM G85-A5. Adhesive tape was used for masking the edges and uncoated areas on the coated panels. Artificial defect was introduced in the coating in the form of X-shape. The panels were taken out of the exposure cabinets after a set period of intervals for visual assessment. The accelerated exposure test was performed on triplicates. EIS was performed using Gamry Reference 600 potentiostat with Gamry Framework Version 5.58 software. EIS cell was prepared using a cylinder clamped to the coating using a rubber ring, allowing 7.6 cm^2 of the coating area exposed to the constant immersion of 5% NaCl solution. Platinum mesh electrode was used as a counter electrode, saturated calomel electrode was used as a reference electrode, and the coated substrate acted as a working electrode. EIS spectra were obtained for the frequencies ranging from 100,000 – 0.01 Hz frequency range at an AC voltage of 10 mV. The scans were performed at set period of intervals. All experiments were performed in triplicates.

7.3. Results and discussions

7.3.1. Characterization of organic corrosion inhibitor entrapped PPy (OCI-PPy)

In previous studies it was observed that the PPy nanospheres grow in particle size over a period of time before approaching to a stable particle size. During this period of the particle growth the OCIs viz. BTA, SCDM and QA were added to the synthesis in order to incorporate them in the PPy nanospheres. The ozone oxidation provides aqueous dispersion of PPy nanospheres with hydrophobic PPy in the core of the nanospheres and hydrophilic overoxidized PPy in the shell. Considering the aforementioned property of PPy nanospheres and their

accumulative growth during the synthesis, OCIs with a partial hydrophilic and hydrophobic character were chosen for the study (Figure 7.1).

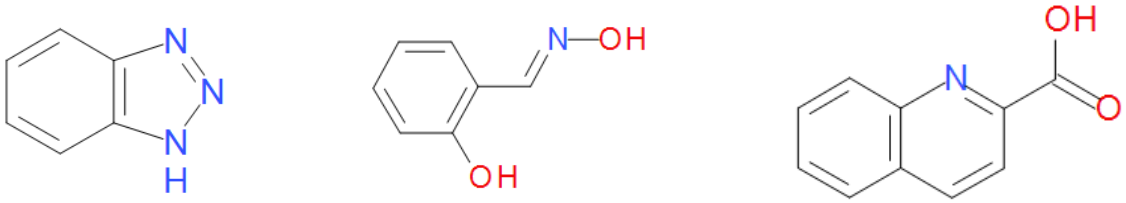

Benzotriazole (BTA) Salicylaldoxime (SCDM) Quinaldic Acid (QA

Figure 7.1. Chemical structures of OCIs used for the synthesis of OCI modified PPy.

The addition of the OCIs affected the stability, morphology and size of PPy particles. (Figure 7.2 and Figure 7.3) The dispersions were not stable particularly at 0.005 M or higher concentrations of OCIs (Figure 7.2). Among the three OCIs, particle size was not affected significantly when BTA was incorporated in the PPy nanospheres. Addition of SCDM at higher concentrations (> 0.001 M) negatively influenced the particle size as well as particle size distribution of SCDM-PPy; particles in the range of 1-2 µm and 200-300 µm were evident from SEM images. In the case of QA, apart from the concentration of 0.02 M, the particle size and morphology was not influenced at lower concentrations of QA. The significant influence on the morphology and size of PPy especially in the case of SCDM may be related to the incompatibility between pyrrole oligomers and SCDM during growth of the PPy nanospheres. [17]

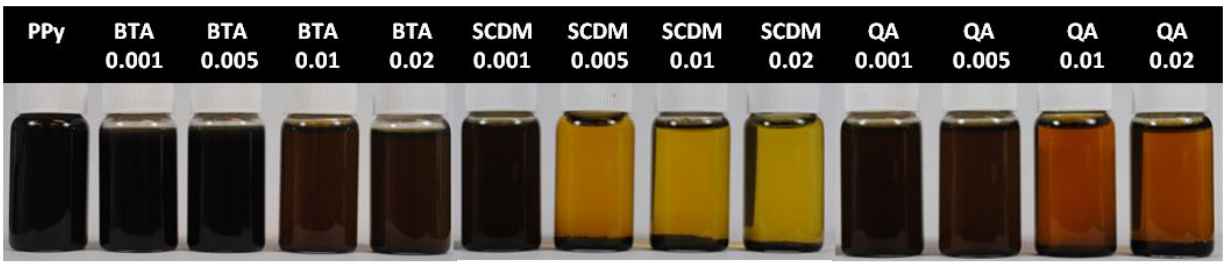

Figure 7.2. Stability of the aqueous dispersion after seven days of the synthesis.

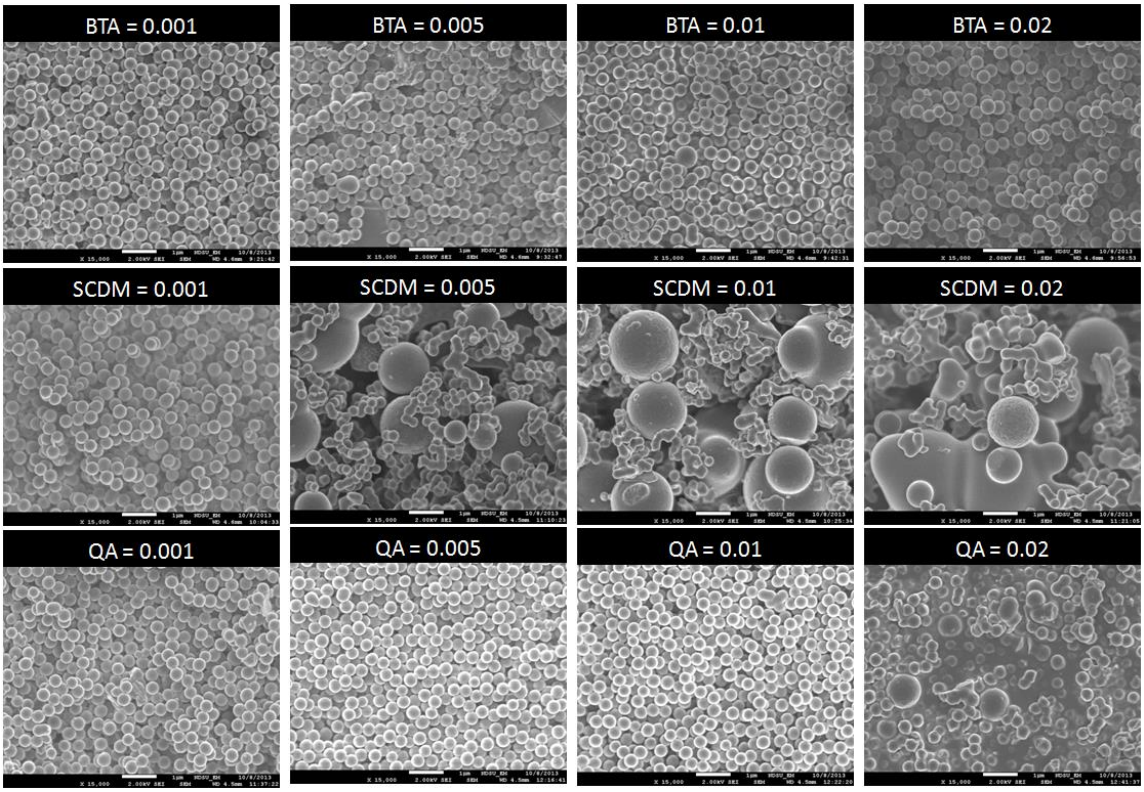

Figure 7.3. SEM images of the reactions performed with various OCIs at various concentrations of OCIs.
(*Note: The scale bar denotes 1 µm for all the images.)*

The entrapment of OCIs was investigated using FTIR and TGA. The peaks associated with PPy were observed (Figure 7.4, Figure 7.5 and Figure 7.6), for example PPy ring vibrations at approximately 1380 cm^{-1} and 1489 cm^{-1}, =C-H in plane vibrations at approximately 1090 cm^{-1} and 1220 cm^{-1}, and =C-H out of plane vibrations at approximately 774 cm^{-1} and 881 cm^{-1}.[18-22] Apart from that, the peaks which indicate the presence of BTA, SCDM and QA were also observed in the FTIR spectra. Triazole vibration peak associated with BTA were detected in BTA-PPy at approximately 1210 cm^{-1} (Figure 7.4).[23, 24] Oxime vibration peak associated with SCDM was present in the FTIR spectra at about 1458 cm^{-1} (Figure 7.5).[25, 26] The shoulder peaks present between 1480 cm^{-1} and 1640 cm^{-1} may indicate the presence of pyridine stretching vibrations in QA (Figure 7.6). [27, 28]

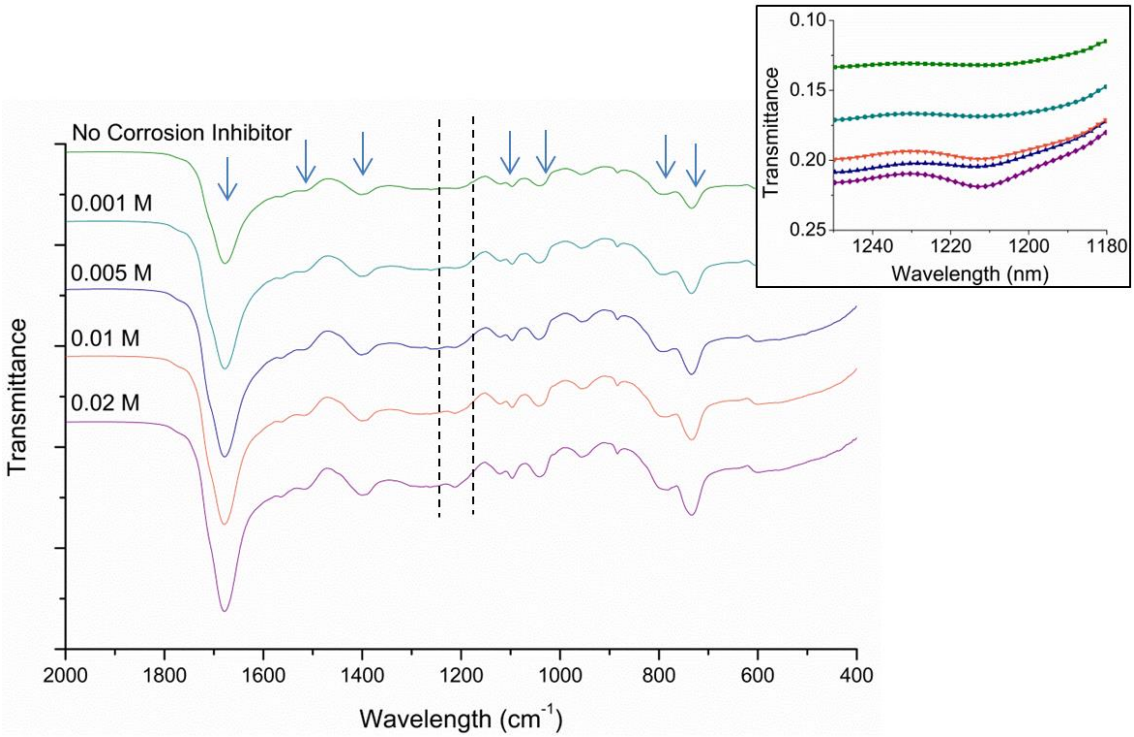

Figure 7.4. FTIR spectra for BTA-PPy at various concentration of BTA (Concentrations provided on each spectra) Inset: The magnified spectra.

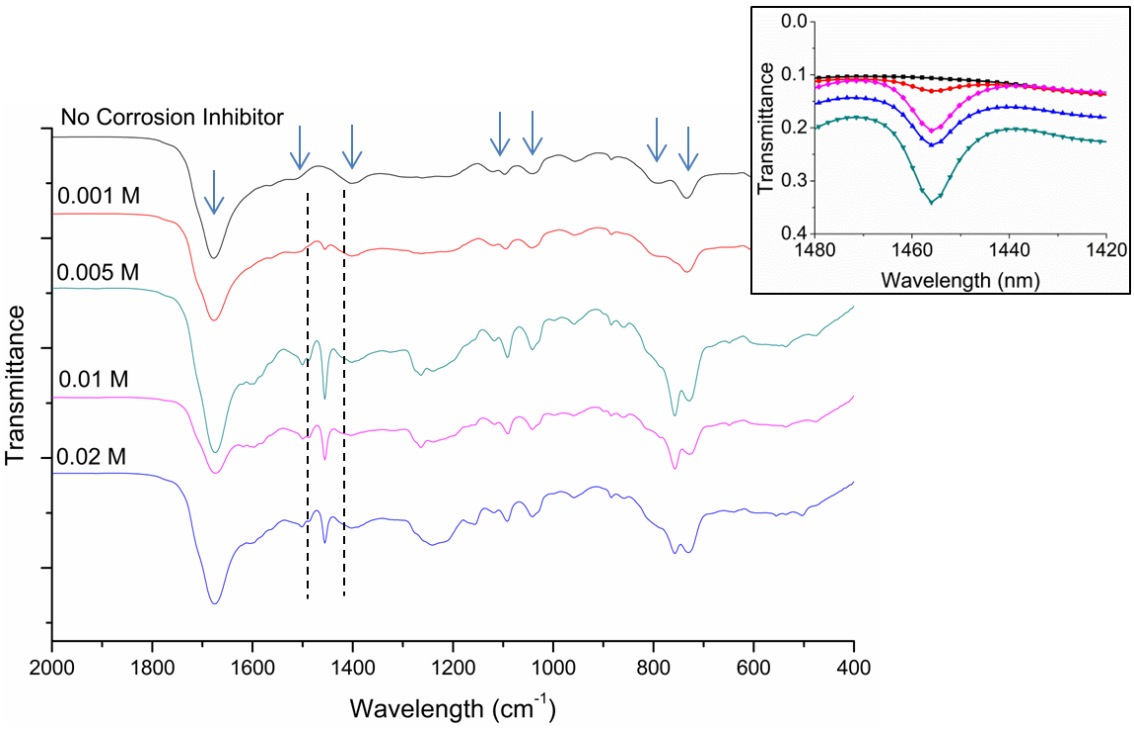

Figure 7.5. FTIR spectra for SCDM-PPy at various concentration of SCDM (Concentrations provided on each spectra) Inset: The magnified spectra.

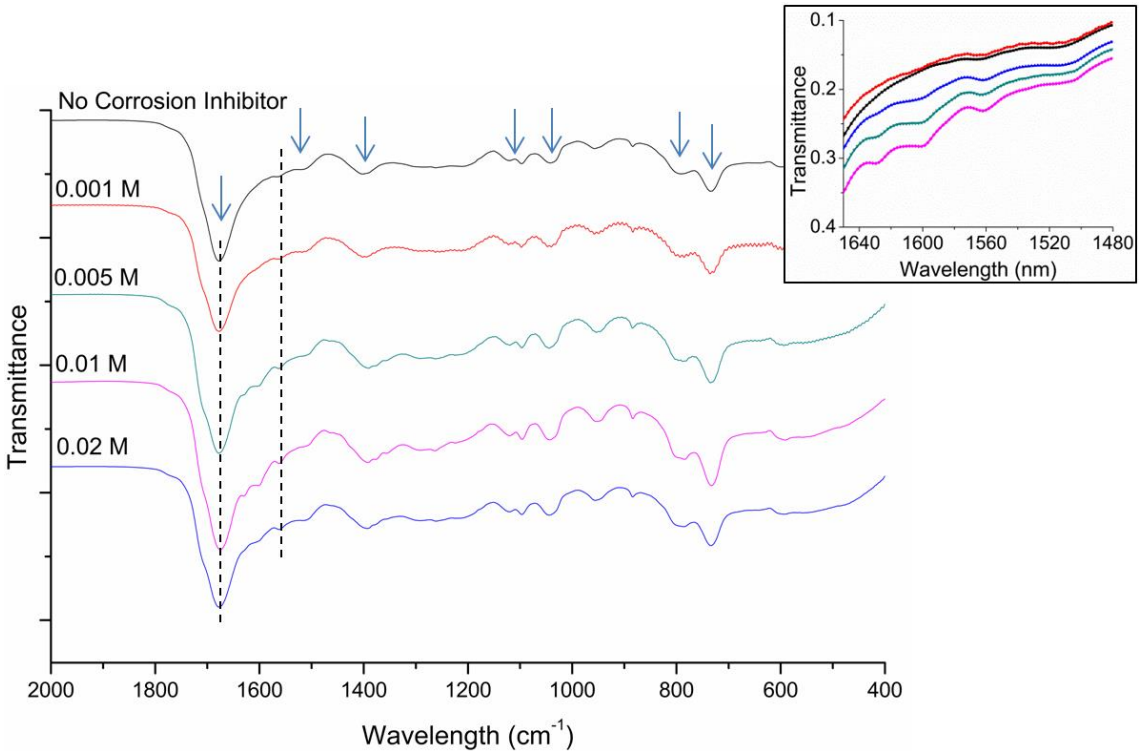

Figure 7.6. FTIR spectra for QA-PPy at various concentration of QA (Concentrations provided on each spectra) Inset: The magnified spectra.

This suggests the successful entrapment of BTA, SCDM and QA in BTA-PPy, SCDM-PPy, and QA-PPy, respectively. Moreover, with the increase in concentration of the OCIs, the peak intensities associated with the OCIs also increased. If the OCIs are successfully entrapped in PPy nanospheres, TGA should show distinct degradation peak in the thermal degradation that belong to the OCIs. TGA was performed on the three individual OCIs; the degradation peaks for BTA, SCDM and QA were found to be at 247°C, 235°C, and 220°C, respectively (Figure 7.7). TGA was also performed on the composites containing OCI and PPy to analyze if the peaks associated with the degradation of individual OCIs are present in the composite. The derivative weight vs. temperature plots are provided in Figure 7.8 for PPy without corrosion inhibitor, BTA-PPy (0.02M), SCDM-PPy (0.02M), and QA-PPy (0.02M). The degradation peaks which were present in the individual OCIs (Figure 7.7) can also be observed in the composites with

OCI and PPy, particularly in the range of 210°C to 250°C, further emphasizing on the successful incorporation of OCIs in the PPy.

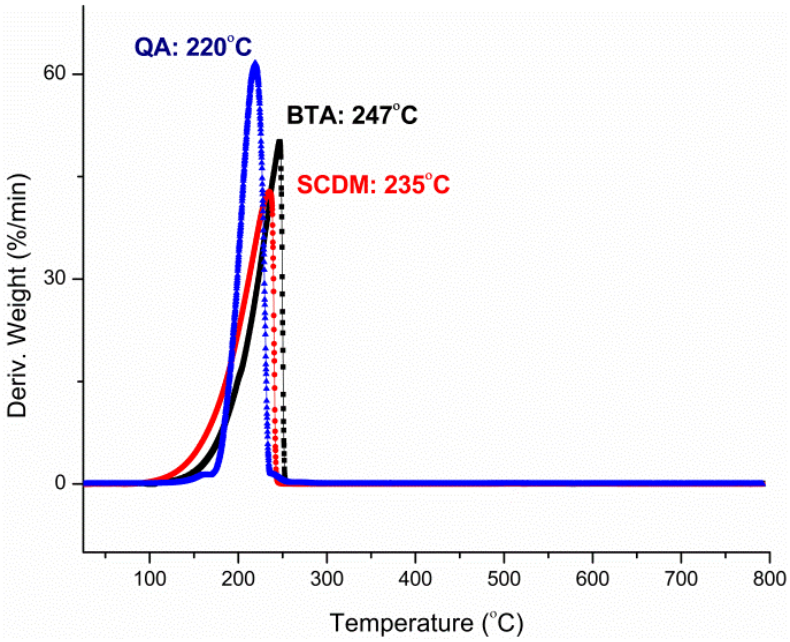

Figure 7.7. Derivative weight vs temperature plots for individual OCIs.

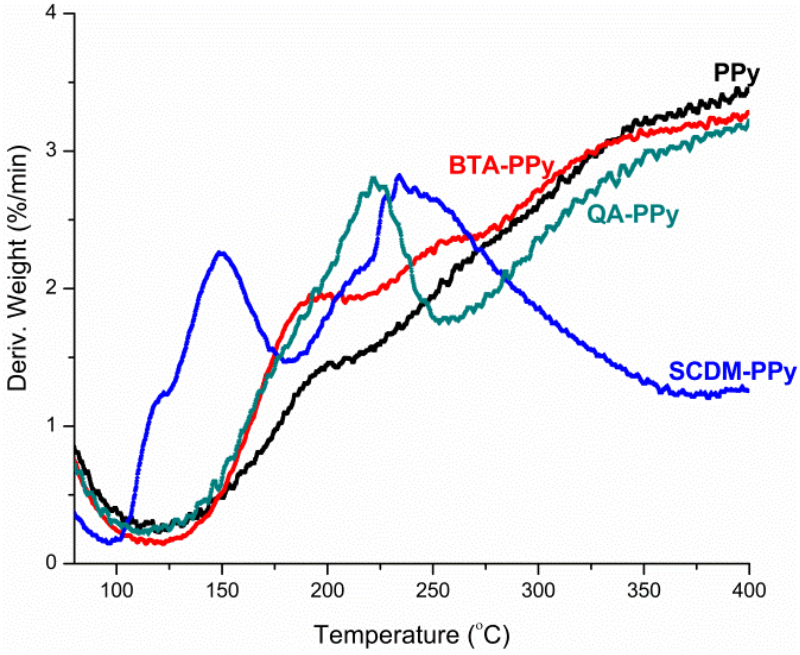

Figure 7.8. Derivative weight vs temperature plots for only PPy, BTA-PPy, SCDM-PPy and QA-PPy synthesized at 0.02 M concentration of OCIs.

7.3.2. Release studies of OCI-PPy

In addition to the entrapment of the OCIs in the PPy, the release of the OCIs from the PPy plays an important role in determining the efficiency of the corrosion inhibiting system. Prior to performing the release studies; about 5 mg of each OCI (BTA, SCDM, and QA) was dissolved in 20 ml 18 MΩ Millipore water. UV-Vis spectroscopy was performed on the solution to determine the absorbance peaks of individual OCIs (Appendix Figure 7A). BTA provides with the absorbance peaks at 260 nm and 278 nm; SCDM provides the absorbance peaks at 213 nm, 257 nm, and 303 nm; while QA provides the absorbance peaks at 240 nm to 320 nm. The release behavior of the organic corrosion inhibitor was studied in 18 MΩ Millipore water. 30 mgs of each OCI-PPy was added to 100 ml water and was kept under magnetic stirring. At periodic intervals about 5 ml of the dispersion was filtered and UV-Vis spectroscopy was performed on the filtrate. The OCIs are expected to release from PPy and show increased peak intensities in the UV-Vis spectra. The peaks of the individual OCIs in each filtrate were observed, approving the fact that the OCIs were indeed being released from PPy.

The peak at 260 nm for BTA-PPy, 257 nm for SCDM-PPy, and 238 nm for QA-PPy, were monitored with the dispersion under constant magnetic stirring over a period of five days, to estimate the release behavior of the OCI. Approximately 100% of the OCIs were released at the end of the five days of magnetic stirring for each sample (Figure 7.9). Maximum release of about 50% was observed at the end of the 24 hours of the immersion of the OCI-PPy in water. This release property corresponds with the release behavior shown by silica and halloysite nanocontainers.[29] Thus, this system makes the case for being an advanced corrosion inhibitor owing to not only the corrosion inhibition ability of PPy but also the corrosion inhibition provided by the released OCIs. It should also be noted that all the corrosion inhibitors show

almost identical release behavior, which can be attributed to the similar entrapment mechanism used for the incorporation of the three OCIs in PPy.

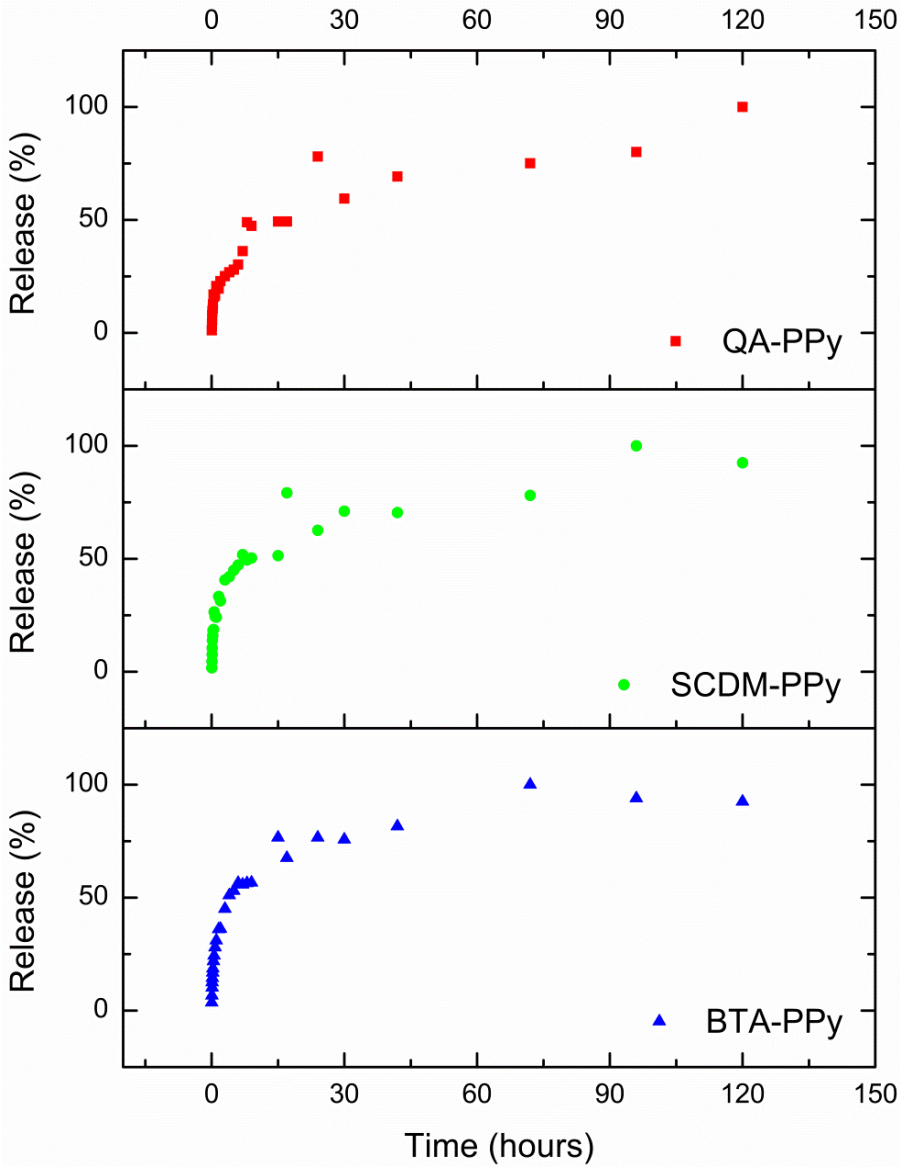

Figure 7.9. Release behavior of OCIs from OCI-PPy (Top: QA, Middle: SCDM, Bottom: BTA).

7.3.3. Corrosion inhibition studies of OCI-PPy

As previously discussed in the experimental section, six coatings were formulated with 1% of the three OCI-PPy; unmodified PPy nanospheres; with 1% mesoporous silica; and clear coat without any particles. The OCI-PPy synthesized at 0.02 M concentration was used for

accelerated weathering studies. The coating matrix used was water based epoxy-amine. The formulation with silica was used to compare between the corrosion inhibition properties of the PPy nanospheres and the mesoporous silica, without entrapment of the OCIs.

The scribed coatings of all the six formulations were exposed to accelerated salt spray according to ASTM B 117 and to the prohesion conditions according to ASTM G85-A5. Figure 7.10 displays the images of the panels exposed to ASTM B 117 salt spray. Among all the formulations, the formulation containing 1% BTA-PPy performed superior, characterized by low blistering around the defect and less corrosion on the scribed area. It can be observed in the Figure 7.10 that corrosion did not progress after 168 hours of the salt spray exposure in the coatings containing 1% BTA-PPy.

The clearcoat (without any particles) showed formation of blisters as well as increased corrosion in and around the scribed area (Figure 7.10). The coatings containing 1% mesoporous silica were the poorest amongst the formulations prepared in this study. This could be attributed to the pores present in the mesoporous silica which provide easier paths for penetration of the electrolyte.

The clearcoat and the coatings containing silica were also severely affected by the filiform corrosion in the unsribed areas of the exposed panels. The coatings containing PPy nanospheres (without OCI) performed better than both clearcoat as well as coatings containing silica. This demonstrates the importance of using PPy as the host material for OCIs as compared to inert containers for instance mesoporous silica.

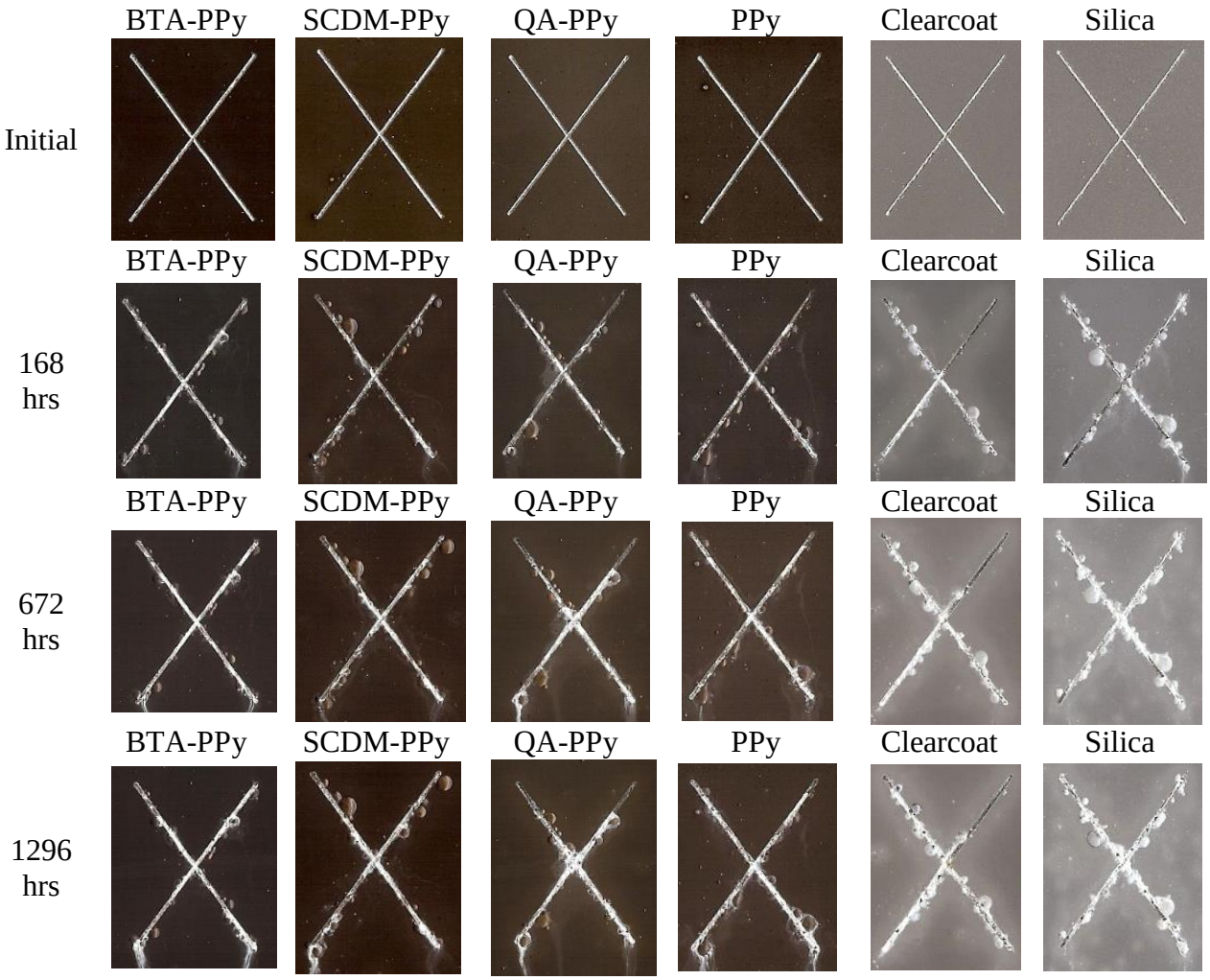

Figure 7.10. Photographs of Al 2024-T3 panels coated with epoxy amine after exposure to ASTM B 117 salt spray.

Although the blister size was slightly large for the coatings containing 1% SCDM-PPy and 1% QA-PPy, the blister density was less, as compared to the clearcoat and the coating containing silica. Less corrosion in and around the scribed area was observed in the coatings containing 1% SCDM-PPy and 1% QA-PPy as compared to the control coatings (clearcoat and silica). Finally, according to the visual assessment of the corrosion performance of the six coatings, they may be rated in the following order (from superior to inferior) with respect to the ASTM B117 salt spray exposure. BTA-PPy > SCDM-PPy > PPy > QA-PPy > Clearcoat > Silica.

In addition to the ASTM B117 salt spray exposure, the Prohesion® testing on the six coating formulations was performed to gain more insights into the performance of the developed formulations. The corrosion under the prohesion condition was characterized by the formation of white rust on the scribed area (Figure 7.11). The worst performance was shown by the coatings containing mesoporous silica. Acute corrosion on and around the scribed area can be observed in Figure 7.11. The clearcoat was also prone to corrosion in the prohesion conditions particularly at 1296 hours of the exposure.

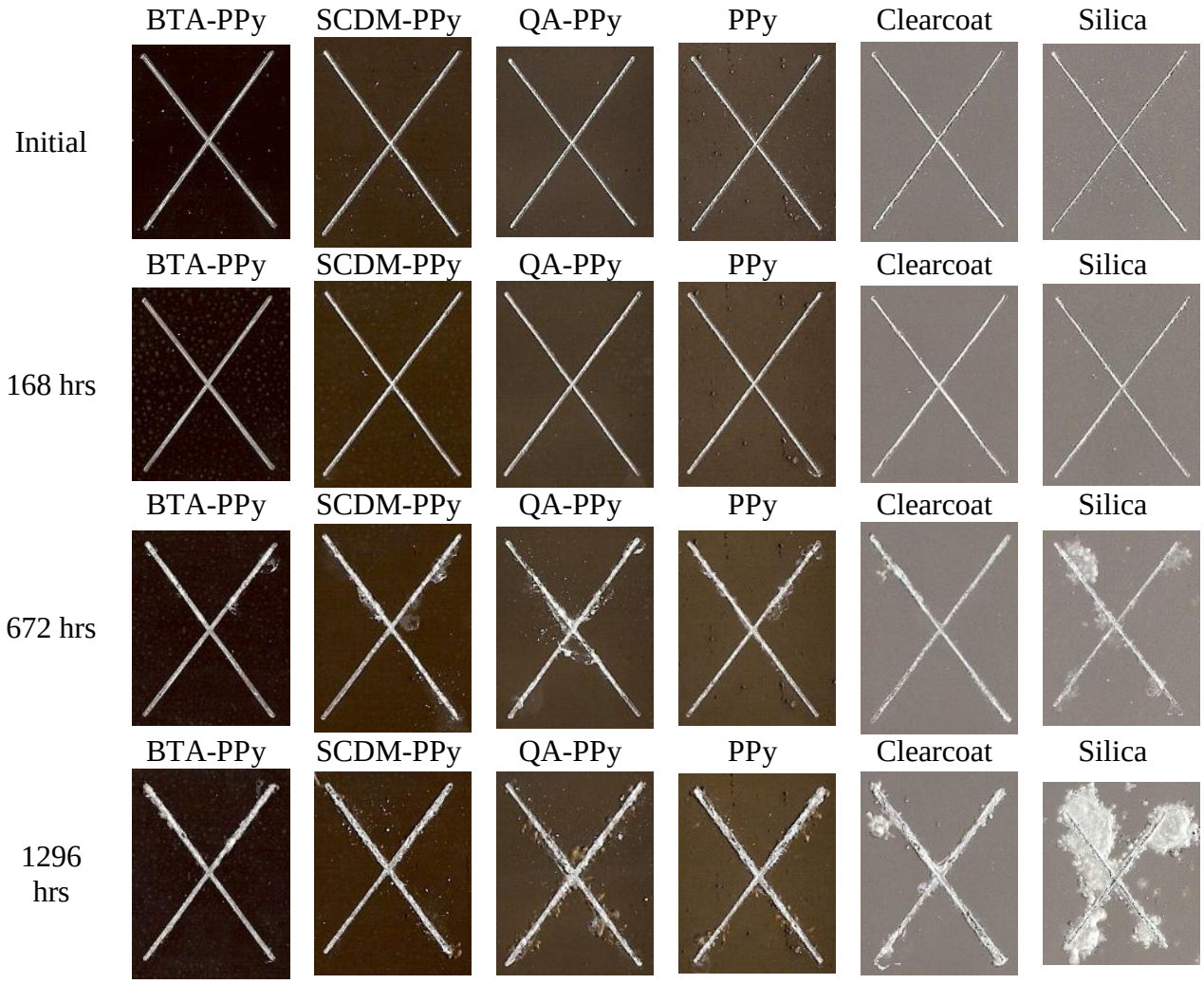

Figure 7.11. Photographs of Al 2024-T3 panels coated with epoxy amine after exposure to prohesion conditions according to ASTM G85-A5.

The best performing coating was observed to be the coating containing 1% BTA PPy. Even after 1296 hours of salt spray exposure the scribed area did not undergo any significant corrosion. The coatings containing 1%PPy, 1% SCDM-PPy, and 1% QA-PPy performed better than the clearcoat as well as the silica containing coating.

The performance ratings for the coatings followed the similar trend that was observed in the ASTM B 117 salt spray study. BTA-PPy > SCDM-PPy > PPy > QA-PPy > Clearcoat > Silica. The improved corrosion inhibition with BTA-PPy systems may be attributed to the uniform size and greater dispersion stability of the BTA-PPy system as compared to the SCDM-PPy and QA-PPy.

The corrosion resistance performance of PPy nanosphere on aluminum alloy 2024-T3 was previously studied (Chapter 6). Important information regarding the improvement in barrier protection provided by PPy nanospheres was obtained. In this study, EIS was performed on the four different formulations containing 1% of BTA-PPy, 1% of SCDM-PPy, 1% of QA-PPy and clearcoat (without any particles).

EIS was conducted with a 5% NaCl solution as an electrolyte at 10 mV of AC potential. Working electrode was the coated substrate (Al 2024 T-3), reference electrode was the saturated calomel electrode while, counter electrode was the platinum mesh electrode. Bode modulus and phase plots for the coatings containing 1% BTA-PPy, 1% SCDM-PPy, and 1% QA-PPy are provided in Figure 7.12A, Figure 7.12B, Figure 7.12C and Figure 7.12D respectively.

Initial decrease in the low frequency impedance may be attributed to the penetration of the electrolyte in the coating. The low frequency impedance for the coatings containing 1% BTA-PPy (Figure 7.12A) and 1% SCDM-PPy (Figure 7.12B) were in the range of 10^7 Ω and 10^8 Ω. The low frequency impedance for the coatings containing 1% QA-PPy (Figure 7.12C) and for

the coatings without any particles (Figure 7.12D) was between 10^6 Ω to 10^7 Ω. The low frequency impedance was the lowest for the clearcoat among all the coatings analyzed in this study. This indicates improved barrier for the electrolyte penetration through the coating. The circuit modeling of EIS results will further emphasize on the various events taking place during the electrolyte penetration and during the corrosion reaction.

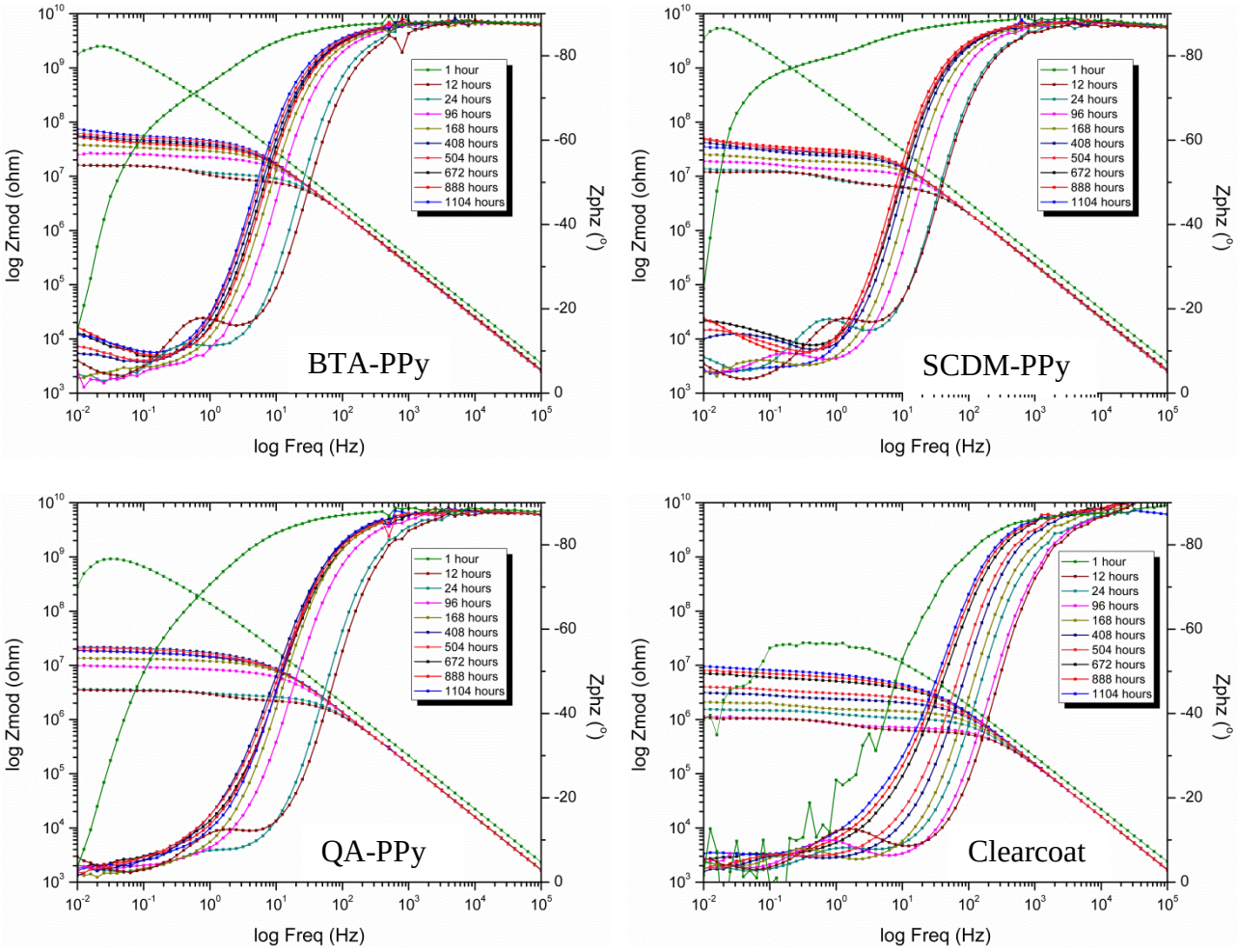

Figure 7.12. A) Top left - Bode phase and modulus plots for coatings with 1% BTA-PPy on Al 2024-T3, B) Top right - Bode phase and modulus plots for coatings with 1% SCDM-PPy on Al 2024-T3, C) Bottom Left - Bode phase and modulus plots for coatings with 1% QA-PPy on Al 2024-T3, and D) Bottom right - Bode phase and modulus plots for clearcoat without any particles on Al 2024-T3.

The OCIs used in this study are expected to form an insoluble complex with copper granules present in the Al 2024-T3 matrix. Literature suggests that the OCIs form a stable oxide layer on the Al 2024-T3 substrates consequently indicating enhanced protection. [3] On the other hand, in the absence of the OCIs, the oxide layer may not be stable with exposure time.

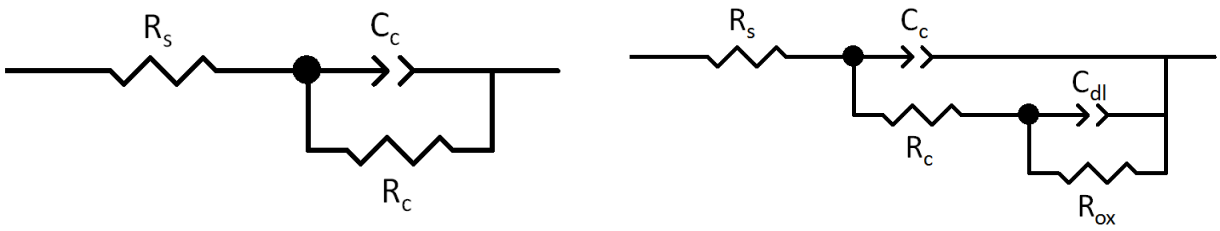

Figure 7.13. A) Left - Equivalent circuit analogous to initial ingress of electrolyte. B) Right - Equivalent circuit analogous to the oxide layer formation.

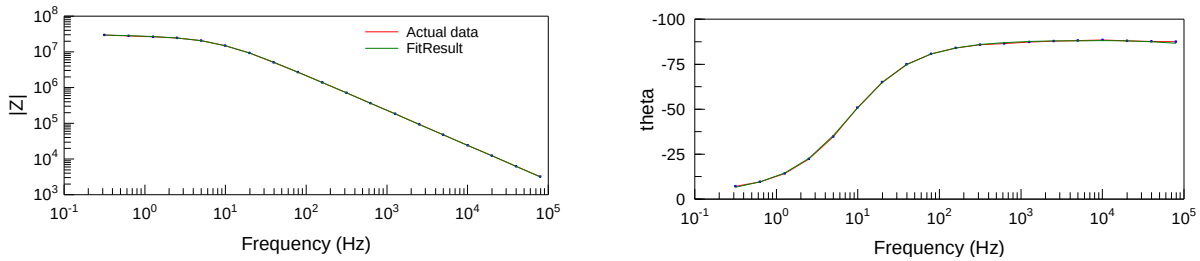

Figure 7.14. Representative fit result showing agreement between actual data and fit result.

Equivalent circuit models represented in the Figure 7.13 are used to study the improvement of corrosion inhibition utilizing the OCIs. In the equivalent circuits shown in Figure 7.13, R_s, C_c and R_c correspond to solution resistance, coating capacitance and coating resistance respectively. C_{dl} and R_{ox} correspond to the double layer capacitance and oxide layer resistance respectively.

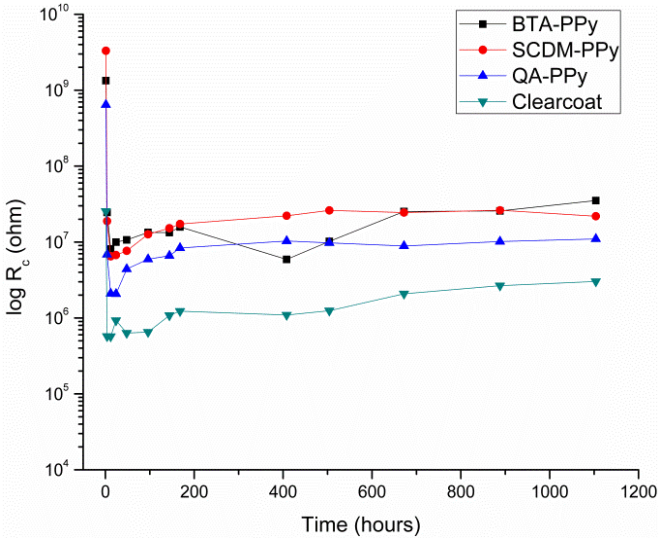

Figure 7.15. Evolution of R_c over immersion time.

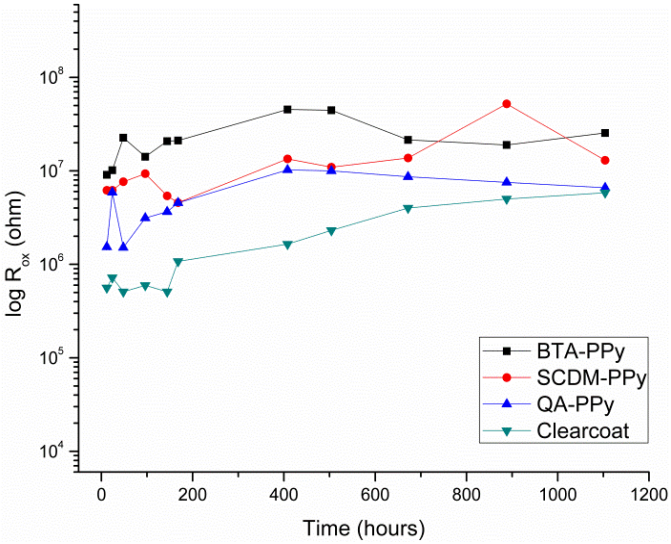

Figure 7.16. Evolution of R_{ox} over immersion time.

The initial ingress of the electrolyte is modeled using the equivalent circuit shown in Figure 7.13A. As the oxide layer develops underneath the coating model shown in Figure 7.13B is employed. These models are used particularly to assess the stability of the coating layer (R_c) and the oxide layer (R_{ox}) under constant immersion. The fitting was performed so that lowest chi-squared value is obtained. Representative fitting models are shown in Figure 7.14.

The coating resistance for the coatings containing OCI-PPy was higher by approximately an order of magnitude throughout the immersion time, indicating better barrier provided OCI-PPy. The oxide layer resistance (Figure 7.16) for the coatings containing OCI-PPy was relatively stable with the increase in immersion time. This was particularly true for the coatings containing 1% BTA-PPy. On the contrary, for the clearcoat (without OCI) the oxide layer resistance was not stable under constant immersion and was marked with an increase in the R_{ox} with immersion time. This result approve of the fact that the coatings containing OCI-PPy may be providing the corrosion protection through the formation of a stable oxide layer on the Al2024-T3 substrate.

7.4. Conclusion

An efficient corrosion inhibiting system has been designed using synergistic effects of PPy and organic corrosion inhibitors. Unlike the traditional entrapment systems where the host materials are often inert; in the OCI-PPy system, both the host (PPy) as well as the releasing organic corrosion inhibitor takes part in mitigating corrosion of Al 2024-T3 alloy. The organic corrosion inhibitors were incorporated in the PPy nanospheres during the growth of the particles. The entrapment of OCI was studied using SEM, FTIR and TGA. While BTA and QA did not show significant effect on particle size and morphology after entrapment of OCI into PPy, the SCDM modified PPy was adversely affected resulting in increased particles size and destabilization of the dispersion. The release studies confirmed that the release of the OCI from PPy was as efficient as is observed traditionally with the entrapment systems consisting of silica or halloysite.

Although, all the three systems (OCI-PPy) displayed improved corrosion inhibition when compared to the clearcoat and silica containing coatings, BTA-PPy was the most efficient corrosion inhibitor as evidenced by accelerated salt spray exposure according to the standards

ASTM B117 and ASTM G-85 A5. EIS results validated that the oxide layer was more stable when OCI-PPy was added to the coatings as compared to the clearcoat.

7.5. References

1. Pinc, W., et al., *Effects of acid and alkaline based surface preparations on spray deposited cerium based conversion coatings on Al 2024-T3.* Applied surface science, 2009. **255**(7): p. 4061-4065.
2. Clark, W.J., et al., *A galvanic corrosion approach to investigating chromate effects on aluminum alloy 2024-T3.* Journal of The Electrochemical Society, 2002. **149**(5): p. B179-B185.
3. Lamaka, S., et al., *High effective organic corrosion inhibitors for 2024 aluminium alloy.* Electrochimica acta, 2007. **52**(25): p. 7231-7247.
4. Racicot, R., R. Brown, and S.C. Yang, *Corrosion protection of aluminum alloys by double-strand polyaniline.* Synthetic metals, 1997. **85**(1): p. 1263-1264.
5. Sukiman, N., et al., *Durability and corrosion of aluminium and its alloys: overview, property space, techniques and developments*. Aluminium Alloys - New Trends in Fabrication and Applications. 2012: InTech.
6. Zheludkevich, M., et al., *Triazole and thiazole derivatives as corrosion inhibitors for AA2024 aluminium alloy*. Corrosion science, 2005. **47**(12): p. 3368-3383.
7. Samuels, B., K. Sotoudeh, and R. Foley, *Inhibition and acceleration of aluminum corrosion.* Corrosion, 1981. **37**(2): p. 92-97.
8. Zheludkevich, M.L., et al., *Anticorrosion coatings with self-healing effect based on nanocontainers impregnated with corrosion inhibitor.* Chemistry of materials, 2007. **19**(3): p. 402-411.

9. Abdullayev, E., et al., *Halloysite tubes as nanocontainers for anticorrosion coating with benzotriazole.* ACS applied materials & interfaces, 2009. **1**(7): p. 1437-1443.

10. Shchukin, D.G., et al., *Active anticorrosion coatings with halloysite nanocontainers.* The Journal of Physical Chemistry C, 2008. **112**(4): p. 958-964.

11. Borisova, D., H. Möhwald, and D.G. Shchukin, *Mesoporous silica nanoparticles for active corrosion protection.* ACS nano, 2011. **5**(3): p. 1939-1946.

12. Borisova, D., H. Möhwald, and D.G. Shchukin, *Influence of Embedded Nanocontainers on the Efficiency of Active Anticorrosive Coatings for Aluminum Alloys Part I: Influence of Nanocontainer Concentration.* ACS applied materials & interfaces, 2012. **4**(6): p. 2931-2939.

13. Poznyak, S., et al., *Novel inorganic host layered double hydroxides intercalated with guest organic inhibitors for anticorrosion applications.* ACS applied materials & interfaces, 2009. **1**(10): p. 2353-2362.

14. Snihirova, D., et al., *Hydroxyapatite microparticles as feedback-active reservoirs of corrosion inhibitors.* ACS applied materials & interfaces, 2010. **2**(11): p. 3011-3022.

15. Li, G.L., et al., *Monodisperse Polymeric Core–Shell Nanocontainers for Organic Self-Healing Anticorrosion Coatings.* Advanced Materials Interfaces, 2013. **1**(1): p. 1300019 (1-6).

16. Plawecka, M., et al., *Self healing ability of inhibitor-containing nanocapsules loaded in epoxy coatings applied on aluminium 5083 and galvanneal substrates.* Electrochimica acta, 2014. **140**: p. 282-293.

17. Scher, H.B., *Microencapsulated chelating agents and their use in removing metal ions from aqueous solutions*, S.C. Company, Editor. 1985, Stauffer Chemical Company.

18. Bhat, N., A. Gadre, and V. Bambole, *Structural, mechanical, and electrical properties of electropolymerized polypyrrole composite films.* Journal of Applied Polymer Science, 2001. **80**(13): p. 2511-2517.

19. Rinaldi, A., et al., *Solid phase photopolymerization of pyrrole in poly (vinylchloride) matrix.* European polymer journal, 2005. **41**(11): p. 2711-2717.

20. Vishnuvardhan, T., et al., *Synthesis, characterization and ac conductivity of polypyrrole/Y2O3 composites.* Bulletin of Materials Science, 2006. **29**(1): p. 77-83.

21. Thombare, J., et al., *Synthesis of Hydrophilic Polypyrrole Thin Films By Silar Method.* Materials Physics and Mechanics, 2013. **16**: p. 118-125.

22. Jing, S., et al., *Synthesis and characterization of Ag/polypyrrole nanocomposites based on silver nanoparticles colloid.* Materials Letters, 2007. **61**(23): p. 4528-4530.

23. Ling, Y., Y. Guan, and K. Han, *Corrosion inhibition of copper with benzotriazole and other organic surfactants.* Corrosion, 1995. **51**(5): p. 367-375.

24. Popova, I. and J.T. Yates, *Adsorption and thermal behavior of benzotriazole chemisorbed on γ-Al2O3.* Langmuir, 1997. **13**(23): p. 6169-6175.

25. Gerlach, T., F.-W. Schütze, and M. Baerns, *An FTIR study on the mechanism of the reaction between nitrogen dioxide and propene over acidic mordenites.* Journal of Catalysis, 1999. **185**(1): p. 131-137.

26. Sedlmair, C., et al., *An in situ IR study of the NOx adsorption/reduction mechanism on modified Y zeolites.* Physical Chemistry Chemical Physics, 2003. **5**(9): p. 1897-1905.

27. Wu, K., Y. Wang, and W. Hwu, *FTIR and TGA studies of poly (4-vinylpyridine-co-divinylbenzene)–Cu (II) complex.* Polymer Degradation and Stability, 2003. **79**(2): p. 195-200.

28. Gunasekaran, S., et al., *FTIR, FT Raman spectra and molecular structural confirmation of isoniazid.* Indian J Pure Appl Phys, 2009. **47**(1): p. 12-8.

29. Shchukin, D.G. and H. Möhwald, *Surface-Engineered Nanocontainers for Entrapment of Corrosion Inhibitors.* Advanced Functional Materials, 2007. **17**(9): p. 1451-1458.

CHAPTER 8. SUMMARY AND FUTURE WORK

8.1. Summary

Because of their useful properties, electroactive polymers (EAPs) such as polypyrrole (PPy) and polyaniline (PANI) have generated a lot of interest in the scientific community. Nanostructures of EAPs have potential applications in the fields of sensors, catalysis, energy storage, biomedical devices and corrosion inhibition. Conventionally, EAP nanostructures are synthesized using a template which drives the growth and morphology of the nanostructures. In this study, a template free method was introduced, for the synthesis of aqueous dispersions of EAP nanostructures using ozone oxidation. The advantages of the template free method over the template based methods are decreased number of steps, reduced cost, and unmodified properties. The aqueous dispersion of nanostructures facilitates the processing of the nanostructures in commonly used coatings and polymers. The simplicity of the ozone oxidation lies in the fact that only monomer, water, and ozone are required for the synthesis.

Stable dispersions of PPy and PANI nanospheres were synthesized successfully using ozone oxidation. The nanospheres synthesized in this study exhibit low particle size distribution and uniform morphology. It is proposed that the high nucleation rate, resulting from the reactive radicals produced in water ozone reaction, leads to the uniform morphology and low particle size distribution. The effect of various reaction parameters on the size and morphology of PPy nanospheres was investigated. The particle size of the synthesized nanospheres can be controlled by temperature of the reaction. Low temperature synthesis, near freezing point of water, resulted in the nanosphere diameters of less than 100 nm. The aqueous dispersion stability of the PPy and PANI nanospheres was attributed to the electrostatic repulsion as well as steric repulsion

provided by the overoxidized oligomers present on the periphery of the nanospheres as evidenced by X-ray photoelectron spectroscopy (XPS) and zeta potential experiments.

This simple method is further explored for the synthesis of silver-PPy core shell nanospheres. The carefully designed experiments combine ozone oxidation and silver nitrate reduction for the synthesis of silver-PPy core shell nanospheres. After nucleation of pyrrole by ozone, silver nitrate is added to the system, which further oxidizes un-reacted pyrrole and pyrrole oligomers by reducing itself to silver. It is believed that the silver nanoparticles provide hydrophobic support for the further growth of PPy resulting into the formation of core shell nanospheres. The synthesized dispersions of silver-PPy core shell nanospheres can potentially be used in the formulations of flexographic ink for food packaging considering their electroactive and antibacterial properties.

The corrosion inhibition of PPy nanospheres was investigated using conventional accelerated salt spray technique as well as modern electrochemical techniques. The facile processability of aqueous dispersions of PPy nanospheres assisted in the straightforward formulations of water based epoxy-amine coatings. These formulations were applied on both cold rolled steel as well as aluminum alloy 2024-T3 substrates. Even at a concentration of 1% by weight of PPy nanospheres in the epoxy-amine coatings, the coatings show improved corrosion inhibition characterized by reduction in the filiform corrosion, particularly for Al-2024 substrates. The results obtained from potentiodynamic scans (PDS), galvanic corrosion experiment, and scanning vibrating electrode technique (SVET) suggested that the oxygen scavenging by reduced form of PPy may be a possible corrosion protection mechanism.

The organic corrosion inhibitor (OCI) modified PPy (OCI-PPy) were synthesized in order to increase the corrosion inhibition efficiency of PPy nanospheres. The OCIs were incorporated

in the PPy nanospheres during the growth of the particles after ozone oxidation. The entrapment of OCIs was confirmed using Fourier transform infrared spectroscopy (FTIR) and thermogravimmetric analysis (TGA). The OCI-PPy is especially useful for corrosion resistance of aluminum alloy 2024-T3. The OCI used in the study were benzotriazole, salicylaldoxime, and quinaldic acid. The synergistic effect of PPy and the OCI was utilized to improve the corrosion inhibition efficiency. OCI are believed to form an insoluble complex with copper granules in Al 2024 thereby reducing the galvanic interaction between copper and aluminum matrix. Among the designed systems benzotriazole modified PPy was observed to be the most effective corrosion inhibitor for Al 2024.

8.2. Future work

As earlier noted, the combination of organic and inorganic nanostructures presents immense opportunities to achieve optimized properties for specific applications, especially in the electronics industry. Silver-PPy (Ag-PPy) core shell nanospheres were synthesized using ozone oxidation in Chapter 5. The *in-situ* reduction of silver nitrate and ozone oxidation was employed for the synthesis of Ag-PPy core shell nanosphere. It will be interesting to examine if the same hypothesis can be utilized for the synthesis of gold-PPy (Au-PPy), palladium-PPy (Pd-PPy) and platinum-PPy (Pt-PPy) core shell nanospheres. The Au-PPy, Pd-PPy and Pt-PPy core shell nanospheres may be synthesized utilizing chloroauric acid ($HAuCl_4$), chloroplatinic acid hexahydrate ($H_2PtCl_6.6H_2O$) and palladium chloride ($PdCl_2$) respectively. Initial studies were performed in our lab to synthesize gold-PPy core shell nanospheres. This synthesis method may further be explored for other electroactive polymers such as PANI.

In Chapter 4, PANI submicron spheres were synthesized, however, the electrochemical activity of PANI was not investigated. The ectrochemical activity of PANI may be investigated

utilizing electrochemical techniques such as cyclic voltammetry. It was observed that the acidic pH as well as shorter ozone exposure duration were essential in controlling over-oxidation of PANI. The effect of reaction pH and ozone exposure time on electrochemical activity of PANI may be investigated to determine the best reaction conditions for achieving efficient electrochemical activity from PANI.

It was proposed that the burst nucleation due to radicals produced in the ozone water reaction may be responsible for the uniformity in PPy and PANI nanospheres. This may be explored in other systems utilizing oxidants such as hydrogen peroxide. In the presented dissertation ozone has been utilized for the synthesis of uniform PPy and PANI nanospheres. The experiments were performed on the lab scale. The scale up of the synthesis to large scale batch is required for commercial success. Traditionally, in the synthesis of conductive polymers the ratio of oxidant to monomer is more than 2. In the case of ozone oxidation, longer ozone exposure to monomer solution leads to over-oxidation. On the other hand short ozone exposure provides with the low yields of the reaction. The yields of the reaction may be improved with assistance from other oxidizing agents with the careful considerations of particle size and morphology.

Although, the PPy synthesized in this research presented electrochemical activity, the conductive forms of PPy were not synthesized. Few of the reasons for less conductivity of the PPy nanostructures could be; overoxidation due to ozone oxidation and lesser interaction of PPy nanospheres due to their spherical morphology. This may be verified after careful investigation of cross sections of PPy nanospheres utilizing high resolution electron microscopy. The differences in elemental composition of over-oxidized outer shell material and inner core material may be helpful in determining the reasons behind lesser conductivity. Further work in

the direction of achieving high conductivity from the PPy nanospheres (synthesized utilizing ozone) would be essential to utilize them in the modern day applications.

It was reported in Chapter 6 and Chapter 7 that even at lower concentrations, pristine PPy nanospheres as well as corrosion inhibitor modified PPy nanospheres show very good corrosion resistance to Al 2024 T3 alloy as compared to the control coatings without PPy. It is essential to study the viability of the PPy nanostructures in complete formulations as a replacement to carcinogenic corrosion inhibitors. The formulations may be utilized in full systems possibly consisting of surface treatment, primer, basecoat and topcoat. Accelerated exposure techniques which were used in the Chapter 6 and Chapter 7 may be utilized to analyze the corrosion inhibition performance of the PPy nanostructures in the coating system resembling the real world situation.

APPENDIX

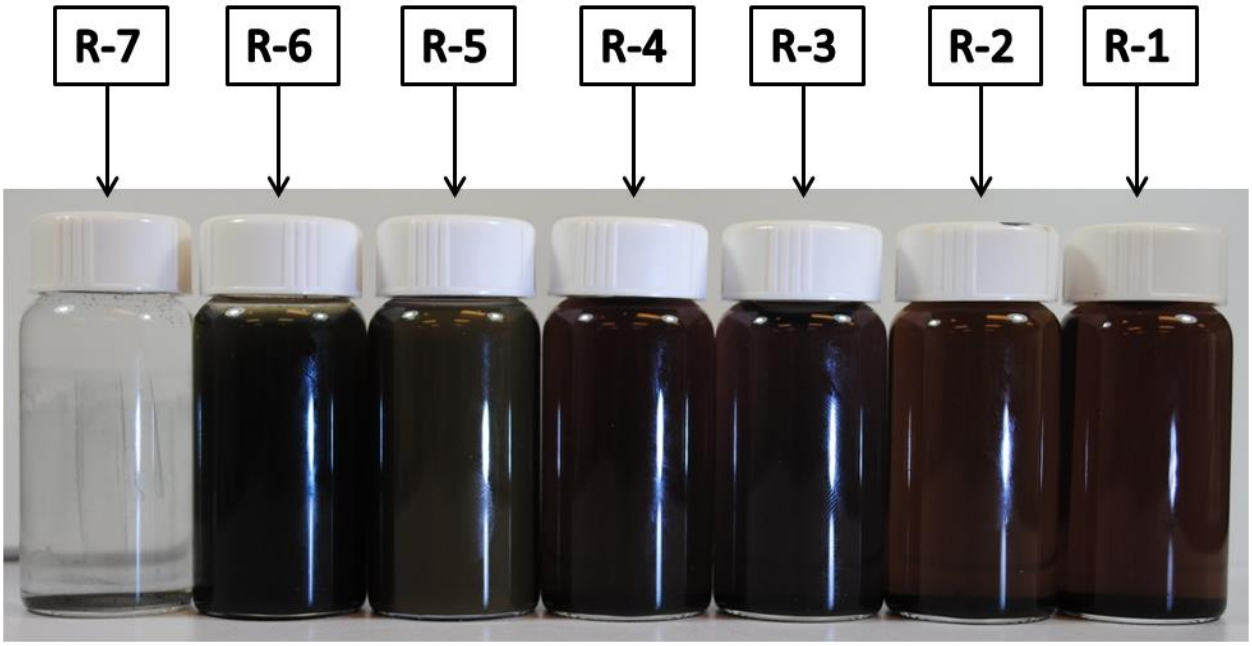

Figure 1A. Reaction vials after 24 Hrs of the reaction. The reactions with more than 0.015 M did not show dispersion stability
(*Note: Please refer to Table 1 for reaction conditions of reactions R-1 to R-7*).

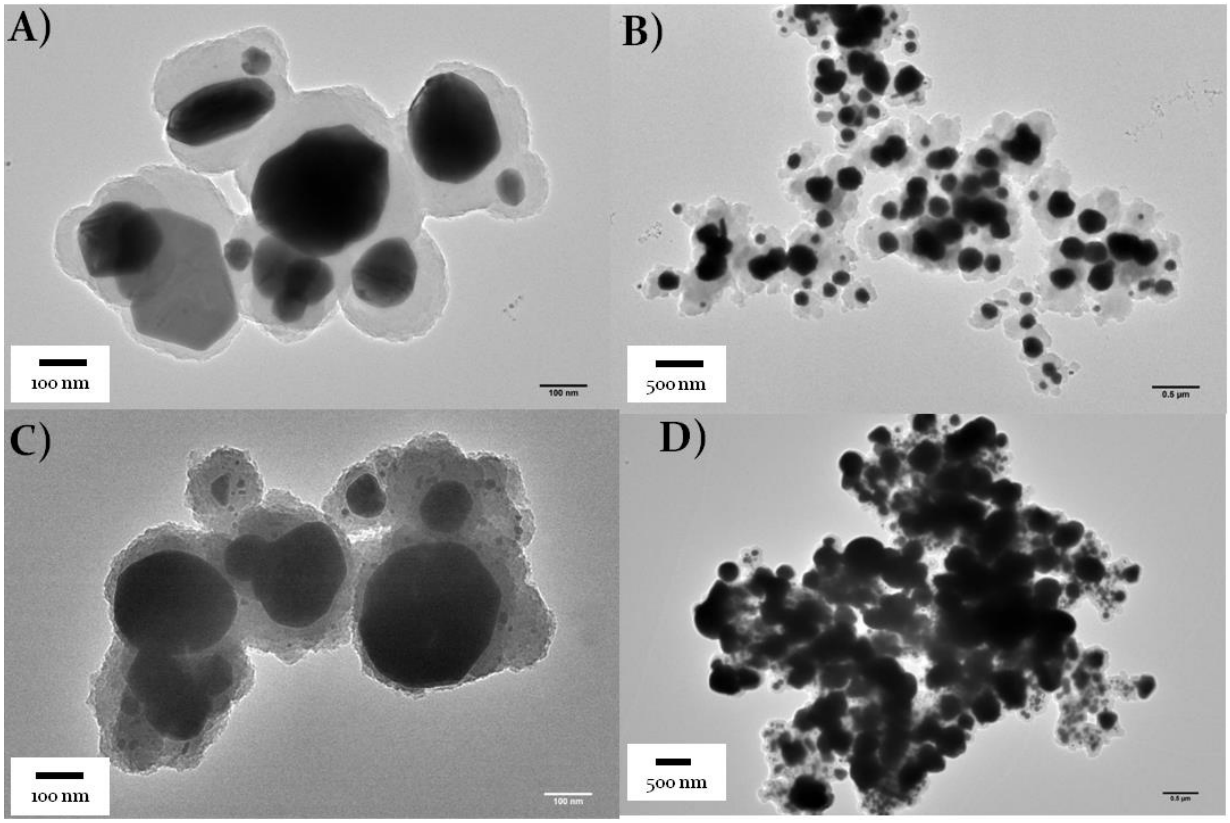

Figure 2A. TEM Images of the Ag/PPy nanocomposites A & B) at 0.04 M silver nitrate concentration C & D) at 0.06 M silver nitrate concentration.

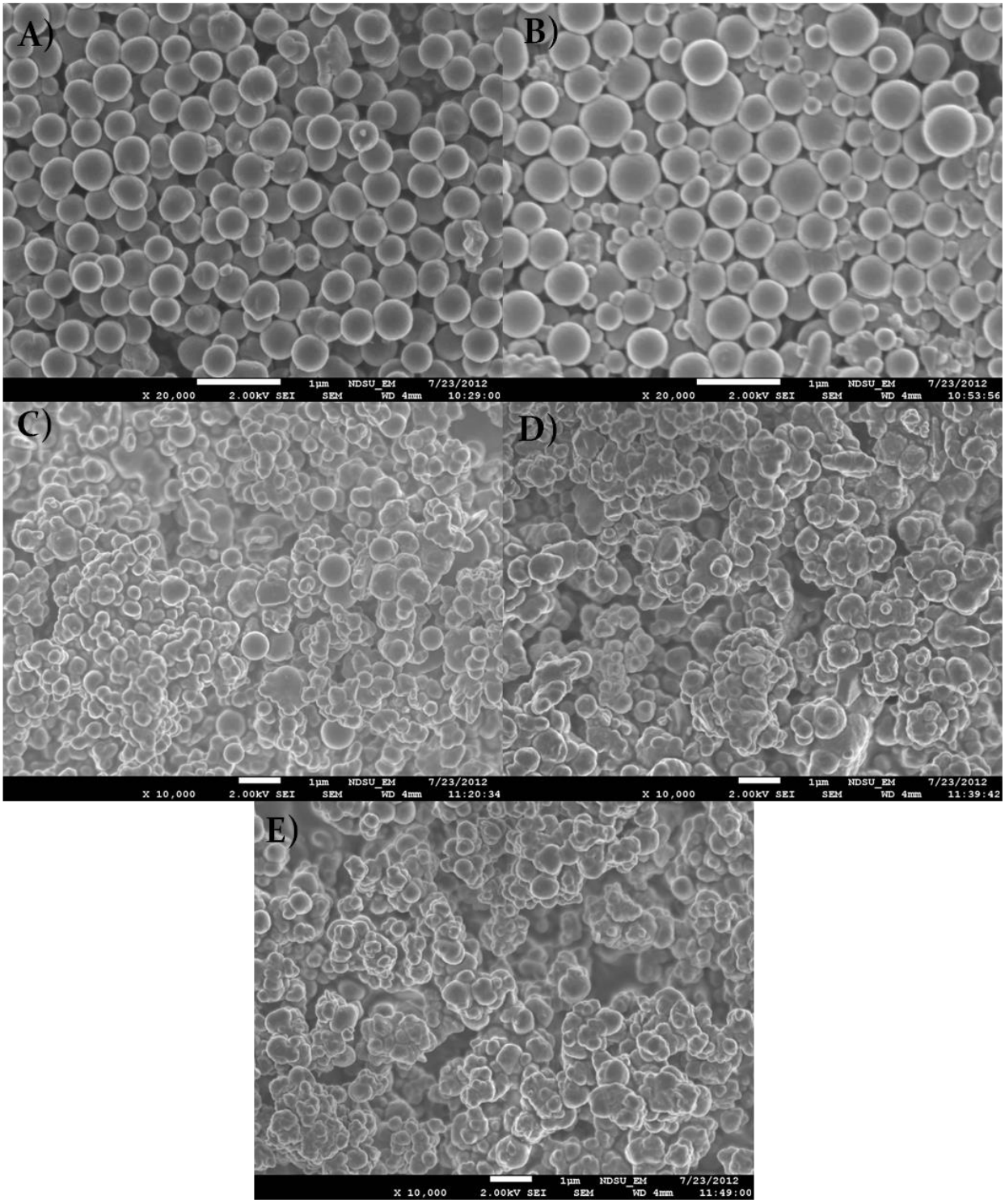

Figure 3A. SEM Images of the Ag/PPy CSNs and nanocomposites at various silver nitrate concentrations A) 0.01 M B) 0.015 M C) 0.02 M D) 0.04 M E) 0.06 M.

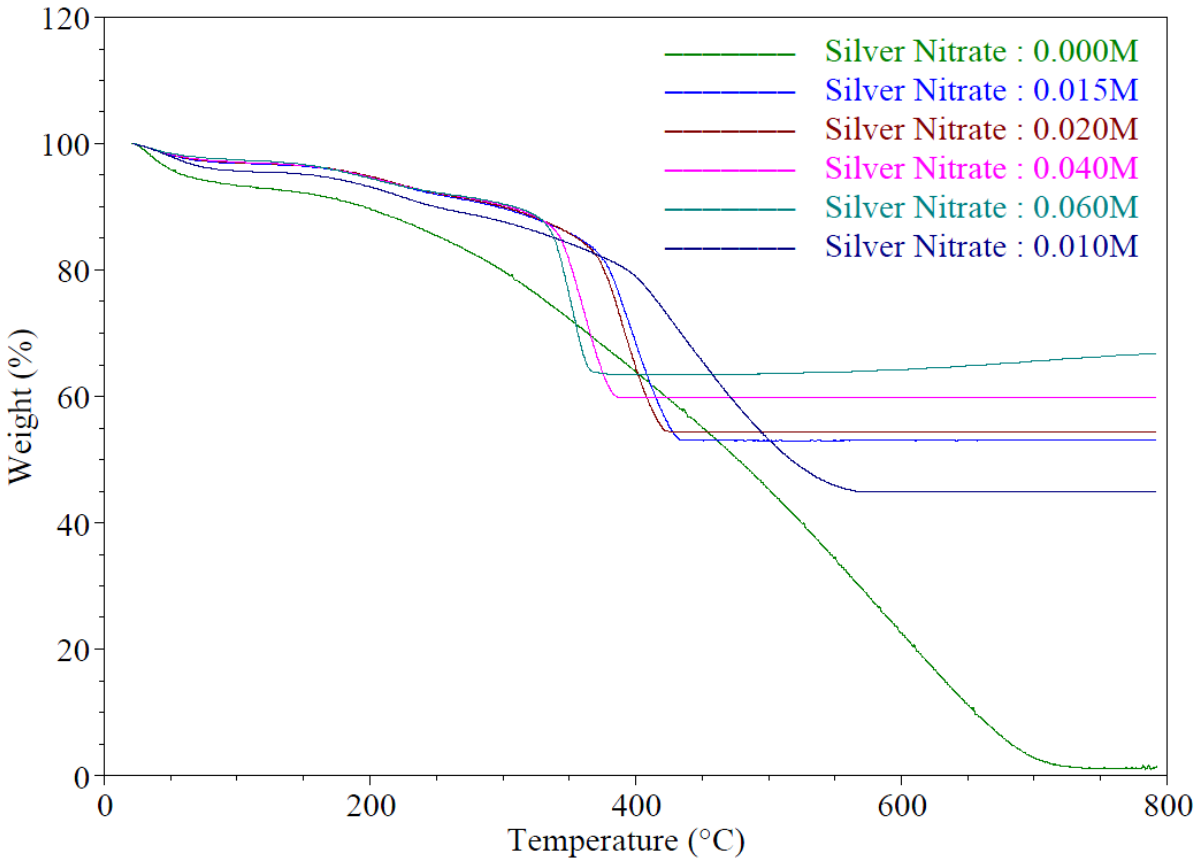

Figure 4A. Thermogravimmetric analysis of the CSNs and nanocomposites. The remaining weight % at 800°C could correspond to silver nanoparticles, since silver nanoparticles do not degrade at 800°C.

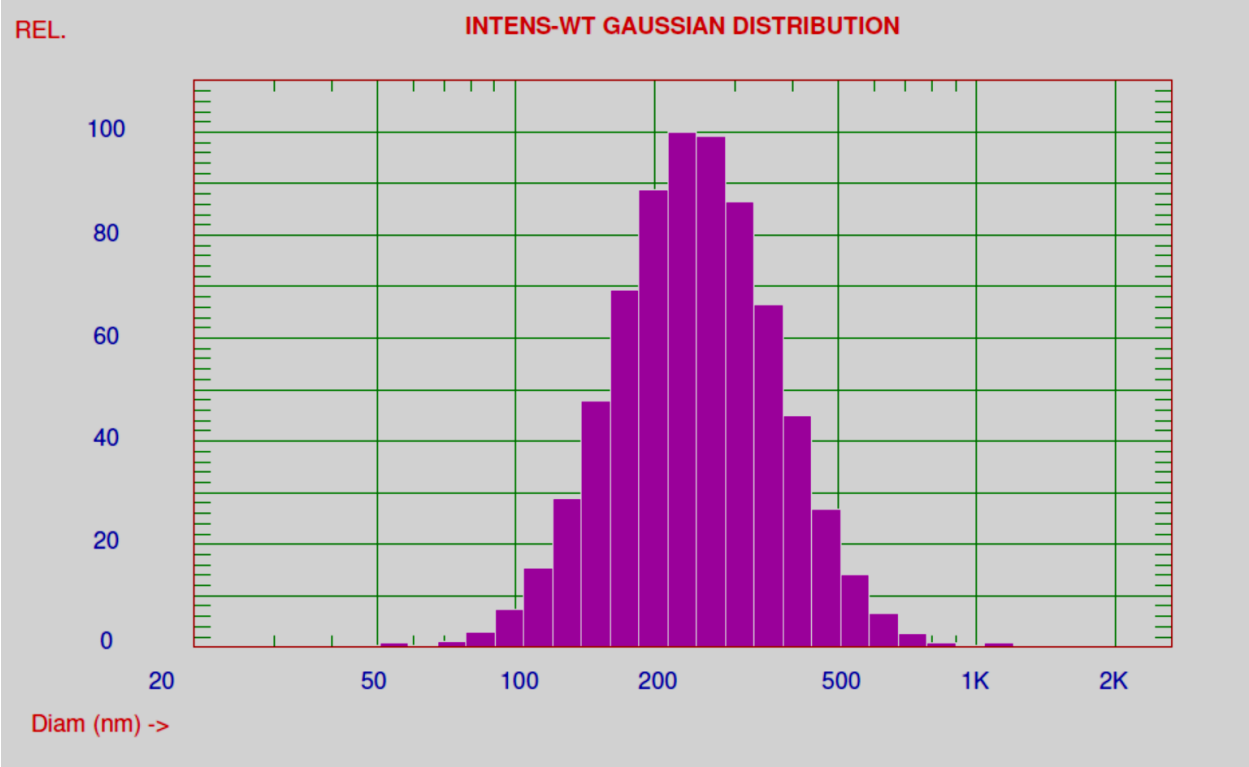
REL.
INTENS-WT GAUSSIAN DISTRIBUTION
100
80
60
40
20
0
20
50
100
200
500
1K
2K
Diam (nm) ->
Figure 5A. Particle size distribution of CSNs synthesized at 0.01M concentration of silver nitrate (R-5).

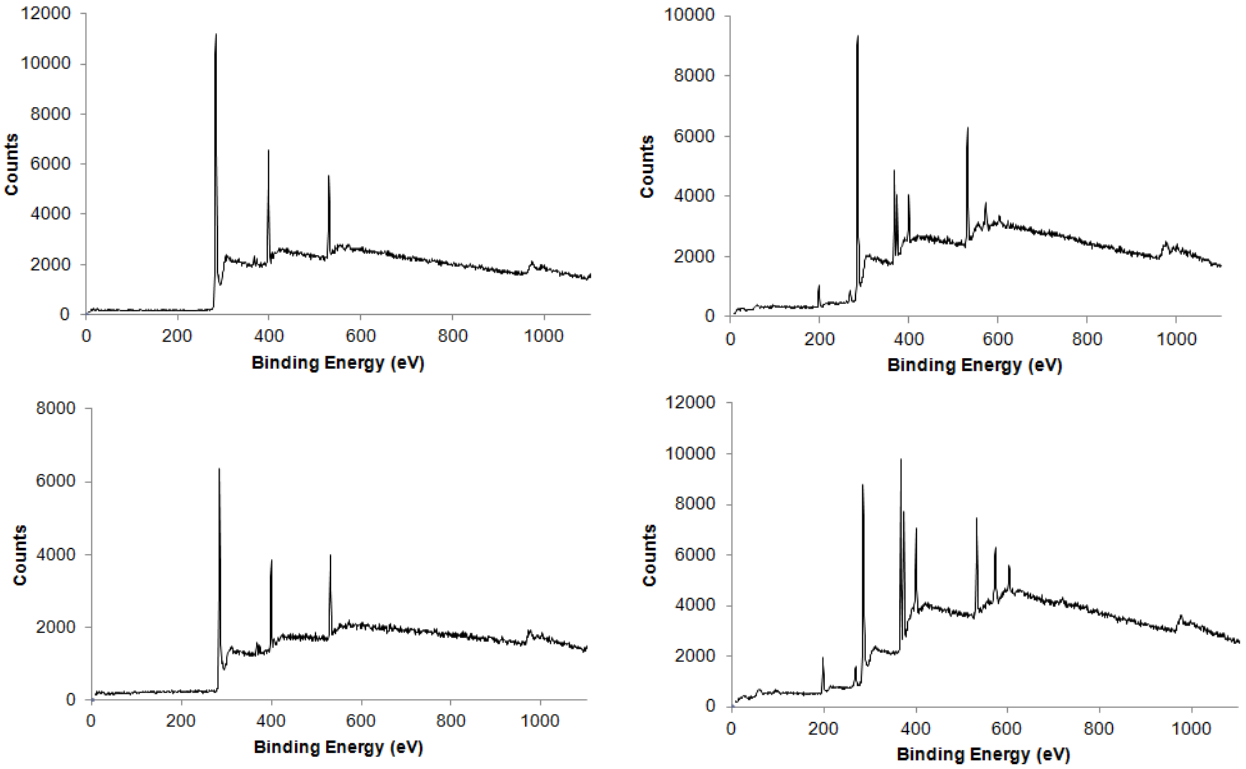

Figure 6A. A) Top left - XPS survey scans for Ag-PPy CSNs (0.01M $AgNO_3$) before cyclic voltammetry, B) Top right - XPS survey scans for Ag-PPy CSNs (0.01M $AgNO_3$) after cyclic voltammetry, C) Bottom left - XPS survey scans for Ag-PPy nanocomposites (0.06M $AgNO_3$) before cyclic voltammetry, and D) Bottom right - XPS survey scans for Ag-PPy nanocomposites (0.06M $AgNO_3$) after cyclic voltammetry.

Table 1A. Atom % after XPS experiments

	Ag-PPy CSNs (0.01M $AgNO_3$)		Ag-PPy nanocomposites (0.06M $AgNO_3$)	
Atom	Atom % before CV	Atom % after CV	Atom % before CV	Atom % after CV
C	76.857	75.320	76.375	66.257
N	14.511	6.692	13.954	12.695
O	8.426	13.658	9.345	11.804
Ag	**0.206**	**2.027**	**0.326**	**4.581**
Cl	--	2.304	--	4.662

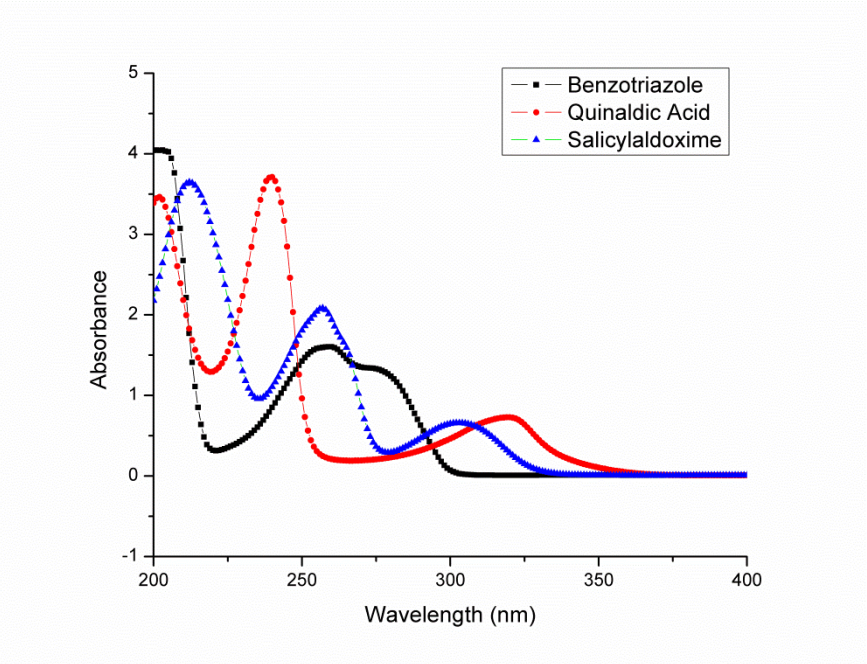

Figure 7A. UV-Vis spectra of corrosion inhibitor solutions in water (5 mg in 20 ml 18 MΩ water).